TOWARDS NEXT GENERATION CRYOPRESERVATION UTILISING MACROMOLECULES AND OSMOLYTES

Trisha L. Bailey

A thesis submitted in fulfilment of the

requirements for the degree of

Doctor of Philosophy

Department of Chemistry, University of Warwick
April 2020

TABLE OF CONTENTS

ACKNOWLEDGMENTS

I would like to first recognize and thank the contribution of my Ph.D. supervisor, Prof Matthew Gibson, your relentless enthusiasm and insights made all this achievable and as painless as possible. Furthermore I would like to thank the Department of Chemistry and the Molecular Analytical Science (MAS) for taking me on and the European Research Council and the Warwick Collaborative Postgraduate Research Scholarship for funding my studies throughout, alongside the Chemistry tech team, stores staff, Rob Jenkins, Sukhjit Takhar, and Rod Wesson, who all solved many problems for me. I would also like to thank Prof Jan Brosens and his group at the University Hospitals Coventry and Warwickshire for allowing me the opportunity to work with their primary cells. I wish to thank Dr Michael Menze for the use of the Biocision CoolCell throughout my reserach. I would like to specifically acknowledge Dr Kathryn Murray, our paths barely crossed but your constant encouragement, help, and presence were a major contributor to this thesis existing, thank you. I also wish to acknowledge my appreciation for the support that the members of the Gibson Group as a whole have provided, from the Postdocs to the rest of my cohort, this is an amazingly kind and knowledgeable group and I am grateful I was a part of it. And finally, to Mike, your unwavering support has made the impossible possible, I just wished you agreed with me that Michael Keaton was the best Batman.

“No one achieves anything alone.”

-Leslie Knope

DECLARATIONS

The work presented in this thesis is entirely my own work, except where acknowledged accordingly in the text:

- All polyampholyte polymers were synthesised and characterised by Dr Christopher Stubbs
- All polyproline polymers were synthesised and characterised by Dr Ben Graham
- Confocal imaging assistance was provided by Ruben Tomás
- Confocal images were processed solely by Ruben Tomás

I confirm that this thesis has not been submitted for a degree at another University.

Parts of the work derived from this thesis have been published by the author.

T. L. Bailey, C. Stubbs, K. Murray, R. M. F. Tomás, L. Otten, and M. I. Gibson, "Synthetically Scalable Poly(ampholyte) Which Dramatically Enhances Cellular Cryopreservation.," Biomacromolecules, vol. 20, no. 8, pp. 3104–3114, Aug. 2019.

B. Graham, **T. L. Bailey**, J. R. J. Healey, M. Marcellini, S. Deville, and M. I. Gibson, "Polyproline as a Minimal Antifreeze Protein Mimic That Enhances the Cryopreservation of Cell Monolayers," *Angew. Chemie - Int. Ed.*, vol. 56, no. 50, pp. 15941–15944, 2017.

ABSTRACT

Complex cell preservation methods, such as attached monolayers, have failed to achieve a level of success that would provide insights and pathways for potential whole organ preservation. Ice crystal growth during freezing can cause both mechanical and osmotic damage to cells, and the ability to control this process by using ice recrystallisation inhibitors has been shown to result in enhanced cryopreservation outcomes. A variety of antifreeze proteins (AFPs) and antifreeze glycoproteins (AFGPs) have been identified in organisms, of which all are ice-binding proteins that are crucial for the species survival. Three different macromolecular cryoprotectants are evaluated: poly(vinyl alcohol) (PVA) due to its high ice recrystallisation inhibition activity, polyproline as a possible AF(G)P mimic, and a polyampholyte due to its scalable synthesis and precise 1:1 ratio of cationic/anionic groups. We also evaluated three potential osmoprotectants: alanine due to the heavy alanine rich regions of AF(G)Ps, betaine for its osmoprotecting properties, and proline due to its previous use as a cryoprotectant and its implications as an osmoprotectant. The macromolecular cryoprotectants and small molecule osmolytes were examined for their physical interactions with ice (Chapter 2), toxicity and proliferation impacts (Chapter 3), the ability to successfully cryopreserve mammalian cells along with post-freeze viability (Chapter 4), and finally, the membrane permeability at various steps throughout the freezing processes was evaluated (Chapter 5). Only PVA was found to have strong ice activity, minimal toxicity was found and proline was shown to down-regulate growth, osmolytes plus PVA or polyproline, and polyampholyte alone, were found to cryopreserve cell monolayers, and polyampholyte showed improved membrane permeability post-freeze. The application of these approaches could provide next generation cryopreservation strategies for many different cell types.

ABBREVIATIONS

A549	Human lung adenocarcinoma cell line
AF(G)P	Antifreeze protein and antifreeze glycoprotein
AFGP	Antifreeze glycoprotein
AFP	Antifreeze protein
ALP	Alkaline phosphatase
ANOVA	Analysis of variance
ATCC	American Tissue Culture Collection
AVD	Apoptotic volume decrease
Bcl-2	B-cell lymphoma cell 2
BGT1	Betaine/GABA transporter 1
Caco-2	Human epithelial colorectal adenocarcinoma cells
CD	Circular dichroism
Cdt-1	Chromatin licensing and DNA replication factor 1
CF	Carboxyfluorescein
CHO	Chinese hamster ovary
CPA	Cryoprotective agent
DCC	Dextran-coated charcoal foetal calf serum
DIS	Dynamic ice shaping
DMEM	Dulbecco's modified eagle medium
DMSO	Dimethyl sulfoxide
DNA	Deoxyribonucleic acid
DSC	Differential scanning calorimetry
DU-145	Human prostate cancer cell line
ECACC	European Collection of Authenticated Cell Cultures
EDTA	Ethylenediaminetetraacetic acid
EEC	Endometrial epithelial cells
EG	Ethylene glycol
EMEM	Eagle’s minimum essential media

ES	Embryonic stem cell line
ESC	Endometrial stromal cells
EthD-1	Ethidium homodimer-1
F-12K	Ham's F-12K (Kaighn's) medium
FBS	Foetal bovine serum
FCS	Foetal calf serum
FDA	Food and Drug Administration
FUCCI	Fluorescence ubiquitination cell cycle indicator
GABA	Gamma aminobutyric acid
GFP	Green fluorescent protein
HCl	Hydrochloric acid
HEK	Human embryonic kidney 293 cells
Hep-G2	Human hepatocyte carcinoma cell line
HeLa	Human cervical cancer cell line
HES	Hydroxyethyl starch
HUVEC	Human umbilical vein endothelial cell line
IIF	Intracellular ice formation
IMINO	Proline, alpha-methylaminoisobutyric acid preferring
IRI	Ice recrystallisation inhibition
IUPAC	International Union of Pure and Applied Chemistry
MC-3T3	Mouse osteoblast precursor cell line
MEM-Alpha	Minimum essential medium α
MLGS	Mean largest grain size
M_n	Average molecular weight of a polymer
mRNA	Messenger ribonucleic acid
mW	milliWatts
MW	Molecular weight
Neuro-2a	Mouse neuroblastoma cell line
NMR	Nuclear magnetic resonance
P-gp	P-glycoprotein

P1	Polyampholyte M_n = 20 kDa
P2	Polyampholyte M_n = 80 kDa
P3	Polyampholyte M_n = 311 kDa
P493	Human B cell lymphoma cell line
PB	Proline biosynthesis
PBS	Phosphate buffered saline
pH	Potential for hydrogen
PHE	Phenylalanine preferring
PLL	Poly(L-lysine)
PSA	Penicillin, streptomycin, and amphotericin B
PUT1	Proline utilisation system
PVA	Poly(vinyl alcohol)
RAW 264.7	Macrophage-like, Abelson leukemia virus transformed cell line
RBC	Red blood cell
RFP	Red fluorescent protein
RFU	Relative fluorescence units
RT	Room temperature
RVI	Regulatory volume increase
SEC	Size exclusion chromatography
SEM	Standard error of the mean
SV-3T3	Simian-virus-40-transformed Balb/c 3T3 cell line
TCA	Tricarboxylic acid
TH	Thermal hysteresis
T_L	Temperature for completion of life cycle
TMAO	Tri-methylamine-*N*-oxide
T_M	Temperature for metabolism
T_{opt}	Optimal temperature
T_S	Temperature for survival
UNOS	United Network for Organ Sharing
UW	University of Wisconsin solution

LIST OF FIGURES, TABLES, AND EQUATIONS

CHAPTER 1

1. INTRODUCTION

1.1 THE GOAL OF CRYOPRESERVATION

According to data from the United Network for Organ Sharing (UNOS), as of April 2020 there are 67,517 people in the United States on the active waiting list for an organ.[1] The average wait time for a deceased donor kidney transplant is 3-5 years, and that for heart transplants is 9 months. Each year, more patients are placed on waiting lists than receive transplants (about one every 10 minutes), causing the wait time to increase. The major limitation of organ transplantation involves the organs themselves, as there is a narrow window of time for the safe transport of live organs. There is currently no process to indefinitely store organs for future use and if a donor cannot be reached in time, the organs will be unable to be used. The ability to store organs in a frozen state (cryostorage) would mitigate many of the current limitations in organ transplantation. Preservation of tissue, the next level of organisation below organs, impacts numerous areas of life, such as fertility, biomedical treatment, and forensic analysis, along with medical and laboratory research. The effects of successful tissue preservation are too vast to list, however one major area of impact, outside the monumental medical impact, is animal research. Currently, molecular studies of experimental animal tissues must be conducted immediately, resulting in long days with limited results per sample, until the tissue is no longer viable. The ability to preserve all the tissue from an animal subject would ease the burden on the researcher along with allowing more samples to be obtained from a single subject, resulting in fewer animals needed per study. Organisationally below tissues, cells are the

chief currency of biological research, with primary cells being the most rare/valuable due to their short lifespan, and stem cells are currently emerging as the backbone for many revolutionary personalised medical treatments due to their programmability. Cell storage currently results in mixed success, with the phenotypic impact of frozen/thawed cells still mostly unknown. A method to reproducibly and unalterably store cells would result in a reliable and robust starting material for an enormous number of bio-medical and research fields. We believe a bottom-up approach is the most beneficial to this field; starting with methods to reliably store cells and then extrapolate those methods and findings to scale up to the more complex networks involved with tissues and then finally, potentially organs.

Temperature is a main focus when talking about cryopreservation and Clark *et al.* succinctly explained the temperature limits for life[2] (Fig 1.1), with emphasis on the fact that the lower limits for life are essentially unknown.[3] Concisely restated from their article, all organisms have an optimal temperature (T_{opt}). On either side of that temperature, is a temperature for completion of the life cycle (T_L), beyond that is a temperature for metabolism (T_M), and at the ends there exists a temperature for survival (T_S). Cryobiologists are attempting to move through lower temperatures such that we stop the life cycle and metabolism while remaining inside the threshold for survival, holding the cells in stasis, yet an undamaged and reversible stasis, such that as the temperature is increased, each of these functions are wholly recovered.

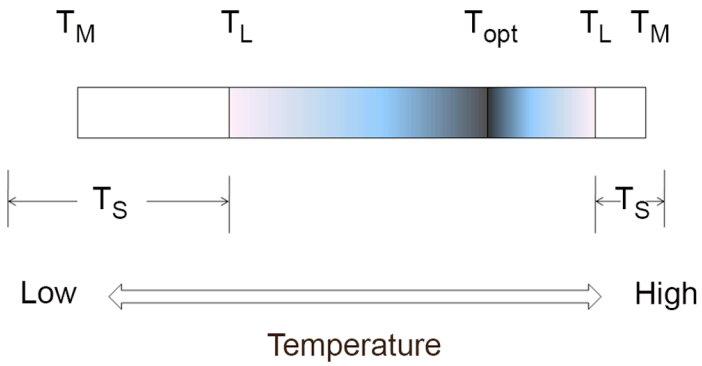

Figure. 1.1. Temperature limits for life. T_L: temperature limit for completion of the life cycle, T_M: temperature limit for metabolism, T_S: temperature limit for survival. Note that T_S can be above, at, or below T_M. The shaded area shows temperature range over which the organism can complete its life cycle, and the white areas show the temperature range (upper and lower) for survival. T_{opt} is the temperature at which growth rate is maximal, which is typically closer to the upper T_L than the lower T_L. Reprinted from Clarke (2013).[2]

1.2 CRYOPRESERVATION STATE-OF-THE-ART

The general principles of organ preservation, static cold storage in a solution to reduce metabolic activity,[4] were developed over 30 years ago and are still standard protocol today. Developed in the 1980s, University of Wisconsin (UW) solution remains the gold standard in organ preservation fluid.[5] The principal components of the UW solution are lactobionate, a large molecular weight anion impermeable to most membranes and thought to suppress hypothermia-induced cell swelling, raffinose, a trisaccharide, and dexamethasone, a corticosteroid. However, UW solution has limitations, principally its incomplete cell protection.[6]

The limitations of organ preservation are also seen on lower levels of cell organisation, such as tissues. Tissues are more challenging to cryopreserve than cells because both cellular integrity and the structure of the extracellular matrix must be preserved, which is complicated by the intimate relationship between both.[7] There is evidence that the core response of cells to cryopreservation is different if the cells are part of a tissue and the scale-up of procedures from a microscopic cellular level to a macroscopic tissue scale will introduce new modes of injury specific to tissue freezing.[8] Most studies of freezing injury have been

carried out with fairly dilute cell suspensions, whereas densely packed cells, such as those seen in tissues, are more likely to be damaged by mechanical stresses due to the space within which they are sequestered changing shape as a result of recrystallisation of the ice that forms their boundaries.[9]

Furthermore, preservation limitations also exist at the cellular level. For the cryopreservation of cells, the standard protocol calls for freezing in a solution containing 5-10% of the cryoprotective agent (CPA) dimethyl sulfoxide (DMSO), which is able to enter cells and at least partly reduce injury by moderating the increase in solute concentration during freezing.[6,10,11] DMSO, discovered in 1959 for its cryoprotective properties,[12] is a small amphiphilic molecule with a hydrophilic sulfoxide and two hydrophobic methyl groups (Fig 1.2). It has been shown that a hydrogen bond between DMSO and water is about 30% stronger than that between two water molecules[13] and this strong hydrogen bonding with water is believed to impart its antifreeze characteristics.[14] Additionally, it has been reported that DMSO reduces membrane rigidity and induces pore formation, a process thought to contribute to reduction of mechanical and osmotic stresses during cellular swelling and shrinking, as well as during ice formation.[15] While suspension freezing in DMSO works for most cell lines, certain cells, such as macrophage-like, Abelson leukaemia virus transformed cells (RAW 264.7) are highly-sensitive to DMSO.[16] These cells are commonly used for the study of cellular responses to microbes and their products, therefore, the ability to reliably store these cells through the use of lower concentrations of DMSO would greatly aid the field of immunology. Additionally, there is a universal concern with using DMSO due to its toxicity at high concentrations and/or room temperature[17–21] as well as the potential for osmotic injuries incurred when loading and unloading cells in the concentrations required for cryopreservation (frequently at levels of 10% w/v).[22]

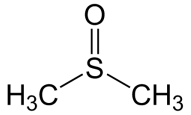

Figure. 1.2. Dimethyl sulfoxide (DMSO) structure.

While cells are typically frozen in cryovials, this format has several disadvantages. Most notably, the need for the cells to be propagated forward through several passages before they are stable enough to be used for reproducible assays. Another disadvantage is that since any *in vitro* culture will undergo phenotypic and genetic changes when propagated for long periods of time, it is neither possible nor practical to maintain a constantly growing culture of cells in order to supply material reproducibly.[23] One answer to this problem is to preserve cells as attached monolayers such that all the required cells for an assay can be frozen from the same cell passage number and thawed as needed. Freezing with just DMSO often protects cells in solution but this method alone does not work well for cell monolayers,[24] typically resulting in only around 20 – 35% recovery[25,26] and adherent attached human embryonic stem cells yield extremely low survival rates of < 5%, which has been shown to be due to apoptosis rather than necrosis from freeze-thaw injury.[24,25] The ability to cryopreserve monolayered cells would facilitate drug development by providing phenotypically identical cells for assays as well as provide insights into the cryopreservation of more complex biological material such as spheroids or tissues. Compared to cryopreservation of suspended cells, protocols for adherent cell monolayers are significantly lacking. To date, there have been few studies on the cryopreservation of monolayered cells that look at recovery post-thaw (Table 1.1). Note in the table that recovery is evaluated in different ways and those which report the highest levels are typically evaluated immediately after freezing, which is not rigorous. At least 24 hours is required to determine if the cells have

functionally recovered[25] and if cells are evaluated before apoptotic processes have had a chance to complete, false positives can be obtained.

Table 1.1. Cell monolayer cryopreservation publications.

Cell Line	Freezing Rate	Condition	DMSO %	Time After Thawing to Assessment	Recovery
HepG2[27]	1 °C·min^{-1}	Trehalose Pre-Incubation	10	24 h	42%
Primary Hepatocytes[28]	1.2 °C·min^{-1}	90% (v/v) FCS	10	48 h	79%
Porcine Aortic Endothelial[29]	0.1 °C·min^{-1}	TiProtec	10	3 h	38%
Porcine Aortic Endothelial[29]	0.1 °C·min^{-1}	Modified TiProtec	10	3 h	50%
Neuro-2a[26]	1 °C·min^{-1}	Trehalose + Proline Pre-Incubation	10	24 h	53%
HeLa[30]	Directional	-	10	5 h	90%
Caco-2[30]	Directional	-	10	5 h	60%
A549[31]	1 °C·min^{-1}	AFPIII	10	24 h	60%
Mouse embryonic stem cell[32]	1 °C·min^{-1}	Virtogel collagen plates	10	6 h	44%
HUVEC[33]	Step-graded	2% Chondroitin Sulfate and 6% HES	5	Immediate	97%
Keratinocytes[34]	3 °C·min^{-1}	10 wt% HES	0	24 h	29%
Keratinocytes[35]	3.3 °C·min^{-1}	10 wt% HES	0	Immediate	80%

There are two main conventional methods for cryopreservation: vitrification and slow cooling (Fig 1.3). Vitrification uses a high concentration of solutes which become viscous through the ultra-rapid lowering of temperature and becomes a glassy solid while avoiding ice nucleation.[36,37] The high CPA concentration results in dehydration of the cells and the potential for extreme ice crystal growth exists upon thawing.[38,39] Additionally, the high concentration of CPA must be quickly removed to prevent toxicity,[19,40] which can involve challenging and complex processes. Due to the high rate of freezing, along with the high CPA concentration required to reach a glassy state, vitrification is not wholly practical for everyday lab use.[41] Slow cooling involves freezing at a controlled rate of 1

°C·min^{-1} in the presence of a CPA which promotes dehydration to avoid intracellular ice formation.[42] Cells can be stored short term at -80 °C or moved to liquid nitrogen for long-term storage at -196 °C. For both methods, upon thawing, ice recrystallisation can damage the cells through the growth of larger ice crystals, at the expense of smaller ones, at temperatures close to the freezing point of the cryoprotectant solution. This crystal growth can cause both mechanical and osmotic damage to cells, and being able to control this process by using ice recrystallisation inhibitors has been shown to result in enhanced post-thaw recovery[43] (further discussed in Section 1.4). In either method, membrane damage can occur at any point where there is molecular movement (> -80 °C).

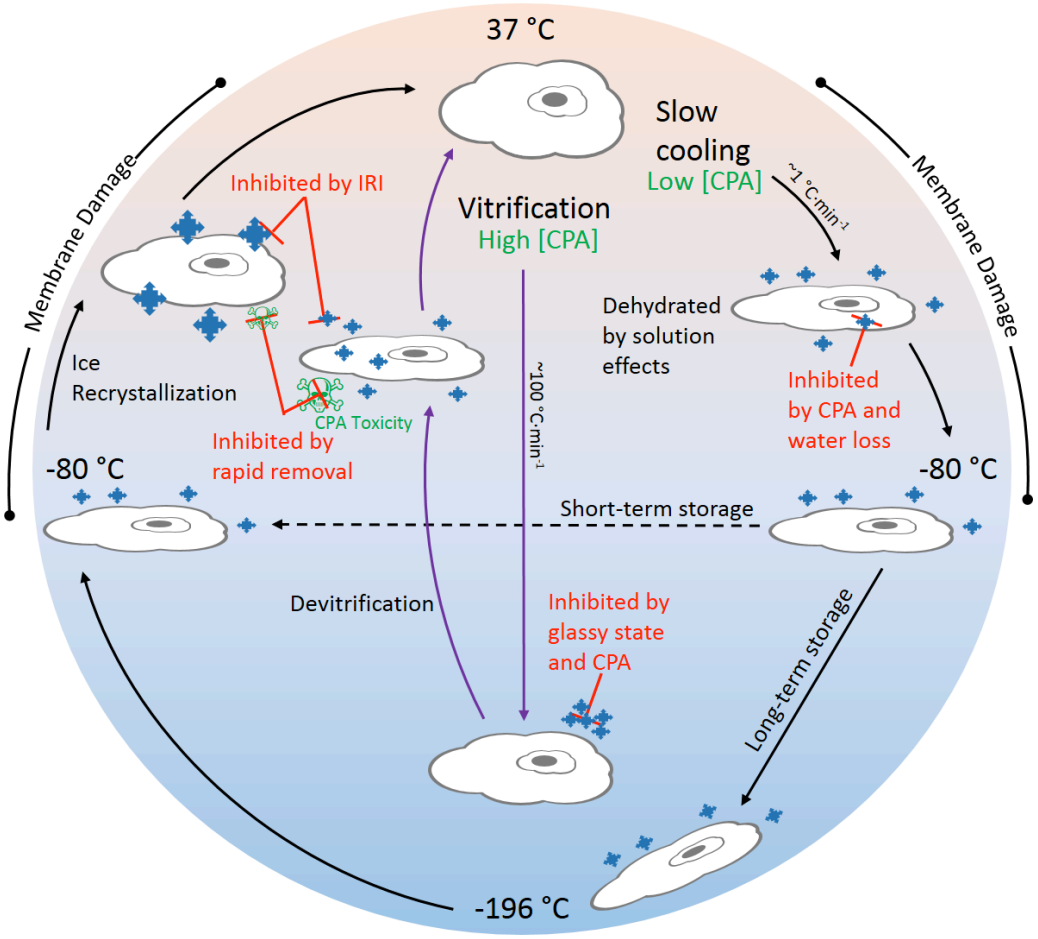

Figure 1.3. Schematic showing conventional cryopreservation processes and sites of damage. Pathways for vitrification (purple) and slow cooling (black) processes are indicated.

1.3 BIOLOGICAL LIMITATIONS

According to Mazur's widely accepted two-factor hypothesis, the main limitations in cryopreservation are ice formation and osmotic stress due to the addition of cryoprotective agents and the increasing concentration of solutes in the remaining water phase during the freezing process.[44] Extensive evidence indicates that ice-formation inside and/or outside of the cell leads to the damage that cells experience when exposed to freezing temperatures, and not the cold temperature itself.[37] Intracellular ice can form when the cooling rate is intermediately high and the cell cannot maintain osmotic equilibrium with the environment.[45] This formation of intracellular ice is almost always lethal.

Intracellular ice formation (IIF) may occur when rates are substantially higher than 1 °C·min^{-1} but are lower than those seen in the ultra-rapid rates used in vitirification.[45,46] A highly controlled rate of freezing is essential to ensure movement of water across the plasma membrane in order for osmotic dehydration to reach equilibrium with intracellular and extracellular contents to prevent IIF.[23,47] It has been demonstrated that the formation of intracellular ice may be less harmful to cells in monolayers than for cells frozen in suspension[48] and IIF may be preceded by damage to the plasma membrane thus IIF could be a result of cell injury and not the cause.[49] Nevertheless, extracellular ice always forms prior to intracellular ice[10] and as extracellular ice forms, a significant increase in the concentration of solutes occurs in the remaining liquid water fraction (Fig 1.4A). If the cooling rate is too low, this can lead to extreme dehydration that may result in irreversible membrane alterations and cell death (Fig 1.4B). However, the optimal cooling rate can vary substantially among cell types and depends on the water permeability of the plasma membrane.[37]

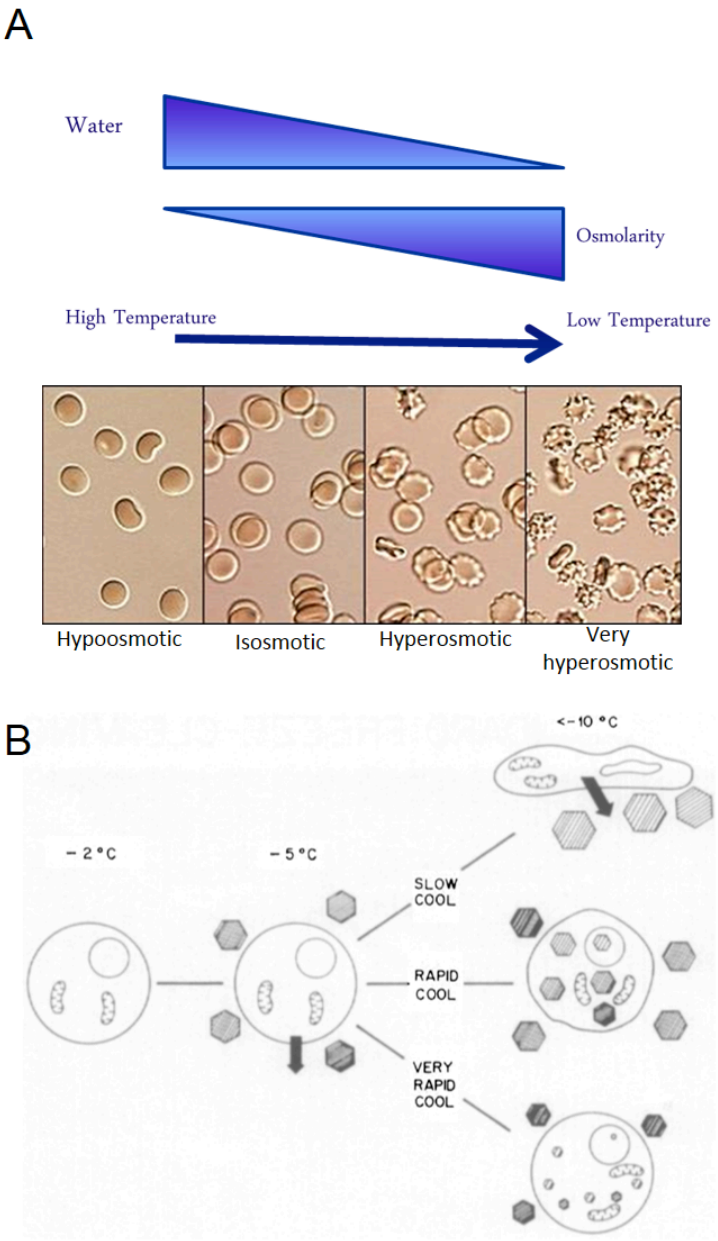

Figure. 1.4. Temperature impact on cells. A) Schematic of temperature, water, and osmolarity of cells. As temperature drops, extracellular water content is reduced as ice forms, the cells experience hyperosmotic conditions, which further draws water out of the cell. **B)** Effect of cooling rate on ice formation and osmolarity during cellular freezing. Reprinted from Mazur[128] Copyright (1977), with permission from Elsevier.

Even with an ideal cooling rate, the formation of extracellular ice results in increased extracellular osmotic pressure that creates an osmotic gradient across the plasma membrane, which provides the driving force for an efflux of water from the cell.[49] There must exist a limit to cell dehydration, as a defining feature of

apoptosis in cells is the apoptotic volume decrease (AVD), which has been considered a passive component of the cell death process. Most cells have inherent volume regulatory increase (RVI) mechanisms to contest an imposed loss in cell size, thus cells exposed to severe shrinkage during freezing will have their apoptotic pathways turned on when thawed.[50] Autophagy, as well as apoptosis, was observed in Chinese hamster ovary (CHO) cells subjected to hyperosmolality and additionally induced apoptosis and tau phosphorylation in human neuroblastoma cells.[51,52] Hyperosmotic stress has been shown to induce metacaspase- and mitochondria-dependent apoptosis in *Saccharomyces cerevisiae* and is thought to kills cells by triggering different molecular pathways, which converge at the mitochondria where pro- and anti-apoptotic members of the Bcl-2 family exert their control.[53,54] Additionally, hyperosmotic stress has also been implicated in cell cycle arrest, DNA damage, oxidative stress, inhibition of transcription and translation, and mitochondrial depolarisation.[55] Conversely, hyperosmotic treatment has been shown to osmotically precondition cardiomyocytes against apoptosis, necrosis,[56] and for an ischemic insult.[57] It appears that hyperosmotic stress has different outcomes based on time experienced and to what extreme, as a tolerable amount of hyperosmotic stress could be beneficial to cells prior to being exposed to stressful conditions.

Temperature also has a strong effect on the physical properties of membrane lipids. Cellular membranes function universally as barriers between the environment, as well as individual cellular components, and play a major role in molecule transport and bioenergetics, and are of critical importance in cell signalling processes. The bilayer typically exists in what is commonly termed a liquid-crystalline phase (a balance between flexibility and order) and at sufficiently low temperatures the regions of the bilayer enter what is termed a gel phase. However, due the heterogeneity of the bilayer, liquid- and gel-phase regions may coexist in the membrane throughout the cooling process, which results in phase

separation[58] (Fig 1.5). Phase separated membranes have been shown to have an increased permeability at the interface of the two regions[59] and upon reheating, phase separated membranes can form non-bilayer lipid structures, due to lipid aggregation[58], which results in membrane integrity damage.[60]

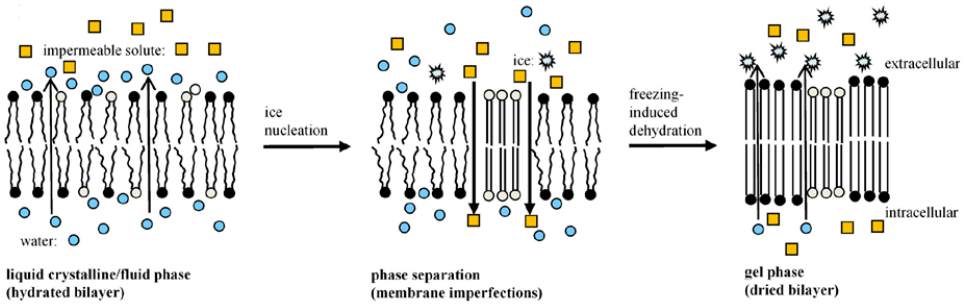

Figure. 1.5. Membrane phase behaviour. Adapted with permission from Wolkers *et al*.[129] Copyright (2018) American Chemical Society.

Cells at low temperatures must also cope with the reduced molecular kinetic energy of the environment and the consequent lower rate of many physical processes.[2] This reduced kinetic energy can limit processes such as ion pumps, as dissipation of ion gradients may occur when energy flow is restricted to the point that ion transport cannot keep up with passive ion leak. This is known to unavoidably trigger the initiation of apoptosis in mammalian species.[61]

Temperature reduction also has an impact on the individual proteins within a cell. Proteins denature at high (~60 °C) and low (~−20 °C) temperatures[62–64] and when a protein experiences this structural instability it loses its functionality. Clathrate cages (particularly ordered structures of water molecules) around non-polar residues were identified as the crucial structure leading to both types of denaturation.[65,66] The hydrophobic effect is one of the main driving forces for the formation of self-assembled biological structures such as lipid membranes and proteins[67] and the strength of the hydrophobic interaction decreases with decreasing temperature. However, proteins have been shown to quickly refold

following a cold denatured temperature jump as opposed to the slower rate following heat denaturation.[68,69]

We have presented many avenues for a cell to become damaged during the cryopreservation process. From extracellular and intracellular ice, hyperosmotic stress, osmotically-triggered apoptosis, membrane disruptions or damage, reduced energy production, and protein damage. This seems like an overwhelming amount of possibilities to manage and control, however, we have a good starting point for how to protect biological materials during freezing from extremophiles found in nature.

1.4 NATURE'S PROTECTION

Organisms in nature have evolved mechanisms to survive desiccation, exposure to sub-zero temperatures, or both. Nature employs a variety of compounds and strategies to enhance the survival of ectothermic animals during extreme environmental conditions.[70] There are many strategies found in nature for the survival of freezing which are not useful to us, for example, blubber, feathers, blood shunting, and metabolic heating are not feasible for the protection of isolated cells in a lab environment. There are, however, a few which can be easily exploited to work in a lab setting.

In 1957, Scholander and colleagues observed that marine teleost fish did not freeze during the winter despite the water temperature being over a degree below the freezing point of their blood serum, which they attributed to osmoadaptation induced by temperature.[71] In 1967, DeVries found that these three species of Antarctic fish could survive temperatures of -2.5 °C[72] and upon further investigation found that a freezing point depression was responsible which could not be due to colligative properties alone, but was owed to carbohydrate containing protein (glycoproteins) (later termed antifreeze glycoproteins (AFGP)),

in the serum.[73,74] Since then, a variety of non-carbohydrate containing antifreeze proteins (AFPs) and AFGPs have since been identified in a number of different fish, insects, plants, and bacteria and they are all ice-binding proteins that are crucial for the species survival in the harsh cold environments to which they are exposed (Fig 1.6).

Characteristic	AFGP	Type I AFP	Type II AFP	Type III AFP	Type IV AFP
Mass (kDa)	2.6 - 33	3.3 – 4.5	11 – 24	6.5	12
Key Properties	AAT repeat; disaccharide	Alanine-rich α-helix	Disulfide bonded	β-sandwich	Alanine rich; helical bundle
Representative Structure	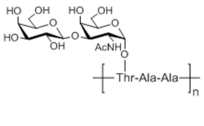	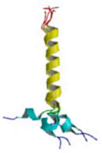			
Natural Source	Antarctic Notothenioids; northern cods	Right-eyed flounders; sculpins	Sea raven; smelt; herring	Ocean pout; wolfish; eel pout	Longhorn sculpin

Figure 1.6. Classification and structural differences between fish antifreeze proteins (AFPs) and antifreeze glycoproteins (AFGPs). Adapted from Capicciotti.[81]

AF(G)Ps have three main activities in regard to freezing: thermal hysteresis (TH), dynamic ice shaping (DIS), and ice recrystallisation inhibition (IRI). Thermal hysteresis refers to the non-colligative lowering of freezing temperature while the melting temperature remains unchanged.[75] TH and DIS are interlinked such that, when the supercooling temperature of the solutions exceeds the level of freezing temperature suppression, growth morphology differs significantly from that of ice growth in pure water with bipyramidal crystallites and columnal spicules forming instead of sheets[75] (Fig 1.7) and both TH and DIS are linked to concentration and protein length.[76,77] The mechanism for DIS has recently been attributed to a semi-clathrate water network on the protein, similar to what was discussed previously in Section 1.3, which merges with, and freezes to, a disordered water layer constructing the ice crystal surface,[78] however, there is still much discussion on

the exact mechanism and a unifying hypothesis has not been adopted. Most notably for us, this bipyramidal ice can lead to mechanical damage of cell membranes,[75] which results in minimal benefit when utilising these proteins as a CPA.

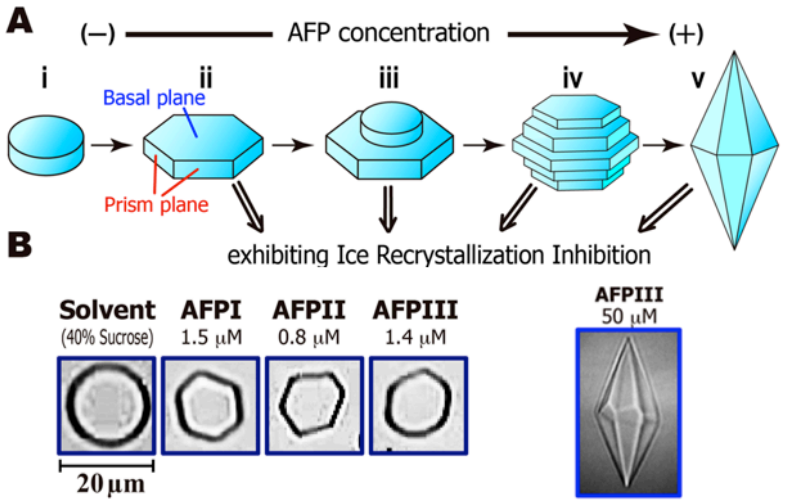

Figure 1.7. Relationship between the morphology of a single ice crystal and AFP concentration. **A)** The crystal forms a round disk without AFP (i), while its six prism planes become visible by AFP-binding to form a hexagonal plate (ii). Further additions of AFP generate a new disk on the hexagonal plate (iii), leading to the formation of a barrel-like ice crystal composed of hexagonal ice layers (iv), and ultimately create a bipyramidal ice crystal (v). **B)** Morphology of ice crystals observed for AFPI-III, at concentrations lower than their IRI endpoint. The hexagonal ice plate is created in the solutions of AFPI-AFPIII and similarly for the solvent (40% sucrose). Adapted from Rahman.[77]

The third property of antifreeze proteins, IRI, appears to operate independently, with little or no correlation to the magnitude of TH activity,[79] such that proteins with high TH activity show relatively low IRI activity, with the opposite being true as well, with proteins showing moderate TH activity showing high IRI.[80] Ice recrystallisation is thought to occur through either grain boundary migration or Ostwald ripening.[81] Grain boundary migration is a phenomenon where large ice grains grow even larger at the expense of small ice grains as individual molecules transfer from unfavourably oriented ice grains to favourably oriented ice grains.[82,83] For the Ostwald ripening process, a constant ice volume is

maintained and water molecules transfer from the surface of smaller ice crystals to bulk-water and then are transferred onto the surface of larger ice crystals. This results in an increase in the average ice crystal size and a decrease in the total number of ice crystals at a constant total ice volume.[84–86] Through either process, the development of these large ice crystals during the thawing process has been shown to mechanically damage cells during cryopreservation.[37,87–90] Antifreeze proteins have the ability to limit this ice recrystallisation so the ice crystals remain small, which results in significantly less damage to membranes[91,92] (Fig 1.8), and this property also appears to be dependent on concentration.[93] However, as stated previously, the DIS properties of AF(G)Ps prohibit their use in applications where IRI activity is highly desirable and attempts at cryopreserving cells with these proteins has resulted in mixed success.[43,94–99]

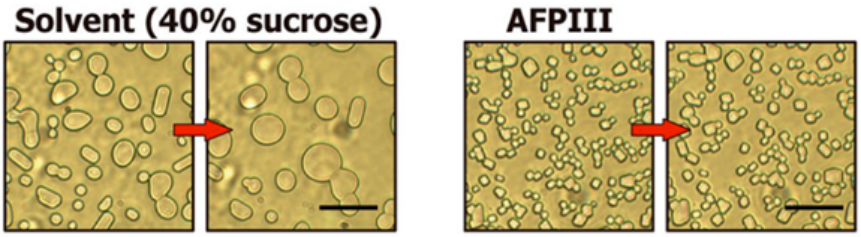

Figure 1.8. Photomicroscope snapshots of ice grains picked up from 40 min videos that recorded the ice recrystallisation process. Photo examples of time-dependent changes in the ice grains in solvent (40% sucrose) and 1.5 μM solutions of AFPIII at −6 °C, taken from the last 20 min. The scale bars represent 50 μm. Adapted from Rahman.[77]

Another approach to cell protection is to view freezing as simply a loss of water event. Cells almost universally respond to the stress of long-term hyperosmolality, such as those seen during freezing, by accumulating compatible organic osmolytes.[100] The major osmolytes in water-stressed eukaryotes are restricted to a few classes of low molecular weight metabolic products: polyhydric alcohols (polyols), such as glycerol and sucrose; free amino acids and amino acid derivatives (taurine and β-alanine); and urea and methylamines, such as

tri-methylamine-*N*-oxide (TMAO), betaine, and sarcosine.[101] Probably the most universally adopted 'compatible' solutes are the *N*-substituted amino acids, particularly betaine and proline.[102] When the freshwater prawn *Macrobrachium rosenbergii* was subjected to a hyperosmotic environment there was shown to be an increase in proline synthesis.[103] Additionally, *Escherichia coli* cells synthesise the osmoprotectant betaine by oxidation of choline when osmotically stressed.[104,105] These strategies could be useful in preconditioning our cells for the stress associated with cryopreservation by simply incubating the cells in these known osmoprotectants.

Another protective mechanism used by natural systems that undergo seasonal exposure to environmental stresses include downregulation of metabolism to enter a hypometabolic state (diapause)[45] and metabolic depression and cell stasis are often prerequisites to survival for animals whose evolutionary history has provided natural adaptations to desiccation, freezing temperatures, and anoxia[106]. As such, a requirement for freezing survival in both *Caenorhabditis elegans*[107] and *Drosophila melanogaster*[108] was a reduction in metabolic activity.[109] Given that there are distinct threshold limits for life, T_M (threshold for metabolism) and T_S (threshold for survival), between T_M and T_S the organism is in a state of suspended animation,[2] it is therefore possible that a reduction in metabolism could be a necessary and inherent step for the suspension of life processes.

1.5 Aims and Objectives

Utilising inspiration obtained from organisms in nature, as well as previous research, there are several novel avenues to be investigated in this work for the successful cryopreservation of biological materials, including explorations into the mechanisms of protection.

We know that AF(G)Ps have a detrimental ice shaping effect which makes their use in cryopreservation difficult. In addition to that, there are also immunogenic and toxicity issues with using these proteins,[110] immense effort required for synthetic production, along with the inherent difficulty of obtaining large quantities of this protein from a source, as it is only produced by extremophiles, usually in specific remote locations.[111] We propose utilising AF(G)P IRI polymer mimics, which allows for tunability of the polymer's properties, such as DIS and IRI since both of the properties are dependent on concentration and protein length, and these polymer mimics mitigate many of the toxicity and immunogenic issues. By using readily available starting materials, we can also ensure the availability of these products for the scale-up to large batch storage. There has previously been success with IRI polymer mimics of AF(G)Ps for freezing cells in suspension,[112–114] but not for cells in a monolayer format. Therefore, we will probe the cryoprotectant properties of these AF(G)P polymer mimics in relation to their protection of cell monolayers. We will additionally investigate non-IRI polymers for the storage of cells, which have been used in the vitrification of cells.[36,115] We will also evaluate the use of osmotic preconditioning compounds with and without our polymer mimics to explore if we can enhance cryopreservation recovery, as this has previously been partially successful in monolayer cryopreservation.[26]

We will primarily use three immortalised cell lines throughout this work; A549, MC-3T3 and Neuro-2a. The human lung adenocarcinoma cell line A549 was established by D.J. Giard in 1972 through an explant culture of a carcinomatous tissue from a 48 year-old Caucasian male[116] and deposited in the American Type Culture Collection (ATCC) bank (CCL-185™) by M. Lieber.[117] The A549 cells are characterised as hypotriploid human alveolar basal epithelial cells and are widely used as an *in vitro* model for type II pulmonary epithelial cells as well as a model of lung adenocarcinoma.[117] These cells grow adherently as monolayers and are suitable as a transfection host.[118] A549 cells were selected as they have been

previously assayed for suspension freezing in the presence of poly(vinyl alcohol)[119] and will allow for comparisons for monolayer freezing. MC3T3 is an osteoblast precursor cell line derived from *Mus musculus* (mouse) calvaria in 1981 by Hiro-aki Kodama[120] and further characterised into the MC3T3-E1 subclone (MC-3T3) by Hiroko Sudo.[121] These cells have been used extensively to define pathways of osteoblast differentiation and equate each stage of differentiation and its gene expression profiles with some function in bone.[122] The cells grow as adherent monolayers and are suitable for *in vitro* osteoblast differentiation. MC-3T3 cells were chosen as they have difficulty attaching and serve as a harsh experiment for cryopreservation outcomes as well as the fact that DMSO has been shown to induce differentiation[123] and thus it would be beneficial to reduce the DMSO exposure of these cells. Gabriella Augusti-Tocco established clonal lines of neurons (Neuro-2a) from mouse neuroblastoma (C1300) for growth in tissue culture in 1969[124] and these cells were further shown to be inducible for in vitro differentiation into mature neurons.[125] This mouse neural crest-derived cell line has been extensively used to study neuronal differentiation, axonal growth and signalling pathways[126] and they grow as adherent monolayers. Neuro-2a cells were chosen as they have previously been used for monolayer cryopreservation after exposure to pre-conditioning osmolytes,[127] a strategy explored in this work.

In addition to finding novel methods and compounds that are successful in cryopreservation, we will also attempt to understand the ways in which these compounds are affording their cryoprotection. This is often not heavily investigated, so we will attempt to scrutinise different avenues involved in the mechanisms of protection. We will assess the compounds' impacts on ice as a mechanism via ice recrystallisation assays and differential scanning calorimetry. We will investigate membrane permeability as a mechanism via calein-AM uptake and retention along with calcein-AM/EthD-1 uptake. As a baseline for the

compound interactions under physiological conditions with the cells we will evaluate the toxicity of the compounds via alamarBlue reduction along with the proliferation impacts of all compounds used via long-term growth assays, in order to assess the impact to the cells of simply being in contact with these compounds. We will additionally assess how well our cells proliferate following cryopreservation via long-term growth assays as a measure of overall cell health. By evaluating cryopreservation outcomes along with cell impacts and mechanisms of protection, we will attempt to identify patterns of protection for cells during cryopreservation.

1.6 References

(1) United Network for Organ Sharing. Transplant Trends https://unos.org/data/transplant-trends/ (accessed Nov 4, 2019).

(2) Clarke, A.; Morris, G. J.; Fonseca, F.; Murray, B. J.; Acton, E.; Price, H. C. A Low Temperature Limit for Life on Earth. *PLoS One* **2013**, *8* (6). https://doi.org/10.1371/journal.pone.0066207.

(3) Pace, N. R. The Universal Nature of Biochemistry. *Proc. Natl. Acad. Sci. U. S. A.* **2001**, *98* (3), 805–808. https://doi.org/10.1073/pnas.98.3.805.

(4) de Rougemont, O.; Lehmann, K.; Clavien, P.-A. Preconditioning, Organ Preservation, and Postconditioning to Prevent Ischemia-Reperfusion Injury to the Liver. *Liver Transpl.* **2009**, *15* (10), 1172–1182. https://doi.org/10.1002/lt.21876.

(5) Feng, S. Donor Intervention and Organ Preservation: Where Is the Science and What Are the Obstacles? *Am. J. Transplant* **2010**, *10* (5), 1155–1162. https://doi.org/10.1111/j.1600-6143.2010.03100.x.

(6) Stéphenne, X.; Najimi, M.; Sokal, E. M. Hepatocyte Cryopreservation: Is It Time to Change the Strategy? *World J. Gastroenterol.* **2010**, *16* (1), 1–14. https://doi.org/10.3748/wjg.v16.i1.1.

(7) Abazari, A.; Jomha, N. M.; Elliott, J. A. W.; McGann, L. E. Cryopreservation of Articular Cartilage. *Cryobiology* **2013**, *66* (3), 201–209.

https://doi.org/10.1016/j.cryobiol.2013.03.001.

(8) Karlsson, J. O. M.; Toner, M. Long-Term Storage of Tissues by Cryopreservation: Critical Issues. *Biomaterials* **1996**, *17* (3), 243–256. https://doi.org/10.1016/0142-9612(96)85562-1.

(9) Pegg, D. E. Principles of Cryopreservation. *Methods Mol. Biol.* **2007**, *368*, 39–57. https://doi.org/10.1007/978-1-59745-362-2_3.

(10) Mazur, P. Cryobiology: The Freezing of Biological Systems. *Science* **1970**, *168* (3934), 939–949. https://doi.org/10.1126/science.168.3934.939.

(11) Mazur, P.; Farrant, J.; Leibo, S. P.; Chu, E. H. Survival of Hamster Tissue Culture Cells after Freezing and Thawing. Interactions between Protective Solutes and Cooling and Warming Rates. *Cryobiology* **1969**, *6* (1), 1–9. https://doi.org/10.1016/s0011-2240(69)80002-7.

(12) Lovelock, J. E.; Bishop, M. W. Prevention of Freezing Damage to Living Cells by Dimethyl Sulphoxide. *Nature* **1959**, *183* (4672), 1394–1395. https://doi.org/10.1038/1831394a0.

(13) MacGregor, W. S. The Chemical and Physical Properties of DMSO. *Ann. N. Y. Acad. Sci.* **1967**, *141* (1), 3–12. https://doi.org/10.1111/j.1749-6632.1967.tb34860.x.

(14) Awan, M.; Buriak, I.; Fleck, R.; Fuller, B.; Goltsev, A.; Kerby, J.; Lowdell, M.; Mericka, P.; Petrenko, A.; Petrenko, Y.; Stolzing, A.; Rogulska, O.; Stacey, G. N. Dimethyl Sulfoxide: A Central Player since the Dawn of Cryobiology, Is Efficacy Balanced by Toxicity? *Regen. Med.* **2020**. https://doi.org/10.2217/rme-2019-0145.

(15) Wang, X.; Hua, T.-C.; Sun, D.-W.; Liu, B.; Yang, G.; Cao, Y. Cryopreservation of Tissue-Engineered Dermal Replacement in Me2SO: Toxicity Study and Effects of Concentration and Cooling Rates on Cell Viability. *Cryobiology* **2007**, *55* (1), 60–65. https://doi.org/10.1016/j.cryobiol.2007.05.006.

(16) Timm, M.; Saaby, L.; Moesby, L.; Hansen, E. W. Considerations Regarding Use of Solvents in in Vitro Cell Based Assays. *Cytotechnology* **2013**, *65* (5), 887–894. https://doi.org/10.1007/s10616-012-9530-6.

(17) Hengstler, J. G.; Utesch, D.; Steinberg, P.; Platt, K. L.; Diener, B.; Ringel, M.;

Swales, N.; Fischer, T.; Biefang, K.; Gerl, M.; Böttger, T.; Oesch, F. Cryopreserved Primary Hepatocytes as a Constantly Available in Vitro Model for the Evaluation of Human and Animal Drug Metabolism and Enzyme Induction. *Drug Metab. Rev.* **2000**, *32* (1), 81–118. https://doi.org/10.1081/DMR-100100564.

(18) Fahy, G. M. Cryoprotectant Toxicity Neutralization. *Cryobiology* **2010**, *60* (3 Suppl), S45-53. https://doi.org/10.1016/j.cryobiol.2009.05.005.

(19) Fahy, G. M. The Relevance of Cryoprotectant "Toxicity" to Cryobiology. *Cryobiology* **1986**, *23* (1), 1–13. https://doi.org/10.1016/0011-2240(86)90013-1.

(20) Arakawa, T.; Carpenter, J. F.; Kita, Y. A.; Crowe, J. H. The Basis for Toxicity of Certain Cryoprotectants: A Hypothesis. *Cryobiology* **1990**, *27* (4), 401–415. https://doi.org/10.1016/0011-2240(90)90017-X.

(21) Da Violante, G.; Zerrouk, N.; Richard, I.; Provot, G.; Chaumeil, J. C.; Arnaud, P. Evaluation of the Cytotoxicity Effect of Dimethyl Sulfoxide (DMSO) on Caco2/TC7 Colon Tumor Cell Cultures. *Biol. Pharm. Bull.* **2002**, *25* (12), 1600–1603. https://doi.org/10.1248/bpb.25.1600.

(22) Farrant, J. Pharmacological Actions and Toxicity of Dimethyl Sulphoxide and Other Compounds Which Protect Smooth Muscle during Freezing and Thawing. *J. Pharm. Pharmacol.* **1964**, *16* (7), 472–483. https://doi.org/10.1111/j.2042-7158.1964.tb07496.x.

(23) Seth, G. Freezing Mammalian Cells for Production of Biopharmaceuticals. *Methods* **2012**, *56* (3), 424–431. https://doi.org/10.1016/j.ymeth.2011.12.008.

(24) Xu, X.; Cowley, S.; Flaim, C. J.; James, W.; Seymour, L.; Cui, Z. The Roles of Apoptotic Pathways in the Low Recovery Rate after Cryopreservation of Dissociated Human Embryonic Stem Cells. *Biotechnol. Prog.* **2010**, *26* (3), 827–837. https://doi.org/10.1002/btpr.368.

(25) Heng, B. C.; Ye, C. P.; Liu, H.; Toh, W. S.; Rufaihah, A. J.; Yang, Z.; Bay, B. H.; Ge, Z.; Ouyang, H. W.; Lee, E. H.; Cao, T. Loss of Viability during Freeze-Thaw of Intact and Adherent Human Embryonic Stem Cells with Conventional Slow-Cooling Protocols Is Predominantly Due to Apoptosis Rather than Cellular Necrosis. *J. Biomed. Sci.* **2006**, *13* (3), 433–445. https://doi.org/10.1007/s11373-

005-9051-9.

(26) Bailey, T. L.; Wang, M.; Solocinski, J.; Nathan, B. P.; Chakraborty, N.; Menze, M. A. Protective Effects of Osmolytes in Cryopreserving Adherent Neuroblastoma (Neuro-2a) Cells. *Cryobiology* **2015**, *71* (3), 472–480. https://doi.org/10.1016/j.cryobiol.2015.08.015.

(27) Stokich, B.; Osgood, Q.; Grimm, D.; Moorthy, S.; Chakraborty, N.; Menze, M. A. Cryopreservation of Hepatocyte (HepG2) Cell Monolayers: Impact of Trehalose. *Cryobiology* **2014**, *69* (2), 281–290. https://doi.org/10.1016/j.cryobiol.2014.08.001.

(28) Stevenson, D. J.; Morgan, C.; Goldie, E.; Connel, G.; Grant, M. H. Cryopreservation of Viable Hepatocyte Monolayers in Cryoprotectant Media with High Serum Content: Metabolism of Testosterone and Kaempherol Post-Cryopreservation. *Cryobiology* **2004**, *49* (2), 97–113. https://doi.org/10.1016/j.cryobiol.2004.05.006.

(29) Pless-Petig, G.; Knoop, S.; Rauen, U. Serum- and Albumin-Free Cryopreservation of Endothelial Monolayers with a New Solution. *Organogenesis* **2018**, *14* (2), 107–121. https://doi.org/10.1080/15476278.2018.1501136.

(30) Bahari, L.; Bein, A.; Yashunsky, V.; Braslavsky, I. Directional Freezing for the Cryopreservation of Adherent Mammalian Cells on a Substrate. *PLoS One* **2018**, *13* (2), e0192265. https://doi.org/10.1371/journal.pone.0192265.

(31) Tomás, R. M. F.; Bailey, T. L.; Hasan, M.; Gibson, M. I. Extracellular Antifreeze Protein Significantly Enhances the Cryopreservation of Cell Monolayers. *Biomacromolecules* **2019**, *20* (10), 3864–3872. https://doi.org/10.1021/acs.biomac.9b00951.

(32) Miyamoto, Y.; Enosawa, S.; Takeuchi, T.; Takezawa, T. Cryopreservation in Situ of Cell Monolayers on Collagen Vitrigel Membrane Culture Substrata: Ready-to-Use Preparation of Primary Hepatocytes and ES Cells. *Cell Transplant.* **2009**, *18* (5), 619–626. https://doi.org/10.1016/j.cryobiol.2009.10.036.

(33) Eskandari, N.; Marquez-curtis, L. A.; Mcgann, L. E.; Elliott, J. A. W. Cryobiology Cryopreservation of Human Umbilical Vein and Porcine Corneal Endothelial Cell Monolayers. *Cryobiology* **2018**, *85* (September), 63–72.

https://doi.org/10.1016/j.cryobiol.2018.10.001.

(34) Pasch, J.; Schiefer, A.; Heschel, I.; Rau, G. Cryopreservation of Keratinocytes in a Monolayer. *Cryobiology* **1999**, *39* (2), 158–168. https://doi.org/10.1006/cryo.1999.2197.

(35) Pasch, J.; Schiefer, A.; Heschel, I.; Dimoudis, N.; Rau, G. Variation of the HES Concentration for the Cryopreservation of Keratinocytes in Suspensions and in Monolayers. *Cryobiology* **2000**, *41* (2), 89–96. https://doi.org/10.1006/cryo.2000.2270.

(36) Meryman, H. T. Cryopreservation of Living Cells: Principles and Practice. *Transfusion* **2007**, *47* (5), 935–945. https://doi.org/10.1111/j.1537-2995.2007.01212.x.

(37) Fowler, A.; Toner, M. Cryo-Injury and Biopreservation. *Ann. N. Y. Acad. Sci.* **2005**, *1066*, 119–135. https://doi.org/10.1196/annals.1363.010.

(38) Asghar, W.; El Assal, R.; Shafiee, H.; Anchan, R. M.; Demirci, U. Preserving Human Cells for Regenerative, Reproductive, and Transfusion Medicine. *Biotechnol. J.* **2014**, *9* (7), 895–903. https://doi.org/10.1002/biot.201300074.

(39) Polge, C.; Smith, A. U.; Parkes, A. S. Revival of Spermatozoa after Vitrification and Dehydration at Low Temperatures. *Nature* **1949**, *164* (4172), 666–666. https://doi.org/10.1038/164666a0.

(40) Meryman, H. T.; Hornblower, M. A Method for Freezing and Washing Red Blood Cells Using a High Glycerol Concentration. *Transfusion* **1972**, *12* (3), 145–156. https://doi.org/10.1111/j.1537-2995.1972.tb00001.x.

(41) Fahy, G. M.; Saur, J.; Williams, R. J. Physical Problems with the Vitrification of Large Biological Systems. *Cryobiology* **1990**, *27* (5), 492–510. https://doi.org/10.1016/0011-2240(90)90038-6.

(42) De Santis, L.; Coticchio, G. Theoretical and Experimental Basis of Slow Freezing. *Reprod. Biomed. Online* **2011**, *22* (2), 125–132. https://doi.org/10.1016/j.rbmo.2010.10.012.

(43) Chao, H.; Davies, P. L.; Carpenter, J. F. Effects of Antifreeze Proteins on Red Blood Cell Survival during Cryopreservation. *J. Exp. Biol.* **1996**, *199* (Pt 9), 2071–

2076. https://doi.org/10.1177/00220345300100030901.

(44) Mazur, P.; Leibo, S. P.; Chu, E. H. Y. A Two-Factor Hypothesis of Freezing Injury. Evidence from Chinese Hamster Tissue-Culture Cells. *Exp. Cell Res.* **1972**, *71* (2), 345–355. https://doi.org/10.1016/0014-4827(72)90303-5.

(45) Mazur, P. Principles of Cryobiology. In *Life in the Frozen State*; Fuller, B., Lane, N., Benson, E. E., Eds.; CRC Press: Boca Raton, 2005; Vol. 17, pp 301–302.

(46) Mazur, P. Freezing of Living Cells: Mechanisms and Implications. *Am. J. Physiol.* **1984**, *247* (3 Pt 1), C125-42. https://doi.org/10.1152/ajpcell.1984.247.3.C125.

(47) Mazur, P.; Miller, R. H.; Leibo, S. P. Survival of Frozen-Thawed Bovine Red Cells as a Function of the Permeation of Glycerol and Sucrose. *J. Membr. Biol.* **1974**, *15* (2), 137–158. https://doi.org/10.1007/bf01870085.

(48) Acker, J. P.; McGann, L. E. Protective Effect of Intracellular Ice during Freezing? *Cryobiology* **2003**, *46* (2), 197–202. https://doi.org/10.1016/s0011-2240(03)00025-7.

(49) Muldrew, K.; McGann, L. E. The Osmotic Rupture Hypothesis of Intracellular Freezing Injury. *Biophys. J.* **1994**, *66* (2 Pt 1), 532–541. https://doi.org/10.1016/S0006-3495(94)80806-9.

(50) Bortner, C. D.; Scoltock, A. B.; Sifre, M. I.; Cidlowski, J. A. Osmotic Stress Resistance Imparts Acquired Anti-Apoptotic Mechanisms in Lymphocytes. *J. Biol. Chem.* **2012**, *287* (9), 6284–6295. https://doi.org/10.1074/jbc.M111.293001.

(51) Han, Y. K.; Kim, Y.-G.; Kim, J. Y.; Lee, G. M. Hyperosmotic Stress Induces Autophagy and Apoptosis in Recombinant Chinese Hamster Ovary Cell Culture. *Biotechnol. Bioeng.* **2010**, *105* (6), 1187–1192. https://doi.org/10.1002/bit.22643.

(52) Stoothoff, W. H.; Johnson, G. V. Hyperosmotic Stress-Induced Apoptosis and Tau Phosphorylation in Human Neuroblastoma Cells. *J. Neurosci. Res.* **2001**, *65* (6), 573–582. https://doi.org/10.1002/jnr.1187.

(53) Silva, R. D.; Sotoca, R.; Johansson, B.; Ludovico, P.; Sansonetty, F.; Silva, M. T.; Peinado, J. M.; Côrte-Real, M. Hyperosmotic Stress Induces Metacaspase- and Mitochondria-Dependent Apoptosis in Saccharomyces Cerevisiae. *Mol. Microbiol.* **2005**, *58* (3), 824–834. https://doi.org/10.1111/j.1365-2958.2005.04868.x.

(54) Criollo, A.; Galluzzi, L.; Chiara Maiuri, M.; Tasdemir, E.; Lavandero, S.; Kroemer, G. Mitochondrial Control of Cell Death Induced by Hyperosmotic Stress. *Apoptosis* **2007**, *12* (1), 3–18. https://doi.org/10.1007/s10495-006-0328-x.

(55) Burg, M. B.; Ferraris, J. D.; Dmitrieva, N. I. Cellular Response to Hyperosmotic Stresses. *Physiol. Rev.* **2007**, *87* (4), 1441–1474. https://doi.org/10.1152/physrev.00056.2006.

(56) Pastukh, V.; Ricci, C.; Solodushko, V.; Mozaffari, M.; Schaffer, S. W. Contribution of the PI 3-Kinase/Akt Survival Pathway toward Osmotic Preconditioning. *Mol. Cell. Biochem.* **2005**, *269* (1), 59–67. https://doi.org/10.1007/s11010-005-2536-z.

(57) Falck, G.; Schjott, J.; Jynge, P. Hyperosmotic Pretreatment Reduces Infarct Size in the Rat Heart. *Physiol. Res.* **1999**, *48* (5), 331–340.

(58) Hazel, J. R. Thermal Adaptation in Biological Membranes: Is Homeoviscous Adaptation the Explanation? *Annu. Rev. Physiol.* **1995**, *57* (1), 19–42. https://doi.org/10.1258/jhsrp.2009.009096.

(59) Cordeiro, R. M. Molecular Structure and Permeability at the Interface between Phase-Separated Membrane Domains. *J. Phys. Chem. B* **2018**, *122* (27), 6954–6965. https://doi.org/10.1021/acs.jpcb.8b03406.

(60) Quinn, P. J. A Lipid-Phase Separation Model of Low-Temperature Damage to Biological Membranes. *Cryobiology* **1985**, *22* (2), 128–146. https://doi.org/10.1016/0011-2240(85)90167-1.

(61) Hand, S. C.; Menze, M. A. Mitochondria in Energy-Limited States: Mechanisms That Blunt the Signaling of Cell Death. *J. Exp. Biol.* **2008**, *211* (12), 1829–1840. https://doi.org/10.1242/jeb.000299.

(62) Kunugi, S.; Tanaka, N. Cold Denaturation of Proteins under High Pressure. *Biochim. Biophys. Acta* **2002**, *1595* (1–2), 329–344. https://doi.org/10.1016/s0167-4838(01)00354-5.

(63) Privalov, P. L.; Griko YuV; Venyaminov SYu; Kutyshenko, V. P. Cold Denaturation of Myoglobin. *J. Mol. Biol.* **1986**, *190* (3), 487–498. https://doi.org/10.1016/0022-2836(86)90017-3.

(64) Privalov, P. L. Thermodynamics of Protein Folding. *J. Chem. Thermodyn.* **1997**,

29 (4), 447–474. https://doi.org/10.1006/jcht.1996.0178.

(65) Dias, C. L.; Ala-Nissila, T.; Wong-ekkabut, J.; Vattulainen, I.; Grant, M.; Karttunen, M. The Hydrophobic Effect and Its Role in Cold Denaturation. *Cryobiology* **2010**, *60* (1), 91–99. https://doi.org/10.1016/j.cryobiol.2009.07.005.

(66) Dias, C. L.; Ala-Nissila, T.; Karttunen, M.; Vattulainen, I.; Grant, M. Microscopic Mechanism for Cold Denaturation. *Phys. Rev. Lett.* **2008**, *100* (11), 118101. https://doi.org/10.1103/PhysRevLett.100.118101.

(67) Dill, K. A.; Truskett, T. M.; Vlachy, V.; Hribar-Lee, B. Modeling Water, the Hydrophobic Effect, and Ion Solvation. *Annu. Rev. Biophys. Biomol. Struct.* **2005**, *34*, 173–199. https://doi.org/10.1146/annurev.biophys.34.040204.144517.

(68) Dyer, R. B.; Maness, S. J.; Franzen, S.; Fesinmeyer, R. M.; Olsen, K. A.; Andersen, N. H. Hairpin Folding Dynamics: The Cold-Denatured State Is Predisposed for Rapid Refolding. *Biochemistry* **2005**, *44* (30), 10406–10415. https://doi.org/10.1021/bi050698z.

(69) Nölting, B. Temperature-Jump Induced Fast Refolding of Cold-Unfolded Protein. *Biochem. Biophys. Res. Commun.* **1996**, *227* (3), 903–908. https://doi.org/10.1006/bbrc.1996.1603.

(70) Brockbank, K. G. M.; Campbell, L. H.; Greene, E. D.; Brockbank, M. C. G.; Duman, J. G. Lessons from Nature for Preservation of Mammalian Cells, Tissues, and Organs. *Vitr. Cell. Dev. Biol. - Anim.* **2011**, *47* (3), 210–217. https://doi.org/10.1007/s11626-010-9383-2.

(71) Scholander, P. F.; van Dam, L.; Kanwisher, J. W.; Hammel, H. T.; Gordon, M. S. Supercooling and Osmoregulation in Arctic Fish. *J. Cell. Comp. Physiol.* **1957**, *49* (1), 5–24. https://doi.org/10.1002/jcp.1030490103.

(72) Somero, G. N.; DeVries, A. L. Temperature Tolerance of Some Antarctic Fishes. *Science* **1967**, *156* (3772), 257–258. https://doi.org/10.1126/science.156.3772.257.

(73) DeVries, A. L.; Wohlschlag, D. E. Freezing Resistance in Some Antarctic Fishes. *Science* **1969**, *163* (3871), 1073–1075. https://doi.org/10.1126/science.163.3871.1073.

(74) DeVries, A. L.; Komatsu, S. K.; Feeney, R. E. Chemical and Physical Properties of Freezing Point-Depressing Glycoproteins from Antarctic Fishes. *J. Biol. Chem.* **1970**, *245* (11), 2901–2908. https://doi.org/07/1970; 245(11):2909-13.

(75) Raymond, J. A.; Wilson, P.; DeVries, A. L. Inhibition of Growth of Nonbasal Planes in Ice by Fish Antifreezes. *Proc. Natl. Acad. Sci. U. S. A.* **1989**, *86* (3), 881–885. https://doi.org/10.1073/pnas.86.3.881.

(76) Ben, R. N. Antifreeze Glycoproteins--Preventing the Growth of Ice. *Chembiochem* **2001**, *2* (3), 161–166. https://doi.org/10.1002/1439-7633(20010302)2:3<161::AID-CBIC161>3.0.CO;2-F.

(77) Rahman, A. T.; Arai, T.; Yamauchi, A.; Miura, A.; Kondo, H.; Ohyama, Y.; Tsuda, S. Ice Recrystallization Is Strongly Inhibited When Antifreeze Proteins Bind to Multiple Ice Planes. *Sci. Rep.* **2019**, *9* (1), 2212. https://doi.org/10.1038/s41598-018-36546-2.

(78) Garnham, C. P.; Campbell, R. L.; Davies, P. L. Anchored Clathrate Waters Bind Antifreeze Proteins to Ice. *Proc. Natl. Acad. Sci. U. S. A.* **2011**, *108* (18), 7363–7367. https://doi.org/10.1073/pnas.1100429108.

(79) Sidebottom, C.; Buckley, S.; Pudney, P.; Twigg, S.; Jarman, C.; Holt, C.; Telford, J.; McArthur, A.; Worrall, D.; Hubbard, R.; Lillford, P. Heat-Stable Antifreeze Protein from Grass. *Nature* **2000**, *406* (6793), 256. https://doi.org/10.1038/35018639.

(80) Scotter, A. J.; Marshall, C. B.; Graham, L. A.; Gilbert, J. A.; Garnham, C. P.; Davies, P. L. The Basis for Hyperactivity of Antifreeze Proteins. *Cryobiology* **2006**, *53* (2), 229–239. https://doi.org/10.1016/j.cryobiol.2006.06.006.

(81) Capicciotti, C. J.; Doshi, M.; Ben, R. N. Ice Recrystallization Inhibitors: From Biological Antifreezes to Small Molecules. In *Recent Developments in the Study of Recrystallization*; InTech, 2013; pp 177–224. https://doi.org/10.5772/54992.

(82) Alley, R. B.; Perepezko, J. H.; Bentley, C. R. Grain Growth in Polar Ice: I. Theory. *J. Glaciol.* **1986**, *32* (112), 415–424. https://doi.org/10.3189/S0022143000012120.

(83) Alley, R. B.; Perepezko, J. H.; Bentley, C. R. Grain Growth in Polar Ice: II. Application. *J. Glaciol.* **1986**, *32* (112), 425–433.

https://doi.org/10.3189/s0022143000012132.

(84) Sutton, R. L.; Lips, A.; Piccirillo, G.; Sztehlo, A. Kinetics of Ice Recrystallization in Aqueous Fructose Solutions. *J. Food Sci.* **1996**, *61* (4), 741–745. https://doi.org/10.1111/j.1365-2621.1996.tb12194.x.

(85) Hagiwara, T.; Hartel, R. W.; Matsukawa, S. Relationship between Recrystallization Rate of Ice Crystals in Sugar Solutions and Water Mobility in Freeze-Concentrated Matrix. *Food Biophys.* **2006**, *1* (2), 74–82. https://doi.org/10.1007/s11483-006-9009-0.

(86) Budke, C.; Heggemann, C.; Koch, M.; Sewald, N.; Koop, T. Ice Recrystallization Kinetics in the Presence of Synthetic Antifreeze Glycoprotein Analogues Using the Framework of LSW Theory. *J. Phys. Chem. B* **2009**, *113* (9), 2865–2873. https://doi.org/10.1021/jp805726e.

(87) Baust, J. M.; Buskirk, R. V. A. N.; Baust, J. G. Cell Viability Improves Following Inhibition of Cryopreservation-Induced Apoptosis. *Vitr. Cell. Dev. Biol. - Anim.* **2000**, *36* (April), 262–270. https://doi.org/10.1290/1071-2690(2000)036<0262.

(88) Baust, J. M.; Vogel, M. J.; Van Buskirk, R.; Baust, J. G. A Molecular Basis of Cryopreservation Failure and Its Modulation to Improve Cell Survival. *Cell Transplant.* **2001**, *10* (7), 561–571. https://doi.org/10.3727/000000001783986413.

(89) Baust, J. M. Molecular Mechanisms of Cellular Demise Associated with Cryopreservation Failure. *Cell Preserv. Technol.* **2002**, *1* (1), 17–31. https://doi.org/10.1089/15383440260073266.

(90) Jin, B.; Kusanagi, K.; Ueda, M.; Seki, S.; Valdez, D. M.; Edashige, K.; Kasai, M. Formation of Extracellular and Intracellular Ice during Warming of Vitrified Mouse Morulae and Its Effect on Embryo Survival. *Cryobiology* **2008**, *56* (3), 233–240. https://doi.org/10.1016/j.cryobiol.2008.03.004.

(91) Knight, C. A.; Hallett, J.; DeVries, A. L. Solute Effects on Ice Recrystallization: An Assessment Technique. *Cryobiology* **1988**, *25* (1), 55–60. https://doi.org/10.1016/0011-2240(88)90020-X.

(92) Knight, C. A.; Wen, D.; Laursen, R. A. Nonequilibrium Antifreeze Peptides and the Recrystallization of Ice. *Cryobiology* **1995**, *32* (1), 23–34.

https://doi.org/10.1006/cryo.1995.1002.

(93) Knight, C. A.; DeVries, A. L.; Oolman, L. D. Fish Antifreeze Protein and the Freezing and Recrystallization of Ice. *Nature* **1984**, *308* (5956), 295–296. https://doi.org/10.1038/308295a0.

(94) Nishijima, K.; Tanaka, M.; Sakai, Y.; Koshimoto, C.; Morimoto, M.; Watanabe, T.; Fan, J.; Kitajima, S. Effects of Type III Antifreeze Protein on Sperm and Embryo Cryopreservation in Rabbit. *Cryobiology* **2014**, *69* (1), 22–25. https://doi.org/10.1016/j.cryobiol.2014.04.014.

(95) O'Neil, L.; Paynter, S. J.; Fuller, B. J.; Shaw, R. W.; DeVries, A. L. Vitrification of Mature Mouse Oocytes in a 6 M Me2SO Solution Supplemented with Antifreeze Glycoproteins: The Effect of Temperature. *Cryobiology* **1998**, *37* (1), 59–66. https://doi.org/10.1006/cryo.1998.2098.

(96) Koshimoto, C.; Mazur, P. Effects of Warming Rate, Temperature, and Antifreeze Proteins on the Survival of Mouse Spermatozoa Frozen at an Optimal Rate. *Cryobiology* **2002**, *45* (1), 49–59. https://doi.org/10.1016/S0011-2240(02)00105-0.

(97) Carpenter, J. F.; Hansen, T. N. Antifreeze Protein Modulates Cell Survival during Cryopreservation: Mediation through Influence on Ice Crystal Growth. *Proc. Natl. Acad. Sci. U. S. A.* **1992**, *89* (19), 8953–8957. https://doi.org/10.1073/pnas.89.19.8953.

(98) Geng, H.; Liu, X.; Shi, G.; Bai, G.; Ma, J.; Chen, J.; Wu, Z.; Song, Y.; Fang, H.; Wang, J. Graphene Oxide Restricts Growth and Recrystallization of Ice Crystals. *Angew. Chem. Int. Ed. Engl.* **2017**, *56* (4), 997–1001. https://doi.org/10.1002/anie.201609230.

(99) Wang, T.; Zhu, Q.; Yang, X.; Layne, J. R.; Devries, A. L. Antifreeze Glycoproteins from Antarctic Notothenioid Fishes Fail to Protect the Rat Cardiac Explant during Hypothermic and Freezing Preservation. *Cryobiology* **1994**, *31* (2), 185–192. https://doi.org/10.1006/cryo.1994.1022.

(100) Burg, M. B. Molecular Basis of Osmotic Regulation. *Am.J Physiol* **1995**, *268* (6 Pt 2), F983–F996. https://doi.org/10.1152/ajprenal.1995.268.6.F983.

(101) Yancey, P. H.; Clark, M. E.; Hand, S. C.; Bowlus, R. D.; Somero, G. N. Living with

Water Stress: Evolution of Osmolyte Systems. *Science* **1982**, *217* (4566), 1214–1222. https://doi.org/10.1126/science.7112124.

(102) Higgins, C. F.; Cairney, J.; Stirling, D. A.; Sutherland, L.; Booth, I. R. Osmotic Regulation of Gene Expression: Ionic Strength as an Intracellular Signal? *Trends Biochem. Sci.* **1987**, *12* (C), 339–344. https://doi.org/10.1016/0968-0004(87)90158-7.

(103) Armstrong, D. A.; Strange, K.; Crowe, J.; Knight, A.; Simmons, M. High Salinity Acclimation by the Prawn Macrobrachium Rosenbergii: Uptake of Exogenous Nitrogenous Compounds. *Biol. Bull.* **1981**, *160* (3), 349–365. https://doi.org/10.2307/1540844.

(104) Styrvold, O. B.; Falkenberg, P.; Landfald, B.; Eshoo, M. W.; Bjørnsen, T.; Strøm, A. R. Selection, Mapping, and Characterization of Osmoregulatory Mutants of Escherichia Coli Blocked in the Choline-Glycine Betaine Pathway. *J. Bacteriol.* **1986**, *165* (3), 856–863. https://doi.org/10.1128/jb.165.3.856-863.1986.

(105) Ly, A.; Henderson, J.; Lu, A.; Culham, D. E.; Wood, J. M. Osmoregulatory Systems of Escherichia Coli: Identification of Betaine-Carnitine-Choline Transporter Family Member BetU and Distributions of BetU and TrkG among Pathogenic and Nonpathogenic Isolates. *J. Bacteriol.* **2004**, *186* (2), 296–306. https://doi.org/10.1128/jb.186.2.296-306.2004.

(106) Hand, S. C.; Patil, Y. N.; Li, S.; Chakraborty, N.; Borcar, A.; Menze, M. A.; Boswell, L. C.; Moore, D.; Toner, M. Diapause and Anhydrobiosis in Embryos of Artemia Franciscana : Metabolic Depression, LEA Proteins and Water Stress (Papers Presented at the Seminar, “NIAS International Seminar for Cryobiology and Cryotechnology”). *Cryobiol. Cryotechnology* **2013**, *59* (1), 41–46. https://doi.org/10.20585/cryobolcryotechnol.59.1_41.

(107) Erkut, C.; Penkov, S.; Fahmy, K.; Kurzchalia, T. V. How Worms Survive Desiccation: Trehalose pro Water. *Worm* **2012**, *1* (1), 61–65. https://doi.org/10.4161/worm.19040.

(108) Koštál, V.; Šimek, P.; Zahradníčková, H.; Cimlová, J.; Štětina, T. Conversion of the Chill Susceptible Fruit Fly Larva (Drosophila Melanogaster) to a Freeze

Tolerant Organism. *Proc. Natl. Acad. Sci. U. S. A.* **2012**, *109* (9), 3270–3274. https://doi.org/10.1073/pnas.1119986109.

(109) Neven, L. G.; Duman, J. G.; Beals, J. M.; Castellino, F. J. Overwintering Adaptations of the Stag Beetle,Ceruchus Piceus: Removal of Ice Nucleators in the Winter to Promote Supercooling. *J. Comp. Physiol. B* **1986**, *156* (5), 707–716. https://doi.org/10.1007/BF00692749.

(110) Liu, S.; Wang, W.; von Moos, E.; Jackman, J.; Mealing, G.; Monette, R.; Ben, R. N. In Vitro Studies of Antifreeze Glycoprotein (AFGP) and a C -Linked AFGP Analogue. *Biomacromolecules* **2007**, *8* (5), 1456–1462. https://doi.org/10.1021/bm061044o.

(111) Peltier, R.; Brimble, M. A.; Wojnar, J. M.; Williams, D. E.; Evans, C. W.; DeVries, A. L. Synthesis and Antifreeze Activity of Fish Antifreeze Glycoproteins and Their Analogues. *Chem. Sci.* **2010**, *1* (5), 538. https://doi.org/10.1039/c0sc00194e.

(112) Deller, R. C.; Vatish, M.; Mitchell, D. A.; Gibson, M. I. Synthetic Polymers Enable Non-Vitreous Cellular Cryopreservation by Reducing Ice Crystal Growth during Thawing. *Nat. Commun.* **2014**, *5*, 1–7. https://doi.org/10.1038/ncomms4244.

(113) Leclère, M.; Kwok, B. K.; Wu, L. K.; Allan, D. S.; Ben, R. N. C-Linked Antifreeze Glycoprotein (C-AFGP) Analogues as Novel Cryoprotectants. *Bioconjug. Chem.* **2011**, *22* (9), 1804–1810. https://doi.org/10.1021/bc2001837.

(114) Tam, R. Y.; Ferreira, S. S.; Czechura, P.; Chaytor, J. L.; Ben, R. N. Hydration Index--a Better Parameter for Explaining Small Molecule Hydration in Inhibition of Ice Recrystallization. *J. Am. Chem. Soc.* **2008**, *130* (51), 17494–17501. https://doi.org/10.1021/ja806284x.

(115) Sputtek, A.; Kühnl, P.; Rowe, A. W. Cryopreservation of Erythrocytes, Thrombocytes, and Lymphocytes. *Transfus. Med. Hemotherapy* **2007**, *34* (4), 262–267. https://doi.org/10.1159/000104136.

(116) Giard, D. J.; Aaronson, S. A.; Todaro, G. J.; Arnstein, P.; Kersey, J. H.; Dosik, H.; Parks, W. P. In Vitro Cultivation of Human Tumors: Establishment of Cell Lines Derived From a Series of Solid Tumors2. *JNCI J. Natl. Cancer Inst.* **1973**, *51* (5), 1417–1423. https://doi.org/10.1093/jnci/51.5.1417.

(117) Lieber, M.; Todaro, G.; Smith, B.; Szakal, A.; Nelson-Rees, W. A Continuous Tumor-cell Line from a Human Lung Carcinoma with Properties of Type II Alveolar Epithelial Cells. *Int. J. Cancer* **1976**, *17* (1), 62–70. https://doi.org/10.1002/ijc.2910170110.

(118) Korrodi-Gregório, L.; Soto-Cerrato, V.; Vitorino, R.; Fardilha, M.; Pérez-Tomás, R. From Proteomic Analysis to Potential Therapeutic Targets: Functional Profile of Two Lung Cancer Cell Lines, A549 and SW900, Widely Studied in Pre-Clinical Research. *PLoS One* **2016**, *11* (11), e0165973. https://doi.org/10.1371/journal.pone.0165973.

(119) Deller, R. C.; Pessin, J. E.; Vatish, M.; Mitchell, D. A.; Gibson, M. I. Enhanced Non-Vitreous Cryopreservation of Immortalized and Primary Cells by Ice-Growth Inhibiting Polymers. *Biomater. Sci.* **2016**, *4* (7), 1079–1084. https://doi.org/10.1039/c6bm00129g.

(120) Kodama, H.; Amagai, Y.; Sudo, H.; Kasai, S.; Yamamoto, S. Establishment of a Clonal Osteogenic Cell Line from Newborn Mouse Calvaria. *Japanese J. Oral Biol.* **1981**, *23*, 899–901. https://doi.org/10.2330/joralbiosci1965.23.899.

(121) Sudo, H.; Kodama, H. A.; Amagai, Y.; Yamamoto, S.; Kasai, S. In Vitro Differentiation and Calcification in a New Clonal Osteogenic Cell Line Derived from Newborn Mouse Calvaria. *J. Cell Biol.* **1983**, *96* (1), 191–198. https://doi.org/10.1083/jcb.96.1.191.

(122) Sims, N. A.; Martin, T. J. *The Osteoblast Lineage*; Elsevier Inc., 2020; Vol. 23. https://doi.org/10.1016/b978-0-12-814841-9.00004-x.

(123) Cheung, W. M. W.; Ng, W. W.; Kung, A. W. C. Dimethyl Sulfoxide as an Inducer of Differentiation in Preosteoblast MC3T3-E1 Cells. *FEBS Lett.* **2006**, *580* (1), 121–126. https://doi.org/10.1016/j.febslet.2005.11.062.

(124) Augusti-Tocco, G.; Sato, G. Establishment of Functional Clonal Lines of Neurons from Mouse Neuroblastoma. *Proc. Natl. Acad. Sci. U. S. A.* **1969**, *64* (1), 311–315. https://doi.org/10.1073/pnas.64.1.311.

(125) Schubert, D.; Humphreys, S.; Baroni, C.; Cohn, M. In Vitro Differentiation of a Mouse Neuroblastoma. *Proc. Natl. Acad. Sci. U. S. A.* **1969**, *64* (1), 316–323.

https://doi.org/10.1073/pnas.64.1.316.

(126) Tremblay, R. G.; Sikorska, M.; Sandhu, J. K.; Lanthier, P.; Ribecco-Lutkiewicz, M.; Bani-Yaghoub, M. Differentiation of Mouse Neuro 2A Cells into Dopamine Neurons. *J. Neurosci. Methods* **2010**, *186* (1), 60–67. https://doi.org/10.1016/j.jneumeth.2009.11.004.

(127) Bailey, T. L.; Wang, M.; Solocinski, J.; Nathan, B. P.; Chakraborty, N.; Menze, M. A. Protective Effects of Osmolytes in Cryopreserving Adherent Neuroblastoma (Neuro-2a) Cells. *Cryobiology* **2015**, *71* (3), 472–480. https://doi.org/10.1016/j.cryobiol.2015.08.015.

(128) Mazur, P. The Role of Intracellular Freezing in the Death of Cells Cooled at Supraoptimal Rates. *Cryobiology* **1977**, *14* (3), 251–272. https://doi.org/10.1016/0011-2240(77)90175-4.

(129) Wolkers, W. F.; Oldenhof, H.; Tang, F.; Han, J.; Bigalk, J.; Sieme, H. Factors Affecting the Membrane Permeability Barrier Function of Cells during Preservation Technologies. *Langmuir* **2018**, acs.langmuir.8b02852. https://doi.org/10.1021/acs.langmuir.8b02852.

CHAPTER 2

2. BIOPHYSICAL EFFECTS OF MACROMOLECULAR AND SMALL MOLECULAR CRYOPROTECTANTS

2.1 DECLARATIONS

All polyampholyte polymers were synthesised and functionally analysed by Dr Christopher Stubbs and all polyproline polymers were synthesised and characterised by Dr Ben Graham, both under the supervision of Prof Matthew Gibson.

2.2 CHAPTER SUMMARY

Ice recrystallisation upon thawing is a major contributor to cell death, which is not controlled by traditional cryoprotective agents. We evaluated the ice recrystallisation inhibition capabilities of several compounds in two different solvents. We additionally assessed the enthalpy of crystallisation and melting temperature of our compounds. We observed that poly(vinyl alcohol) retained its inhibition properties regardless of solvent or the presence of compatible osmolytes and our polymers of polyproline and polyampholyte had weak inhibition capabilities. We further observed no significant non-colligative deviations for the enthalpy of crystallisation or melting temperature for our solutions.

2.3 INTRODUCTION

2.3.1 Synthetic Polymers

Antifreeze (glyco)proteins (AF(G)Ps) are potent ice recrystallisation inhibitors (IRIs), but are typically unsuitable for cryopreservation applications due to their potential toxicity/immunogenicity and their secondary effect of dynamic ice shaping (DIS), which leads to 'needle like' ice crystals that pierce cell membranes.[1] Due to this, chemical synthesis of biologically and chemically stable AF(G)P analogues (as they are structurally simpler than exact AF(G)P structures) is a growing research field. This approach started with Eniade *et al*. discovering a short glycopeptide with moderate IRI activity but little to no thermal hysteresis (TH) activity,[2] which is necessary for DIS, therefore showing that these properties could be decoupled in an advantageous way.[1,3] Since then, synthetic polymers with potent IRI have emerged as a new paradigm for controlling ice growth.[4] In this work, we started by investigating the IRI properties of several chemically distinct polymers which have been suggested as potential CPAs to determine what level of IRI activity they possess, if any.

2.3.1.1 Poly(vinyl alcohol)

The most studied IRI active synthetic polymer is poly(vinyl alcohol) (PVA), (Fig 2.1). PVA is a simple, scalable and biocompatible polymer which has potent IRI activity, shown by the ability to inhibit ice growth at less than 1 mg·mL^{-1}, and has low TH activity.[5–7]

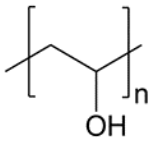

Figure 2.1. Structure of PVA.

It was first suggested that the presentation of hydrophobic domains, without the onset of self-assembly, contributed to PVA's high IRI activity,[8] however, more recently it has been ascribed to the ability to hydrogen bond with the planes of ice.[9,10] Chain length has also been shown to be important, with a longer chain length corresponding to stronger IRI activity, though the stronger IRI activity is offset by a reduction in solubility, thereby lowering the final usable concentration. The IRI activity of PVA has also been shown to be strongly concentration dependent (Fig 2.2).[11] Simulations show that PVA binds to the prismatic plane of ice *via* direct hydrogen bonding with two out of every three hydroxyl groups hydrogen bonded to the ice parallel to the *c*-axis.[9]

PVA is an attractive cell additive, as it is known to have minimal toxicity and is already approved by the Food and Drug Administration (FDA) for use in dietary applications and eyedrops.[12] PVA has been shown to moderately enhance the cryopreservation of cells in suspension,[13-15] but has not been previously used for monolayer cell freezing, making this polymer an ideal selection for monolayer cryopreservation enhancement.

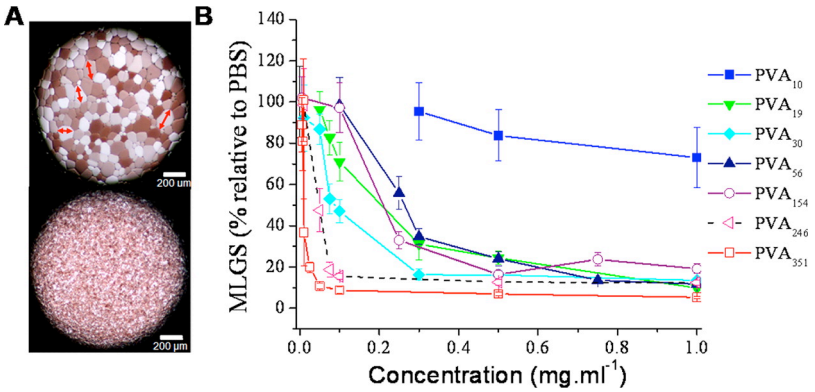

Figure 2.2. Ice recrystallization inhibition activity of PVA homopolymers as measured by the splat assay. A) Example micrographs showing ice crystals grown in PBS alone (upper) and with PVA_{351}, 1 mg·mL^{-1}). **B)** IRI activity as a function of polymer concentration. MLGS = mean largest grain size relative to a PBS control, expressed as %. Error bars represent the standard deviation from at least three measurements. Reprinted with permission from (Congdon, 2013).[11] Copyright (2013) American Chemical Society.

2.3.1.2 Polyproline

There are currently no crystal structures for antifreeze glycoproteins (AFGP)s but nuclear magnetic resonance (NMR) and ultra-ultraviolet circular dichroism (CD) suggest a polyproline II type helix.[16] Synthetic peptides with a polyproline II helical topology and proline oligomers have been shown to have IRI activity.[17,18] Polyproline (Fig 2.3) is unique as it has a tertiary amide and cannot form intramolecular hydrogen bonds which makes it water soluble despite being hydrophobic, similar to antifreeze protein (AFP) I, which is comprised of 70% alanine (a hydrophobic amino acid).[19] Polyproline has also been confirmed to have a PPII helix via circular dichroism spectroscopy (CD).[20] $PPRO_{11}$ (1250 $g \cdot mol^{-1}$, $Đ$ = 1.03) is used throughout this work.

Due to its amphiphilicity and tertiary structure, we believe that polyproline may be a minimal AF(G)P mimic, making it an ideal candidate for investigation as a monolayer cell cryoprotectant as AF(G)Ps have been shown to be detrimental to cells and this mimic has the potential to protect without the damaging side effects of the native proteins.

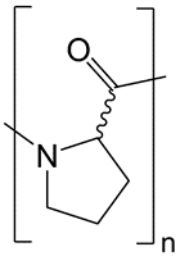

Figure 2.3. Structure of polyproline.

2.3.1.2.1 Characterisation of polyproline[21] – *Performed and written solely by Dr Ben Graham and included here for completeness*

Following dialysis, polymers were characterised by SEC (size exclusion chromatography), Table 2.1. The polymers were less disperse than expected due

to fractionation during dialysis. Table 1 also contains polymers from previous work, which are included for later critical IRI activity analysis (*vide infra*). CD confirmed that $PPro_{15}$ adopted a PPII helix (Figure 2.4)[22] with characteristic signals present at 207 and 228 nm, whilst a random coli would exhibit slight peak shifting, with signals absent in the 220 nm region.[23] $P(D)Pro_{15}$ gave the mirror spectrum whilst the D/L racemic mixture showed no secondary structure.

Table 2.1. Polyproline SEC (size exclusion chromatography). [a] Determined by SEC; [b] Value from supplier; [c] Mass Spectrometry; [d] Single species; [e] From literature.[80,81,82] ***Performed and analysed solely by Dr Ben Graham.***

	M_n, (g.mol^{-1})	$Đ$, SEC [a] (-)	DP (-)	Secondary Structure
$PPro_{11}$	1300 [a]	1.03	11	
$PPro_{15}$	1700 [a]	2.12	15	PPII
$PPro_{19}$	2100 [a]	1.50	19	
$P(D)Pro_{15}$	1700 [a]	1.01	15	Enantiomeric PPII
$P(DL)Pro_{21}$	2400 [a]	1.01	21	Random coil
$PPro_{10\text{-}100}$	1 – 10k [b]	-	10-100	PPII [e]
$PPro_{10}$	900 [c]	[d]	10	PPII [e]
$PPro_{10\text{-}25}$	1 – 3k	1.01 – 1.03	10 - 25	PPII [e]
$PPro_{20}$	2000 [c]	[d]	20	PPII [e]

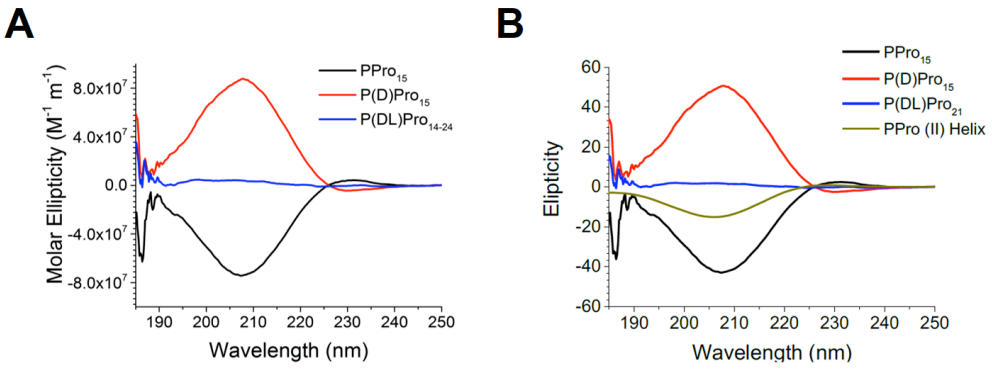

Figure 2.4. Polyproline circular dichroism spectra. A) Spectra of synthesised polyproline polymers. **B)** Spectra of synthesised proline polypeptides compared to a polyproline II helical reference (PPro (II) Helix)[2] not corrected for concentration to enable comparison against reference standard. ***Performed and analysed solely by Dr Ben Graham.***

2.3.1.3 Polyampholyte

Synthetic poly(ampholyte)s bearing mixed positive and negative charges have been evaluated in cryopreservation. Carboxylated poly(lysine) (PLL) has shown good recovery in the slow freezing of suspended cells in vials 6h after thawing and the degree of carboxylation was shown to have an impact on both cell recovery and IRI, with COOH fractions between 50 and 75% giving the best cell recovery and IRI.[24] PLL has also been used for the vitrification of cell suspensions and monolayers, but 6.5 M ethylene glycol is needed to provide good recovery, which was shown to be toxic in less than three minutes and equilibrium solutions are needed to prepare the cells for the addition of PLL.[25,26] The mechanism of PLL's protection is thought to be either through membrane interaction, reduction of cytotoxicity or devitrification, or the prevention of overexpansion osmotic injury, and not IRI, due to its weak activity.[24–26]

Our polyampholyte of interest (Fig 2.5) utilised a poly(methyl vinyl ether-*alt*-maleic anhydride) precursor since this precursor is produced on a multi-ton scale, is safe as both a food additive and a bioadhesive,[27] and the use of an anhydride precursor guarantees a 1:1 ratio of cationic/anionic groups. As the distribution of carboxylation has been shown to be important and ampholytes have been demonstrated to provide cryoprotection, we believe our finely tuned polymer will provide interesting insights into the cryoprotection of monolayered cells.

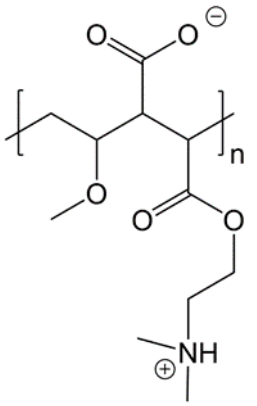

Figure 2.5. Structure of polyampholyte.

2.3.1.3.1 Characterisation of Polyampholyte[28] – *Performed and written solely by Dr Christopher Stubbs and included here for completeness*

The initial precursor polymer of gantrez was not characterised as it is an industrial polymer with relatively poor quality control for molecular weight and dispersity, therefore, the exact characterisation becomes difficult. Dimethyl aminoethanol functionalised polyampholyte was characterised by ^{1}H NMR and infrared spectroscopy (IR) (Figure 2.6).

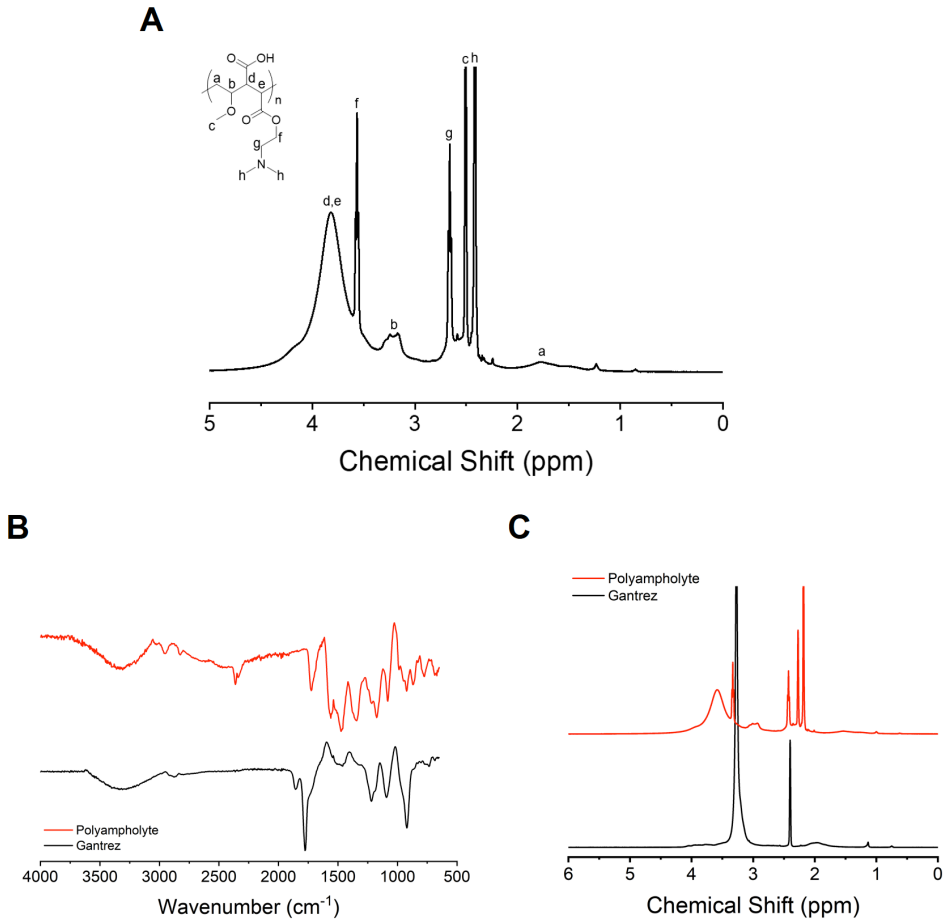

Figure 2.6. Characterisation of polyampholyte. A) Annotated ^{1}H NMR of dimethyl aminoethanol functionalised polyampholyte. **B)** Infrared spectra of the poly(methyl vinyl ether-*alt*-maleic anhydride) precursor (black) and the aminoethanol functionalised polyampholyte (red), the anhydride peak at ca. 1750 cm^{-1} is removed, and the new carboxylate and ester stretches produced. **C)** ^{1}H NMR spectra of the poly(methyl vinyl ether-*alt*-maleic anhydride) precursor (black) and the aminoethanol functionalised polyampholyte (red). ***Performed and analysed solely by Dr Christopher Stubbs.***

2.3.2 Osmotic Preconditioning

Cells in freeze-tolerant organisms experience dehydration in highly organised tissues and cells almost universally respond to the stress of long-term hyperosmolality (such as those seen during freezing) by accumulating compatible organic osmolytes.[29] Therefore, we hypothesised that the osmolytes of alanine, betaine, and proline (Fig 2.7) might be useful in the cryopreservation of cell monolayers.

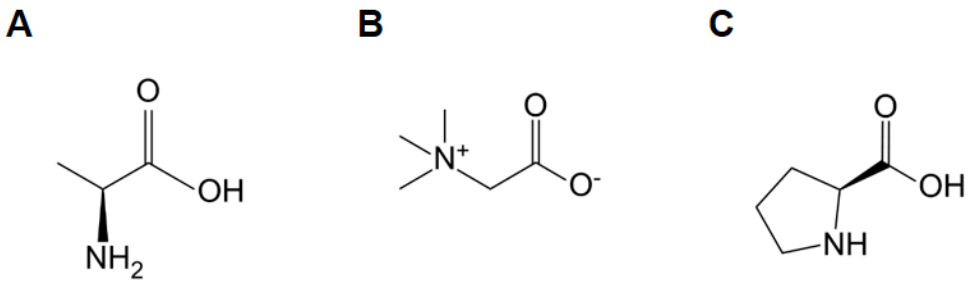

Figure 2.7. Structure of osmolytes. A) Structure of L-alanine. **B)** Structure of betaine. **C)** Structure of L-proline.

2.3.2.1 Alanine

Alanine is a simple nonpolar aliphatic amino acid that is zwitterionic under biological conditions. Alanine is the second most prevalent amino acid occurring in proteins and is therefore used heavily for protein synthesis. Even though alanine is a zwitterion, it has not been used extensively in cryopreservation. Alanine was shown to have a detrimental effect on ram semen during cryopreservation[30] and only marginally increased the post-thaw motility of striped bass (*Morone saxatilis*) spermatozoa.[31]

Alanine is an interesting supplement for cryopreservation investigation due to the alanine-heavy regions of many AF(G)Ps[32] and will allow us to investigate if the presence of alanine is a contributing protective factor for native proteins.

2.3.2.2 Betaine

Glycine betaine (referred to in this text as simply “betaine”) is an amino acid derivative that was originally discovered in beets that required osmolytes in order to survive in the salty soils of coastal areas. Betaine is an *N*-trimethylated amino acid, and the quaternary ammonium exists as a zwitterion at neutral pH. Betaine’s osmoprotection is thought to be attributed to the osmoregulated betaine/GABA transporter (BGT1) which couples the transport of betaine to Cl^- and Na^+ across the cell membrane.[33] These ion gradients strengthen the transport of betaine, providing a driving force that can raise betaine from

micromolar levels to millimolar levels within the plasma of the cells. Hypertonicity has also been shown to increase the transcription of the BGT1 gene, followed by a rise in its mRNA and transport activity.[34] Thus, tonicity controls betaine transporter activity by affecting BGT1 transcription. BGT1 is regulated not only by transcription, but also by insertion into the plasma membrane.[35] The small amount of BGT1 that exists under normal conditions is mainly located in the cytoplasm and following hypertonicity, BGT1 is seen mainly within membranes. This transport is upregulated without change in the total abundance of BGT1, only its location.[36] In addition to its osmoprotectant role, betaine has also been implicated to have a role in cellular metabolism and DNA methylation.[37] Betaine's osmoprotection is found throughout nature, as one example, when the dogfish shark *Squalus acanthias* was exposed to hypotonic conditions, there was an efflux of betaine and this efflux was shown to be responsible for the loss of osmotically obliged water during regulatory volume decrease.[38] Within the laboratory, renomedullary cells grown in hyperosmotic media contained higher concentrations of betaine than cells grown in isotonic media[39] and simian-virus-40-transformed Balb/c 3T3 (SV-3T3) cells were resistant to osmotic stress, which typically resulted in inhibition of protein synthesis and decreased proliferation, when treated exogenously with betaine.[40] Betaine has been shown to reduce leakage from frozen multilamellar liposomes,[41] and significantly enhance the vitrification of mammalian cells in suspension.[42]

Betaine, due to its osmoprotectant role, could provide the necessary preconditioning and/or protections to aid cells through the harsh event of cryopreservation, as the freezing process consists of a loss of water from the cells.

2.3.2.3 Proline

Proline is a proteinogenic amino acid that contains a side chain pyrrolidine, classifying it as a nonpolar aliphatic amino acid and it is the only proteinogenic amino acid with a secondary amine. Proline is membrane permeable regardless of pH,[43] and transfer may also occur by either a classical sodium-dependent A-type system with a wide substrate specificity or by the combination of sodium-dependent PHE (phenylalanine preferring) and IMINO (proline, alpha-methylaminoisobutyric acid preferring) systems.[44] Proline has also been implicated as a survival factor that protects the cell against apoptosis and maintains the progression of the cell cycle through a signal recognition function of the transporters that may take part in the control of cell cycle progression and programmed cell death.[45] In biological organisms, proline utilisation (PUT1)-disrupted *Saccharomyces cerevisiae,* supplemented with external proline, accumulated higher levels of proline in cells and conferred a higher tolerance to freezing and desiccation stresses.[46] Further, increased proline transport is also suggested to generate or maintain an osmoprotective transmembrane proline gradient in the bacterium *Escherichia coli*.[47] Even more striking, when a high level of proline was incorporated into the tissues of *Drosophila melanogaster*, a chill susceptible insect, it was able to survive with 50% of its total water volume frozen.[48] Proline has been used with success to cryopreserve mouse oocytes,[49] vitrify red blood cells (RBCs) and mammalian cells,[50] and has shown moderate protection for mammalian cell monolayers.[51]

Proline, similar to betaine above, has been chosen for its potential osmoprotective role, however, proline also has implications in protection from apoptosis which could be very beneficial to cells following the harsh event of cryopreservation.

The first aim of this thesis was to examine the physical properties on ice of our potential cryoprotective agents. This will be accomplished via ice recrystallisation

assays, to determine if our compounds alter ice growth upon melting and differential scanning calorimetry of the compounds to evaluate ice crystal fractions and melting temperatures. This will allow us a first look as to how our compounds may be affording their protection, if any exists, either through interaction with and influence on the ice, allowing us to begin to classify our compounds. We wanted to specifically address if: (i) our compounds effected the recrystallisation of ice, (ii) the solvent affected the results, (iii) compatible osmolytes affected the properties of ice or (iv) compatible osmolytes affected another compound's interaction with ice, and (v) any of the compounds induced vitrification or affect melting temperature. Should we find large variances in our physical assays, we can propose a mechanism of action via ice influence or interaction.

2.4 RESULTS AND DISCUSSION

2.4.1 Ice Recrystallisation Inhibition (IRI)

Ice recrystallisation is a major problem in cell and tissue cryopreservation[1,52,53] and we will start our investigation by assaying our compounds' ability to inhibit ice recrystallisation, as this will allow us to identify a potential protective mechanism. IRI is routinely evaluated by using an assay developed by Knight *et al*., typically referred to as the "splat test", which addressed the difficulties of previous assays in inconsistent nucleation and grain growth.[54] The splat test involves a small (10 μL) droplet released from a height of ~2 m onto a pre-cooled aluminium plate sitting atop dry ice (~ -70 °C). This impact causes an instantaneous phase change that results in the formation of a single layer of ice crystals. The layer is then annealed at -8 °C for 30 min on a cryostage, which allows for ice crystal growth due to melting. The ice crystals themselves are transparent and a polariser sits between the light source and the crystal specimen causing a

change in the brightness and/or the colour of the crystals being examined. Polarisation colours result from the interference of the two components of light split by the anisotropic specimen and is a result of white light minus those colours that are interfering destructively, our resultant images appear to be in the sixth order wavelength in the pink field. The orientation and thickness of the ice will have an impact on the observed colour. Images are taken after 30 min and crystals are then counted using imageJ software. The overall size of the picture capture area is 652.22 μm x 434.81 μm (at 7.2859 pixels·μm^{-1}) for a total area of 271851.908 μm^2, therefore using the crystal counts and the known area we can calculate the average crystal size. Values are reported as true averages for the solvent (control) and experimental samples to allow for statistical analysis. Smaller ice crystals indicate IRI properties for the compound tested, while larger ice crystals reflect little to no IRI activity.

2.4.1.1 PVA IRI

We first wanted to test and compare the IRI activity of both phosphate buffered saline (PBS) and cell culture media (Ham's F-12K (Kaighn's) Medium (F-12K)), as the cell media contains proteins and additives which are typically not taken into account when translating results in PBS to a more complex solution. We saw no significant difference in the average crystal sizes between PBS and F-12K (Fig 2.8), suggesting the cell culture media (F-12K) was not affecting the assay. Following our solvent tests, we wanted to evaluate the IRI activity of PVA in both PBS and F-12K to note any differences cell media may have on the IRI ability of PVA. As expected, PVA had significantly higher IRI activity than either solvent tested, but we saw no significant difference in the ice crystal sizes of PVA when dissolved in either PBS or F-12K (Fig 2.8, n = 3, P = 0.000003). PVA is known to have potent IRI activity in the ranges of 1 - 10 mg·mL^{-1} when dissolved

in PBS[13] and our results demonstrate that PVA retains its strong IRI activity when dissolved in completed cell media (F-12K).

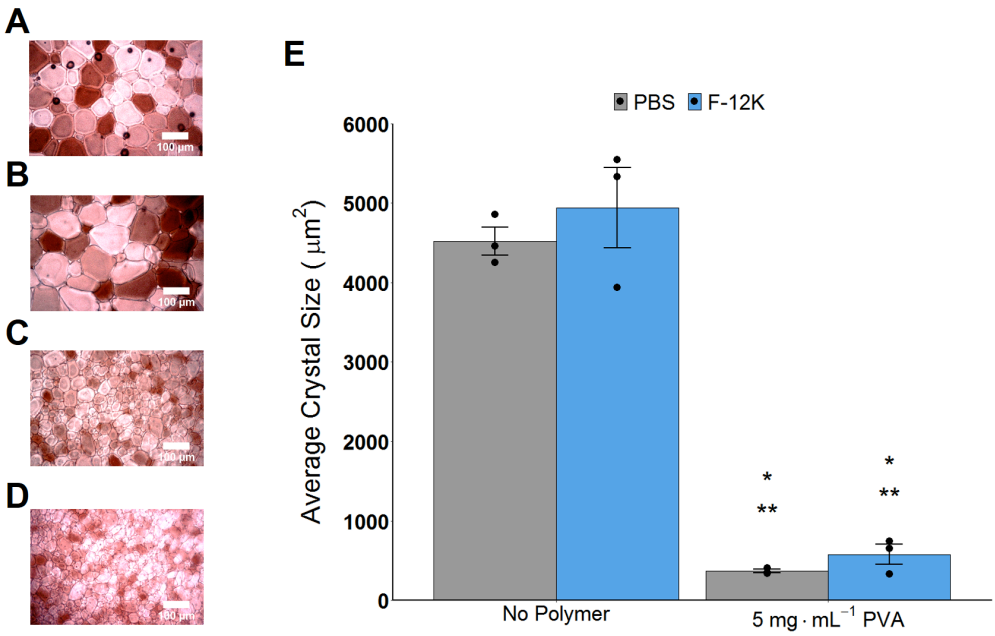

Figure 2.8. Splat of PVA solutions. **A)** Splat micrograph of PBS. **B)** Splat micrograph of F-12K. **C)** Splat micrograph of 5 mg·mL^{-1} PVA in PBS. **D)** Splat micrograph of 5 mg·mL^{-1} PVA in F-12K. Scale bar = 100 μm. **E)** Average ice crystal size of solutions calculated from splat wafers. * P < 0.001 from PBS, ** P < 0.001 from F-12K. Error bars represent ± SEM of 3 independent experiments.

2.4.1.2 Polyproline IRI

We next evaluated the IRI activity of our polyproline polymer in both PBS and F-12K. We found that 5 and 20 mg·mL^{-1} polyproline had significantly smaller crystals than PBS alone, but significantly larger crystals than 5 mg·mL^{-1} PVA (Fig 2.9, n = 3, P = 0.00000002). We additionally saw that 20 mg·mL^{-1} polyproline in F-12K was statistically similar to 5 mg·mL^{-1} PVA in F-12K (Fig 2.25, n = 3, P = 0.00004). While we do see a reduction in ice crystal size, due to the dissimilarity to PVA and the concentration needed to be statistically similar, for the samples in F-12K, our results show that polyproline would be considered a “weak inhibitor” of ice recrystallisation.[55] Poly(hydroxyl proline) has previously been shown to also have moderate IRI activity, which was thought to be due to the spacing of the

hydroxyl groups.[7] Whilst we haven't tested poly(hydroxyl proline), our results suggest that the moderate activity of both polyproline and poly(hydroxyl proline) is due to the polyproline II type helix,[16] rather than the hydroxyl groups, and that IRI activity may require segregated hydrophilic and hydrophobic domains.[19,56,57]

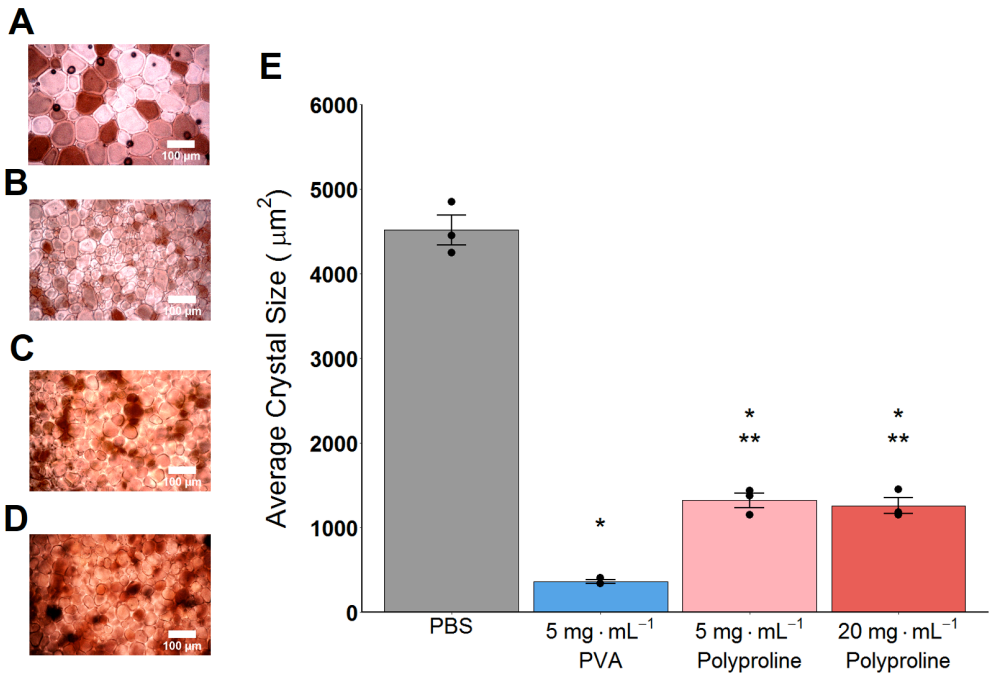

Figure 2.9. Splat of polyproline and PVA solutions in PBS. A) Splat micrograph of PBS. **B)** Splat micrograph of 5 mg·mL^{-1} PVA in PBS. **C)** Splat micrograph of 5 mg·mL^{-1} polyproline in PBS. **D)** Splat micrograph of 20 mg·mL^{-1} polyproline in PBS. Scale bar = 100 µm. **E)** Average ice crystal size of solutions calculated from splat wafers. * P < 0.001 from PBS, ** P < 0.001 from 5 mg·mL^{-1} PVA in PBS. Error bars represent ± SEM of 3 independent experiments.

2.4.1.3 Polyampholyte IRI

We next evaluated the IRI activity of our novel polyampholyte polymer (which is shown in later chapters to be a potent cryoprotectant) at an average M_n value of 80 kDa (P2). We saw that 5 and 40 mg·mL^{-1} P2 had smaller crystals than PBS, suggesting both samples were more IRI active than PBS alone. However, 5 mg·mL^{-1} P2 had significantly larger crystals than 5 mg·mL^{-1} PVA (Fig 2.10, n = 3, P = 0.00003), indicating it was far less IRI active than PVA. Similar to

polyproline in F-12K, the high concentration of 40 mg·mL^{-1} P2 in PBS was statistically similar to 5 mg·mL^{-1} PVA in PBS, however, the concentration of P2 needed to achieve IRI activity similar to PVA, while also showing larger crystals, would result in P2 being considered a "weak inhibitor" of ice recrystallisation.[55] We saw the same trends for P2 in F-12K (Fig 2.26, n = 3, P = 0.00002).

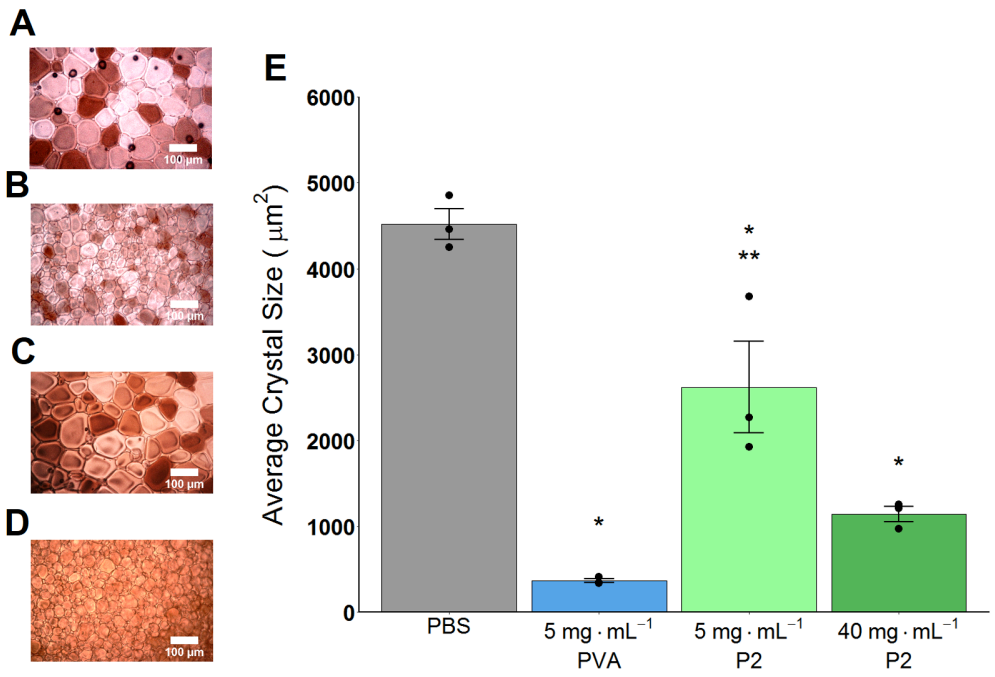

Figure 2.10. Splat of polyampholyte P2 and PVA solutions in PBS. A) Splat micrograph of PBS. **B)** Splat micrograph of 5 mg·mL^{-1} PVA in PBS. **C)** Splat micrograph of 5 mg·mL^{-1} P2 in PBS. **D)** Splat micrograph of 40 mg·mL^{-1} P2 in PBS. Scale bar = 100 µm. **E)** Average ice crystal size of solutions calculated from splat wafers. * P < 0.0001 from PBS, ** P < 0.0001 from 5 mg·mL^{-1} PVA in PBS. Error bars represent ± SEM of 3 independent experiments.

2.4.1.4 Compatible Osmolyte IRI

We next wanted to evaluate the IRI properties of alanine, betaine, and proline. Our osmolytes were tested individually in both PBS and F-12K and the individual results are shown in Figures 2.27-2.32. Osmolyte concentrations were chosen based on the best cryopreservation conditions used later (Section 4.4.1.2). Combining the results for comparison, 100 mM alanine, 100 mM betaine, and

200 mM proline had statistically significant smaller crystal sizes than PBS alone, yet all also had statistically significant larger crystal sizes than 5 mg·mL^{-1} PVA in PBS (Fig 2.11, n = 3, P = 0.0000000001), suggesting that while the osmolytes may have some IRI activity compared to PBS, the osmolytes alone would not be considered IRI active compounds, as their activity is well below that needed to even be considered "weak inhibitors" of ice recrystallisation.[55] It is emerging that IRI is very dependent not only on the IRI active compound, but also any ions that may be present, with the concentration and type of ion presenting variable results in IRI activity,[58,59] yet we did not see statistically significant effects with the addition of our osmolytes. All osmolyte solutions containing PVA had statistically significant smaller ice crystals than PBS but were not statistically significantly different from PVA alone, showing that the osmolytes neither inhibited nor enhanced PVA's IRI activity. While alanine showed the most reduction in mean grain size, it was still statistically significantly higher than the IRI active PVA. Although alanine is found predominantly in AFPs, it is believed that there is a strong hydrogen bond interaction with the threonine-hydroxyl groups of these AFPs and that the methyl groups of threonine and alanine do not bind water but instead insert into the cavity of ice.[60] Our results show that free alanine is not a potent IRI active compound. Betaine is well known for its hydrophilic property of strongly binding water molecules, *via* ionic solvation effects due to its charged groups.[61] However, it had the largest mean grain size of our three osmolytes and its IRI activity is more comparable to PBS than PVA, thus we would not consider it's mechanism to consist of ice inhibition. Proline showed statistically significantly smaller ice crystals than PBS and it has been hypothesised that water-proline hydrogen bonding is significant, and upon cooling becomes stronger, which affects the rate of crystallisation.[62] However, again, it is statistically significantly higher than PVA, and thus would not be considered an IRI active substance.

These results establish that our osmolytes have no impact on the IRI activity of PVA and contain very little of their own inherent IRI activity.

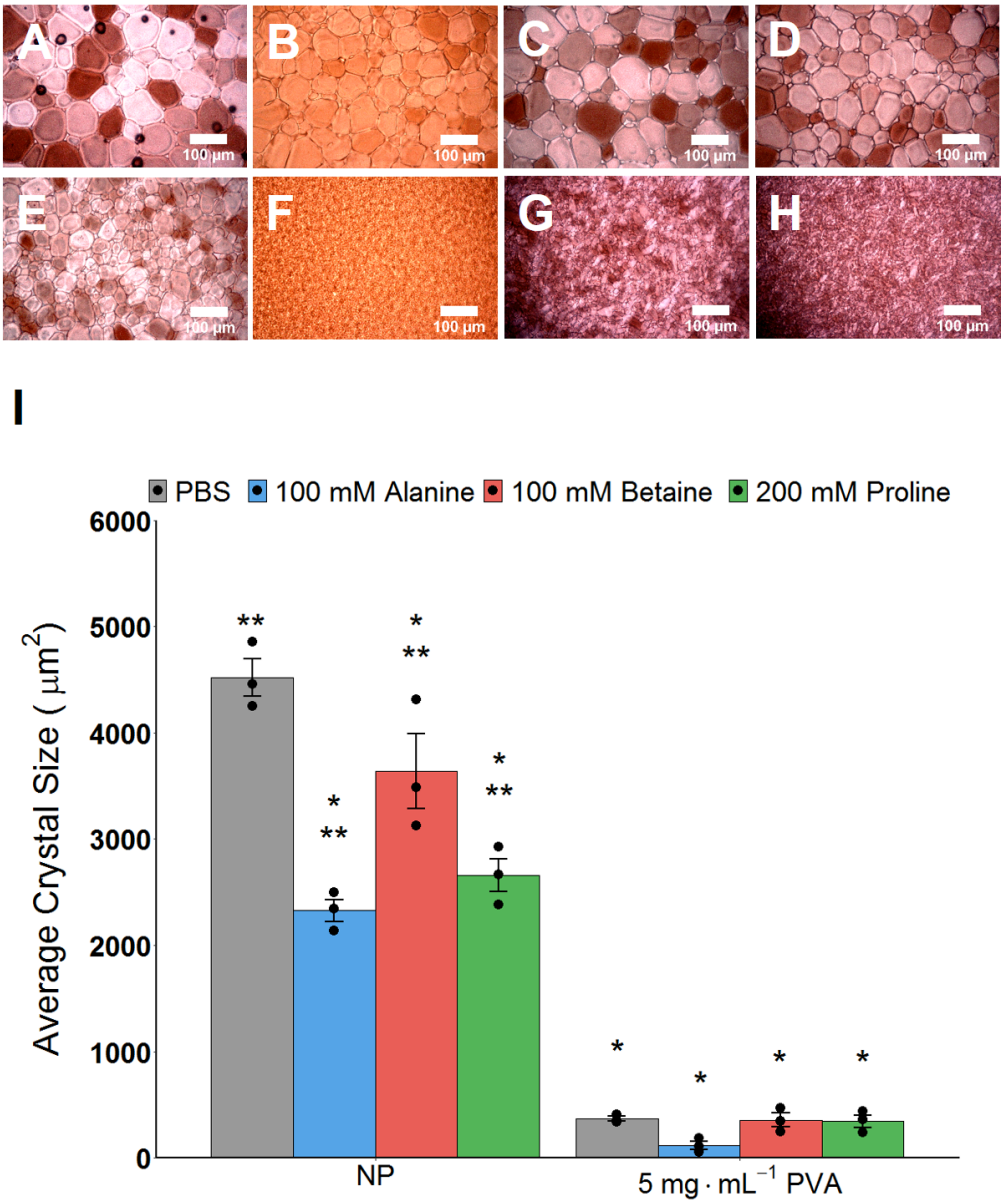

Figure 2.11. Splat of osmolyte solutions in PBS. A) Splat of PBS. **B)** Splat of 100 mM alanine in PBS. **C)** Splat of 100 mM betaine in PBS. **D)** Splat of 200 mM proline in PBS. **E)** Splat of 5 mg·mL^{-1} PVA in PBS. **F)** Splat of 100 mM alanine + 5 mg·mL^{-1} PVA in PBS. **G)** Splat of 100 mM betaine + 5 mg·mL^{-1} PVA in PBS. **H)** Splat of 200 mM proline + 5 mg·mL^{-1} PVA in PBS. Scale bar = 100 µm. **I)** Average crystal size of solutions calculated from splat ice wafers. * P < 0.0001 from PBS, ** P < 0.0001 from 5 mg·mL^{-1} PVA in PBS. Error bars represent ± SEM of 3 independent experiments. (NP = no polymer).

This section has demonstrated that PVA has high IRI activity regardless of utilising either PBS or F-12K as a solvent and hence we can be confident that IRI activity is retained under cell culture conditions. We have additionally demonstrated the moderate IRI activity of polyproline and a statistically relevant, but rather weak, IRI of polyampholyte. We have further shown that compatible osmolytes do not possess strong IRI activity but also do not hinder the IRI activity of PVA. These results allow a starting point for the classification of these macromolecular and molecular compounds.

2.4.2 Differential Scanning Calorimetry (DSC)

We next wanted to evaluate the phase transitions of our solutions during freezing, along with the melting point. We primarily sought to verify that our solutions were indeed freezing and not vitrifying (ice-free phase). We utilised differential scanning calorimetry (DSC), a thermo-analytical technique that can precisely measure the differences in energy required between a reference and sample to detect exothermic and endothermic events (presented as peaks) and therefore phase transitions. If our solutions were freezing, we would expect to see a crystallisation peak where heat is released during the formation of ice crystals. If vitrification was occurring, we would expect to see a step bump resulting in a baseline shift. Both of these curves are represented in Figure 2.12 (adapted from Schawe and Löffler[63]) from the cooling of metallic alloy, with freezing curves illustrated at ≤ 200 $K \cdot s^{-1}$ and vitrification curves illustrated at ≥ 500 $K \cdot s^{-1}$.

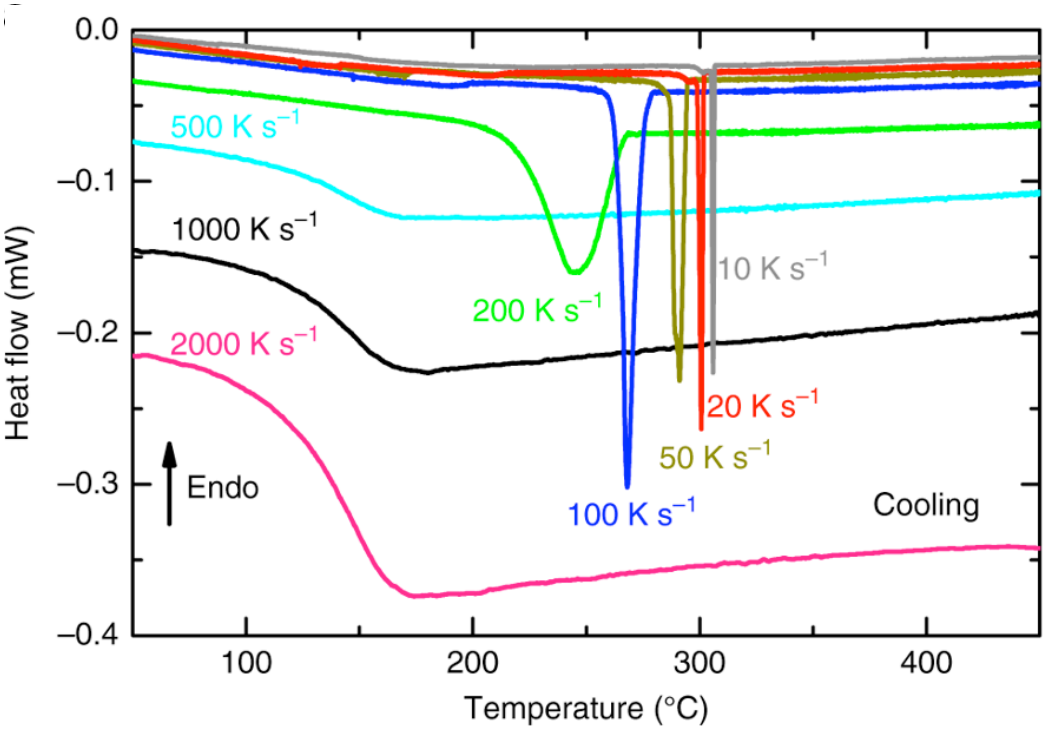

Figure 2.12. DSC phase transformations upon cooling. Adapted with permission under a Creative Commons Attribution 4.0 International License from Schawe and Löffler[63] (2019). The green, blue, gold, red, and grey lines show clear crystallisation peaks, whereas the pink, black, and cyan show no peaks and indicate vitrification.

By measuring the enthalpy of crystallisation (obtained by taking the area under the curve of each crystallisation peak in the DSC trace), we were able to evaluate any non-colligative properties of the solutions. By heating our solutions after cooling, we could also evaluate the onset of the melting point to identify changes in the solid to liquid phase transition upon heating. We also looked at peak shifts from the effects of the added solutes to our standards, for both heating and cooling, as we would expect small scale changes, since solutes are known to result in freezing point depression.[64,65]

2.4.2.1 PVA DSC

Similar to our IRI assessment, we first evaluated the phase transition and melting temperature of both PBS and F-12K, followed by 5 mg·mL^{-1} PVA and 10%

dimethyl sulfoxide (DMSO) in both PBS and F-12K, and then finally, the combination of PVA + DMSO in both PBS and F-12K to note any differences cell media may have on the assessed properties. Evaluating the DSC freezing traces for solutions in PBS (Fig 2.13A) and F-12K (Fig 2.13B) we saw subtle differences between two solutions that we analysed further by measuring the area under the curve of each of the peaks to find the average ice crystallisation enthalpy. We saw no differences in enthalpy between PBS and F-12K, or for PVA in either solvent (Fig 2.13C, n = 3, P = 0.00000004), which was anticipated as PVA has been shown not to greatly alter the ice content, even in a concentration dependent manner.[13] We saw a statistically significant difference in the ice crystallisation enthalpy of solutions containing DMSO, which was expected as the viscosity increase of DMSO is thought to decrease molecular mobility and hence crystallisation.[66] None of the solutions containing DMSO significantly differed from each other statistically, showing that neither the solvent used, nor the presence of PVA, affected the crystallisation enthalpy of DMSO.

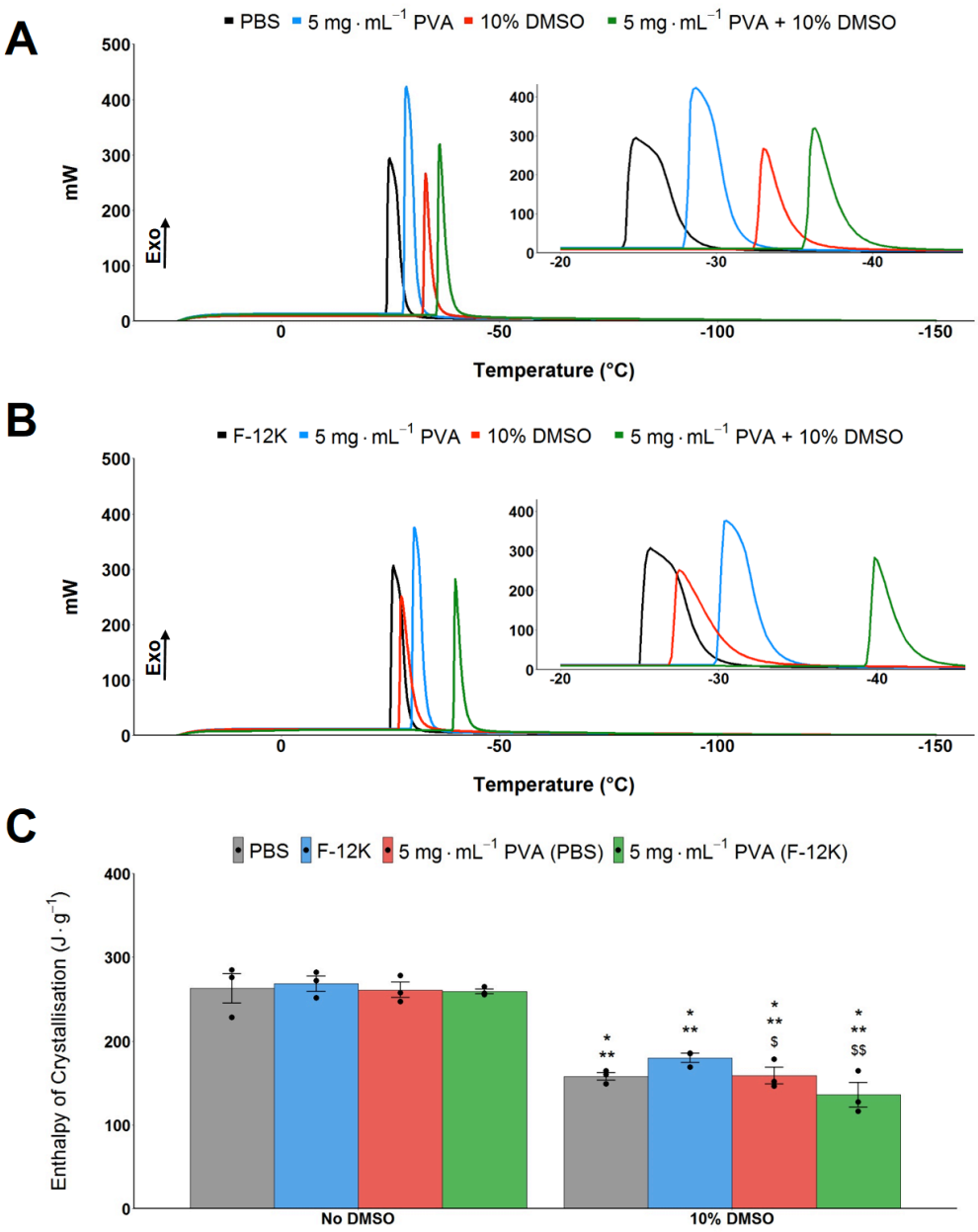

Figure 2.13. DSC cooling of PVA solutions. A) DSC trace of PBS solutions cooling to -150 °C at 10 °C·min^{-1}. **B)** DSC trace of F-12K solutions cooling to -150 °C at 10 °C·min^{-1}. **C)** Average enthalpy of ice crystallisation of solutions calculated from area under curve on DSC trace. Error bars represent ± SEM of 3 independent experiments. * P < 0.001 from PBS, ** P < 0.001 from F-12K, $ P < 0.001 from 5 mg·mL^{-1} PVA in PBS, $$ P < 0.001 from 5 mg·mL^{-1} PVA in F-12K.

Assessing the DSC melting traces for PBS (Fig 2.14A) we can see two distinctive peaks in the PBS sample and upon zooming into the -30 ˚C region we can see there are a total of four unique peaks, three small peaks (labelled antemelting (AM), incipient melting (IM), and eutectic melting (EM)) followed a large melting

peak. Slow freezing causes ice to separate and the exothermic peak AM might be the result of the unfrozen water fraction freezing upon warming,[67,68] with the IM peak relating to a grain boundary melting phase directly prior to the EM peak. The endothermic peak (labelled (EM)) is thought to be the melting of the equilibrium eutectic phase due to the crystal phase of the unfrozen water fraction[69] and previous EM values of -25 ˚C have been reported[70] which align with our reported values here. Eutectic crystallisation has been shown to occur only with supercooling during freezing but melting occurred at the thermodynamic equilibrium eutectic temperatures.[70] In the samples containing DMSO, we see no AM, IM, or EM peak, suggesting an amorphous state for the unfrozen fraction and this has been previously demonstrated as glycerol and DMSO have been shown to prevent eutectic formation.[71] In the samples with F-12K (Fig 2.14B) there was a larger AM peak with a smaller EM peak. The disappearance of eutectic formation has been observed for more complex mixtures[72] with cell media eutectic values of ~ -30 ˚C,[70] however our cell media is complete in this solution, so we have the additional impacts of the heavy protein content of the foetal bovine serum and we see that the further addition of PVA fully removes the eutectic peak from the F-12K solution, which speaks more to complexity of the solution and not the IRI activity of the polymer as AFPs have been shown not to alter premelting peaks.[73] While eutectic crystallization is thought to directly injure cells during freezing,[70] all of our solutions used as CPAs contain DMSO, which eliminate the eutectic melting peak, therefore we can disregard the influence of the eutectic melting as a mode of damage in our later cryopreservation studies.

We saw no differences in melting temperature between PBS and F-12K, or for PVA in either solvent (Fig 2.14C, n = 3, P = 0.000002). We did see a statistically significant difference in the melting temperature of solutions containing DMSO, which was expected as DMSO has been shown to decrease the melting temperature.[66,74] None of the solutions containing DMSO significantly differed

from each other statistically, showing that neither the solvent used, nor the presence of PVA, affected the melting temperature of DMSO. This mirrored our findings for crystallisation enthalpies.

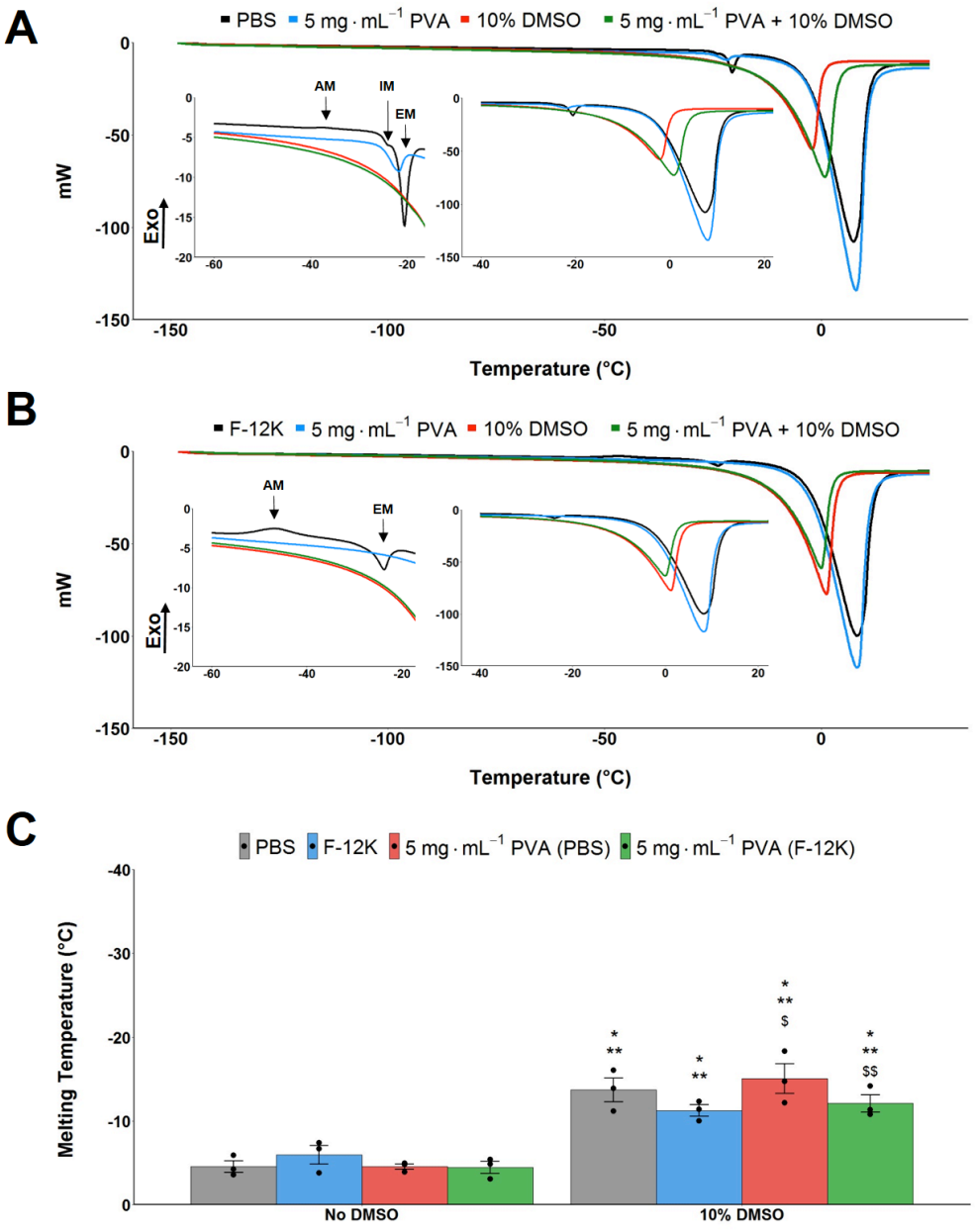

Figure 2.14. DSC heating of PVA solutions. A) DSC trace of warming PBS solutions from -150 °C to 25 °C at 10 °C·min^{-1}. **B)** DSC trace of warming F-12K solutions from -150 °C to 25 °C at 10 °C·min^{-1}. **C)** Average melting temperature calculated from onset of DSC exothermic drop. Error bars represent ± SEM of 3 independent. * P < 0.001 from PBS, ** P < 0.001 from F-12K, $ P < 0.001 from 5 mg·mL^{-1} PVA in PBS, $$ P < 0.001 from 5 mg·mL^{-1} PVA in F-12K.

These results have shown that PVA does not alter the ice crystallisation enthalpy or melting temperature compared to the standards of PBS/F-12K or 10% DMSO in either PBS or F-12K.

2.4.2.2 Polyproline Proline DSC

In evaluating the phase transition and melting temperatures of polyproline we saw that all combinations of our solutions were freezing and not vitrifying (Fig 2.15A). Looking at the enthalpy of crystallisation, there were no statistically significant differences among any of solutions, most likely due to the high variability of the polyproline solutions (Fig 2.15B, n = 3). We did observe a statistically significant lower enthalpy for 200 mM proline + 5 mg·mL^{-1} polyproline both with and without 10% DMSO in F-12K compared to F-12K alone (Fig 2.33B, n = 3, P = 0.01), we believe this is due to colligative effects due to the high concentration of proline used (explored more in Section 2.4.2.4).

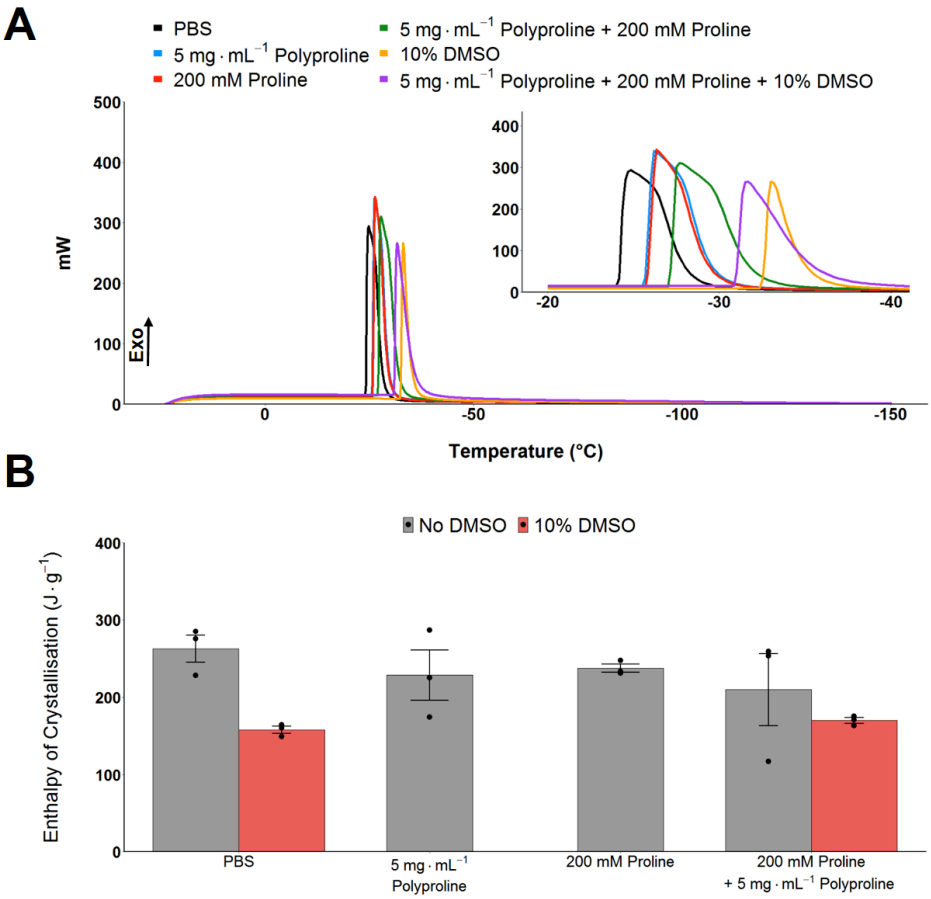

Figure 2.15. DSC cooling of polyproline solutions in PBS. A) DSC trace of polyproline solutions cooled to -150 °C at 10 °C·min^{-1}. **B)** Average enthalpy of ice crystallisation of solutions calculated from area under curve on DSC trace. Error bars represent ± SEM of 3 independent experiments.

From the heating curves, there are not large peak shifts from controls with polyproline suggesting the polymer is not affecting the ice fraction (Fig 2.16A). Antemelting and eutectic melt peaks were observed for PBS and also for polyproline. Upon the addition of proline, the peak was no longer observed, which aligns with previous research demonstrating the disappearance of the eutectic peak in the presence of proline.[69]

Obtaining the melting point from the onset of the exothermic peak, we saw no statistically significant differences in melting temperature for polyproline compared to the standards of solutions containing either PBS or 10% DMSO, with all solutions containing 10% DMSO statistically significantly different to

solutions containing only PBS (Fig 2.16B, n = 3, P = 0.00005). For solutions in F-12K, we saw a statistically significant lower melting temperature for 5 mg·mL^{-1} polyproline + 200 mM proline + 10% DMSO, again most likely due to colligative effects from the proline concentration (Fig 2.34B, n = 3, P = 0.000008).

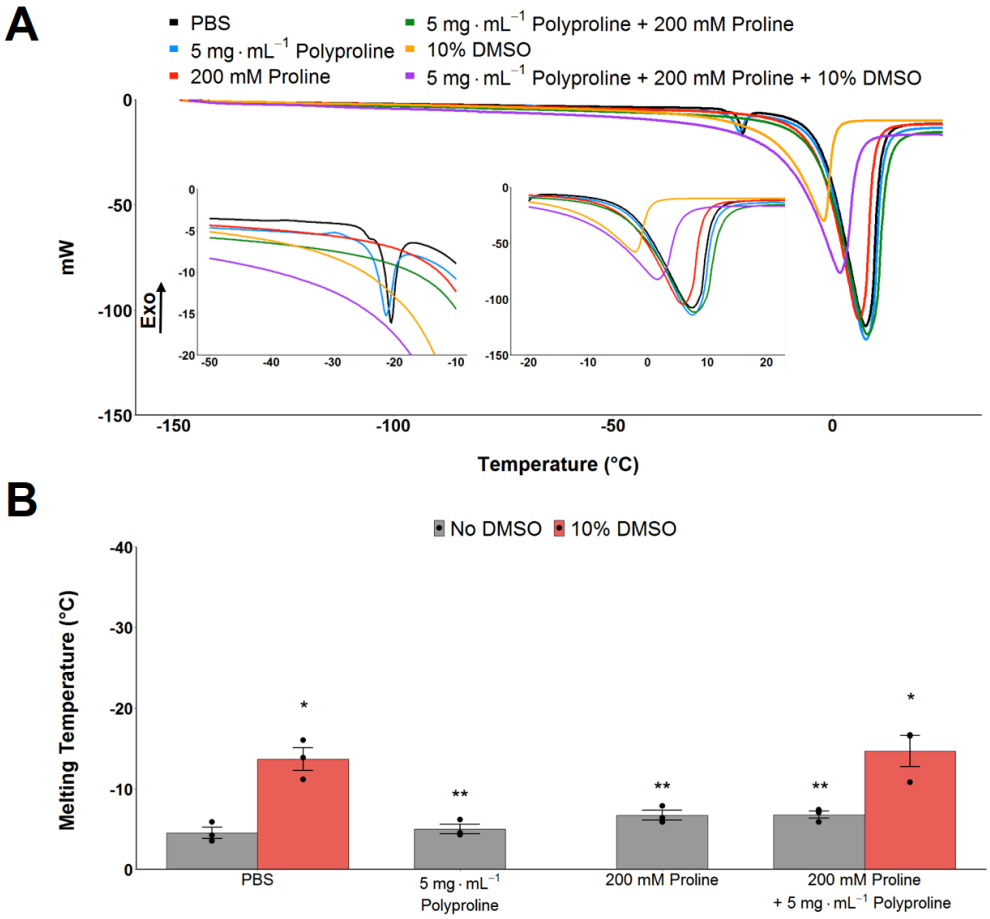

Figure 2.16. DSC heating of polyproline solutions in PBS. A) DSC trace of warming polyproline solutions from -150 °C to 25 °C at 10 °C·min^{-1}. **B)** Average melting temperature calculated from onset of DSC exothermic drop. Error bars represent ± SEM of 3 independent experiments. * P < 0.0001 from PBS, ** P < 0.0001 from 10% DMSO in PBS.

2.4.2.3 Polyampholyte DSC

In evaluating the phase transition of our polyampholyte solutions, we saw that all molecular weights of our polymer (M_n = 20 kDa (P1), 80 kDa (P2), and 311 kDa (P3)) were freezing and not vitrifying (Fig 2.17A). Looking at the enthalpy of

crystallisation, we saw only statistically significant differences from F-12K for solutions containing 10% DMSO (Fig 2.17B, *n* = 3 (5 mg·mL^{-1} P3 (No DMSO and 10% DMSO) N=2 and was not included in statistical analysis), *P* = 0.000005).

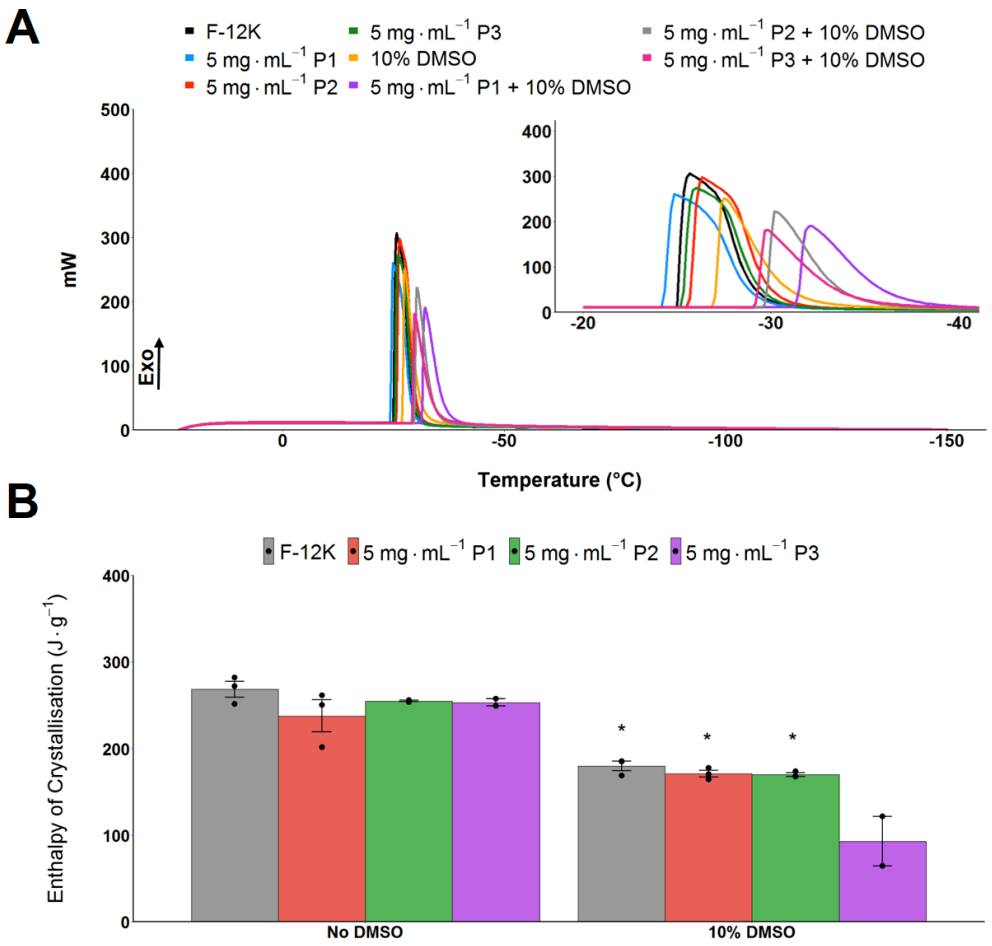

Figure 2.17. DSC cooling of polyampholyte MW solutions in F-12K. A) DSC trace of P1-P3 solutions cooled to -150 °C at 10 °C·min^{-1}. **B)** Average enthalpy of ice crystallisation of solutions calculated from area under curve on DSC trace. Error bars represent ± SEM of 3 independent experiments (5 mg·mL^{-1} P3 (No DMSO and 10% DMSO) N=2). * P < 0.0001 from F-12K.

From our heating curves, we saw that our peak shifts aligned with the presence of DMSO (Fig 2.18A) and premelting peaks only exist in the F-12K solution, most likely due to the increased complexity of complete F-12K as a base solution. Obtaining the melting point from the onset of the exothermic peak, we saw statistically significant differences in melting temperature only for solutions

containing 10% DMSO compared to F-12K (Fig 2.18B, n = 3 (5 mg·mL^{-1} P3 (No DMSO and 10% DMSO) N=2 and was not included in statistical analysis), P = 0.0000001).

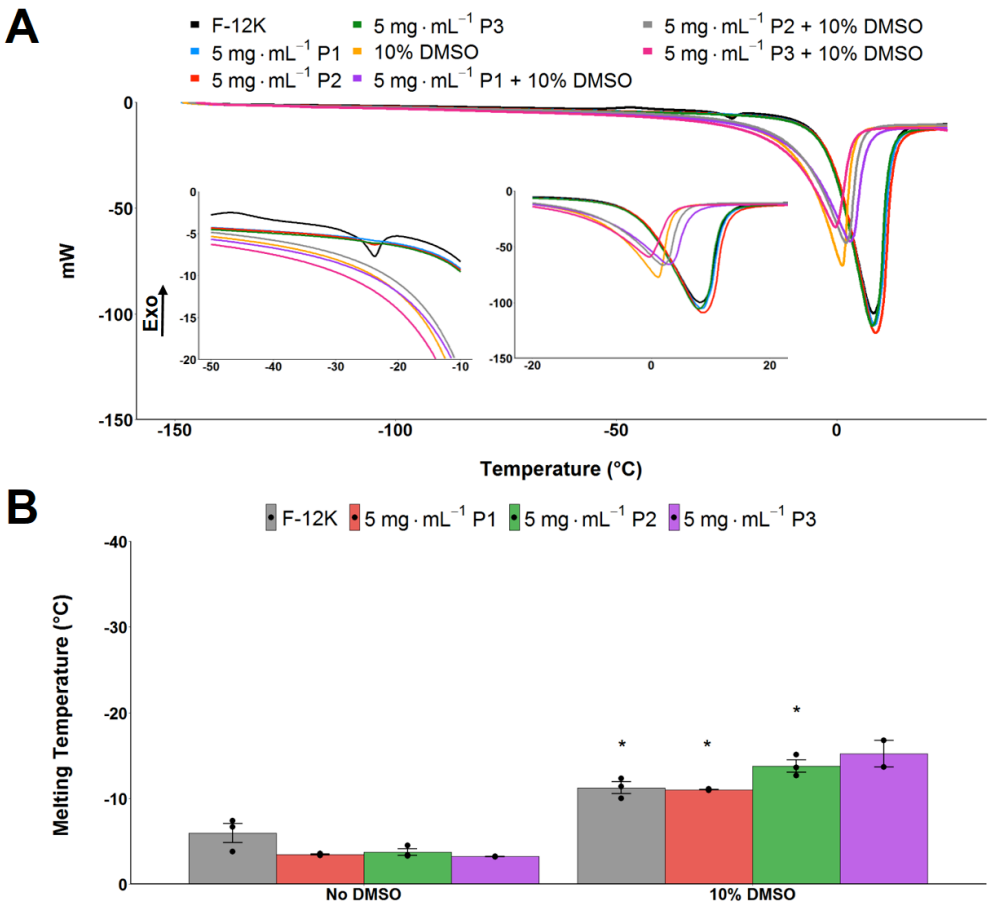

Figure 2.18. DSC heating of polyampholyte MW solutions in F-12K. A) DSC trace of warming P1-P3 solutions from -150 °C to 25 °C at 10 °C·min^{-1}. **B)** Average melting temperature calculated from onset of DSC exothermic drop. Error bars represent ± SEM of 3 independent experiments (5 mg·mL^{-1} P3 (No DMSO and 10% DMSO) N=2). * P < 0.0001 from F-12K.

A single molecular weight (P2, M_n = 80 kDa) was selected for further analysis. In evaluating the phase transition of the concentration effects of P2 we saw that all combinations of our solutions in PBS were freezing and not vitrifying (Fig 2.19A). Looking at the enthalpy of crystallisation, we saw only statistically significant differences for solutions containing DMSO (Fig 2.19B, n = 3, P = 0.000003). We

observed the same trend for these solutions in F-12K (Fig 2.35B, n = 3, P = 0.0000000004).

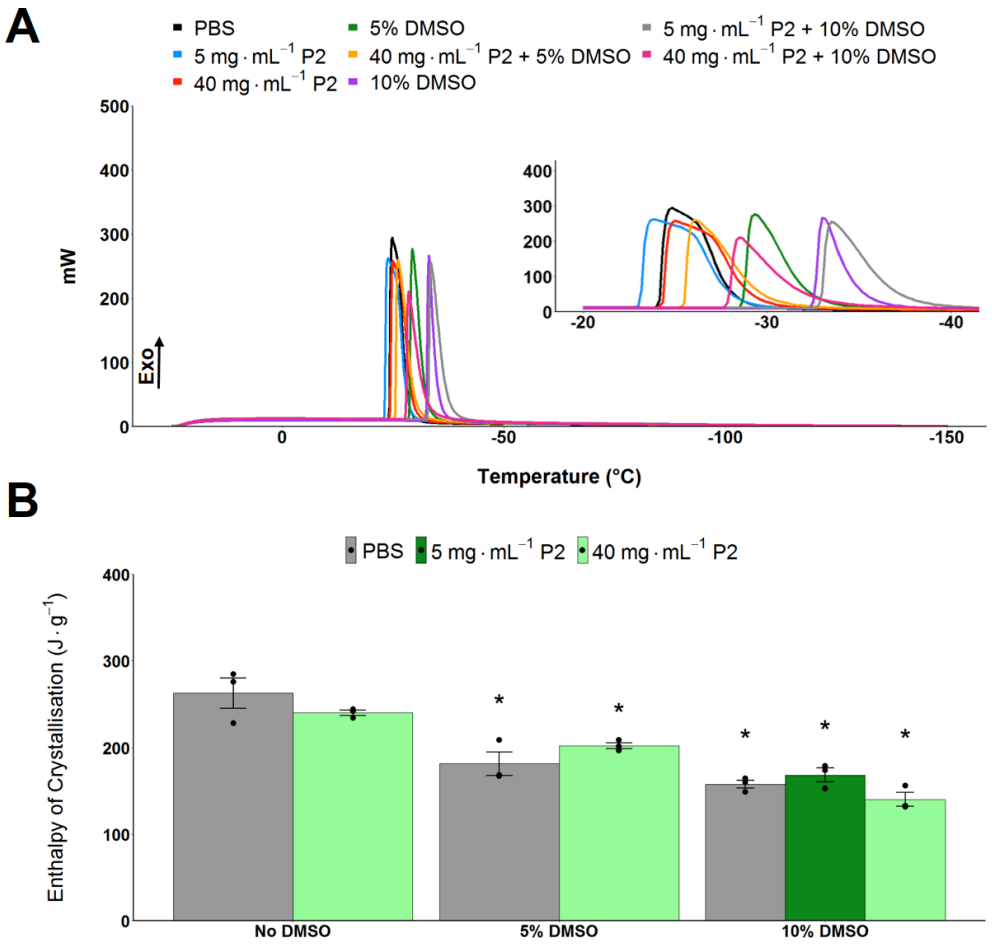

Figure 2.19. DSC cooling of polyampholyte P2 solutions in PBS. A) DSC trace of P2 solutions cooled to -150 °C at 10 °C·min^{-1}. **B)** Average enthalpy of ice crystallisation of solutions calculated from area under curve on DSC trace. Error bars represent ± SEM of 3 independent experiments. * P < 0.0001 from PBS.

From our heating curves, we saw that our small peak shifts aligned with the DMSO concentration (Fig 2.20A) and eutectic peaks exist for PBS and 5 mg·mL^{-1} P2 but disappear upon higher concentrations/more complex mixtures. Obtaining the melting point from the onset of the exothermic peak, we saw statistically significant differences in melting temperature for solutions containing 5 and 10% DMSO compared to PBS along with a statistically significant lower melting

temperature for 40 mg·mL^{-1} P2 + 10% DMSO compared to 10% DMSO, similar to the concentration effects we have seen previously (Fig 2.20B, n = 3, P = 0.00000003). For solutions in F-12K, we saw statistically significant differences only for solutions containing 10% DMSO, as well as a statistically significant lower melting temperature for 40 mg·mL^{-1} P2 + 10% DMSO compared to 10% DMSO (Fig 2.36B, n = 3, P = 0.0000001).

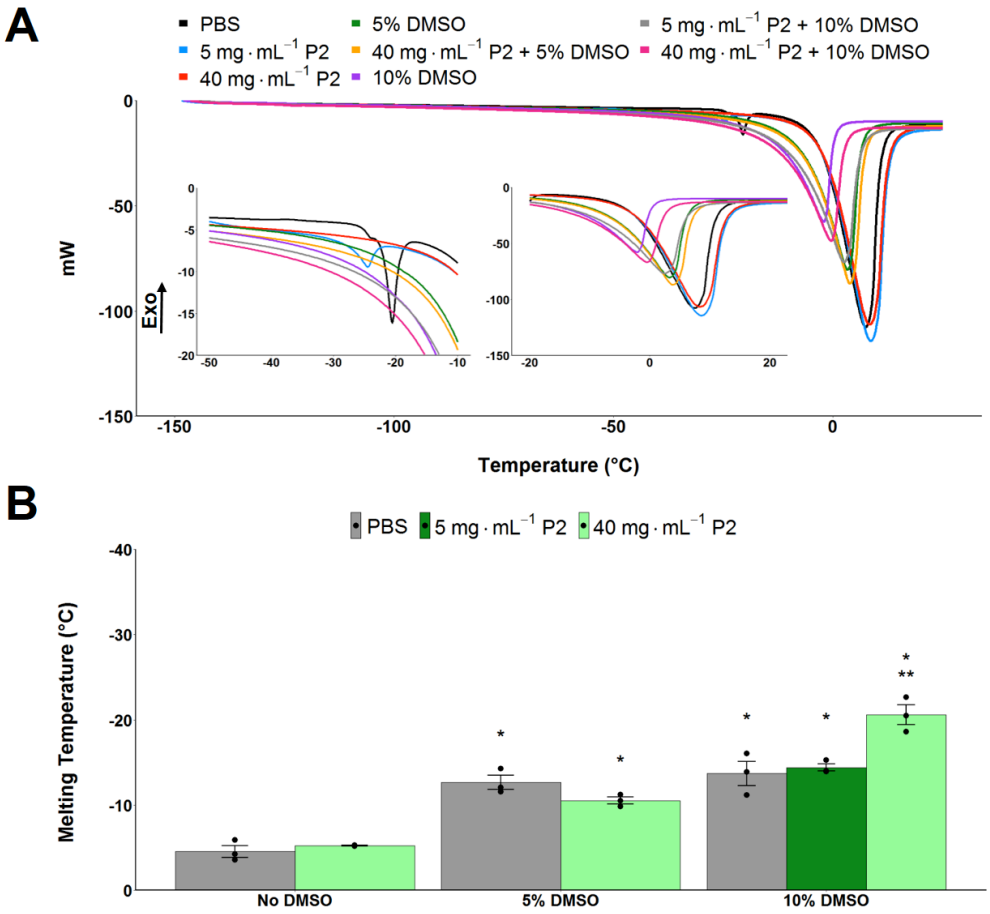

Figure 2.20. DSC heating of polyampholyte P2 solutions in PBS. A) DSC trace of warming P2 solutions from -150 °C to 25 °C at 10 °C·min^{-1}. **B)** Average melting temperature calculated from onset of DSC exothermic drop. Error bars represent ± SEM of 3 independent experiments. * P < 0.0001 from PBS, ** P < 0.0001 from 10% DMSO in PBS.

None of our macromolecular cryoprotectants significantly altered the ice crystallisation enthalpy or the melting temperature compared to standards. We

did see significant differences for high concentration solutions, owing to colligative effects rather than inherent properties of the compounds themselves. We have additionally shown that all of our macromolecular cryoprotectant solutions are freezing and not vitrifying.

2.4.2.4 Combined Osmolyte PVA DSC

Although osmolytes have not been reported to heavily influence the ice fraction, we wanted to extensively test these compounds, on their own and in combination with PVA, to ensure there were no agonistic/antagonistic interactions or alterations of phase transitions that could be attributed to any cryoprotection these small molecule osmolytes may afford. We measured the phase transition and melting temperatures of our individual osmolyte solutions in both PBS and F-12K, followed by combinations in solution of 5 $mg \cdot mL^{-1}$ PVA and 10% DMSO in both PBS and F-12K, and then finally, the combination of PVA + DMSO in both PBS and F-12K (Fig 2.37-2.48). Combining the data for comparison, we can see that with the addition of osmolytes, our solutions are freezing and not vitrifying (Fig 2.21). Looking at the enthalpy of crystallisation, there were no significant differences among our solutions which contained DMSO, showing that our osmolytes in combination with PVA did not induce vitrification (Fig 2.22, $n = 3$, $P = 0.0000004$). We did observe a lower enthalpy for both alanine and proline (+PVA+DMSO) solutions. There exists very little literature on alanine's interaction with ice and we believe that alanine may be affecting ice nucleation in some way, however, this requires further study. Proline has been shown to reduce the glass transition temperature at high concentrations,[75] however, for 100 mM proline (+PVA+DMSO) we saw no change in the ice crystallisation enthalpy or a phase change from freezing to vitrification. Similar to our results, proline-fed larvae of two *Drosophilia melanogaster* flies (resulting in cold-acclimation[76]) showed

relatively small differences in ice fraction dynamics.[77] This suggests that the lower ice crystal enthalpy for 200 mM proline (+PVA+DMSO) is due to concentration colligative effects.

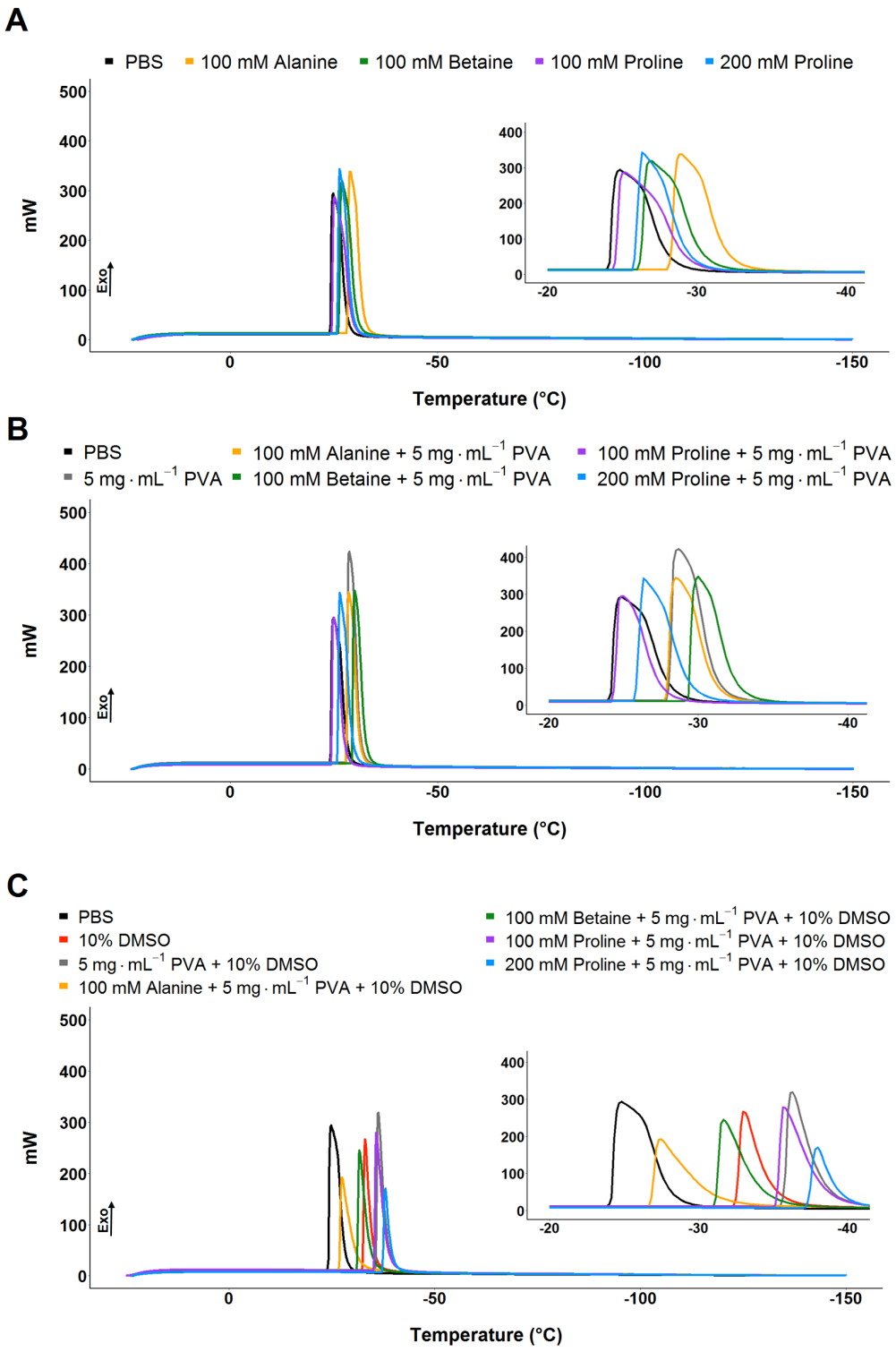

Figure 2.21. DSC cooling of osmolyte solutions to -150 °C at 10 °C·min^{-1}. A) Solutions in PBS. **B)** Solutions with 5 mg·mL^{-1} PVA in PBS. **C)** Solutions with 5 mg·mL^{-1} PVA + 10% DMSO in PBS.

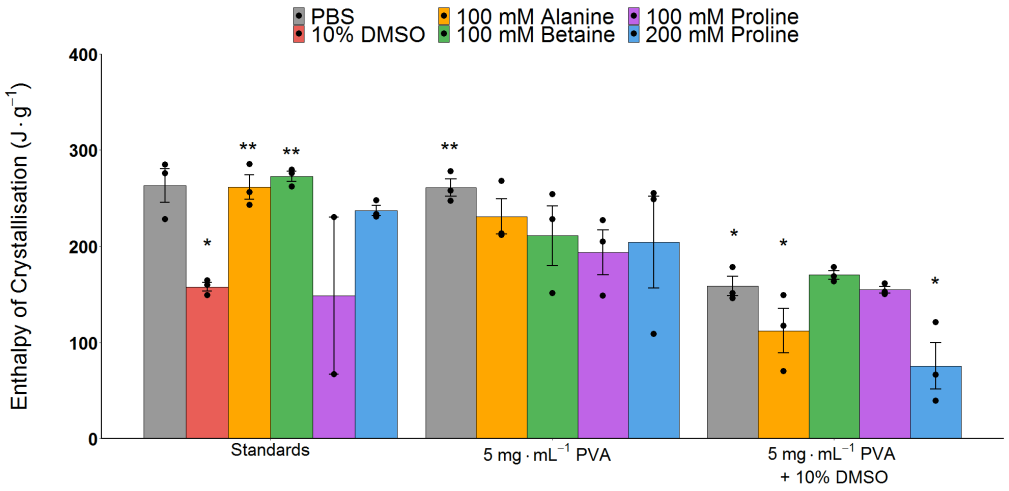

Figure 2.22. Average enthalpy of ice crystallisation for osmolyte solutions. Average enthalpy of ice crystallisation of solutions calculated from area under curve on DSC trace. Error bars represent ± SEM of 3 independent experiments (100 mM proline in PBS (standards) N=2 and was not included in statistical analyses). * P < 0.001 from PBS. ** P < 0.001 from 10% DMSO.

From our heating curves, we saw that we did not have large peak shifts with the addition of our osmolytes (Fig 2.23), suggesting there were no large freezing point depression alterations and we observed no premelting peaks for any of the osmolyte solutions. Obtaining the melting point from the onset of the exothermic peak, we saw no significant differences in melting temperature for our osmolyte solutions containing PVA+DMSO (Fig 2.24, n = 3, P = 0.0000002). Betaine has been shown to slightly increase the melting temperature[42] but we did not see any difference for the concentration tested. We did see a slightly lower melting temperature for 200 mM proline (+PVA+DMSO), however it was not observed with 100 mM proline so we believe this is also a concentration colligative effect.

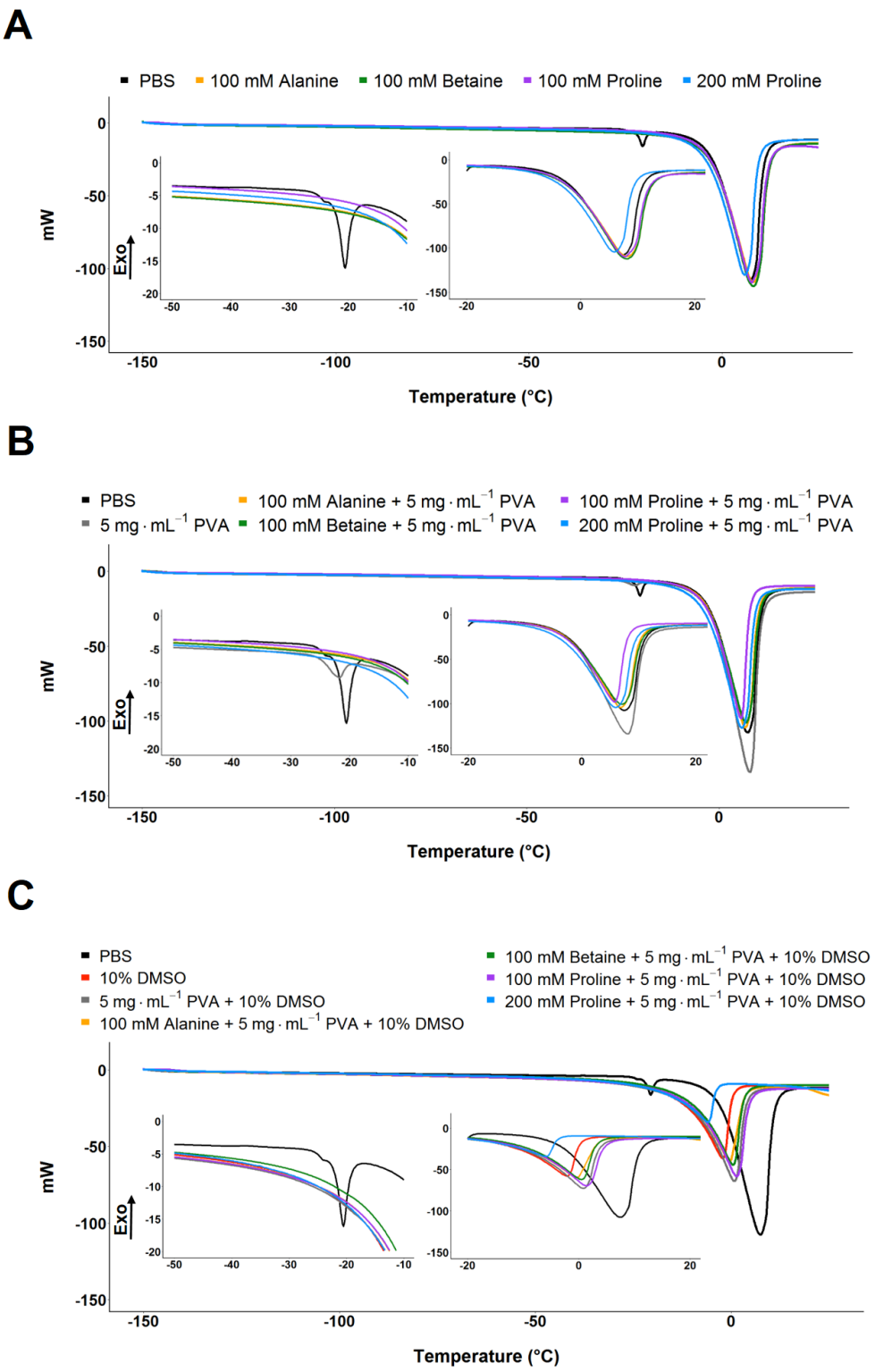

Figure 2.23. DSC heating of osmolyte solutions warmed from -150 °C to 25 °C at 10 °C·min^{-1}. A) Solutions in PBS. **B)** Solutions with 5 mg·mL^{-1} PVA in PBS. **C)** Solutions with 5 mg·mL^{-1} PVA + 10% DMSO in PBS.

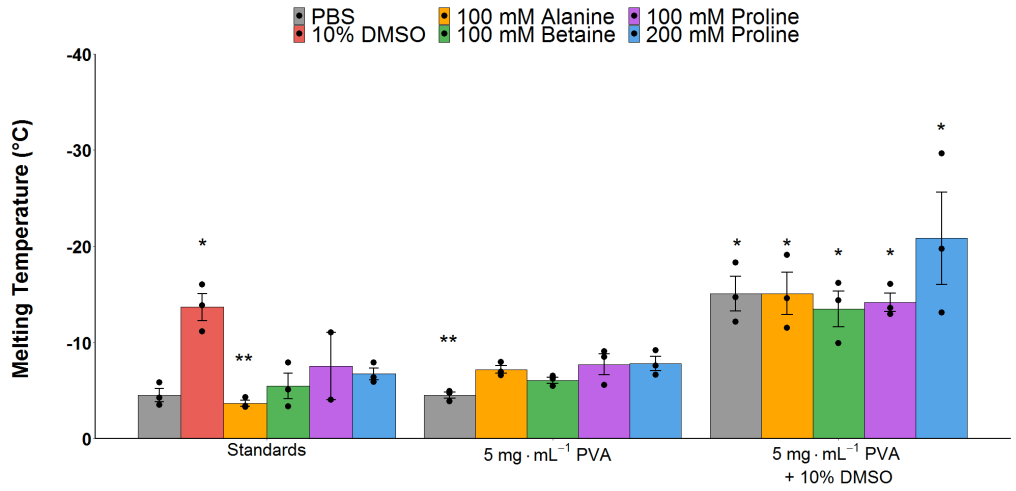

Figure 2.24. Melting temperature for osmolyte solutions. Average melting temperature of solutions calculated from onset of exothermic drop on DSC trace. Error bars represent ± SEM of 3 independent experiments (100 mM proline in PBS (standards) N=2 and was not included in statistical analyses). * P < 0.0001 from PBS. ** P< 0.0001 from 10% DMSO.

We saw no significant changes for the addition of osmolytes in our solutions and are confident that phase change alterations are not responsible for cryopreservation outcomes. Our results thus far have shown that PVA, osmolytes, or a combination of both do not alter the phase transitions of ice.

There may be aspirations to extrapolate data from our two physical assays, IRI and DSC, to explain the results of each other. However, our conditions and assays are not wholly comparable. The IRI assay is an artificial environment which allows us to observe crystallisation. Our solutions of interest are usually quenched at $CO_{2(s)}$ temperatures and this deep supercooling can give rise to the small ice crystals seen.[78] Therefore, ice grains within the DSC pans are unlikely to ever be as small as those seen in the splat assays. Additionally, the DSC cooling rates are slow cooling rates with variable temperatures and that results in a much different environment than those used for the IRI assay which are held at one single temperature. These assays independently explore the potential for ice recrystallisation inhibition along with the enthalpy of crystallisation and melting

temperatures, which allows us to answer questions as to the ice interactions and influences of these compounds.

2.5 Conclusion

In this chapter our aim was to assess the IRI activity of our macromolecular and molecular compounds along with any influence on the enthalpy of crystallisation and melting temperature. We found that PVA is a potent IRI polymer, regardless of solvent (PBS or cell media) and polyproline and polyampholyte showed weak IRI activity in comparison. The osmolytes themselves showed weak IRI activity yet did not inhibit PVA's high IRI activity. All solutions containing macromolecular cryoprotectants, osmolytes, DMSO, or a combination of, have been shown to freeze and not vitrify and the polymers and osmolytes did not affect DMSO's phase transitions. Our results have been summarised in Table 2.2. The results of this chapter have shown that PVA would be considered to have a large impact on the physical properties of the ice as a potential mechanism via ice recrystallisation inhibition, while the polymers of polyproline and polyampholyte, along with the osmolytes of alanine, betaine, and proline, have only a minimal influence on the physical properties of ice for the IRI. This is most likely due to the orientation and spacing of the hydroxyl groups of PVA, which allow it to bind to and inhibit the recrystallisation of ice upon thawing, and therefore, it would follow that the rest of our compounds do not have the necessary groups and/or a favourable orientation of those groups to influence ice recrystallisation in the same manner as PVA. An interesting next step would be to assay the phase transitions of the solutions via DSC in the presence of cells attached as a monolayer as we don't know how the presence of cells influences the phase transitions of the solutions. Additionally, Raman spectroscopy of the solutions on their own and in the presence of cells could also provide further insights into the

shape and size of the ice fractions, allowing a baseline of starting fraction sizes which could then be correlated to the amount of potential IRI needed.

Table 2.2. Chapter 2 Results Summary. Control = [a]PBS, [b]5 mg·mL^{-1} PVA in PBS, [c]10% DMSO in PBS, [d]+200 mM proline. Significantly higher than control, significant from control and indicated solution, significantly lower than control.

Target	Average Ice Crystal Size (μm^2) ↓	Enthalpy of Crystallisation ($J \cdot g^{-1}$) -	Melting Temperature (°C) -
Control	4519.59[a]	157.65[c]	-13.68[c]
5 mg·mL^{-1} PVA	**365.87**	158.54	-15.05
100 mM Alanine	2326.05[b]	–	–
Alanine + PVA	**117.9**	112.13	-15.09
100 mM Betaine	3641.71[b]	–	–
Betaine + PVA	**354.71**	170.03	-13.49
200 mM Proline	2657.67[b]	–	–
Proline + PVA	**344.34**	75.54	-20.82
5 mg·mL^{-1} Polyproline	1323.41[b]	169.78[d]	-14.65[d]
5 mg·mL^{-1} P2 Polyampholyte	2622.38[b]	168.33	-14.40

2.6 Materials and Methods

2.6.1 Chemical structures

All structures were drawn with ChemDraw 19.0 (PerkinElmer, Waltham, MA).

2.6.2 Reagents and solutions

PVA (M_w 9,000-10,000, 80% hydrolysed, CAS Number: 9002-89-5) was obtained from Sigma Aldrich Co Ltd, (Irvine, UK). Standard cell culture medium was composed of Ham's F-12K (Kaighn's) Medium (F-12K) (Gibco, Paisley, UK) supplemented with 10% USA-origin foetal bovine serum (FBS) purchased from

Sigma Aldrich (Dorset, UK) and 100 units·mL^{-1} penicillin, 100 µg·mL^{-1} streptomycin, and 250 ng·mL^{-1} amphotericin B (PSA) (HyClone, Cramlington, UK). Solutions for experiments were prepared by dissolving the individual compounds in PBS or base cell media supplemented with 10% FBS and 1x PSA (solutions to be used as CPAs did not contain PSA) and sterile filtering prior to use.

2.6.2.1 Synthesis of polyproline

Performed and written by Dr Ben Graham from the University of Warwick and reproduced here for completeness. EDCI (0.50 g, 2.60 mmol) was dissolved in dry DCM (20 mL) and stirred at room temperature under a flow of nitrogen for 20 minutes, followed by cooling to 0 ºC. Within 5 minutes of cooling, L-proline (0.30 g, 2.60 mmol, 1 eqv) and OxymaPureTM (0.37 g, 2.60 mmol, 1 eqv) were added together to the reaction mixture, resulting in an instantaneous colour change to yellow. The mixture was stirred on ice under nitrogen for 1 further hour, and then warmed to RT with stirring overnight. The dark yellow solution was condensed *in vacuo*, dissolved in Milli-Q water (10 mL) acidified to pH 3-4 with 3M HCl, and a minimum volume of methanol added until residual solids dissolved. Dialysis (> 1 kDa) for 48 hours was subsequently performed with regular water changes. The resulting solution was freeze dried, yielding an offwhite solid. 31.4 mg (10.4%). The DL racemate, P(DL)Pron, utilised a 1:1 ratio of L- and D-proline (2.60 mmol prolines).

2.6.2.1.1 Polyproline physical and analytical methods

Performed and written by Dr Ben Graham and included here for completeness. SEC (size exclusion chromatography) was acquired a DMF Agilent 390-LC MDS instrument equipped with differential refractive index (DRI), viscometry (VS), dual angle light scatter (LS) and dual wavelength UV detectors. The system was equipped with 2 x PLgel Mixed D columns (300 x 7.5 mm) and a

PLgel 5 μm guard column. The eluent is DMF with 5 mmol NH4BF4 additive. Samples were run at 1 mL/min at 50'C. Poly(methyl methacrylate) standards (Agilent EasyVials) were used for calibration. Analyte samples were filtered through a nylon membrane with 0.22 μm pore size before injection. Respectively, experimental molar mass (Mn,SEC) and dispersity (Đ) values of synthesised polymers were determined by conventional calibration (relative to poly(methyl methacrylate) standards) using Agilent GPC/SEC software. Refractive index recorded.

2.6.2.2 Synthesis of polyampholyte

Performed and written by Dr Christopher Stubbs and included here for completeness. As a representative example, poly(methyl vinyl ether-*alt*-maleic anhydride), average M_n ~80,000 Da, (1 g) was dissolved in tetrahydrofuran (50 mL) and heated to 50 °C with stirring. After dissolution, dimethylamino ethanol (2 g) was added in excess, forming a pink waxy solid, which was allowed to stir for 30 minutes. 50 mL water was added, and the reaction left to stir overnight followed by purification in dialysis tubing (Spectrapor, 12 – 14 kDa MWCO) for 48 hours with 7 water changes. The resulting solution was freeze-dried to evolve a white solid.

2.6.2.2.1 Polyampholyte physical and analytical methods

Performed and written by Dr Christopher Stubbs, from the University of Warwick and included here for completeness. ^{1}H and ^{13}C NMR spectra were recorded on Bruker Avance III HD 300 MHz, HD 400 MHz or HD 500 MHz spectrometers using deuterated solvents obtained from Sigma-Aldrich. Chemical shifts are reported relative to residual non-deuterated solvent.

2.6.3 Splat Assays

A 10 μL droplet of compound in solution was dropped using a Hamilton gastight 1750 syringe (Hamilton Bonaduz AG, GR, Switzerland) coupled with a BD microlance 3 21G needle (BD, Oxfordshire, UK) from a fixed height of 1.4 m onto a 22x22 mm no.1 glass cover slip (Fisher Scientific UK Ltd, Leicestershire, UK) placed on a $CO_{2(s)}$ cooled aluminium plate (~ -70 °C). The droplet froze instantly upon impact with the plate, spread out, and formed a thin wafer of ice. This wafer was then placed on a liquid nitrogen cooled BCS196 cryostage (Linkam Scientific, Surrey, UK) and held at -8 °C to anneal for 30 min using the LNP96 cooling system (Linkam Scientific). Photographs were taken using a Canon EOS 500D SLR digital camera (Canon (UK) Ltd, Surrey, UK) after 0 and 30 minutes coupled to an Olympus CX41 microscope (Olympus, Southend-on-Sea, UK) equipped with UIS-2 20x/0.45/∞/0-2/FN22, UIS-2 4x/0.1/∞/-/FN22 and UIS-2 10x/0.2/∞/-/FN22 lenses (Olympus Ltd, Essex, UK) through cross polarisers. The number of crystals in the image were counted using ImageJ (version 1.52a)[79] and the area of the field of view divided by the number of crystals gave the average crystal size per wafer.

2.6.4 Differential Scanning Calorimetry

Samples were prepared by weighing standard 40 μL aluminium crucibles (Mettler Toledo, Leicestershire, UK) and adding 15 μL of analyte before sealing (hermetically) and reweighing in order to quantify the exact mass of sample. Each sample was then transferred to a liquid nitrogen cooled DSC 1 STAR® system (Mettler Toledo, Leicestershire, UK) differential scanning calorimeter. The mass of the aluminium crucible and sample mass was input into the complimentary STARe thermal analysis software to retain a digital record and aid analysis. Each DSC sample was individually cooled from +25 ºC to -150 ºC at a rate of 10 ºC·min^{-1} whilst concurrently monitoring the heat flow (mW) of the

system to detect any endothermic or exothermic transitions. When samples were cooled to -150 ºC, each sample was held for 10 min and then warmed at a rate of 10 ºC·min^{-1} from -150 ºC to +25 ºC. Raw data from each experiment was exported and plotted in R (R Foundation for Statistical Computing, Vienna, Austria) and individual peaks highlighted for comparison using the STARe thermal analysis software built-in modelling functions for linear curve fitting and area under the curve when required.

2.6.5 Statistical Analysis

Data were analysed with a one-way analysis of variance (ANOVA) on ranks followed by comparison of experimental groups with the appropriate control group (Holm–Sidak method) followed by Tukey's post hoc test. Excel 2013 (Microsoft, Redmond, WA) and R were used for the analyses and graphs. Data sets are presented as mean ± (SEM).

2.7 Appendix

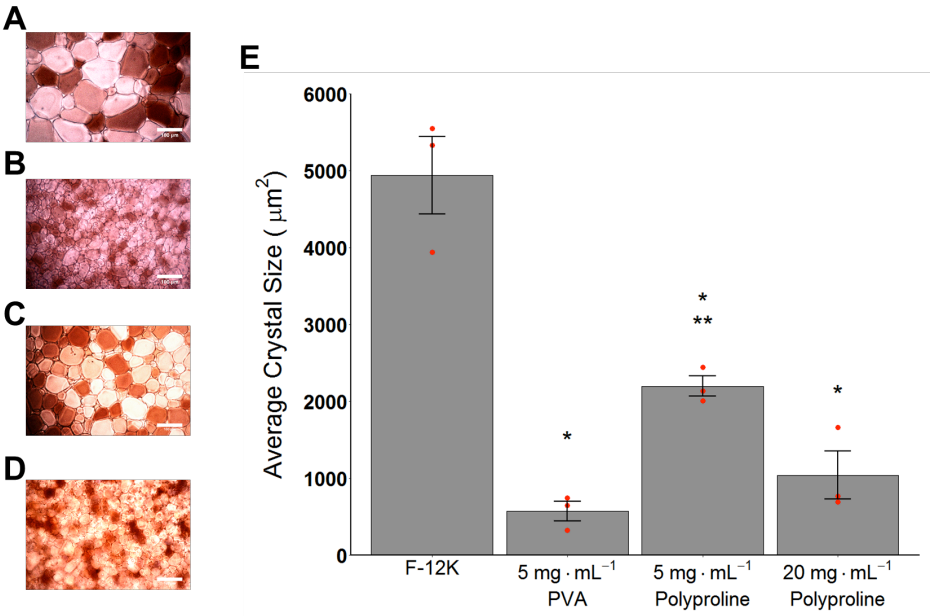

Figure 2.25. Splat of polyproline and PVA solutions in F-12K. A) Splat micrograph of F-12K. **B)** Splat micrograph of 5 mg·mL^{-1} PVA in F-12K. **C)** Splat micrograph of 5 mg·mL^{-1} polyproline in F-12K. **D)** Splat micrograph of 20 mg·mL^{-1} polyproline in F-12K. Scale bar = 100 μm. **E)** Average ice crystal size of solutions calculated from splat wafers. * $P < 0.001$ from F-12K, ** $P < 0.001$ from 5 mg·mL^{-1} PVA in F-12K. Error bars represent ± SEM of 3 independent experiments.

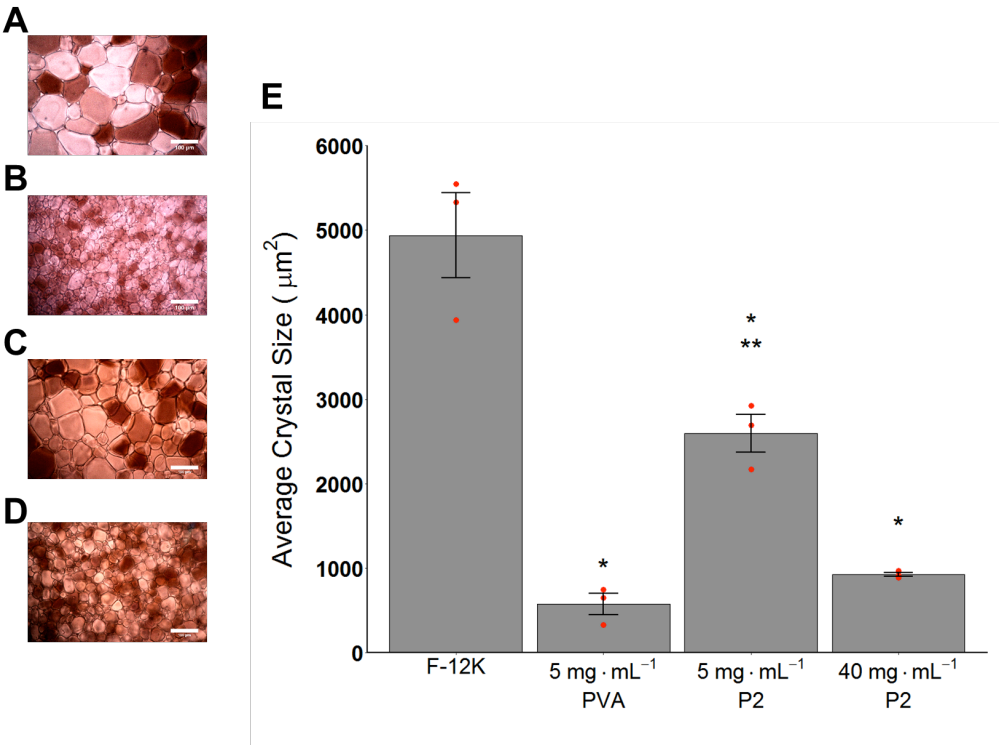

Figure 2.26. Splat of polyampholyte P2 and PVA solutions in F-12K. A) Splat micrograph of F-12K. **B)** Splat micrograph of 5 mg·mL^{-1} PVA in F-12K. **C)** Splat micrograph of 5 mg·mL^{-1} P2 in F-12K. **D)** Splat micrograph of 40 mg·mL^{-1} P2 in F-12K. Scale bar = 100 μm. **E)** Average ice crystal size of solutions calculated from splat wafers. * P < 0.001 from F-12K, ** P < 0.001 from 5 mg·mL^{-1} PVA in F-12K. Error bars represent ± SEM of 3 independent experiments.

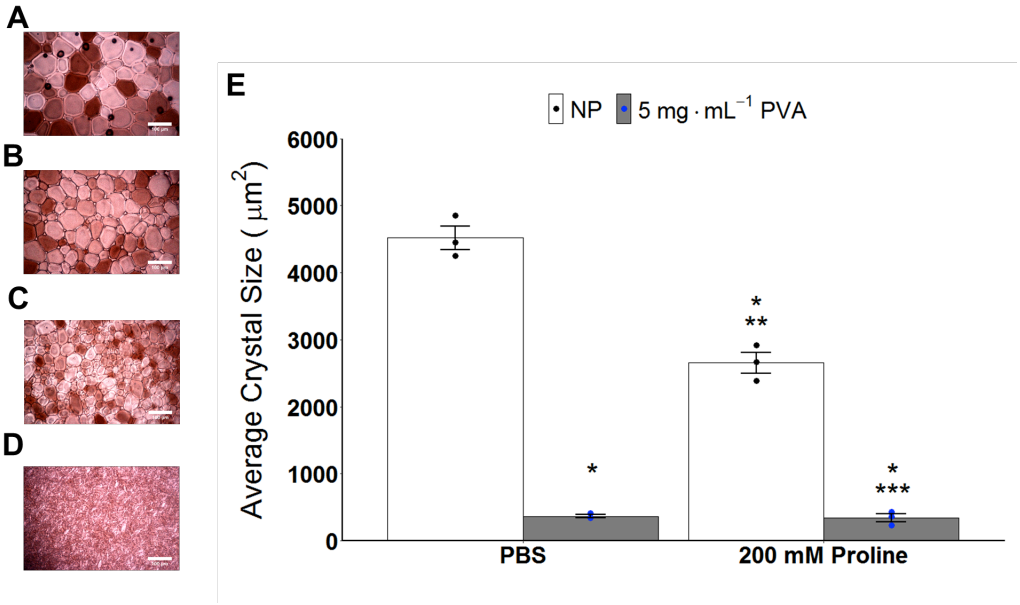

Figure 2.27. Splat of proline solutions in PBS. **A)** Splat of PBS. **B)** Splat of 200 mM proline in PBS. **C)** Splat of 5 mg·mL^{-1} PVA in PBS. **D)** Splat of 200 mM proline + 5 mg·mL^{-1} PVA in PBS. **E)** Average crystal size of solutions calculated from splat ice wafers. * P < 0.0001 from PBS, ** P < 0.0001 from 5 mg·mL^{-1} PVA in PBS, *** P < 0.0001 from 200 mM proline in PBS. Error bars represent ± SEM of 3 independent experiments. Scale bar = 100 µm (NP=No polymer).

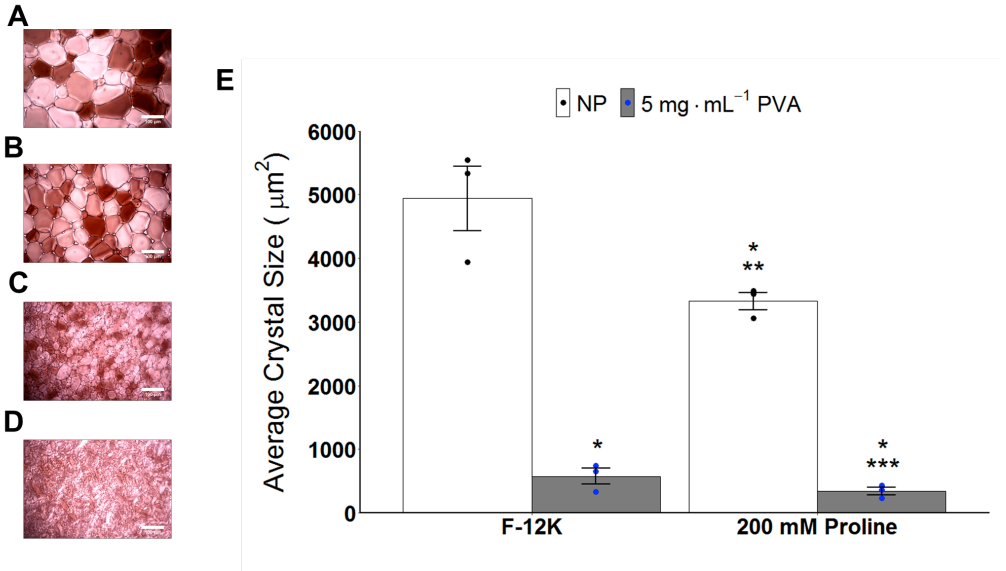

Figure 2.28. Splat of proline solutions in F-12K. **A)** Splat of F-12K. **B)** Splat of 200 mM proline in F-12K. **C)** Splat of 5 mg·mL^{-1} PVA in F-12K. **D)** Splat of 200 mM proline + 5 mg·mL^{-1} PVA in F-12K. **E)** Average crystal size of solutions calculated from splat ice wafers. * P < 0.0001 from F-12K, ** P < 0.0001 from 5 mg·mL^{-1} PVA in F-12K, *** P < 0.0001 from 200 mM proline in F-12K. Error bars represent ± SEM of 3 independent experiments. Scale bar = 100 µm (NP=No polymer).

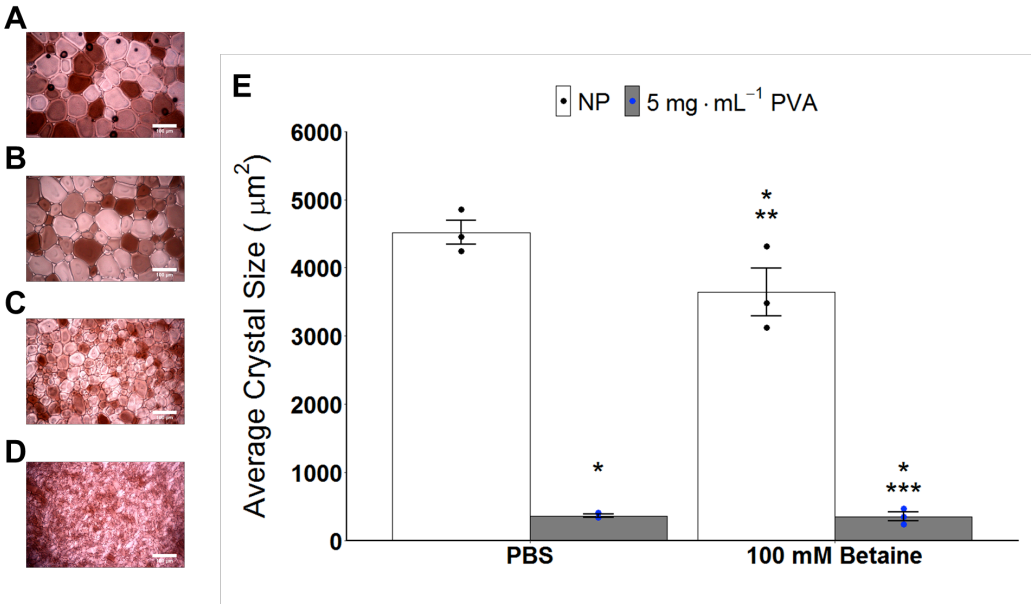

Figure 2.29. Splat of betaine solutions in PBS. **A)** Splat of PBS. **B)** Splat of 100 mM betaine in PBS. **C)** Splat of 5 mg·mL^{-1} PVA in PBS. **D)** Splat of 100 mM betaine + 5 mg·mL^{-1} PVA in PBS. **E)** Average crystal size of solutions calculated from splat ice wafers. * P < 0.0001 from PBS, ** P < 0.0001 from 5 mg·mL^{-1} PVA in PBS, *** P < 0.0001 from 100 mM betaine in PBS. Error bars represent ± SEM of 3 independent experiments. Scale bar = 100 μm (NP=No polymer).

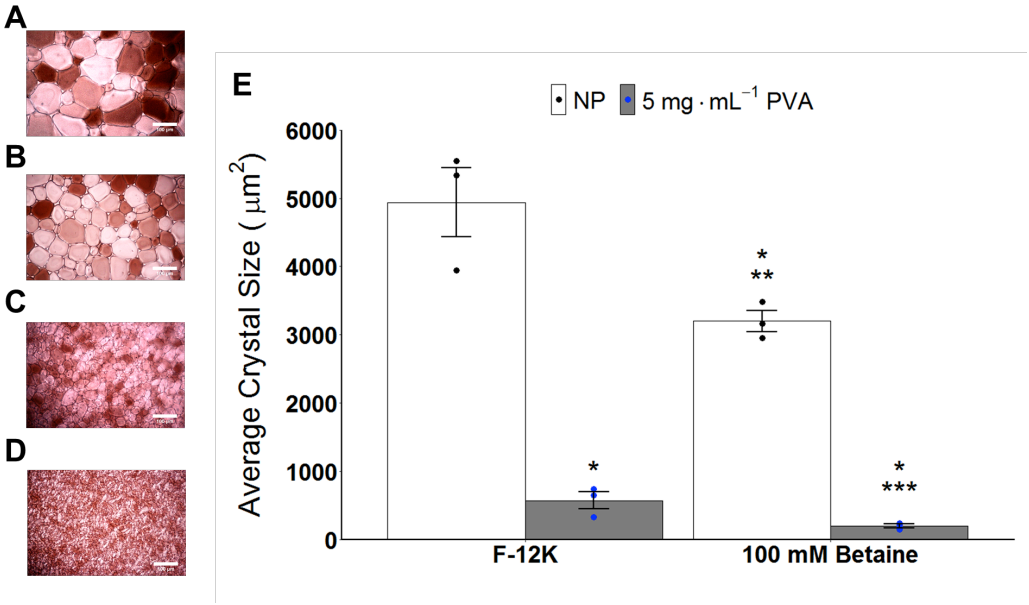

Figure 2.30. Splat of betaine solutions in F-12K. **A)** Splat of F-12K. **B)** Splat of 100 mM betaine in F-12K. **C)** Splat of 5 mg·mL^{-1} PVA in F-12K. **D)** Splat of 100 mM betaine + 5 mg·mL^{-1} PVA in F-12K. **E)** Average crystal size of solutions calculated from splat ice wafers. * P < 0.0001 from F-12K, ** P < 0.0001 from 5 mg·mL^{-1} PVA in F-12K, *** P < 0.0001 from 100 mM betaine in F-12K. Error bars represent ± SEM of 3 independent experiments. Scale bar = 100 μm (NP=No polymer).

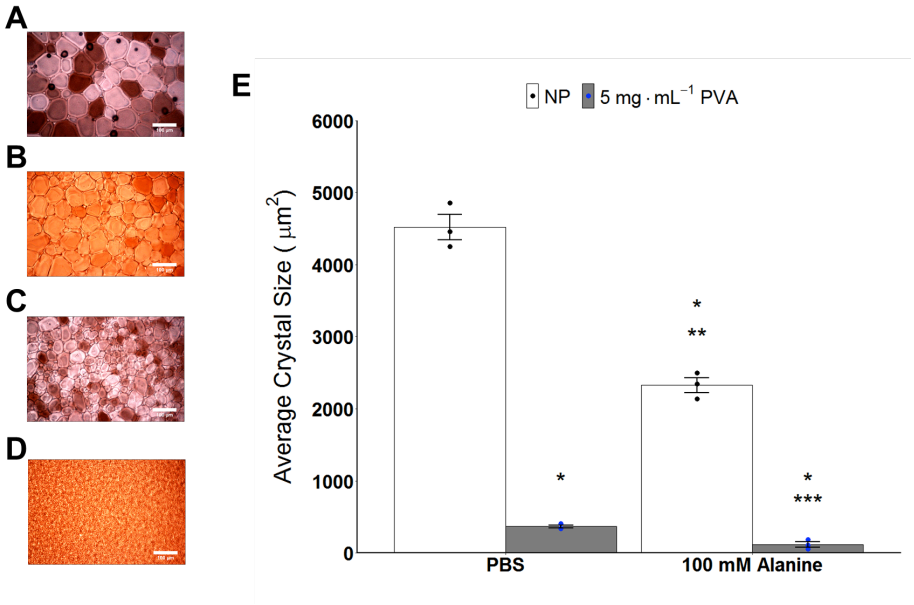

Figure 2.31. Splat of alanine solutions in PBS. **A)** Splat of PBS. **B)** Splat of 100 mM alanine in PBS. **C)** Splat of 5 mg·mL^{-1} PVA in PBS. **D)** Splat of 100 mM alanine + 5 mg·mL^{-1} PVA in PBS. **E)** Average crystal size of solutions calculated from splat ice wafers. * P < 0.0001 from PBS, ** P < 0.0001 from 5 mg·mL^{-1} PVA in PBS, *** P < 0.0001 from 100 mM alanine in PBS. Error bars represent ± SEM of 3 independent experiments. Scale bar = 100 µm (NP=No polymer).

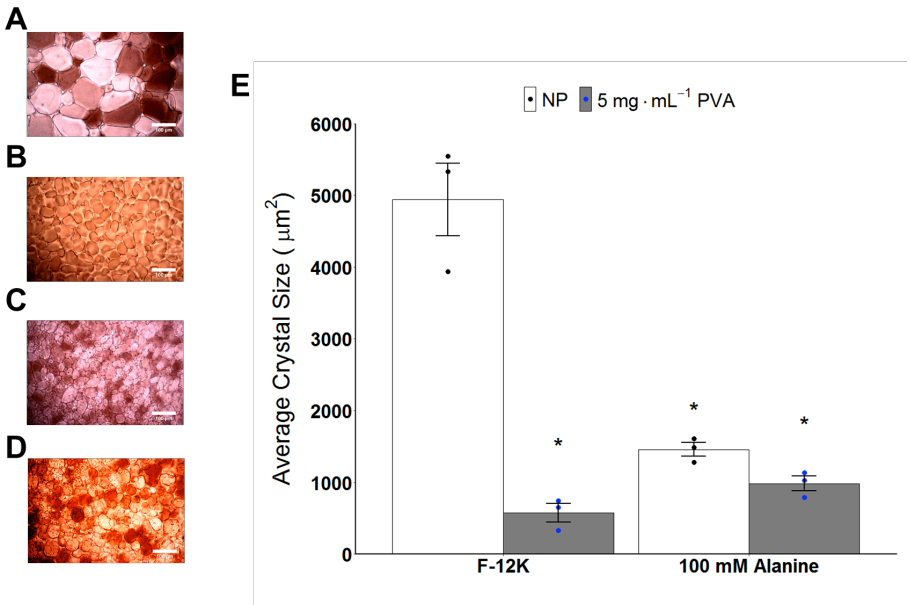

Figure 2.32. Splat of alanine solutions in F-12K. **A)** Splat of F-12K. **B)** Splat of 100 mM alanine in F-12K. **C)** Splat of 5 mg·mL^{-1} PVA in F-12K. **D)** Splat of 100 mM alanine + 5 mg·mL^{-1} PVA in F-12K. **E)** Average crystal size of solutions calculated from splat ice wafers. * P < 0.0001 from F-12K. Error bars represent ± SEM of 3 independent experiments. Scale bar = 100 µm (NP=No polymer).

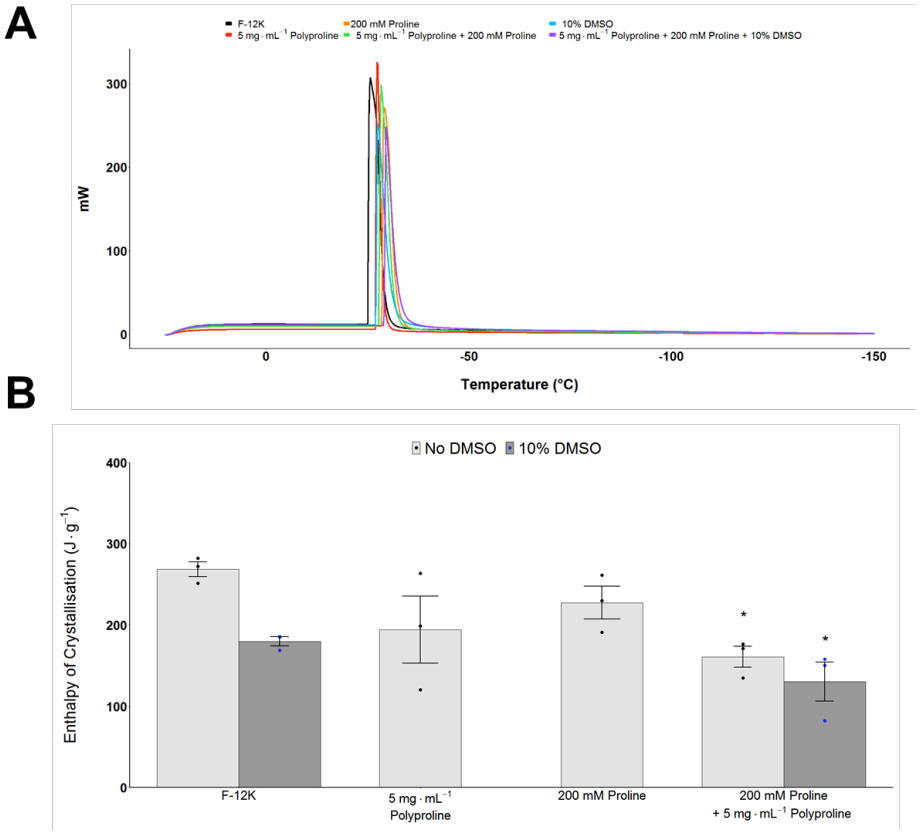

Figure 2.33. DSC cooling of polyproline solutions in F-12K. A) DSC trace of cooling to -150 °C at 10 °C·min^{-1}. **B)** Average enthalpy of ice crystallisation of solutions calculated from area under curve on DSC trace. Error bars represent ± SEM of 3 independent experiments. * P < 0.0001 from F-12K.

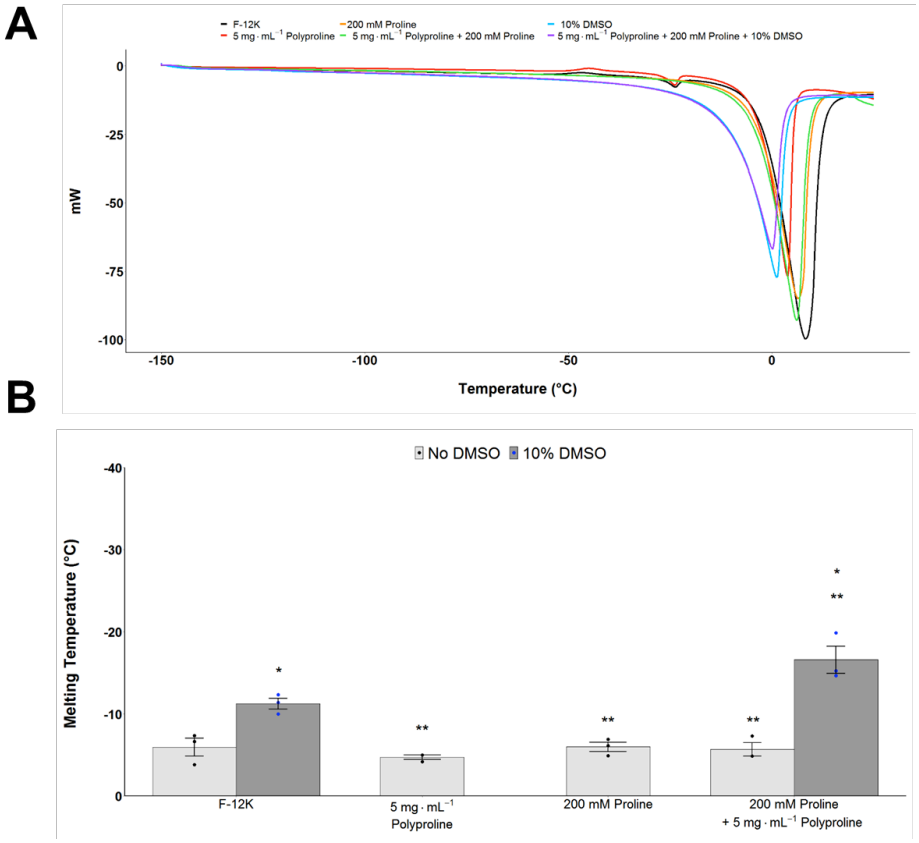

Figure 2.34. DSC heating of polyproline solutions in F-12K. A) DSC trace of warming polyproline solutions from -150 °C to 25 °C at 10 °C·min^{-1}. **B)** Average melting temperature calculated from onset of DSC exothermic drop. Error bars represent ± SEM of 3 independent. * P < 0.001 from F-12K, ** P < 0.001 from 10% DMSO in F-12K.

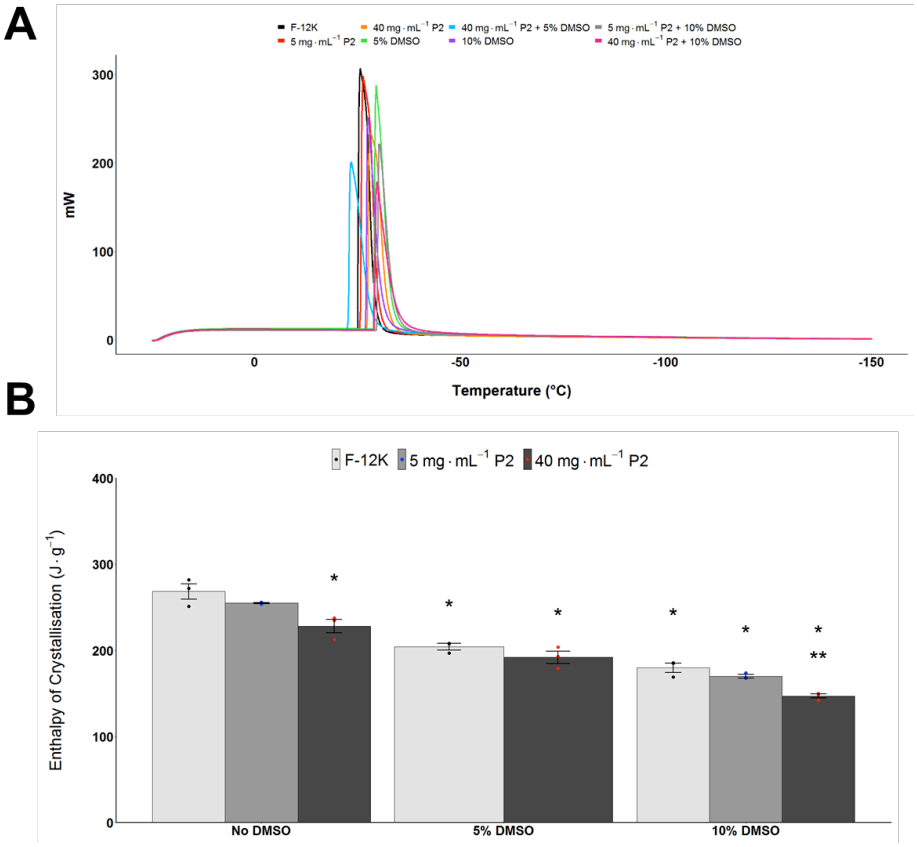

Figure 2.35. DSC cooling of polyampholyte P2 solutions in F-12K. A) DSC trace of P2 solutions cooled to -150 °C at 10 °C·min^{-1}. **B)** Average enthalpy of ice crystallisation of solutions calculated from area under curve on DSC trace. Error bars represent ± SEM of 3 independent experiments. * P < 0.0001 from F-12K, ** P < 0.0001 from 10% DMSO in F-12K.

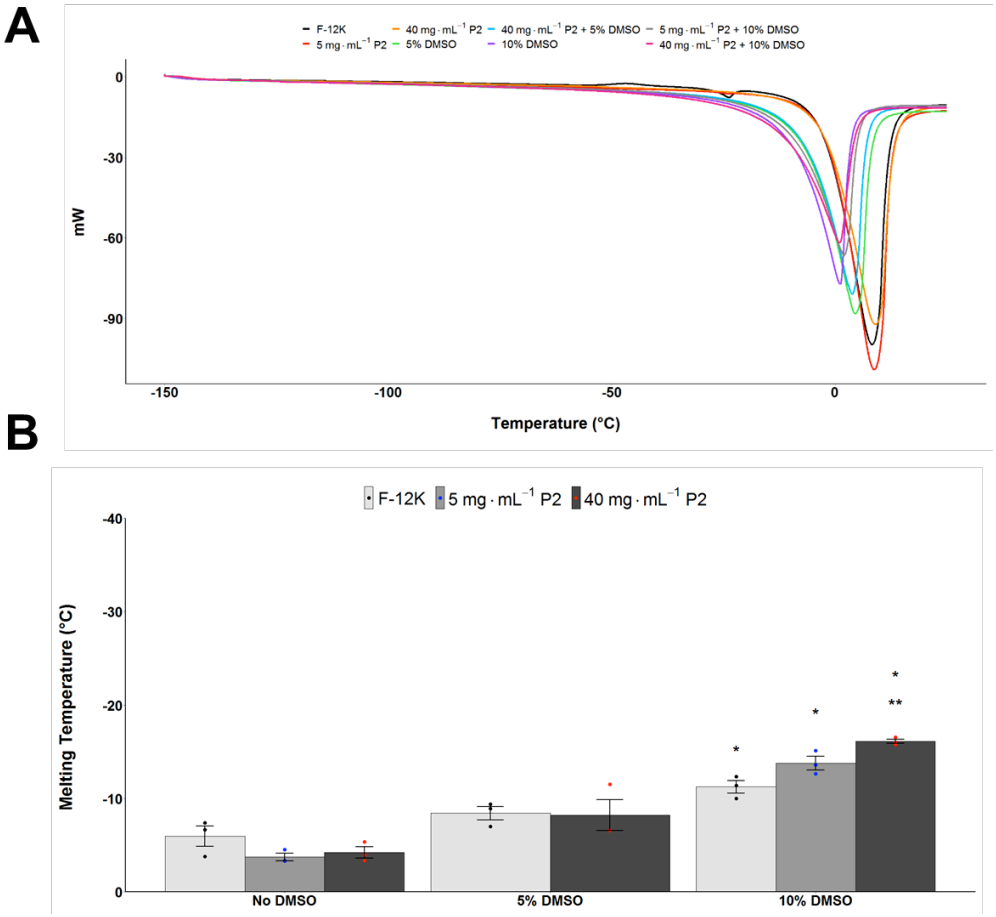

Figure 2.36. DSC heating of polyampholyte P2 solutions in F-12K. A) DSC trace of warming P2 solutions from -150 °C to 25 °C at 10 °C·min^{-1}. **B)** Average melting temperature calculated from onset of DSC exothermic drop. Error bars represent ± SEM of 3 independent. * P < 0.001 from F-12K, ** P < 0.001 from 10% DMSO in F-12K.

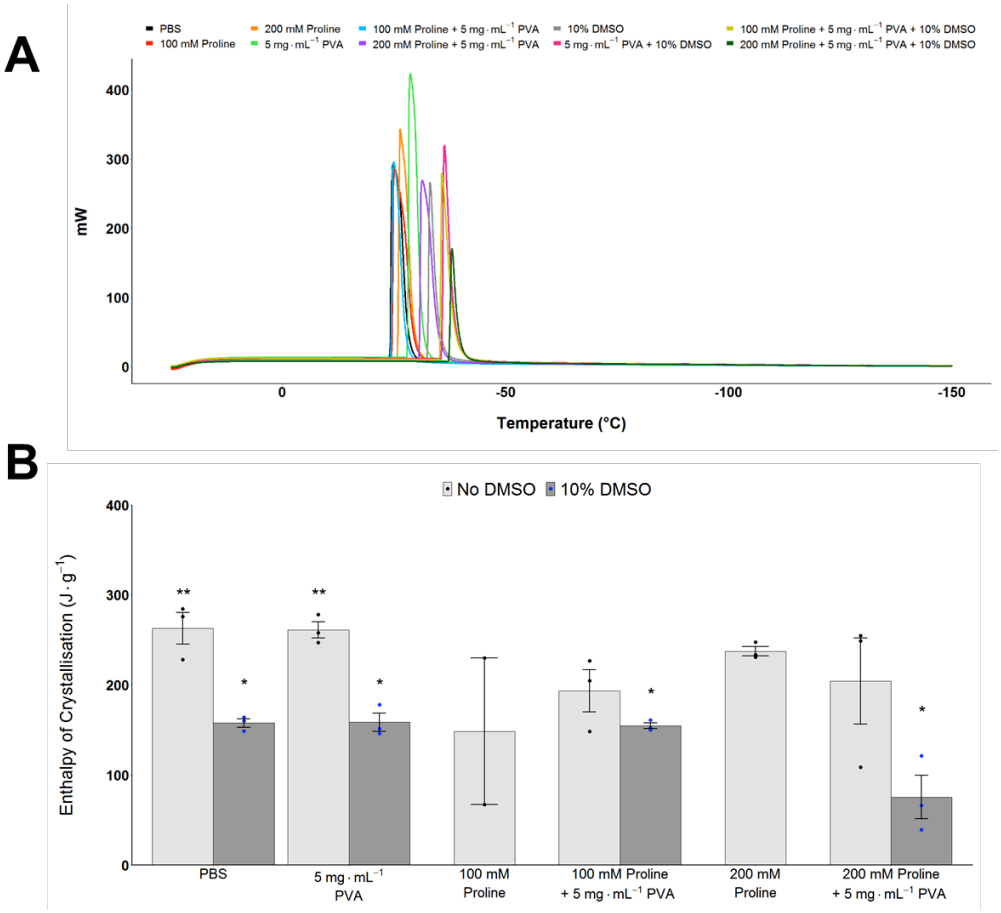

Figure 2.37. DSC cooling of proline solutions in PBS. A) DSC trace of cooling to -150 °C at 10 °C·min^{-1}. **B)** Average enthalpy of ice crystallisation of solutions calculated from area under curve on DSC trace. Error bars represent ± SEM of 3 independent experiments. * P < 0.001 from PBS. ** P< 0.001 from 10% DMSO. (100 mM proline N=2 and not included in statistical analysis.)

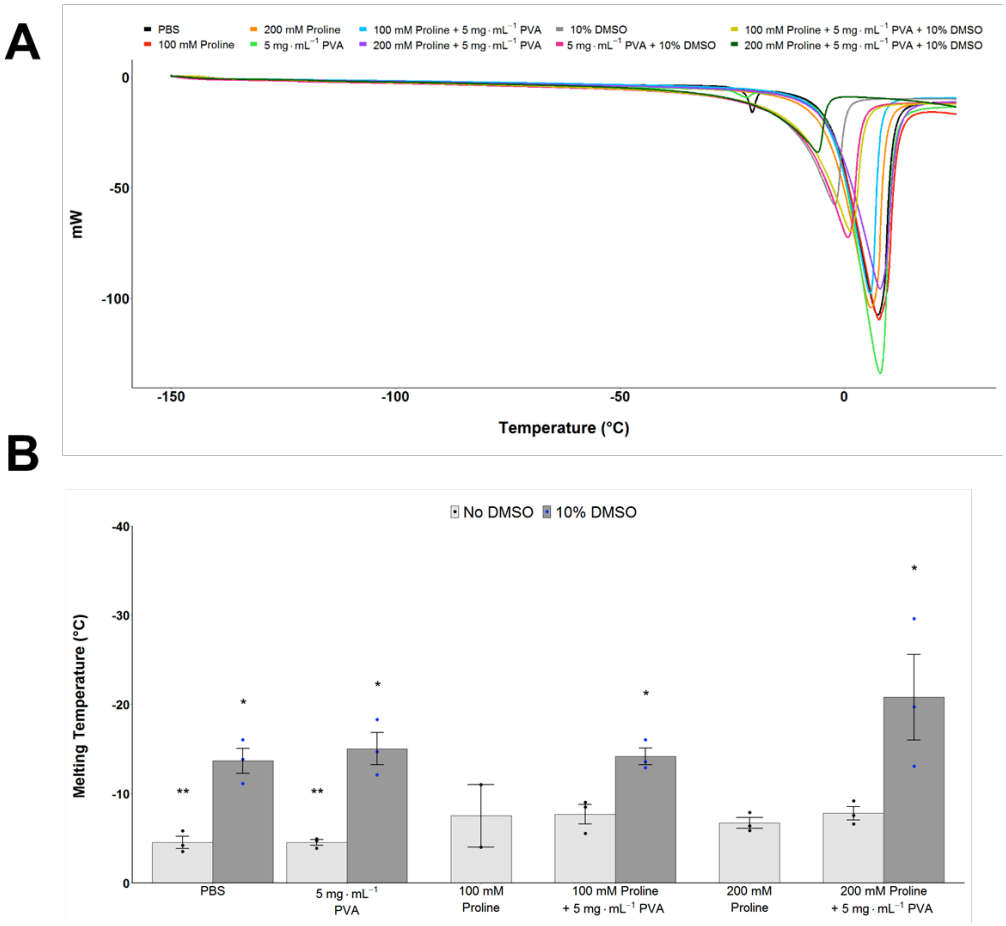

Figure 2.38. DSC heating of proline solutions in PBS. A) DSC trace of warming from -150 °C to 25 °C at 10 °C·min^{-1}. **B)** Average melting temperature calculated from onset of DSC mW drop. Error bars represent ± SEM of 3 independent experiments (100 mM proline N=2 and not included in statistical analysis). * P < 0.0001 from PBS. ** P < 0.0001 from 10% DMSO.

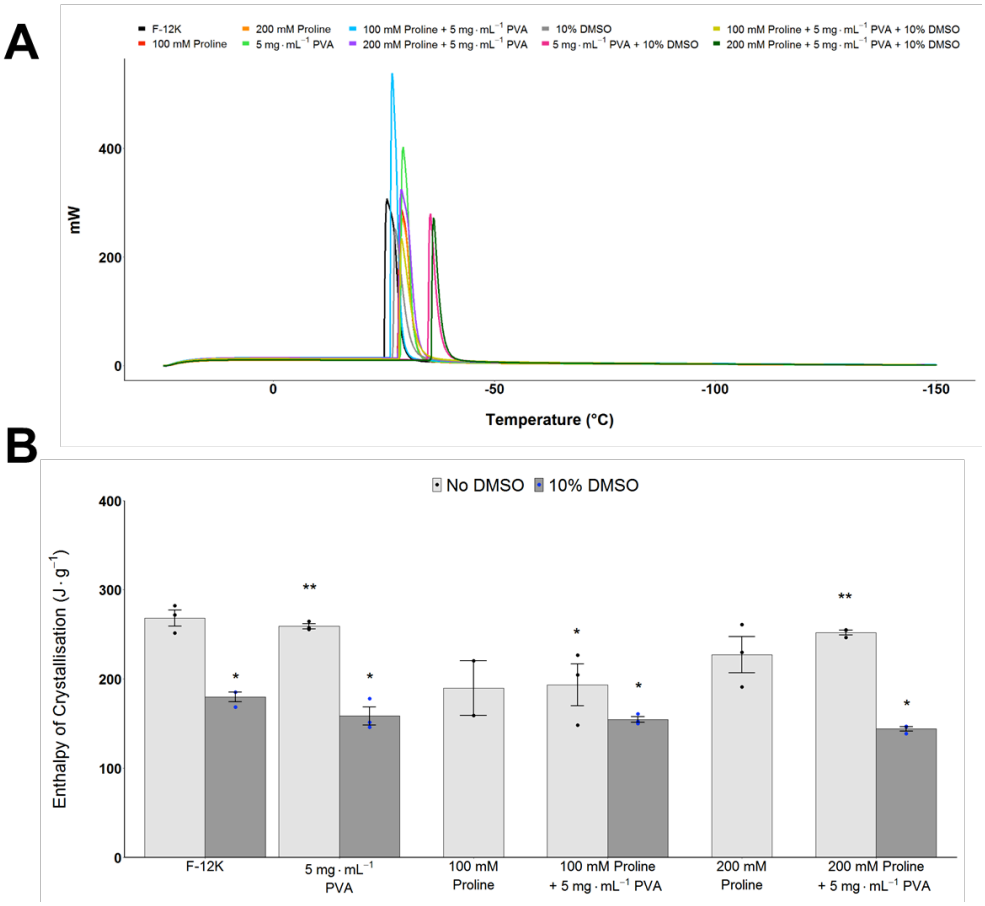

Figure 2.39. DSC cooling of proline solutions in F-12K. A) DSC trace of cooling to -150 °C at 10 °C·min^{-1}. **B)** Average enthalpy of ice crystallisation of solutions calculated from area under curve on DSC trace. Error bars represent ± SEM of 3 independent experiments (100 mM proline N=2 and was not included in statistical analysis). * P < 0.00001 from F-12K. ** P < 0.00001 from 10% DMSO.

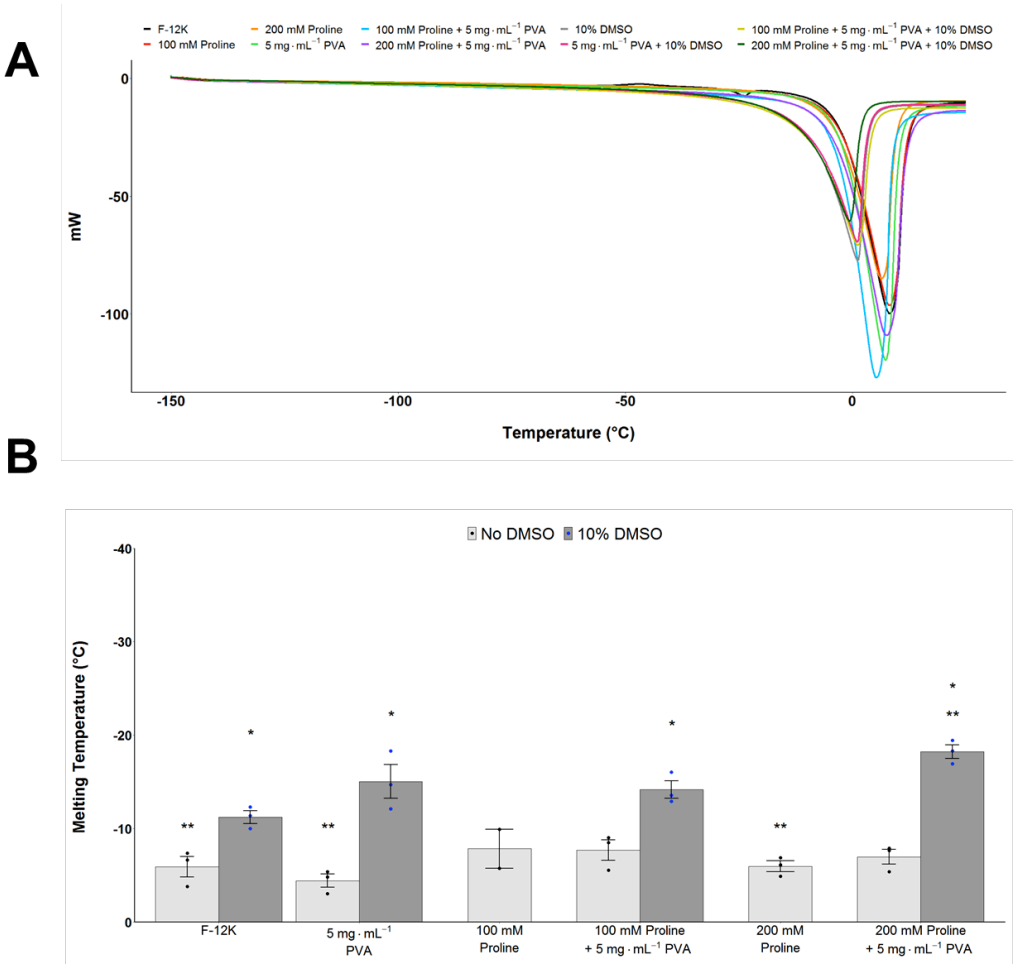

Figure 2.40. DSC heating of proline solutions in F-12K. A) DSC trace of warming from -150 °C to 25 °C at 10 °C·min^{-1}. **B)** Average melting temperature calculated from onset of DSC mW drop. Error bars represent ± SEM of 3 independent experiments. * P < 0.00001 from F-12K. ** P < 0.0001 from 10% DMSO. (100 mM proline N=2 and was not included in statistical analysis.)

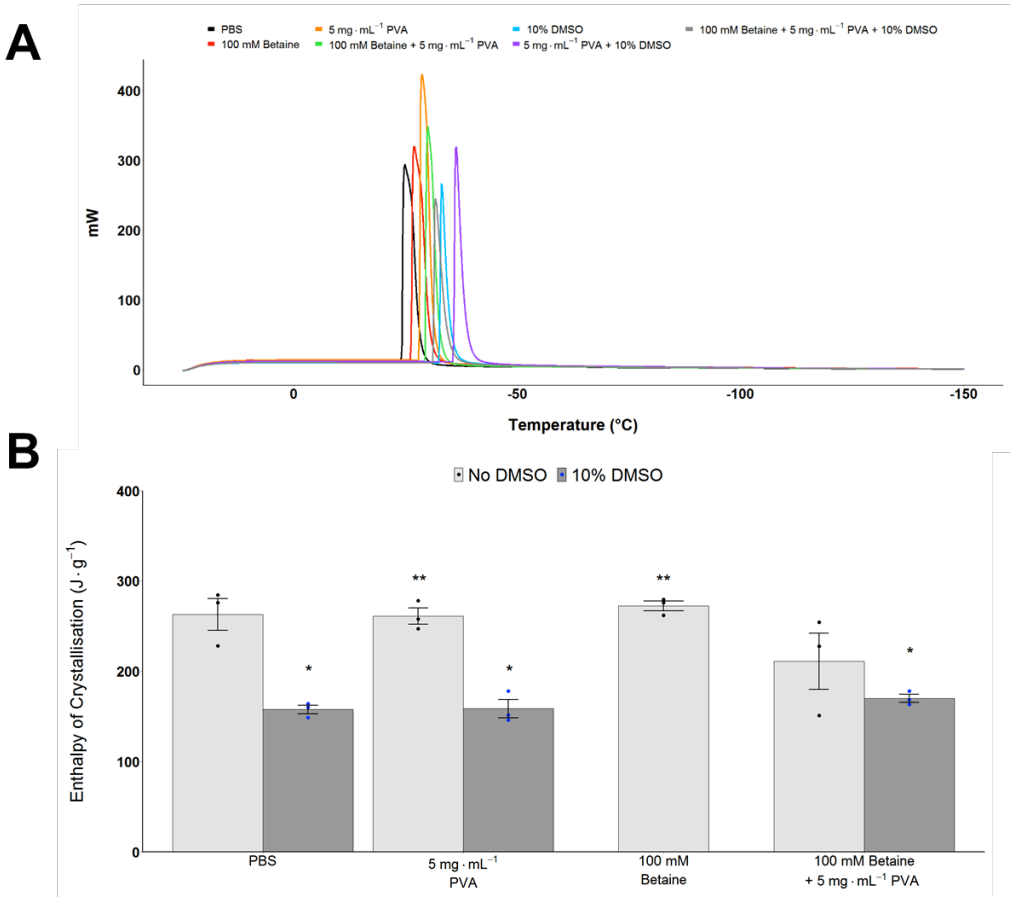

Figure 2.41. DSC cooling of betaine solutions in PBS. A) DSC trace of cooling to -150 °C at 10 °C·min^{-1}. **B)** Average enthalpy of ice crystallisation of solutions calculated from area under curve on DSC trace. Error bars represent ± SEM of 3 independent experiments. * P < 0.0001 from PBS. ** P< 0.001 from 10% DMSO.

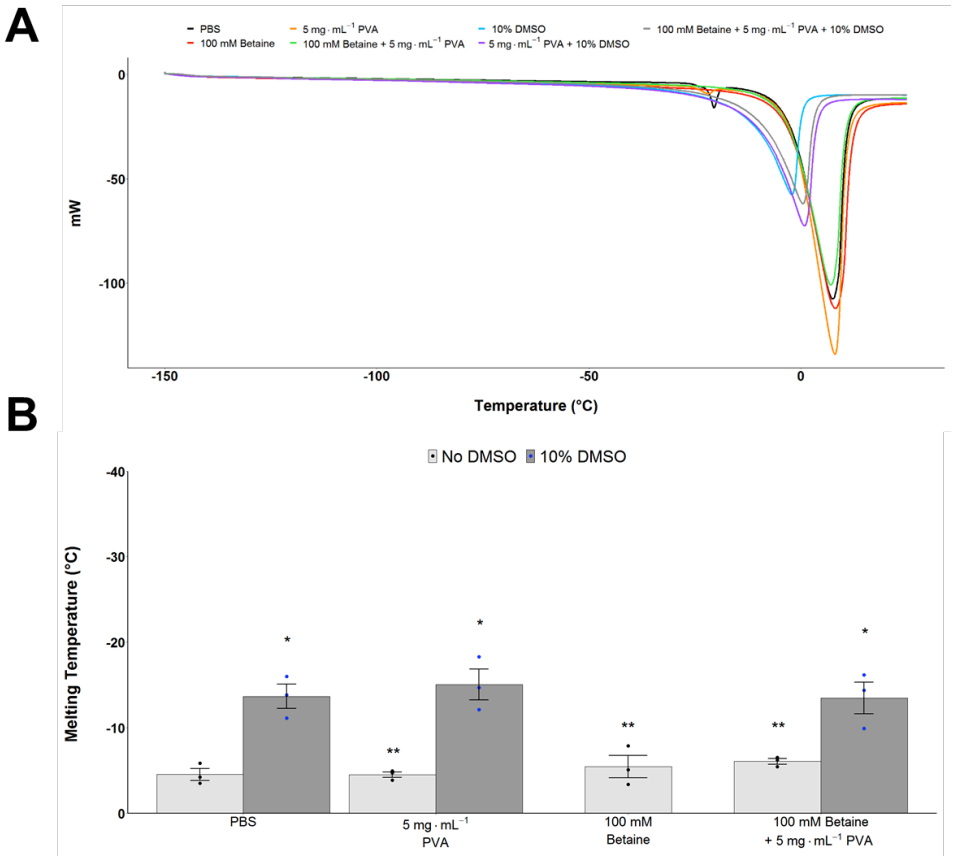

Figure 2.42. DSC heating of betaine solutions in PBS. A) DSC trace of warming from -150 °C to 25 °C at 10 °C·min^{-1}. **B)** Average melting temperature calculated from onset of DSC mW drop. Error bars represent ± SEM of 3 independent experiments. * P < 0.00001 from PBS. ** P < 0.0001 from 10% DMSO.

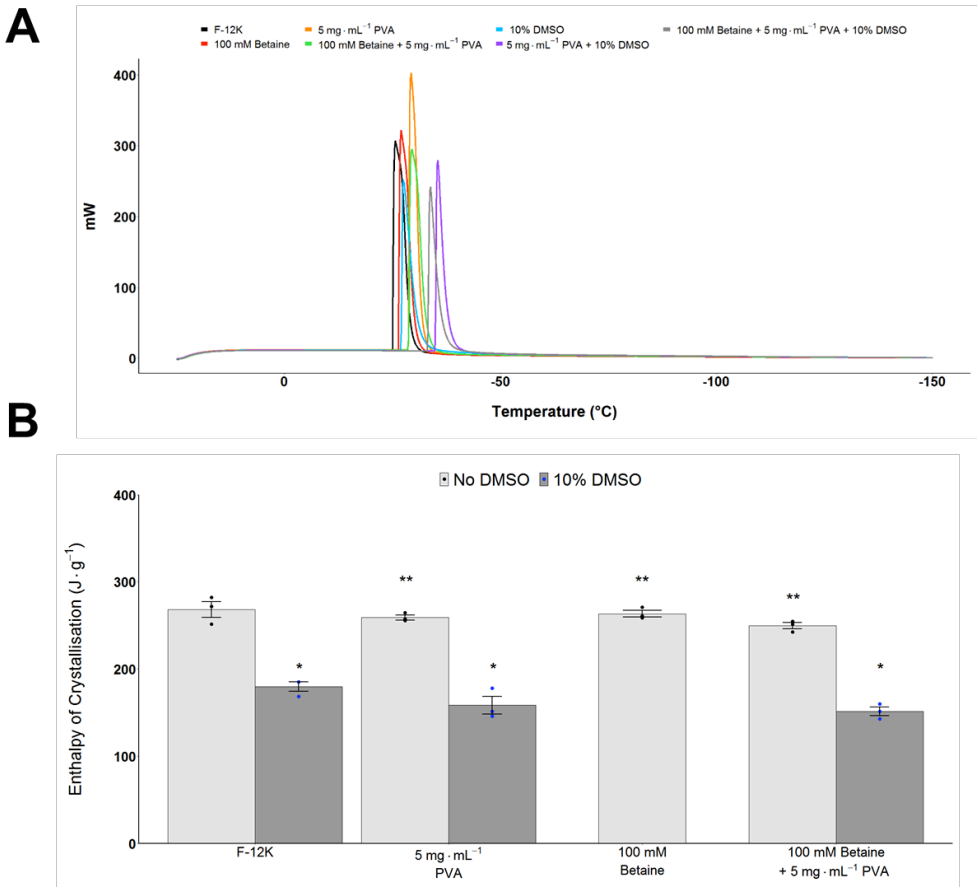

Figure 2.43. DSC cooling of betaine solutions in F-12K. A) DSC trace of cooling to -150 °C at 10 °C·min^{-1}. **B)** Average enthalpy of ice crystallisation of solutions calculated from area under curve on DSC trace. Error bars represent ± SEM of 3 independent experiments. * P < 0.0001 from F-12K. ** P< 0.001 from 10% DMSO.

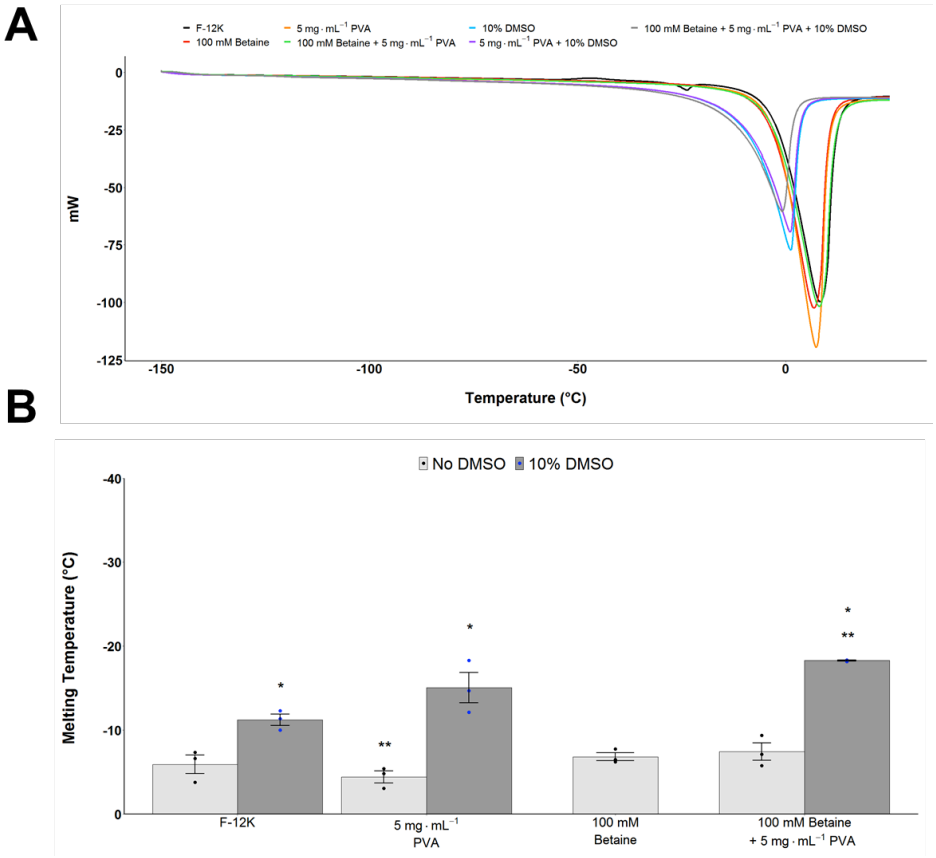

Figure 2.44. DSC heating of betaine solutions in F-12K. A) DSC trace of warming from -150 °C to 25 °C at 10 °C·min^{-1}. **B)** Average melting temperature calculated from onset of DSC mW drop. Error bars represent ± SEM of 3 independent experiments. * P < 0.00001 from F-12K. ** P < 0.0001 from 10% DMSO.

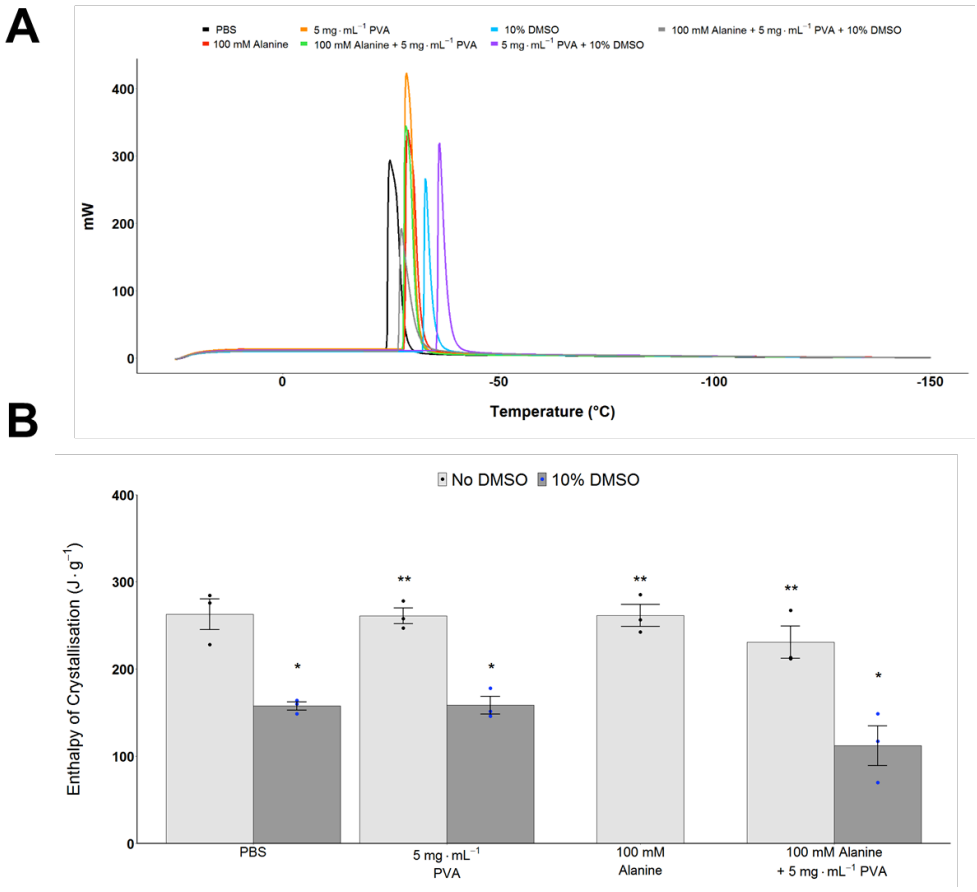

Figure 2.45. DSC cooling of alanine solutions in PBS. A) DSC trace of cooling to -150 °C at 10 °C·min^{-1}. **B)** Average enthalpy of ice crystallisation of solutions calculated from area under curve on DSC trace. Error bars represent ± SEM of 3 independent experiments. * P < 0.0001 from PBS. ** P< 0.001 from 10% DMSO.

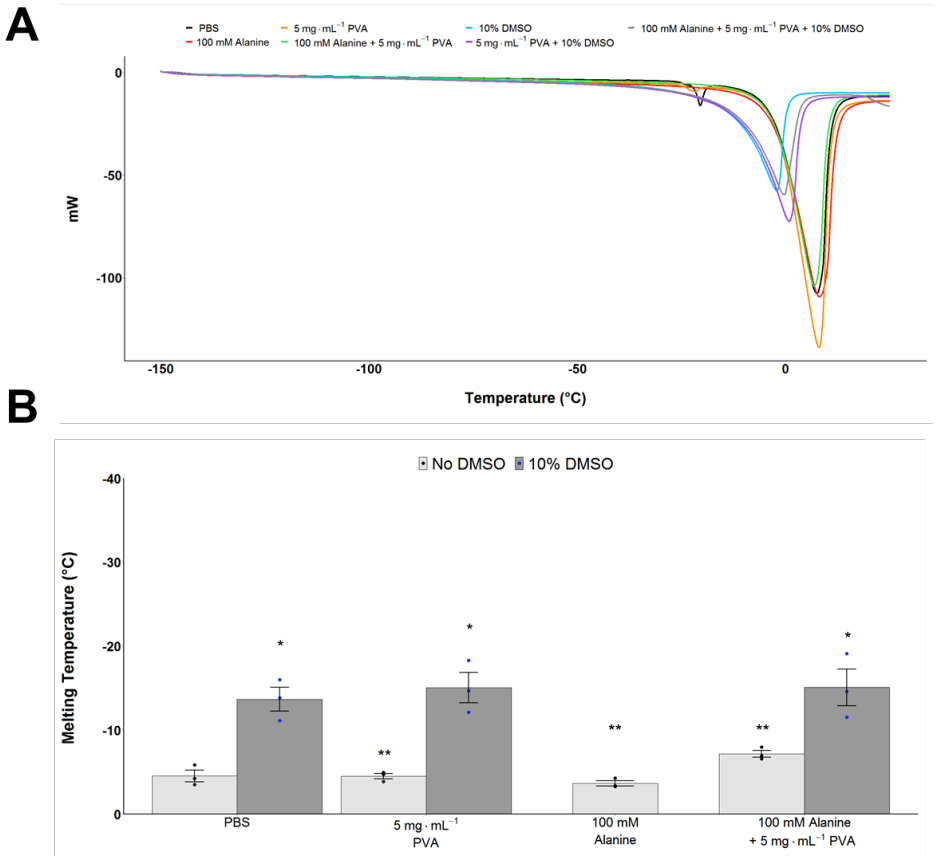

Figure 2.46. DSC heating of alanine solutions in PBS. A) DSC trace of warming from -150 °C to 25 °C at 10 °C·min^{-1}. **B)** Average melting temperature calculated from onset of DSC mW drop. Error bars represent ± SEM of 3 independent experiments. * P < 0.00001 from PBS. ** P < 0.0001 from 10% DMSO.

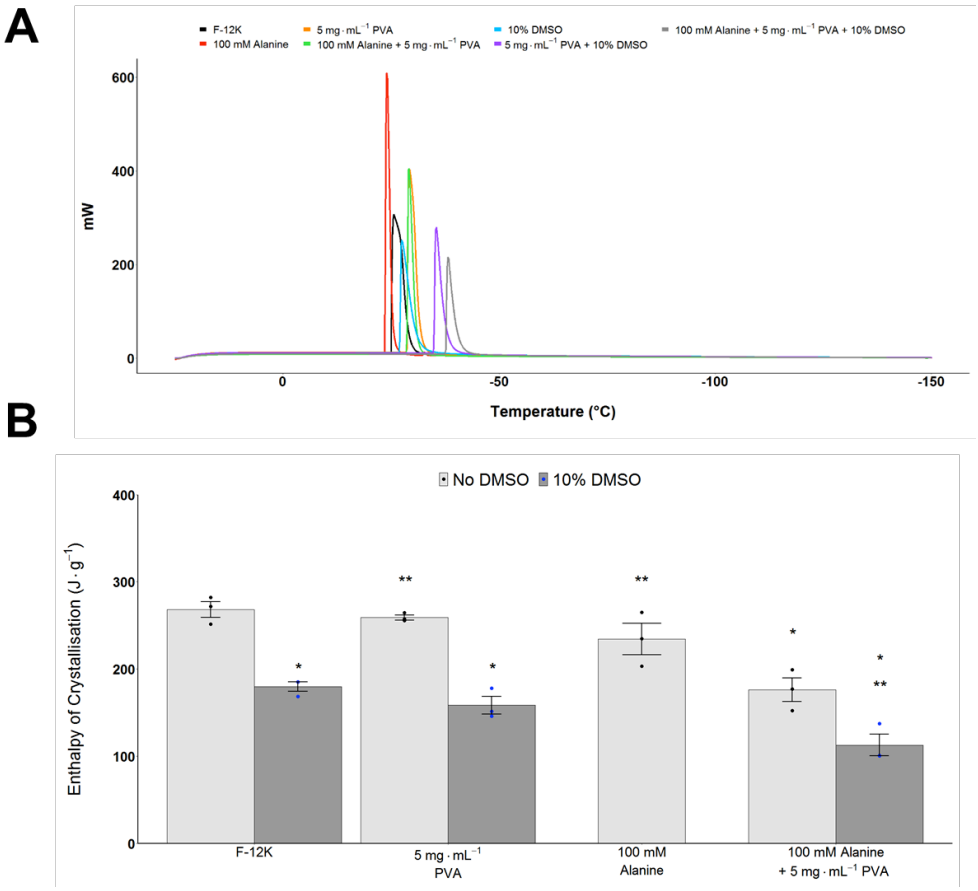

Figure 2.47. DSC cooling of alanine solutions in F-12K. A) DSC trace of cooling to -150 °C at 10 °C·min^{-1}. **B)** Average enthalpy of ice crystallisation of solutions calculated from area under curve on DSC trace. Error bars represent ± SEM of 3 independent experiments. * P < 0.0001 from F-12K. ** P< 0.001 from 10% DMSO.

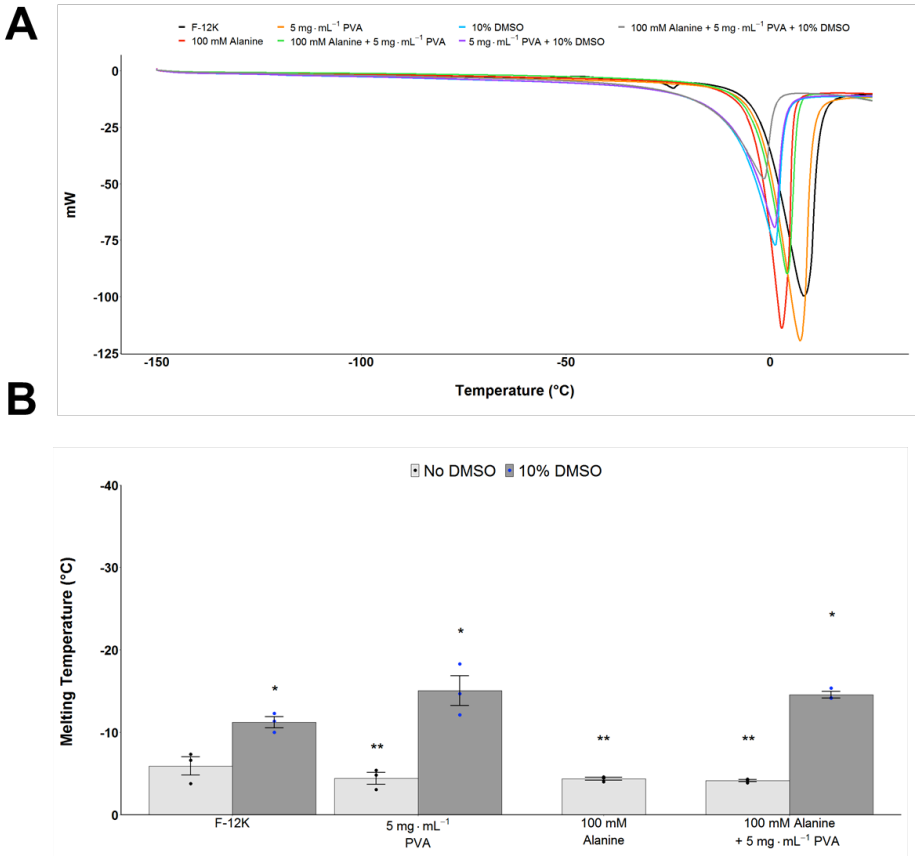

Figure 2.48. DSC heating of alanine solutions in F-12K. A) DSC trace of warming from -150 °C to 25 °C at 10 °C·min^{-1}. **B)** Average melting temperature calculated from onset of DSC mW drop. Error bars represent ± SEM of 3 independent experiments. * P < 0.00001 from F-12K. ** P < 0.0001 from 10% DMSO.

2.8 References

(1) Chao, H.; Davies, P. L.; Carpenter, J. F. Effects of Antifreeze Proteins on Red Blood Cell Survival during Cryopreservation. *J. Exp. Biol.* **1996**, *199* (Pt 9), 2071–2076. https://doi.org/10.1177/0022034530010003090l.

(2) Eniade, A.; Purushotham, M.; Ben, R. N.; Wang, J. B.; Horwath, K. A Serendipitous Discovery of Antifreeze Protein-Specific Activity in C-Linked Antifreeze Glycoprotein Analogs. *Cell Biochem. Biophys.* **2003**, *38* (2), 115–124. https://doi.org/10.1385/CBB:38:2:115.

(3) Carpenter, J. F.; Hansen, T. N. Antifreeze Protein Modulates Cell Survival during Cryopreservation: Mediation through Influence on Ice Crystal Growth. *Proc. Natl.*

Acad. Sci. U. S. A. **1992**, *89* (19), 8953–8957. https://doi.org/10.1073/pnas.89.19.8953.

(4) Gibson, M. I. Slowing the Growth of Ice with Synthetic Macromolecules: Beyond Antifreeze(Glyco) Proteins. *Polym. Chem.* **2010**, *1* (8), 1141. https://doi.org/10.1039/c0py00089b.

(5) Inada, T.; Lu, S.-S. Inhibition of Recrystallization of Ice Grains by Adsorption of Poly(Vinyl Alcohol) onto Ice Surfaces. *Cryst. Growth Des.* **2003**, *3* (5), 747–752. https://doi.org/10.1021/cg0340300.

(6) Budke, C.; Koop, T. Ice Recrystallization Inhibition and Molecular Recognition of Ice Faces by Poly(Vinyl Alcohol). *Chemphyschem* **2006**, *7* (12), 2601–2606. https://doi.org/10.1002/cphc.200600533.

(7) Knight, C. A.; Wen, D.; Laursen, R. A. Nonequilibrium Antifreeze Peptides and the Recrystallization of Ice. *Cryobiology* **1995**, *32* (1), 23–34. https://doi.org/10.1006/cryo.1995.1002.

(8) Deller, R. C.; Congdon, T.; Sahid, M. A.; Morgan, M.; Vatish, M.; Mitchell, D. A.; Notman, R.; Gibson, M. I. Ice Recrystallisation Inhibition by Polyols: Comparison of Molecular and Macromolecular Inhibitors and Role of Hydrophobic Units. *Biomater. Sci.* **2013**, *1* (5), 478. https://doi.org/10.1039/c3bm00194f.

(9) Naullage, P. M.; Lupi, L.; Molinero, V. Molecular Recognition of Ice by Fully Flexible Molecules. *J. Phys. Chem. C* **2017**, *121* (48), 26949–26957. https://doi.org/10.1021/acs.jpcc.7b10265.

(10) Naullage, P. M.; Molinero, V. Slow Propagation of Ice Binding Limits the Ice-Recrystallization Inhibition Efficiency of PVA and Other Flexible Polymers. *J. Am. Chem. Soc.* **2020**, *142* (9), 4356–4366. https://doi.org/10.1021/jacs.9b12943.

(11) Congdon, T.; Notman, R.; Gibson, M. I. Antifreeze (Glyco)Protein Mimetic Behavior of Poly(Vinyl Alcohol): Detailed Structure Ice Recrystallization Inhibition Activity Study. *Biomacromolecules* **2013**, *14* (5), 1578–1586. https://doi.org/10.1021/bm400217j.

(12) DeMerlis, C. C.; Schoneker, D. R. Review of the Oral Toxicity of Polyvinyl Alcohol (PVA). *Food Chem. Toxicol.* **2003**, *41* (3), 319–326.

https://doi.org/10.1016/S0278-6915(02)00258-2.

(13) Deller, R. C.; Vatish, M.; Mitchell, D. A.; Gibson, M. I. Synthetic Polymers Enable Non-Vitreous Cellular Cryopreservation by Reducing Ice Crystal Growth during Thawing. *Nat. Commun.* **2014**, *5*, 1–7. https://doi.org/10.1038/ncomms4244.

(14) Wowk, B.; Leitl, E.; Rasch, C. M.; Mesbah-Karimi, N.; Harris, S. B.; Fahy, G. M. Vitrification Enhancement by Synthetic Ice Blocking Agents. *Cryobiology* **2000**, *40* (3), 228–236. https://doi.org/10.1006/cryo.2000.2243.

(15) Deller, R. C.; Pessin, J. E.; Vatish, M.; Mitchell, D. A.; Gibson, M. I. Enhanced Non-Vitreous Cryopreservation of Immortalized and Primary Cells by Ice-Growth Inhibiting Polymers. *Biomater. Sci.* **2016**, *4* (7), 1079–1084. https://doi.org/10.1039/c6bm00129g.

(16) Nguyen, D. H.; Colvin, M. E.; Yeh, Y.; Feeney, R. E.; Fink, W. H. The Dynamics, Structure, and Conformational Free Energy of Proline-Containing Antifreeze Glycoprotein. *Biophys. J.* **2002**, *82* (6), 2892–2905. https://doi.org/10.1016/S0006-3495(02)75630-0.

(17) Corcilius, L.; Santhakumar, G.; Stone, R. S.; Capicciotti, C. J.; Joseph, S.; Matthews, J. M.; Ben, R. N.; Payne, R. J. Synthesis of Peptides and Glycopeptides with Polyproline II Helical Topology as Potential Antifreeze Molecules. *Bioorg. Med. Chem.* **2013**, *21* (12), 3569–3581. https://doi.org/10.1016/j.bmc.2013.02.025.

(18) Sumii, Y.; Hibino, H.; Saidalimu, I.; Kawahara, H.; Shibata, N. Design and Synthesis of Galactose-Conjugated Fluorinated and Non-Fluorinated Proline Oligomers: Towards Antifreeze Molecules. *Chem. Commun. (Camb).* **2018**, *54* (70), 9749–9752. https://doi.org/10.1039/c8cc05588b.

(19) Mitchell, D. E.; Clarkson, G.; Fox, D. J.; Vipond, R. A.; Scott, P.; Gibson, M. I. Antifreeze Protein Mimetic Metallohelices with Potent Ice Recrystallization Inhibition Activity. *J. Am. Chem. Soc.* **2017**, *139* (29), 9835–9838. https://doi.org/10.1021/jacs.7b05822.

(20) Graham, B.; Bailey, T. L.; Healey, J. R. J.; Marcellini, M.; Deville, S.; Gibson, M. I. Polyproline as a Minimal Antifreeze Protein Mimic That Enhances the

Cryopreservation of Cell Monolayers. *Angew. Chemie Int. Ed.* **2017**, *56* (50), 15941–15944. https://doi.org/10.1002/anie.201706703.

(21) Graham, B.; Bailey, T. L.; Healey, J. R. J.; Marcellini, M.; Deville, S.; Gibson, M. I. Polyproline as a Minimal Antifreeze Protein Mimic That Enhances the Cryopreservation of Cell Monolayers. *Angew. Chem. Int. Ed. Engl.* **2017**, *56* (50), 15941–15944. https://doi.org/10.1002/anie.201706703.

(22) Protein Circular Dichroism Data Bank. CD0004553000. 2016, p CD0004553000.

(23) Lopes, J. L. S.; Miles, A. J.; Whitmore, L.; Wallace, B. A. Distinct Circular Dichroism Spectroscopic Signatures of Polyproline II and Unordered Secondary Structures: Applications in Secondary Structure Analyses. *Protein Sci.* **2014**, *23* (12), 1765–1772. https://doi.org/10.1002/pro.2558.

(24) Matsumura, K.; Hyon, S. H. Polyampholytes as Low Toxic Efficient Cryoprotective Agents with Antifreeze Protein Properties. *Biomaterials* **2009**, *30* (27), 4842–4849. https://doi.org/10.1016/j.biomaterials.2009.05.025.

(25) Matsumura, K.; Bae, J. Y.; Kim, H. H.; Hyon, S. H. Effective Vitrification of Human Induced Pluripotent Stem Cells Using Carboxylated ε-Poly-l-Lysine. *Cryobiology* **2011**, *63* (2), 76–83. https://doi.org/10.1016/j.cryobiol.2011.05.003.

(26) Matsumura, K.; Kawamoto, K.; Takeuchi, M.; Yoshimura, S.; Tanaka, D.; Hyon, S. H. Cryopreservation of a Two-Dimensional Monolayer Using a Slow Vitrification Method with Polyampholyte to Inhibit Ice Crystal Formation. *ACS Biomater. Sci. Eng.* **2016**, *2* (6), 1023–1029. https://doi.org/10.1021/acsbiomaterials.6b00150.

(27) European Food Safety Authority (EFSA), Parma, I. Scientific Opinion on the Safety of “Methyl Vinyl Ether-Maleic Anhydride Copolymer” (Chewing Gum Base Ingredient) as a Novel Food Ingredient. *EFSA J.* **2013**, *11* (3423), 1–17. https://doi.org/10.2903/j.efsa.2013.3423.

(28) Otten, L.; Bailey, T. L.; Stubbs, C.; Murray, K.; Toma, R. M. F.; Gibson, M. I. Synthetically Scalable Poly(Ampholyte) Which Dramatically Enhances Cellular Cryopreservation´, †. **2019**. https://doi.org/10.1021/acs.biomac.9b00681.

(29) Burg, M. B. Molecular Basis of Osmotic Regulation. *Am.J Physiol* **1995**, *268* (6 Pt 2), F983–F996. https://doi.org/10.1152/ajprenal.1995.268.6.F983.

(30) Sangeeta, S.; Arangasamy, A.; Kulkarni, S.; Selvaraju, S. Role of Amino Acids as Additives on Sperm Motility, Plasma Membrane Integrity and Lipid Peroxidation Levels at Pre-Freeze and Post-Thawed Ram Semen. *Anim. Reprod. Sci.* **2015**, *161*, 82–88. https://doi.org/10.1016/j.anireprosci.2015.08.008.

(31) He, S.; Woods, L. C. Effects of Glycine and Alanine on Short-Term Storage and Cryopreservation of Striped Bass (Morone Saxatilis) Spermatozoa. *Cryobiology* **2003**, *46* (1), 17–25. https://doi.org/10.1016/S0011-2240(02)00159-1.

(32) Capicciotti, C. J.; Doshi, M.; Ben, R. N. Ice Recrystallization Inhibitors: From Biological Antifreezes to Small Molecules. In *Recent Developments in the Study of Recrystallization*; InTech, 2013; pp 177–224. https://doi.org/10.5772/54992.

(33) Yamauchi, A.; Uchida, S.; Kwon, H. M.; Preston, A. S.; Robey, R. B.; Garcia-Perez, A.; Burg, M. B.; Handler, J. S. Cloning of a Na(+)- and Cl(-)-Dependent Betaine Transporter That Is Regulated by Hypertonicity. *J. Biol. Chem.* **1992**, *267* (1), 649–652.

(34) Uchida, S.; Yamauchi, A.; Preston, A. S.; Kwon, H. M.; Handler, J. S. Medium Tonicity Regulates Expression of the Na(+)- and Cl(-)-Dependent Betaine Transporter in Madin-Darby Canine Kidney Cells by Increasing Transcription of the Transporter Gene. *J. Clin. Invest.* **1993**, *91* (4), 1604–1607. https://doi.org/10.1172/JCI116367.

(35) Kempson, S. A.; Montrose, M. H. Osmotic Regulation of Renal Betaine Transport: Transcription and Beyond. *Pflugers Arch.* **2004**, *449* (3), 227–234. https://doi.org/10.1007/s00424-004-1338-6.

(36) Burg, M. B.; Ferraris, J. D.; Dmitrieva, N. I. Cellular Response to Hyperosmotic Stresses. *Physiol. Rev.* **2007**, *87* (4), 1441–1474. https://doi.org/10.1152/physrev.00056.2006.

(37) Figueroa-Soto, C. G.; Valenzuela-Soto, E. M. Glycine Betaine Rather than Acting Only as an Osmolyte Also Plays a Role as Regulator in Cellular Metabolism. *Biochimie* **2018**, *147*, 89–97. https://doi.org/10.1016/j.biochi.2018.01.002.

(38) Ziyadeh, F. N.; Mills, J. W.; Kleinzeller, A. Hypotonicity and Cell Volume Regulation in Shark Rectal Gland: Role of Organic Osmolytes and F-Actin. *Am. J.*

Physiol. **1992**, *262* (3 Pt 2), F468-79. https://doi.org/10.1152/ajprenal.1992.262.3.F468.

(39) Nakanishi, T.; Balaban, R. S.; Burg, M. B. Survey of Osmolytes in Renal Cell Lines. *Am. J. Physiol.* **1988**, *255* (2 Pt 1), C181-91. https://doi.org/10.1152/ajpcell.1988.255.2.C181.

(40) Petronini, P. G.; De Angelis, E. M.; Borghetti, P.; Borghetti, A. F.; Wheeler, K. P. Modulation by Betaine of Cellular Responses to Osmotic Stress. *Biochem. J.* **1992**, *282 (Pt 1* (1), 69–73. https://doi.org/10.1042/bj2820069.

(41) Lloyd, A. W.; Olliff, C. J.; Rutt, K. J. A Study of Modified Betaines as Cryoprotective Additives. *J. Pharm. Pharmacol.* **1994**, *46* (9), 704–707. https://doi.org/10.1111/j.2042-7158.1994.tb03887.x.

(42) Yang, J.; Cai, N.; Zhai, H.; Zhang, J.; Zhu, Y.; Zhang, L. Natural Zwitterionic Betaine Enables Cells to Survive Ultrarapid Cryopreservation. *Sci. Rep.* **2016**, *6* (1), 37458. https://doi.org/10.1038/srep37458.

(43) Chakrabarti, A. C. Permeability of Membranes to Amino Acids and Modified Amino Acids: Mechanisms Involved in Translocation. *Amino Acids* **1994**, *6* (3), 213–229. https://doi.org/10.1007/BF00813743.

(44) Vilella, S.; Ahearn, G. A.; Cassano, G.; Storelli, C. Na-Dependent L-Proline Transport by Eel Intestinal Brush-Border Membrane Vesicles. *Am. J. Physiol.* **1988**, *255* (4 Pt 2), R648-53. https://doi.org/10.1152/ajpregu.1988.255.4.R648.

(45) Franěk, F.; Srámková, K. Cell Suicide in Starving Hybridoma Culture: Survival-Signal Effect of Some Amino Acids. *Cytotechnology* **1997**, *23* (1–3), 231–239. https://doi.org/10.1023/B:CYTO.0000010400.89582.b8.

(46) Takagi, H.; Sakai, K.; Morida, K.; Nakamori, S. Proline Accumulation by Mutation or Disruption of the Proline Oxidase Gene Improves Resistance to Freezing and Desiccation Stresses in Saccharomyces Cerevisiae. *FEMS Microbiol. Lett.* **2000**, *184* (1), 103–108. https://doi.org/10.1016/S0378-1097(00)00023-9.

(47) Grothe, S.; Krogsrud, R. L.; McClellan, D. J.; Milner, J. L.; Wood, J. M. Proline Transport and Osmotic Stress Response in Escherichia Coli K-12. *J. Bacteriol.* **1986**, *166* (1), 253–259. https://doi.org/10.1128/jb.166.1.253-259.1986.

(48) Koštál, V.; Šimek, P.; Zahradníčková, H.; Cimlová, J.; Štětina, T. Conversion of the Chill Susceptible Fruit Fly Larva (Drosophila Melanogaster) to a Freeze Tolerant Organism. *Proc. Natl. Acad. Sci. U. S. A.* **2012**, *109* (9), 3270–3274. https://doi.org/10.1073/pnas.1119986109.

(49) Zhang, L.; Xue, X.; Yan, J.; Yan, L.-Y.; Jin, X.-H.; Zhu, X.-H.; He, Z.-Z.; Liu, J.; Li, R.; Qiao, J. Cryobiological Characteristics of L-Proline in Mammalian Oocyte Cryopreservation. *Chin. Med. J. (Engl).* **2016**, *129* (16), 1963–1968. https://doi.org/10.4103/0366-6999.187846.

(50) Yang, J.; Pan, C.; Zhang, J.; Sui, X.; Zhu, Y.; Wen, C.; Zhang, L. Exploring the Potential of Biocompatible Osmoprotectants as Highly Efficient Cryoprotectants. *ACS Appl. Mater. Interfaces* **2017**, *9* (49), 42516–42524. https://doi.org/10.1021/acsami.7b12189.

(51) Bailey, T. L.; Wang, M.; Solocinski, J.; Nathan, B. P.; Chakraborty, N.; Menze, M. A. Protective Effects of Osmolytes in Cryopreserving Adherent Neuroblastoma (Neuro-2a) Cells. *Cryobiology* **2015**, *71* (3), 472–480. https://doi.org/10.1016/j.cryobiol.2015.08.015.

(52) Koshimoto, C.; Mazur, P. Effects of Warming Rate, Temperature, and Antifreeze Proteins on the Survival of Mouse Spermatozoa Frozen at an Optimal Rate. *Cryobiology* **2002**, *45* (1), 49–59. https://doi.org/10.1016/S0011-2240(02)00105-0.

(53) Deller, R. C.; Vatish, M.; Mitchell, D. A.; Gibson, M. I. Synthetic Polymers Enable Non-Vitreous Cellular Cryopreservation by Reducing Ice Crystal Growth during Thawing. *Nat. Commun.* **2014**, *5*, 3244. https://doi.org/10.1038/ncomms4244.

(54) Knight, C. A.; Hallett, J.; DeVries, A. L. Solute Effects on Ice Recrystallization: An Assessment Technique. *Cryobiology* **1988**, *25* (1), 55–60. https://doi.org/10.1016/0011-2240(88)90020-X.

(55) Biggs, C. I.; Stubbs, C.; Graham, B.; Fayter, A. E. R.; Hasan, M.; Gibson, M. I. Mimicking the Ice Recrystallization Activity of Biological Antifreezes. When Is a New Polymer “Active”? *Macromol. Biosci.* **2019**, *1900082*, 1900082. https://doi.org/10.1002/mabi.201900082.

(56) Mitchell, D. E.; Gibson, M. I. Latent Ice Recrystallization Inhibition Activity in

Nonantifreeze Proteins: Ca2+-Activated Plant Lectins and Cation-Activated Antimicrobial Peptides. *Biomacromolecules* **2015**, *16* (10), 3411–3416. https://doi.org/10.1021/acs.biomac.5b01118.

(57) Capicciotti, C. J.; Leclère, M.; Perras, F. A.; Bryce, D. L.; Paulin, H.; Harden, J.; Liu, Y.; Ben, R. N. Potent Inhibition of Ice Recrystallization by Low Molecular Weight Carbohydrate-Based Surfactants and Hydrogelators. *Chem. Sci.* **2012**, *3* (5), 1408–1416. https://doi.org/10.1039/c2sc00885h.

(58) Wu, S.; Zhu, C.; He, Z.; Xue, H.; Fan, Q.; Song, Y.; Francisco, J. S.; Zeng, X. C.; Wang, J. Ion-Specific Ice Recrystallization Provides a Facile Approach for the Fabrication of Porous Materials. *Nat. Commun.* **2017**, *8* (May), 15154. https://doi.org/10.1038/ncomms15154.

(59) Surís-Valls, R.; Voets, I. K. The Impact of Salts on the Ice Recrystallization Inhibition Activity of Antifreeze (Glyco)Proteins. *Biomolecules* **2019**, *9* (8), 347. https://doi.org/10.3390/biom9080347.

(60) Lee, H. Effects of Hydrophobic and Hydrogen-Bond Interactions on the Binding Affinity of Antifreeze Proteins to Specific Ice Planes. *J. Mol. Graph. Model.* **2019**, *87*, 48–55. https://doi.org/10.1016/j.jmgm.2018.11.006.

(61) Shao, Q.; Jiang, S. Molecular Understanding and Design of Zwitterionic Materials. *Adv. Mater.* **2015**, *27* (1), 15–26. https://doi.org/10.1002/adma.201404059.

(62) Troitzsch, R. Z.; Vass, H.; Hossack, W. J.; Martyna, G. J.; Crain, J. Molecular Mechanisms of Cryoprotection in Aqueous Proline: Light Scattering and Molecular Dynamics Simulations. *J. Phys. Chem. B* **2008**, *112* (14), 4290–4297. https://doi.org/10.1021/jp076713m.

(63) Schawe, J. E. K.; Löffler, J. F. Existence of Multiple Critical Cooling Rates Which Generate Different Types of Monolithic Metallic Glass. *Nat. Commun.* **2019**, *10* (1), 1337. https://doi.org/10.1038/s41467-018-07930-3.

(64) Lewis, G. N. .; Randall, M. Thermodynamics. *J. Chem. Educ.* **1962**, *39* (1), 53. https://doi.org/10.1021/ed039p53.1.

(65) Fullerton, G. D.; Keener, C. R.; Cameron, I. L. Correction for Solute/Solvent Interaction Extends Accurate Freezing Point Depression Theory to High

Concentration Range. *J. Biochem. Biophys. Methods* **1994**, *29* (3–4), 217–235. https://doi.org/10.1016/0165-022x(94)90034-5.

(66) Murthy, S. S. N. Some Insight into the Physical Basis of the Cryoprotective Action of Dimethyl Sulfoxide and Ethylene Glycol. *Cryobiology* **1998**, *36* (2), 84–96. https://doi.org/10.1006/cryo.1997.2064.

(67) MacKenzie, A. P. Non-Equilibrium Freezing Behaviour of Aqueous Systems. *Philos. Trans. R. Soc. Lond. B. Biol. Sci.* **1977**, *278* (959), 167–189. https://doi.org/10.1098/rstb.1977.0036.

(68) MacKenzie, A. P. MODELLING THE ULTRA-RAPID FREEZING OF CELLS AND TISSUES. In *Microprobe Analysis of Biological Systems*; HUTCHINSON, T. E., SOMLYO, A. P. B. T.-M. A. of B. S., Eds.; Elsevier, 1981; pp 397–421. https://doi.org/10.1016/B978-0-12-362880-0.50028-4.

(69) Liu, W.; Huang, Z.; He, X.; Jiang, P.; Huo, X.; Lu, Z.; Liu, B. Impacts of Trehalose and L-Proline on the Thermodynamic Nonequilibrium Phase Change and Thermal Properties of Normal Saline. *Cryobiology* **2020**. https://doi.org/10.1016/j.cryobiol.2020.07.011.

(70) Han, B.; Bischof, J. C. Direct Cell Injury Associated with Eutectic Crystallization during Freezing. *Cryobiology* **2004**, *48* (1), 8–21. https://doi.org/10.1016/j.cryobiol.2003.11.002.

(71) Meryman, H. T. Review of Biological Freezing. *Cryobiology* **1966**, 1–114.

(72) Izutsu, K.; Yoshioka, S.; Kojima, S. Effect of Cryoprotectants on the Eutectic Crystallization of NaCl in Frozen Solutions Studied by Differential Scanning Calorimetry (DSC) and Broad-Line Pulsed NMR. *Chem. Pharm. Bull. (Tokyo).* **1995**, *43* (10), 1804–1806. https://doi.org/10.1248/cpb.43.1804.

(73) Hansen, T. N.; Carpenter, J. F. Calorimetric Determination of Inhibition of Ice Crystal Growth by Antifreeze Protein in Hydroxyethyl Starch Solutions. *Biophys. J.* **1993**, *64* (6), 1843–1850. https://doi.org/10.1016/S0006-3495(93)81555-8.

(74) Bryant, G. DSC Measurement of Cell Suspensions during Successive Freezing Runs: Implications for the Mechanisms of Intracellular Ice Formation. *Cryobiology* **1995**, *32* (2), 114–128. https://doi.org/10.1006/cryo.1995.1011.

(75) Rudolph, A. S.; Crowe, J. H. A Calorimetric and Infrared Spectroscopic Study of the Stabilizing Solute Proline. *Biophys. J.* **1986**, *50* (3), 423–430. https://doi.org/10.1016/S0006-3495(86)83478-6.

(76) Koštál, V.; Korbelová, J.; Poupardin, R.; Moos, M.; Šimek, P. Arginine and Proline Applied as Food Additives Stimulate High Freeze Tolerance in Larvae of Drosophila Melanogaster. *J. Exp. Biol.* **2016**, *219* (Pt 15), 2358–2367. https://doi.org/10.1242/jeb.142158.

(77) Rozsypal, J.; Moos, M.; Šimek, P.; Koštál, V. Thermal Analysis of Ice and Glass Transitions in Insects That Do and Do Not Survive Freezing. *J. Exp. Biol.* **2018**, *221* (Pt 7). https://doi.org/10.1242/jeb.170464.

(78) Wilson, P. W.; Arthur, J. W.; Haymet, A. D. J. Ice Premelting during Differential Scanning Calorimetry. *Biophys. J.* **1999**, *77* (5), 2850–2855. https://doi.org/10.1016/S0006-3495(99)77116-X.

(79) Schneider, C. A.; Rasband, W. S.; Eliceiri, K. W. NIH Image to ImageJ: 25 Years of Image Analysis. *Nat. Methods* **2012**, *9* (7), 671–675. https://doi.org/10.1038/nmeth.2089.

(80) Adzhubei, A. A.; Sternberg, M. J. E.; Makarov, A. A. Polyproline-II Helix in Proteins: Structure and Function. *J. Mol. Biol.* **2013**, *425* (12), 2100–2132. https://doi.org/10.1016/j.jmb.2013.03.018.

(81) Wilhelm, P.; Lewandowski, B.; Trapp, N.; Wennemers, H. A Crystal Structure of an Oligoproline PPII-Helix, at Last. *J. Am. Chem. Soc.* **2014**, *136* (45), 15829–15832. https://doi.org/10.1021/ja507405j.

(82) Mikhonin, A. V; Myshakina, N. S.; Bykov, S. V; Asher, S. A.; Pennsyl, V. UV Resonance Raman Determination of Polyproline II , Extended 2 . 5 1 -Helix , and -Sheet Ψ Angle Energy Landscape in Poly- L -Lysine and Poly- L -Glutamic Acid. *J. Am. Chem. Soc.* **2005**, *127*, 7712–7720.

CHAPTER 3

3. BIOCOMPATIBILITY OF MOLECULAR AND MACROMOLECULAR COMPOUNDS ON A549 CELLS

3.1 DECLARATIONS

All polyampholyte polymers were synthesised by Dr Christopher Stubbs and all polyproline polymers were synthesised by Dr Ben Graham, both under the supervision of Prof Matthew Gibson.

3.2 CHAPTER SUMMARY

In examining potential cryoprotective agents, the ability of these compounds to provide protection without introducing down-stream ill effects of their own is vital. Here we show the compatibility of three macromolecular cryoprotectants that do not reduce cell metabolism when used for a CPA exposure time of 10 min, which aligns with the cryopreservation conditions used throughout this thesis. We additionally show that our small molecule osmolytes do not show cell cytotoxicity for incubation times up to 24 h. Only one small molecule, proline, was shown to down-regulate cell growth, and growth was shown to be recoverable to normal levels when the proline solution was removed, which may help explain its cryoprotective benefit.

3.3 INTRODUCTION

The aim of this chapter was to understand how our macromolecular cryoprotectants and molecular osmolytes affect cells at physiological conditions and to examine cytotoxicity and proliferation. The ideal test for *in vitro* cytotoxicity is a simple, rapid, efficient, reliable, and cost-effective measurement of cell viability and additionally should not interfere with the compound being tested. AlamarBlue has been widely used over the past 50 years in studies on cell viability and cytotoxicity in a range of biological systems and is one of the most highly referenced substances used for cytotoxicity and viability assays according to PubMed records.[1] AlamarBlue monitors the reducing environment of the living cell. The active ingredient is resazurin (IUPAC name: 7-hydroxy-10-oxidophenoxazin-10-ium-3-one), also known as diazo-resorcinol, azoresorcin, resazoin, or resazurine, which is water-soluble, stable in culture medium, is non-toxic, and permeable through cell membranes.[1] The oxidised, blue, non-fluorescent alamarBlue is reduced to a pink fluorescent dye in the medium by cell activity (likely by oxygen consumption through metabolism).[2] The reduced form, resorufin, is pink and highly fluorescent, and the intensity of the pink colour or fluorescence produced is proportional to the number of living cells respiring. Through detecting the level of reduction during respiration, alamarBlue acts as a direct indicator to quantitatively measure cell viability and cytotoxicity. Spectrophotometric absorbance is taken at two wavelengths (570 and 600 nm).

Since organisms that undergo seasonal exposure to environmental stresses utilise downregulation of metabolism to enter a hypometabolic state (diapause),[3] it follows that we would want to explore if these processes were taking place due to the presence of osmolytes. Metabolic depression and cell stasis are often prerequisites to survival for animals whose evolutionary history has provided natural adaptations to desiccation, freezing temperatures, and anoxia.[4] It has also

been shown that a requirement for freezing survival in both *Caenorhabditis elegans*[5] and *Drosophila melanogaster*[6] is a reduction in metabolic activity. Therefore, we wanted to investigate how incubation with compatible osmolytes affected the proliferation of cells. This was accomplished by simply counting the cells daily throughout a long exposure osmolyte incubation. For a more detailed analysis, we conducted cell cycle analysis to determine if down-regulation or stasis may be occurring.

It is important to understand how any compounds used in the presence of cells will impact those cells under ideal physiological conditions in order to establish a baseline of compound influence. We will evaluate the impact of metabolic activity via alamarBlue reduction to evaluate the potential cytotoxicity of our compounds. In order to evaluate the proliferation impacts of our compounds, we will conduct long-term growth assays of cells incubated in the compounds for the duration of the assay. The specific aims of this chapter were to evaluate if (i) any of our macromolecular cryoprotectants or molecular osmolytes were inherently toxic to our cells and the working ranges thereof, (ii) the osmolytes affected the proliferation rate of cells. The results of this chapter will allow us to identify any potential downstream issues that may result from the cells being in contact with the compound of interest, such as reduced metabolism or up/down-regulation of growth.

3.4 RESULTS AND DISCUSSION

3.4.1 Cytotoxicity

In evaluating the impact the compounds had on A549 cell metabolism as a means of cytotoxicity screening, it is important to note that DMSO, the most common cryoprotective agent (CPA), is cytotoxic at room temperature and high concentrations.[7] In evaluating the cytotoxicity of our macromolecular

cryoprotectants we were not looking to rule out a particular compound but rather to understand how these polymers may be interacting with our cells. Since our polymers will be functioning in a CPA capacity, we tested two incubation times, exposure for 10 min (thereafter replaced with cell media) along with an extreme exposure of 24 h. The 10 min exposure was to replicate the CPA exposure time in our monolayer protocol with a 24 h extreme exposure to test severe responses. The osmolyte compounds will only be utilised for a 24 h incubation treatment as CPAs, and were assayed as such. Following the incubation periods, cells were treated with a 1% alamarBlue (resazurin) solution. Control cells were measured in tandem with experimental cells and values were normalised based on control values of 100% reduction. Less reduction represents less metabolism and thus suggests cell damage.

3.4.1.1 PVA Cytotoxicity

We first investigated PVA toxicity on A549 cells for 10 min and 24 h and compared these results to cells exposed to 10% DMSO. Normalised alamarBlue reduction for all concentrations of PVA was not significantly different from control cells (0 mM) after a 10 min incubation, however, 10% DMSO did show significantly less reduction following a 10 min exposure (Fig 3.1, $n \geq 3$, $P = 0.0000000001$). For our 24 h incubation, PVA led to lower alamarBlue reduction when treated at 1, 2, and 10 $mg \cdot mL^{-1}$. However, this 24 h PVA reduction was not extreme and was comparable to cells treated with 10% DMSO for 10 min. Cells exposed for 24 h to 10% DMSO had a significantly lower alamarBlue reduction of only 31.9%. This correlates with previous data showing that PVA is non-toxic at up to 20 $mg \cdot mL^{-1}$ concentrations[8] as PVA is regularly utilised in eye drops and is FDA approved. We have shown that PVA was non-toxic for the exposure time of

a CPA (10 min) and only minimally reduced metabolic activity when incubated for 24 h (an extreme exposure time).

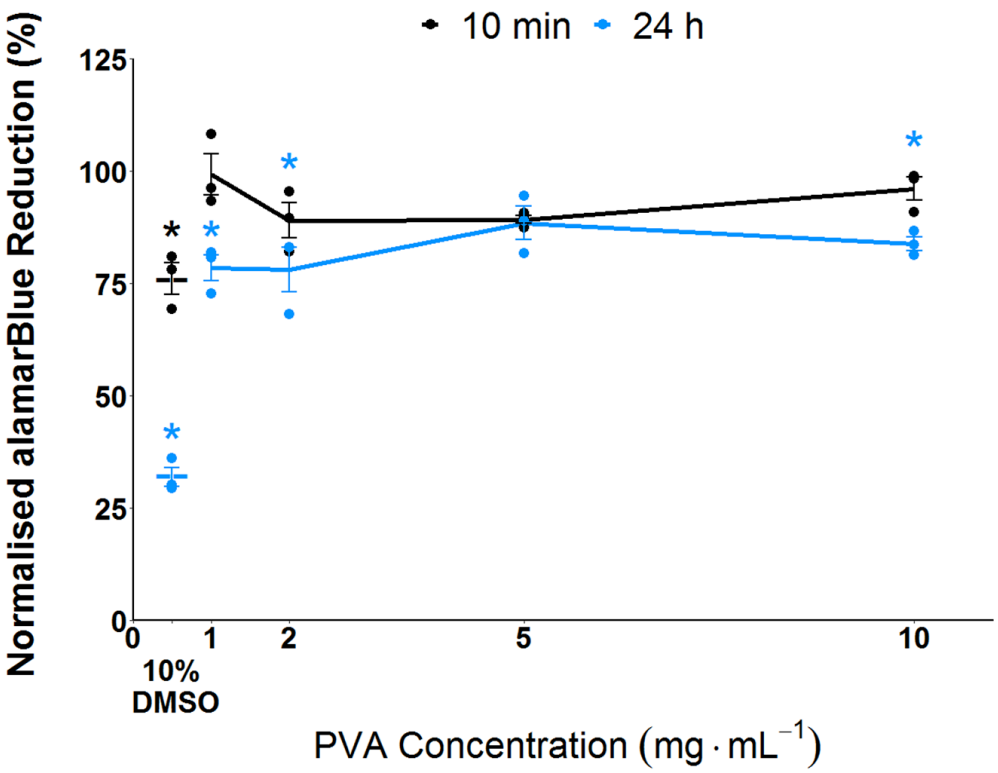

Figure 3.1. A549 PVA cytotoxicity. Average normalised alamarBlue reduction for 10 min and 24 h. * P < 0.0001 from control (0 mM). Error bars represent ± SEM of at least 3 independent experiments.

3.4.1.2 Polyproline Cytotoxicity

Following our screen using PVA, we next wanted to understand how polyproline may affect cell metabolism. Utilising varying concentrations of poly(L-proline) with a 10 min incubation, we did not see significant differences from control cells (0 mM). However, we did see significantly less metabolic activity for concentrations above 1 mg·mL^{-1} poly(L-proline) when incubated for 24 h (Fig 3.2, $n \geq 3$, $P = 0.0000000001$). To evaluate if poly(L-proline) was causing a specific cell response to reduce metabolic activity, we also tested the isomer of poly(L-proline), poly(D-proline). Similar to poly(L-proline), incubating cells in poly(D-

proline) for 24 h showed significantly lower alamarBlue reduction for concentrations above 5 mg·mL^{-1} compared to untreated control cells, suggesting the reduction in metabolic activity was not an isomer specific effect. We have found that poly(L-proline) was non-toxic for the exposure time of a CPA (10 min) and reduced metabolic activity similar to 10% DMSO when incubated for 24 h (an extreme exposure time) when used at concentrations above 5 mg·mL^{-1}.

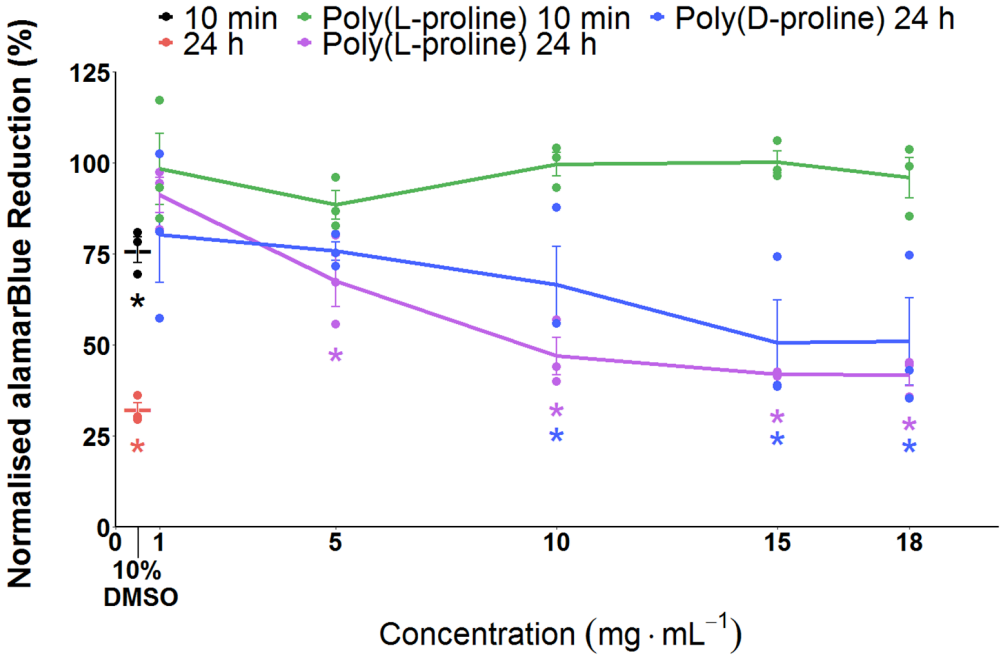

Figure 3.2. A549 polyproline cytotoxicity. Average normalised alamarBlue reduction for 10 min and 24 h. * P < 0.0001 from control (0 mM). Error bars represent ± SEM of at least 3 independent experiments.

3.4.1.3 Polyampholyte Cytotoxicity

Testing the cytotoxicity of our final novel macromolecular cryoprotectant, polyampholyte P2 (M_n = 80 kDa), we saw no difference in reduction for cells incubated with varying concentrations of polyampholyte for 10 min compared to control cells (0 mM) (Fig 3.3, $n \geq 3$, $P = 0.0000000003$). For our 24 h incubation, we saw significant reductions for concentrations higher than 10 mg·mL^{-1}, with

reductions falling midway between reductions seen for 10% DMSO at 10 min and 24 h. This suggests that polyampholyte P2 is non-toxic for the exposure time of a CPA (10 min) and only minimally reduced metabolic activity when incubated for 24 h at high concentrations.

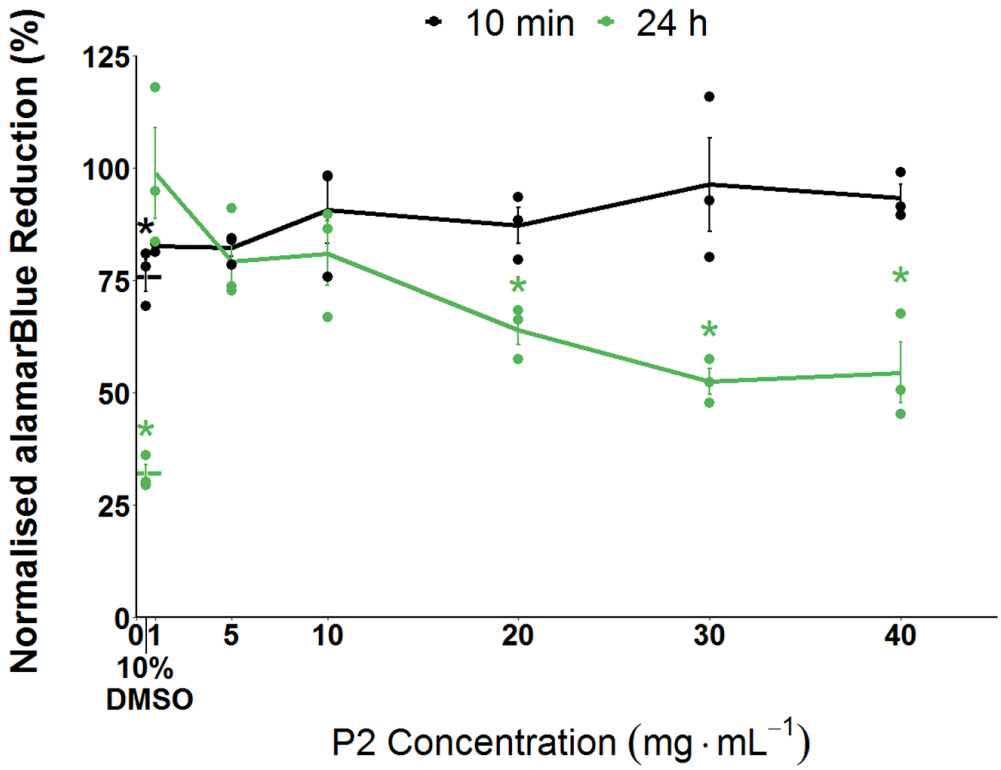

Figure 3.3. A549 polyampholyte P2 cytotoxicity. Average normalised alamarBlue reduction for 10 min and 24 h. * P < 0.0001 from control (0 mM). Error bars represent ± SEM of at least 3 independent experiments.

3.4.1.4 Combined Osmolyte Cytotoxicity

Following analysis of our macromolecular compounds, we next tested the effect our small molecular osmolytes had on cell metabolic activity. We first tested our osmolyte solutions individually for alamarBlue reduction (Fig 3.10-3.12). F-12K media contains 0.2 mM alanine and 0.6 mM proline and the concentrations listed in our assays are in addition to the pre-existing osmolytes in the base cell media formulation. Combining the individual results for comparison, we saw that alamarBlue reduction of A549 cells incubated for 24 h with varying concentrations

of osmolytes showed no significant difference in reduction compared to control (F-12K 0 mM) (Fig 3.4, *n* = 3). These results were somewhat unsurprising, as compatible solutes are highly soluble organic compounds of low molecular weight that maintain osmotic balance (osmoregulation) without interfering with cell metabolism.[9] We have shown that incubation with osmolytes for 24 h did not alter the metabolic capabilities of the cells compared to control and thus appear to be non-toxic to our cell monolayers.

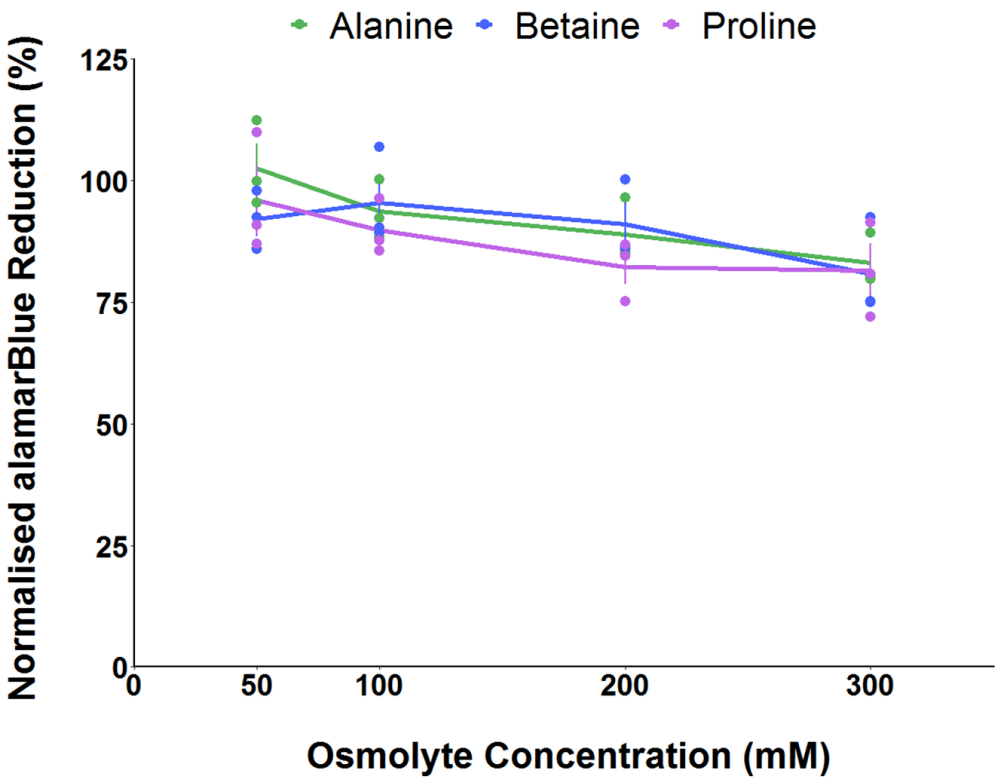

Figure 3.4. A549 osmolyte cytotoxicity. Average normalised alamarBlue reduction after 24 h incubation. Error bars represent ± SEM of 3 independent experiments.

This section has demonstrated that our macromolecular cryoprotectants are not toxic to A549 cells when used for the CPA duration time of 10 min. PVA showed minimal toxicity for longer exposure times, polyproline showed reduced reductions similar to 10% DMSO for long exposure, and polyampholyte showed

lower reduction at high concentrations. It should be noted that DMSO is redox reactive, as several DMSO reductases exist,[10] however all compounds were assayed without cells and no alamarBlue reduction was observed (data not shown). Osmolytes showed no significant difference from control cells when incubated for 24 h at concentrations up to and including 300 mM. These findings illustrate the well-known compatibility of these osmolytes and show the suitability of these small molecules for the investigation of their cryoprotective effects.

3.4.2 Growth in the Presence of Osmolytes

We next evaluated how the cells grew (proliferated) while incubated in the osmolyte solutions. Since the cells would be incubated for 24 h in the solutions prior to cryopreservation, we wanted to assess if any up- or down-regulation of cell growth was taking place during this incubation period and we were particularly interested in any down-regulated cell growth, as Chapter 1 explained that stasis is a requirement for some organisms to survive extreme conditions.

To determine cell growth, cells were plated at an identical density and counted each day (starting with day 2) to obtain cell numbers. Starting density was $12.5 \cdot 10^3$ per well in 6-well plates to allow cells enough room to grow for the duration of the experiment and not become confluent but allow enough cells to be initially plated as to not cause growth arrest due to a low-density environment. Cells were counted using trypan blue exclusion[11] with a hemocytometer. Trypan blue is impermeable to cells with intact membranes and will only be taken up by dead cells with porous membranes, therefore reliable counts of live cells can be obtained. Healthy cells grow in an exponential fashion and the formula for this growth is listed in Equation 3.1.

$$N(t) = N(0)\mathrm{e}^{(\mathrm{rt})}$$

N(t) = number of cells at time (day)
N(0) = number of cells at time zero (initially plated)
r = rate of growth
t = time (day)

Equation 3.1. Equation for exponential cell growth.

Since we are interested in the growth rate of our cells, we can solve for r utilising Equation 3.2 to establish a rate of growth for each of the incubation conditions. A rate of 0 would indicate no change in cell growth from the previous day while a rate of 1 would indicated a complete doubling of the cells from the previous day, negative rates would indicated less cells present than the previous day.

$$r = \frac{\ln\left({}^{N(t)}/_{N(0)}\right)}{t}$$

N(t) = number of cells at time (day)
N(0) = number of cells at time zero (initially plated)
r = rate of growth
t = time (day)

Equation 3.2. Equation for cell growth rate.

We evaluated the 6-day fold change of our cells in individual osmolyte solutions (alanine, betaine and proline) (Fig 3.13-3.15). Combining the results for comparison, we found control cells to have a day 6 rate of growth of 0.68 – 0.71 (Fig 3.5, n = 3, P = 0.00012). Alanine and betaine had comparable rates of 0.62 – 0.70 and 0.71 – 0.78, respectively. Proline had a significantly lower rate of 0.47 – 0.54 compared to control cells.

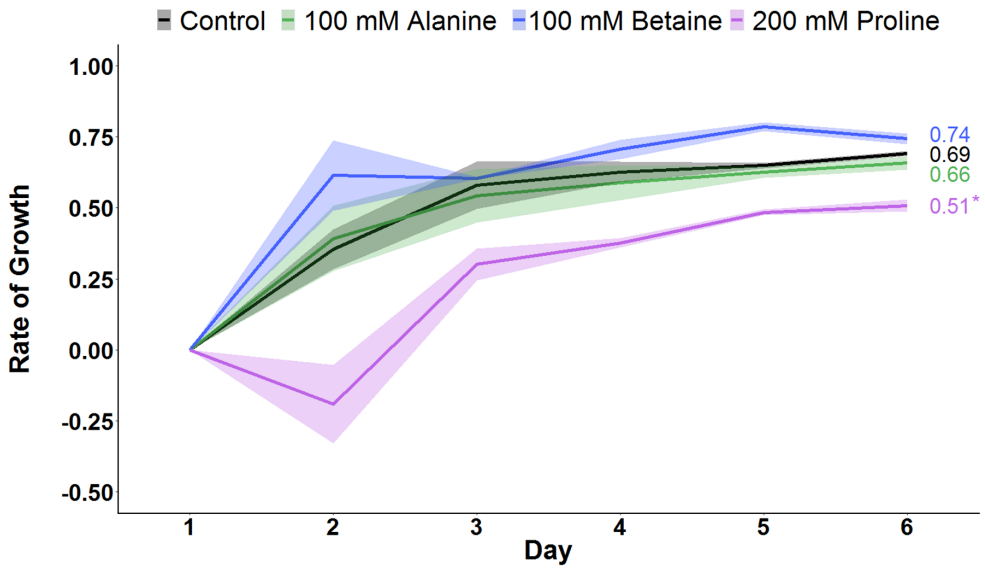

Figure 3.5. A549 osmolyte incubation rate of growth. Growth rates after incubation with F-12K (black) or osmolyte (alanine=green, betaine=blue, proline=purple) for 6 days. Error represents ± SEM of 3 independent experiments.

We also tested for long term effects, or how recoverable the change in regulation would be, if there was one. For this, cells were incubated in the osmolytes for 3 days and then the osmolyte solution was replaced with complete cell media, then cell counts were performed for the subsequent 3 days. We found control cells to have a day 6 rate of growth of 0.38 – 0.41 (Fig 3.6, n = 3, P = 0.01). Alanine and betaine had comparable rates of 0.42 – 0.44 and 0.40 – 0.46, respectively. Proline had a significantly higher rate of 0.45 – 0.52 compared to control cells. This shows that the reduced growth seen for the proline incubated cells is reversible and cells recovery quickly to proliferate faster than control cells. Conducting this experiment in the future, it would be wise to include the previous day counts (days 1-3) to analyse trends from when the osmolyte solutions are replaced.

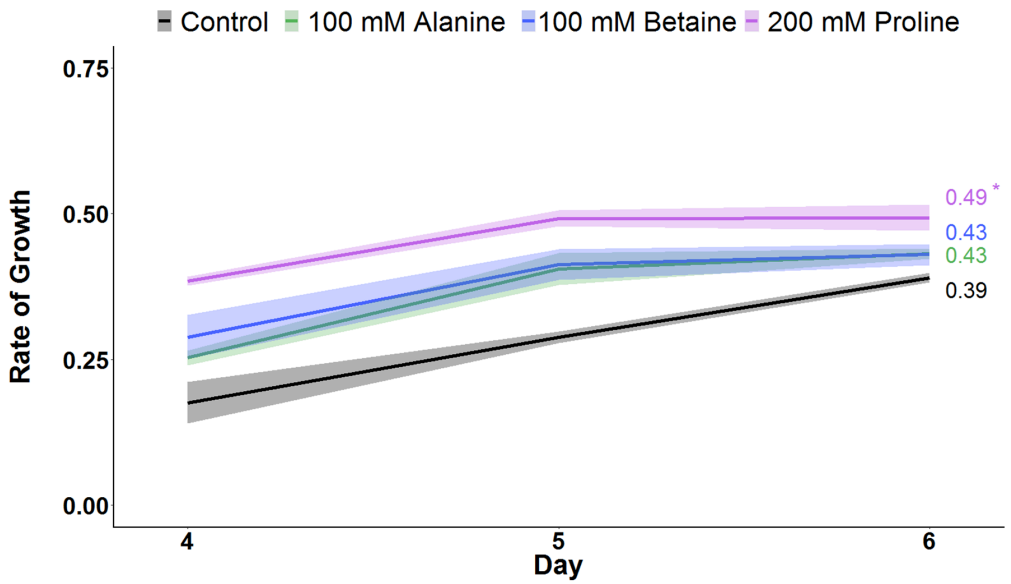

Figure 3.6. A549 osmolyte recovery growth rates. Growth rates after incubation with F-12K for 6 days (black) or osmolyte for 3 days (alanine=green, betaine=blue, proline=purple) then F-12K media for 3 days. Error represents ± SEM of 3 independent experiments.

Alanine has been shown to reduce cell proliferation in epithelial cells,[12] yet showed increased proliferation in thymocyte lobes,[13] however, our cells were not effected in either direction as they did not significantly differ from control when grown in the presence of alanine. Betaine has been shown to reduce the proliferation of HeLa (cervical cancer)[14] and DU-145 (prostate cancer)[15] cells, and most surprising, betaine was shown to suppress tumour formation of A549 cells *in vivo*.[16] Our results differ from these, as our cells, in the presence of betaine, grew much faster than control cells. Proline has been shown to be essential for proliferation in hepatocyte cells in culture[17] and increases the proliferation of embryonic stem (ES) cells.[18] However, proline catabolism effects seem to be dependent on metabolic context and the switches for these responses remain unknown.[19] One explanation for the suppressed growth of our proline-incubated cells comes from P493 (B lymphoma) cells incubated in proline which experience growth inhibition, and thus, results in the proline biosynthesis (PB) pathway being down-regulated with a downstream effect on the glycolytic pathway (Fig 3.7).[20]

This suggests that the lower proliferation rate we see may not be the proline itself, but rather the effects of the PB pathway not running due to an increase in the available free proline, which would be very interesting to evaluate in the future.

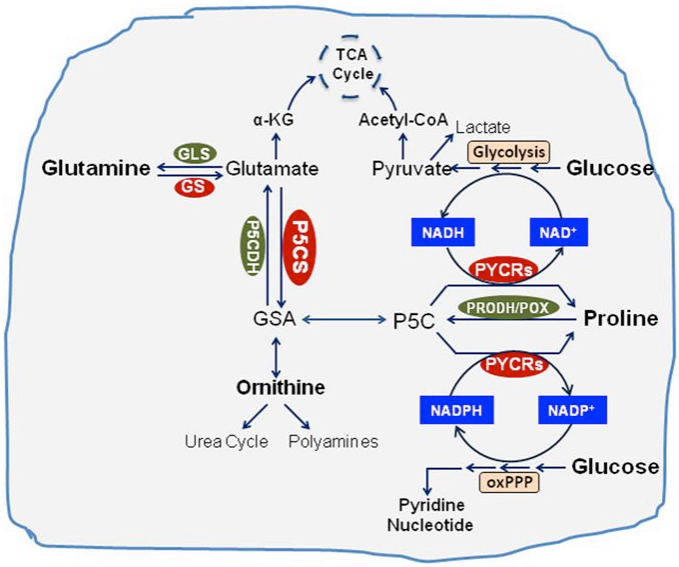

Figure 3.7. Proline biosynthesis from glutamine in cancer cells promotes cell growth through interacting with glycolysis and oxidative arm of pentose phosphate pathway. P5C, Δ^1-pyrroline-5-carboxylate; GSA, glutamic-gamma-semialdehyde; GLS, glutaminase; GS, glutaminesynthase; P5CS, pyrroline-5-carboxylatesynthase; P5CDH, pyrroline-5-carboxylatedehydrogenase; PRODH/POX, proline dehydrogenase/oxidase; PYCR1/2, pyrroline-5-carboxylatereductase1, and 2; PYCRL, pyrroline-5-carboxylatereductase L. oxPPP, oxidative arm of pentose phosphate pathway. Reprinted from Liu (2015).[20]

3.5 Conclusion

We have shown that none of our macromolecular cryoprotectants were toxic to our cells for a 10 min exposure and none of our osmolytes were toxic to the cells after 24 hours. This is promising, as these timescales were chosen as they reflect those used in monolayer cryopreservation protocols; the intended application for our compounds. DMSO was shown to significantly reduce alamarBlue reduction following a 24 h exposure and all of our potential cryoprotective agents performed better than DMSO. Proline was the only osmolyte to affect the growth of our cells,

significantly down-regulating growth during incubation, this is most likely due to the proline biosynthesis pathway not running due to the excess of available proline. Our results have been summarised in Table 3.1. As osmolarity is a key area of damage for cells during cryopreservation, the next step in this work would be to evaluate the osmotic parameters of the cells in the presence of our compounds as well as an osmotic stress assay to evaluate if any of our compounds have the ability to protect cells from stressful osmotic conditions. Having established the effects of our compounds on cell toxicity and proliferation, our next chapter sought to understand how these compounds faired as cryoprotective agents.

Table 3.1. Chapter 3 results summary. Control = F-12K. Significantly higher than control, significantly lower than control.

Target	alamarBlue Reduction (24 h) (%) ↑	Incubation Rate of Growth (Day 6)	Recovery Rate of Growth (Day 6)
Control	100	0.69	0.39
10% DMSO	**31.9**		
5 mg·mL^{-1} PVA	88.3	–	–
5 mg·mL^{-1} Polyproline	**67.5**	–	–
5 mg·mL^{-1} P2 Polyampholyte	79.1	–	–
100 mM Alanine	93.5	0.66	0.43
100 mM Betaine	95.4	0.74	0.43
200 mM Proline	82.1	**0.51**	**0.49**

3.6 Materials and Methods

3.6.1 Reagents

All non-specified chemicals were obtained from Sigma Aldrich Co Ltd, (Irvine, UK).

Polyproline was synthesised as in Section 2.6.1.1.

Polyampholyte was synthesised as in Section 2.6.1.2.

3.6.2 A549 Cell Culture

Human Caucasian lung carcinoma cells (A549) were obtained from the European Collection of Authenticated Cell Cultures (ECACC) (Salisbury, UK) and grown in 175 cm^2 cell culture Nunc flasks (Corning Incorporated, Corning, NY). Standard cell culture medium was composed of Ham's F-12K (Kaighn's) Medium (F-12K) (Gibco, Paisley, UK) supplemented with 10% USA-origin fetal bovine serum (FBS) purchased from Sigma Aldrich (Dorset, UK), 100 units·mL^{-1} penicillin, 100 µg·mL^{-1} streptomycin, and 250 ng·mL^{-1} amphotericin B (PSA) (HyClone, Cramlington, UK). F-12K contains 0.2 mM alanine, 0.6 mM proline and has an osmolarity of 275 to 357 mOsm·kg^{-1}. A549 cells were maintained in a humidified atmosphere of 5% CO_2 and 95% air at 37 °C and the culture medium was renewed every 3–4 days. The cells were subcultured every 7 days or before reaching 90% confluency. To subculture, cells were dissociated using 0.25% trypsin plus 1 mM EDTA in balanced salt solution (Gibco) and reseeded at $1.87 \cdot 10^5$ cells per 175 cm^2 cell culture flasks.

3.6.3 Solution Preparation

Solutions for cell experiments were prepared by dissolving the individual compounds in base cell media supplemented with 10% FBS and 1x PSA (solutions used as CPAs did not contain PSA) and sterile filtering prior to use.

3.6.4 Cytotoxicity of Compounds

A549 cells were seeded at $4 \cdot 10^4$ cells per well in 200 µL of cell culture medium with indicated concentrations of solutions in 96-well plates (ThermoFisher). Cells were incubated with solutions for 10 min and exchanged against complete cell media or incubated with solutions for 24 h in a humidified atmosphere of 5 % CO_2 and 95 % air at 37 °C. Following the incubation period, resazurin sodium salt (Sigma Aldrich) was dissolved in phosphate buffered saline (Sigma Aldrich) and added to wells in an amount of $1/10^{th}$ initial well volume. Readings were taken using a Synergy HTX Multi-Mode Reader (BioTek, Swindon, UK) at 570/600 nm absorbance every 30 m until control cells reached ~70% reduction. These readings enabled the calculation for the percentage of alamarBlue reduction (Equation 3.3). Values were normalised by dividing experimental values by control values. Cells were then imaged using a CKX41 microscope (Olympus) equipped with the XC30 camera (Olympus). Images were captured and processed using the CellSens standard software (Olympus).

$$Percent\,reduction\,of\,alamarBlue = \frac{(O2 * A1) - (O1 * A2)}{(R1 * N2) - (R2 * N1)} * 100$$

O1 = molar extinction coefficient (E) of oxidised alamarBlue (blue) at 570 nm
O2 = E of oxidised alamarBlue at 600 nm
R1 = E of reduced alamarBlue (red) at 570 nm
R2 = E of reduced alamarBlue at 600 nm
A1 = absorbance of test wells at 570 nm
A2 = absorbance of test wells at 600 nm
N1 = absorbance of negative control well (media plus alamarBlue but no cells) at 570 nm
N2 = absorbance of negative control well (media plus alamarBlue but no cells) at 600 nm

Equation 3.3. Equation used for alamarBlue reduction calculation.

3.6.5 Incubation Growth Assay

Cells were seeded at $12.5 \cdot 10^3$ per well in 6-well plates (Thermo Fisher) in 2 mL of complete cell media or in the indicated solutions. Cells were placed in a

humidified atmosphere of 5% CO_2 and 95% air at 37 °C and allowed to grow, with counts starting on day two and commencing on day six. Cell media was renewed on day three. Cells were dissociated using 0.25% trypsin plus 1 mM EDTA in balanced salt solution. The number of viable cells was then determined by counting with a haemocytometer (Sigma Aldrich) at room temperature after 1:1 dilution of the sample with 0.4% trypan blue solution (Sigma Aldrich). Fold increase of cells was calculated by dividing the number of cells with intact cell membranes by the number of cells initially plated.

3.6.6 Incubation Recovery Growth Assay

Cells were seeded at $12.5 \cdot 10^3$ per well in 6-well plates (Thermo Fisher) in 2 mL of complete cell media or in the indicated solutions. Cells were placed in a humidified atmosphere of 5% CO_2 and 95% air at 37 °C and allowed to grow, with counts starting on day two and commencing on day six. Cell media was renewed on day three and cells incubated in solutes were switched back to complete cell media. Cells were dissociated using 0.25% trypsin plus 1 mM EDTA in balanced salt solution. The number of viable cells was then determined by counting with a haemocytometer (Sigma Aldrich) at room temperature after 1:1 dilution of the sample with 0.4% trypan blue solution (Sigma Aldrich). Fold increase of cells was calculated by dividing the number of cells with intact cell membranes by the average number of cells on day three.

3.6.7 Trypan Blue Assay

50 µL of 0.4% trypan blue was combined with 50 µL cell suspension, mixed, and allowed to penetrate for 10 min. After remixing of sample, 10 µL of trypan blue/cell sample was added to each side of a haemocytometer. Four squares on each side of the haemocytometer were counted for viable (non-blue) cells (Fig

3.10) and average cell number for each sample was calculated utilising Equation 3.4.

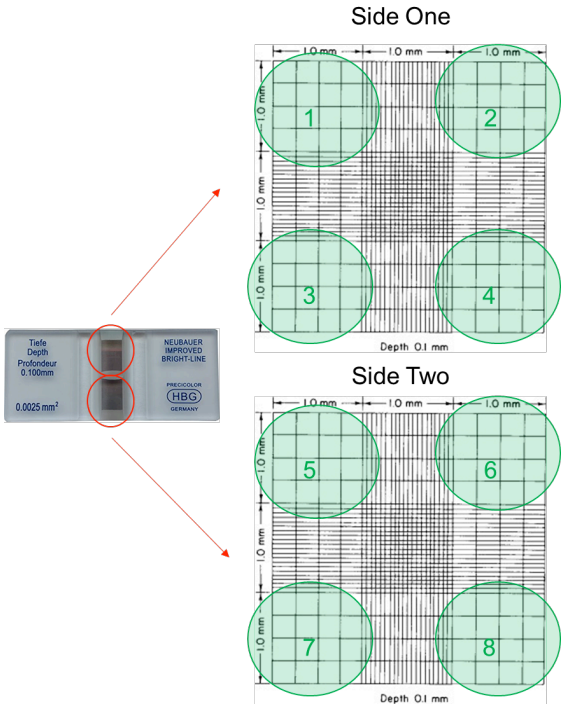

Figure 3.8. Haemocytometer Counting.

$$\frac{Viable\ Cells}{mL} = \frac{Cells}{S} * DF * V$$

S = number of squares counted
DF = dilution factor
V = volume scale up to mL

Equation 3.4. Equation used for trypan blue viable cell calculation.

3.6.8 Statistical Analysis

Data were analysed with a one-way analysis of variance (ANOVA) on ranks followed by comparison of experimental groups with the appropriate control group (Holm–Sidak method) followed by Tukey's post hoc test. Excel 2013 (Microsoft, Redmond, WA) and R were used for the analyses and graphs. Data sets are presented as mean ± (SEM).

3.7 Appendix

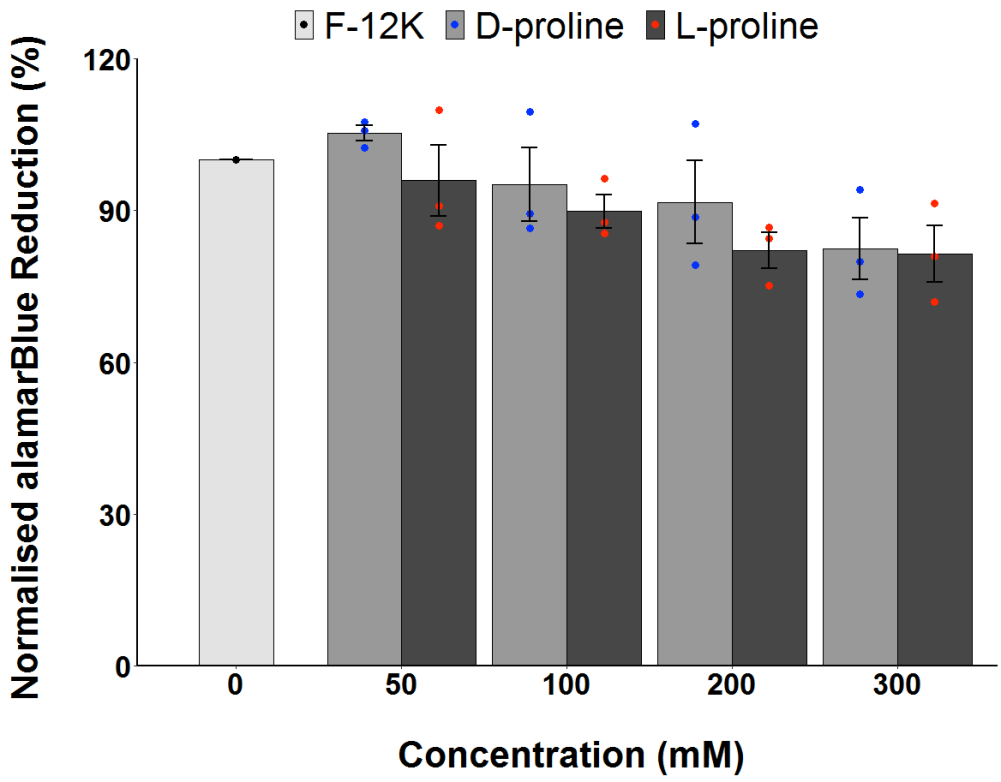

Figure 3.9. A549 proline cytotoxicity. Average normalised alamarBlue reduction after 24 h incubation. Error bars represent ± SEM of 3 independent experiments.

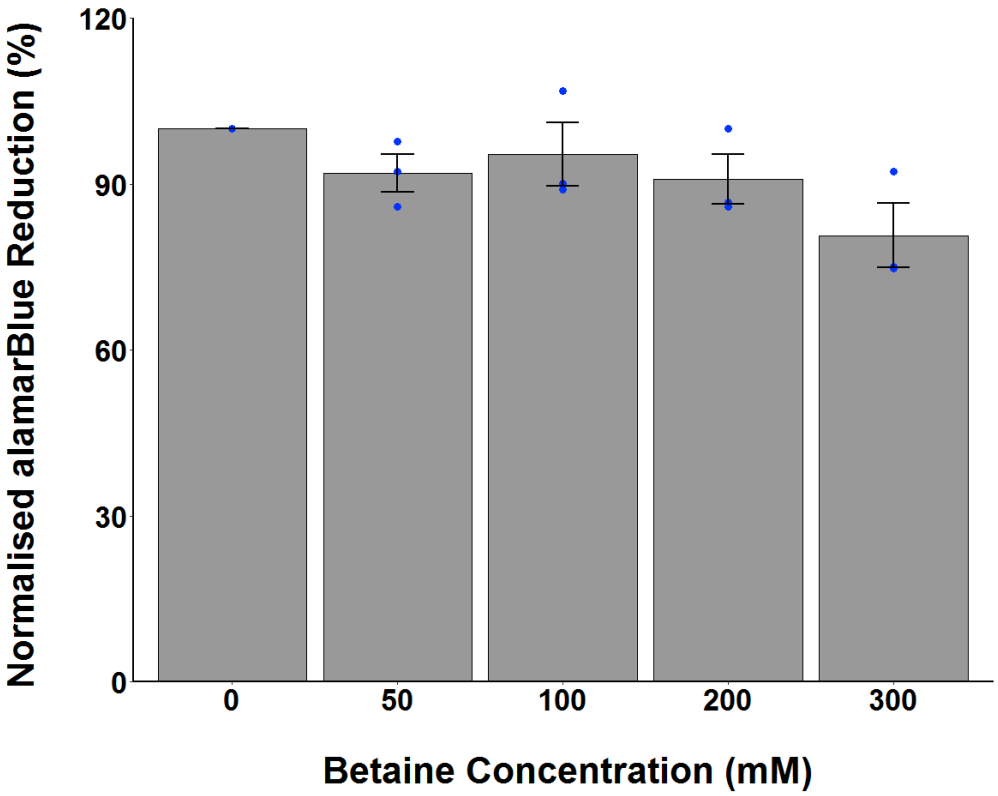

Figure 3.10. A549 betaine cytotoxicity. Average normalised alamarBlue reduction after 24hr incubation. Error bars represent ± SEM of 3 independent experiments.

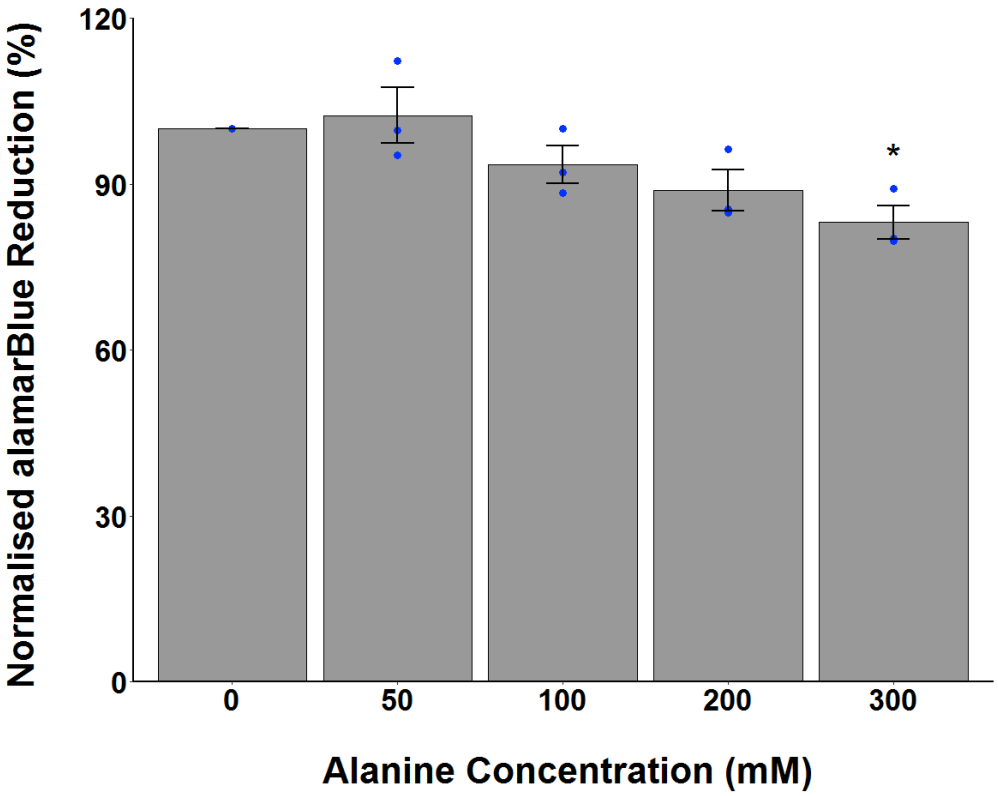

Figure 3.11. A549 alanine cytotoxicity. Average normalised alamarBlue reduction after 24hr incubation. Error bars represent ± SEM of 3 independent experiments. * P < 0.02 from control (0 mM alanine).

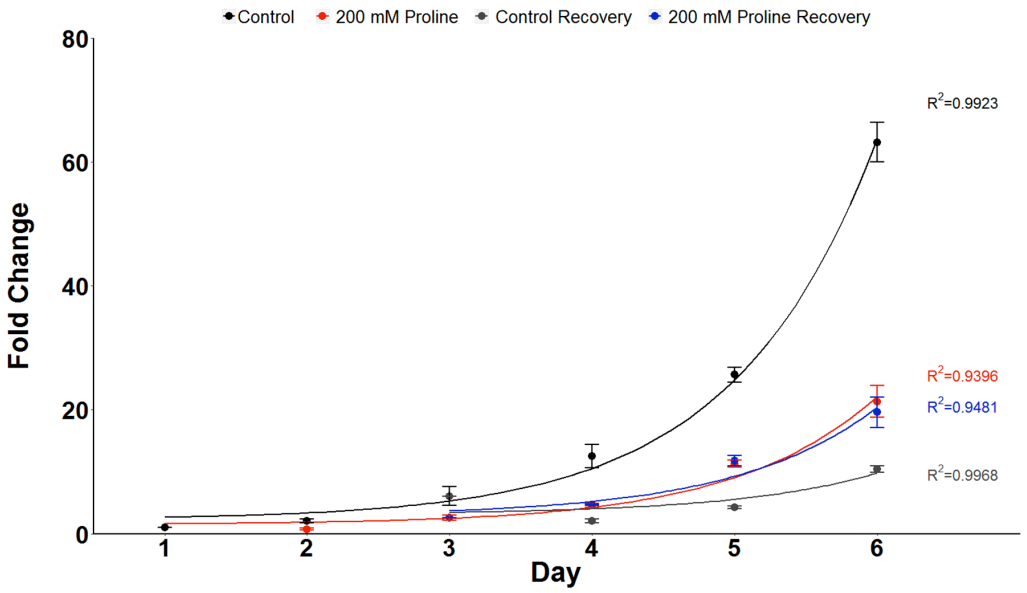

Figure 3.12. A549 proline incubation and recovery growth rates. Growth rates after incubation with F-12K (control) for 6 days (black), 200 mM proline for 6 days (red), control recovery cells (grey), or 200 mM proline for 3 days then F-12K media for 3 days (blue). Error bars represent ± SEM of 3 independent experiments.

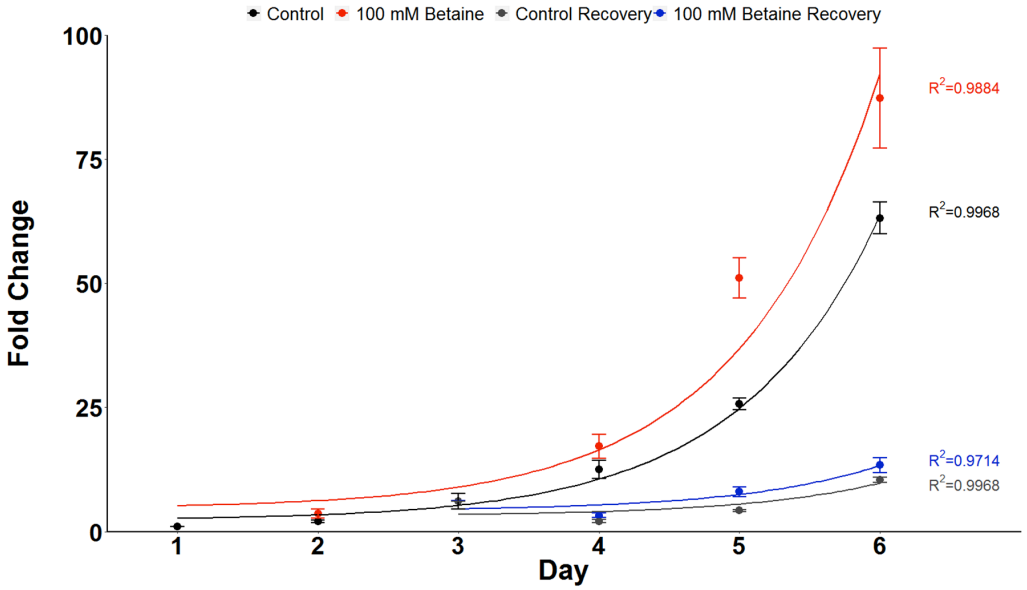

Figure 3.13. A549 betaine incubation and recovery growth rates. Growth rates after incubation with F-12K for 6 days (black), 100 mM betaine for 6 days (red), control recovery cells (grey), or 100 mM betaine for 3 days then F-12K media for 3 days (blue). Error bars represent ± SEM of 3 independent experiments.

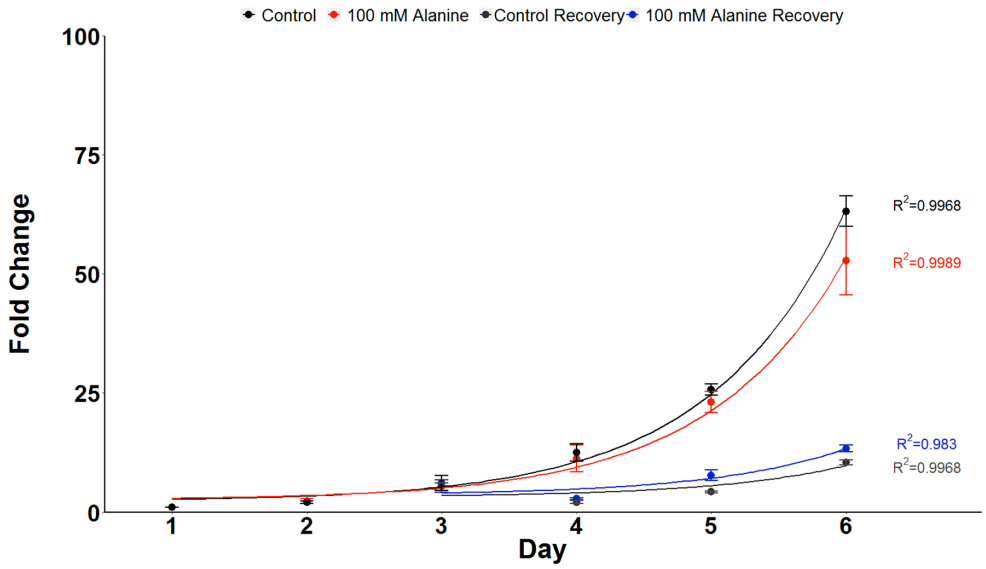

Figure 3.14. A549 alanine incubation and recovery growth rates. Growth rates after incubation with F-12K for 6 days (black), 100 mM alanine for 6 days (red), control recovery cells (grey), or 100 mM alanine for 3 days then F-12K media for 3 days (blue). Error bars represent ± SEM of 3 independent experiments.

3.8 References

(1) Rampersad, S. N. Multiple Applications of Alamar Blue as an Indicator of Metabolic Function and Cellular Health in Cell Viability Bioassays. *Sensors (Basel).* **2012**, *12* (9), 12347–12360. https://doi.org/10.3390/s120912347.

(2) O'Brien, J.; Wilson, I.; Orton, T.; Pognan, F. Investigation of the Alamar Blue (Resazurin) Fluorescent Dye for the Assessment of Mammalian Cell Cytotoxicity. *Eur. J. Biochem.* **2000**, *267* (17), 5421–5426. https://doi.org/10.1046/j.1432-1327.2000.01606.x.

(3) Mazur, P. Principles of Cryobiology. In *Life in the Frozen State*; Fuller, B., Lane, N., Benson, E. E., Eds.; CRC Press: Boca Raton, 2005; Vol. 17, pp 301–302.

(4) Hand, S. C.; Patil, Y. N.; Li, S.; Chakraborty, N.; Borcar, A.; Menze, M. A.; Boswell, L. C.; Moore, D.; Toner, M. Diapause and Anhydrobiosis in Embryos of Artemia Franciscana : Metabolic Depression, LEA Proteins and Water Stress (Papers Presented at the Seminar, "NIAS International Seminar for Cryobiology and Cryotechnology"). *Cryobiol. Cryotechnology* **2013**, *59* (1), 41–46. https://doi.org/10.20585/cryobolcryotechnol.59.1_41.

(5) Erkut, C.; Penkov, S.; Fahmy, K.; Kurzchalia, T. V. How Worms Survive Desiccation: Trehalose pro Water. *Worm* **2012**, *1* (1), 61–65. https://doi.org/10.4161/worm.19040.

(6) Koštál, V.; Šimek, P.; Zahradníčková, H.; Cimlová, J.; Štětina, T. Conversion of the Chill Susceptible Fruit Fly Larva (Drosophila Melanogaster) to a Freeze Tolerant Organism. *Proc. Natl. Acad. Sci. U. S. A.* **2012**, *109* (9), 3270–3274. https://doi.org/10.1073/pnas.1119986109.

(7) Fahy, G. M. The Relevance of Cryoprotectant "Toxicity" to Cryobiology. *Cryobiology* **1986**, *23* (1), 1–13. https://doi.org/10.1016/0011-2240(86)90013-1.

(8) Deller, R. C.; Pessin, J. E.; Vatish, M.; Mitchell, D. A.; Gibson, M. I. Enhanced Non-Vitreous Cryopreservation of Immortalized and Primary Cells by Ice-Growth Inhibiting Polymers. *Biomater. Sci.* **2016**, *4* (7), 1079–1084. https://doi.org/10.1039/c6bm00129g.

(9) Julca, I.; Alaminos, M.; González-López, J.; Manzanera, M. Xeroprotectants for the Stabilization of Biomaterials. *Biotechnol. Adv.* **2012**, *30* (6), 1641–1654. https://doi.org/10.1016/j.biotechadv.2012.07.002.

(10) Miralles-Robledillo, J. M.; Torregrosa-Crespo, J.; Martínez-Espinosa, R. M.; Pire, C. DMSO Reductase Family: Phylogenetics and Applications of Extremophiles. *Int. J. Mol. Sci.* **2019**, *20* (13). https://doi.org/10.3390/ijms20133349.

(11) Stoddart, M. J. *Cell Viability Assays: Introduction.*; 2011; Vol. 740. https://doi.org/10.1007/978-1-61779-108-6_1.

(12) Vaughan, R. A.; Gannon, N. P.; Garcia-Smith, R.; Licon-Munoz, Y.; Barberena, M. A.; Bisoffi, M.; Trujillo, K. A. β-Alanine Suppresses Malignant Breast Epithelial Cell Aggressiveness through Alterations in Metabolism and Cellular Acidity in Vitro. *Mol. Cancer* **2014**, *13* (1), 14. https://doi.org/10.1186/1476-4598-13-14.

(13) Hägglund, B.; Sandberg, G. Effect of L-Alanine and Some Other Amino Acids on Thymocyte Proliferation in Vivo. *Immunobiology* **1993**, *188* (1–2), 62–69. https://doi.org/10.1016/S0171-2985(11)80487-0.

(14) Guo, Y.; Xu, L.-S.; Zhang, D.; Liao, Y.-P.; Wang, H.-P.; Lan, Z.-H.; Guan, W.-J.; Liu, C.-Q. Betaine Effects on Morphology, Proliferation, and P53-Induced

Apoptosis of HeLa Cervical Carcinoma Cells in Vitro. *Asian Pac. J. Cancer Prev.* **2015**, *16* (8), 3195–3201. https://doi.org/10.7314/apjcp.2015.16.8.3195.

(15) Kar, F.; Hacioglu, C.; Kacar, S.; Sahinturk, V.; Kanbak, G. Betaine Suppresses Cell Proliferation by Increasing Oxidative Stress-Mediated Apoptosis and Inflammation in DU-145 Human Prostate Cancer Cell Line. *Cell Stress Chaperones* **2019**. https://doi.org/10.1007/s12192-019-01022-x.

(16) Bingula, R.; Dupuis, C.; Pichon, C.; Berthon, J.-Y.; Filaire, M.; Pigeon, L.; Filaire, E. Study of the Effects of Betaine and/or C-Phycocyanin on the Growth of Lung Cancer A549 Cells In Vitro and In Vivo. *J. Oncol.* **2016**, *2016*, 8162952. https://doi.org/10.1155/2016/8162952.

(17) Nakamura, T.; Teramoto, H.; Tomita, Y.; Ichihara, A. L-Proline Is an Essential Amino Acid for Hepatocyte Growth in Culture. *Biochem. Biophys. Res. Commun.* **1984**, *122* (3), 884–891. https://doi.org/10.1016/0006-291x(84)91173-2.

(18) Washington, J. M.; Rathjen, J.; Felquer, F.; Lonic, A.; Bettess, M. D.; Hamra, N.; Semendric, L.; Tan, B. S. N.; Lake, J. A.; Keough, R. A.; Morris, M. B.; Rathjen, P. D. L-Proline Induces Differentiation of ES Cells: A Novel Role for an Amino Acid in the Regulation of Pluripotent Cells in Culture. *Am. J. Physiol. - Cell Physiol.* **2010**, *298* (5), 982–992. https://doi.org/10.1152/ajpcell.00498.2009.

(19) Phang, J. M. Proline Metabolism in Cell Regulation and Cancer Biology: Recent Advances and Hypotheses. *Antioxid. Redox Signal.* **2019**, *30* (4), 635–649. https://doi.org/10.1089/ars.2017.7350.

(20) Liu, W.; Hancock, C. N.; Fischer, J. W.; Harman, M.; Phang, J. M. Proline Biosynthesis Augments Tumor Cell Growth and Aerobic Glycolysis: Involvement of Pyridine Nucleotides. *Sci. Rep.* **2015**, *5* (1), 17206. https://doi.org/10.1038/srep17206.

CHAPTER 4

4. MACROMOLECULAR CRYOPROTECTANTS AND OSMOTIC PRECONDITIONING FOR ENHANCED MAMMALIAN CELL CRYOPRESERVATION

4.1 DECLARATIONS

All polyampholyte polymers were synthesised by Dr Christopher Stubbs and all polyproline polymers were synthesised by Dr Ben Graham, both under the supervision of Prof Matthew Gibson.

4.2 CHAPTER SUMMARY

We have demonstrated that osmolytes in combination with the highly active IRI polymer PVA, or the moderately IRI active polymer polyproline, and the very low IRI active polyampholyte can be used to improve the cryopreservation of cell monolayers, with each potentially acting by different mechanisms of action. In particular the polyampholyte lead to very large increase in post-thaw cell yield for A549 cells, but also moderate increases with harder to freeze MC-3T3 and Neuro-2a monolayers. We further demonstrate that cells frozen with the combination of osmolytes, plus PVA or polyproline, grow better post-thaw than cells frozen with just 10% DMSO, osmolytes alone, or PVA/polyproline alone. Similarly, cells frozen with a low concentration of polyampholyte P2 were shown to grow better post-freeze than cells frozen with just 10% DMSO. Taken together,

this shows that macromolecular cryoprotectants increase cell yield and health, post-thaw.

4.3 INTRODUCTION

As discussed in Chapter 1, there are only a few studies on monolayer cryopreservation and they often involve complicated processes, such as solvent equilibration steps or specialised freezing processes. For example, Matsumura *et al.* used slow vitrification (10.8 $^{\circ}C \cdot min^{-1}$) in the cryopreservation of monolayered mesenchymal stem cells.[1] Their CPA solutions included a vitrification solution (VS) comprising 6.5 M ethylene glycol (EG) and 0.75 M sucrose or a polymer vitrification solution (P-VS) comprised of the VS plus 10% carboxylated poly-L-lysine (COOH-PLL) – a polyampholyte which we hypothesise has similar functions to the one used in this thesis. Their process involved treating the cells with an equilibrium solution (ES) comprised of 15% EG for 10 min, a CPA exposure of 5 min, slow vitrification utilising $N_{2(l)}$ (distance from the surface dictated the freezing rate) for 20 min, then soaking the plate in $N_{2(l)}$. Plates were then warmed with rewarming solution (RS), comprised of 1M sucrose, for 1 min then treated with dilution solution (DS), a 0.5 M sucrose solution, for 3 min, then washed twice with cell media to ensure all treatment solutions were removed. Cells were assayed immediately after freezing, using trypan blue exclusion, with the cells still attached to the plate, and a 90% recovery for cells frozen with VS and a 95% recovery for cells frozen with P-VS was found. Repeating the trypan blue assay 24 h later found a 50% recovery for cells frozen with VS and a 90% recovery for cells frozen with P-VS, showing a substantial 40% drop in recovery for VS cells from the 90% reported immediately post-thaw. Bahari *et al.* utilised directional freezing, where the monolayers were individually frozen on a cryostage; following nucleation, the slides were moved linearly from hot to cold at variable speeds.[2] The monolayers were assayed 5 h post-thaw via fluorescent

microscopy, with HeLa cells showing a 90% recovery and Caco-2 cells showing at 60% recovery. A study by Pless-Petig *et al.* investigated porcine aortic endothelial cells, utilising a slow freezing rate of 0.1 $^{\circ}C \cdot min^{-1}$ and a proprietary TiProtec® solution containing iron chelators, glycine, alanine, and high chloride and potassium, along with 10% DMSO.[3] Their freezing process involved incubating the cells at 4 °C for 10 min, then transferring to a pre-cooled (4°C) cooling chamber of a controlled-rate freezer and cooled at a linear temperature gradient to -4 °C, followed by a short, rapid temperature drop to -40 °C then immediately back to the approximate sample temperature to initialise crystallisation, and then a linear decrease to -80 °C at the initial cooling rate. The cells were evaluated 3 h post-thaw, with a maximum recovery rate of 50%. The cells were then examined after 24 h re-culture via assessment of intracellular LDH and trends were found to match the 3 h post-thaw assessments. All of these studies provide valuable insights into how cryoprotectants and freezing conditions affect the freezing of monolayers but the scale up of these procedures would be laborious, expensive, and time consuming.

Additionally, there is no universal method or procedure for assessment, which makes comparing studies and results especially difficult. Time from thawing to assessment introduces a large variable for comparability. For example, in 2009, a study by Miyamoto *et al.* used vitrogel collagen matrices in combination with 10% DMSO to cryopreserve primary hepatocytes and mouse embryonic stem cells.[4] The assessment was conducted 3 h post-thaw with the cells attached to the plates via live/dead staining and fluorescent microscopy. They found a 36% recovery for hepatocytes and a 44% recovery for embryonic stem cells. Conversely, Stevenson *et al.* also examined primary rat hepatocytes, utilising a 90% foetal calf serum (FCS) and 10% DMSO solution, the cryopreserved cells were assayed 48 h post-thaw to allow repair to damaged plasma membranes,[5] the cells were not removed from the plates and assessed via carboxyfluorescein

and measured with confocal laser scanning microscopy (CLSM) to find a 79% recovery rate. It is difficult to assess whether the greater recovery value reported in the latter study is due to a superior cryoprotectant or the increased post-thaw incubation time which may allow for cell proliferation to occur.

Another variable for comparability in cryopreservation outcomes is trypsinisation. None of the studies mentioned previously removed their cells from the attached substrate for analysis. In 1999, Pasch *et al.* examined keratinocyte monolayers and found a 29% recovery for cells frozen with 10% hydroxyethyl starch 24 h after thawing.[6] They additionally found that 65% of their cells were damaged during the trypsinisation process. In 2000, they repeated the experiment but assayed the cells immediately after thawing, without removal from the plate, and found an 80% recovery rate for monolayers frozen with 10% hydroxyethyl starch.[7] This shows that the trypsinisation process introduces stress to the cells, and studies that do not remove the cells from the plates may overstate the membrane health of cryopreservation outcomes.

Studies that allow 24 h recovery and removal of cells from the substrate, compared to immediate post-thaw analysis conducted with cells attached, report moderate cell recoveries. Stokich *et al.* incubated hepatocyte cell (HepG2) monolayers in 100 mM trehalose, followed by freezing with 10% DMSO, to achieve a 42% recovery 24 h post thaw and trypsinisation.[8] Bailey *et al.* found that incubating neuronal cell (Neuro-2a) monolayers in 112.5 mM proline and trehalose, followed by freezing with 112.5 mM proline and trehalose plus 10% DMSO resulted in 53% recovery 24 h post-thaw and trypsinisation.[9] Finally, Tomás *et al.* found a 60% recovery for A549 monolayers frozen with 0.8 $mg \cdot mL^{-1}$ AFPIII and 10% DMSO 24 h post-thaw and trypsinisation.[10] With these studies, the results appear to be directly accountable to the cryopreservation processes themselves, as time between thawing and the assay has allowed apoptosis

processes to complete and cells have been removed from the substrate, a rigorous test of cell membrane integrity.

The highest recovery seen for monolayer cryopreservation was the Eskandaria *et al.* study utilising cryopreserved human umbilical vein endothelial cell monolayers with a solution of 2% chondroitin sulfate, 6% hydroxyethyl starch, and 5% DMSO.[11] The cells were measured for viability immediately post-thaw without removal from the substrate via staining with SYTO 13/GelRed, imaging with fluorescent microscopy, and analysis using the Viability3 program to find 97% recovery, with no longevity studies conducted. It is difficult to determine if this high recovery rate was due to the cryoprotectants themselves, the immediate assay time, leaving the cells attached to the substrate, or combinations of, which may be affording the reported protections.

These examples demonstrate that while assessing cells too early can potentially give false positives as apoptotic processes have not had time to complete,[12] assessing later than 24 h post-thaw can potentially allow the cells to repair damage and proliferate.[13,14]

We hoped to find a simple, streamlined approach for freezing cell monolayers that would be researcher and lab-friendly. For the monolayer freezing in this work, we utilised an efficient slow-freezing methodology,[9] which ensured proper recovery time to evaluation (Fig 4.1). We allowed the cells to attach for 2 h, media was then exchanged and cells were incubated for 24 h, and then treated with a CPA for 10 min. In order to freeze the cells in a semi-dry state and allow for a faster thawing process, we then fully removed the CPA from the cells. Cells were frozen at 1 °C·min^{-1} to -80 °C for 24 h and then thawed using 37 °C cell media. We utilised a cooling rate of 1 °C·min^{-1} which allowed the cells to dehydrate so there was less chance of intracellular ice while still retaining a recoverable water content (enough water within the cell to avoid triggering apoptotic processes due to water loss) upon rewarming. The rationale for a 24 h

frozen storage time was due to evidence that post-thaw function is independent of storage time at -80 ˚C, in particular, rat hepatocytes cryopreserved as monolayer cultures for 28 days at -80 ˚C showed no significant differences in cytochrome P-450 activity from those cultures stored for 1 day.[15] The cells were then incubated for 24 h prior to recovery assays.

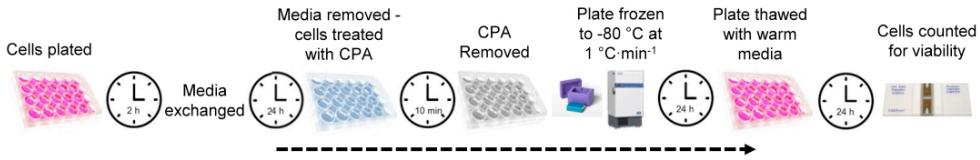

Figure 4.1. Monolayer cell cryopreservation methodology.

Following cryopreservation and our recovery assessment, cells were also plated at equal starting numbers to evaluate growth rates over six days to determine post-freeze viability.

And now, the main event, to evaluate if these compounds are useful in the cryopreservation of monolayered cells. We will evaluate cryopreservation outcomes via our previously outlined cell cryopreservation methodology. In addition to cryopreservation outcomes, we will also assess the proliferation capabilities of cryopreserved cells via long-term growth assays. The main objectives of this chapter were to evaluate (i) if our molecular osmolytes and/or macromolecular polymers were able to successfully cryopreserve mammalian cells, and (ii) how viable the cells were post-freeze when our molecular osmolytes and/or macromolecular polymers were included. The results of this chapter will allow us to identify potentially protective compounds for the cryopreservation of attached monolayered cells while also assessing the downstream effects of the cells several days post-thaw.

4.4 RESULTS AND DISCUSSION

4.4.1 Cell Cryopreservation

Our monolayer method involved plating the cells with a 24 h incubation period (with or without osmolytes as indicated in figures) to allow time for any pre-conditioning. This was followed by a 10 min CPA application, removal of the CPA, controlled rate freezing of 1 °C·min^{-1} to -80 °C for 24 h, and then quickly thawing with 37 °C media, followed by a post-thaw incubation of 24 h, and finally counting with trypan blue to evaluate cell recovery. Since cells have been successfully cryopreserved with PVA utilising suspension freezing[16] (cells suspended in solution and frozen in vials), our first experiment was to evaluate if similar results could be obtained with monolayer freezing. In these assays we were looking for a high percentage of cells recovered after freezing, significantly higher than 10% DMSO on its own.

4.4.1.1 PVA Monolayer Freezing

A549 cells frozen as monolayers with a CPA of only 10% DMSO resulted in a 16.9% (± 3.2) recovery (Fig 4.2, *n* = 3). We next tested cell recovery with different concentrations, from 1 to 10 mg·mL^{-1} PVA, added to the CPA solution. Cells frozen with 5 mg·mL^{-1} PVA inclusion in the CPA (along with 10% DMSO) gave the highest recovery of 23.7% (± 2.8), however, this is still considered to be a very low recovery. These results highlight the difficulty in moving from suspension freezing to freezing cells as a monolayer, as A549 cells frozen in suspension with 10% DMSO resulted in ~ 60% recovery.[17] Cells in solution have free movement and are able to adjust to ice engulfment and often avoid growing ice by moving into the non-frozen solution between crystals,[18] whereas monolayer cells are attached to a substrate and cannot adjust their position throughout the freezing process. While PVA has been successfully utilised in suspension

cryopreservation, it was not sufficient to protect our cell monolayers during freezing.

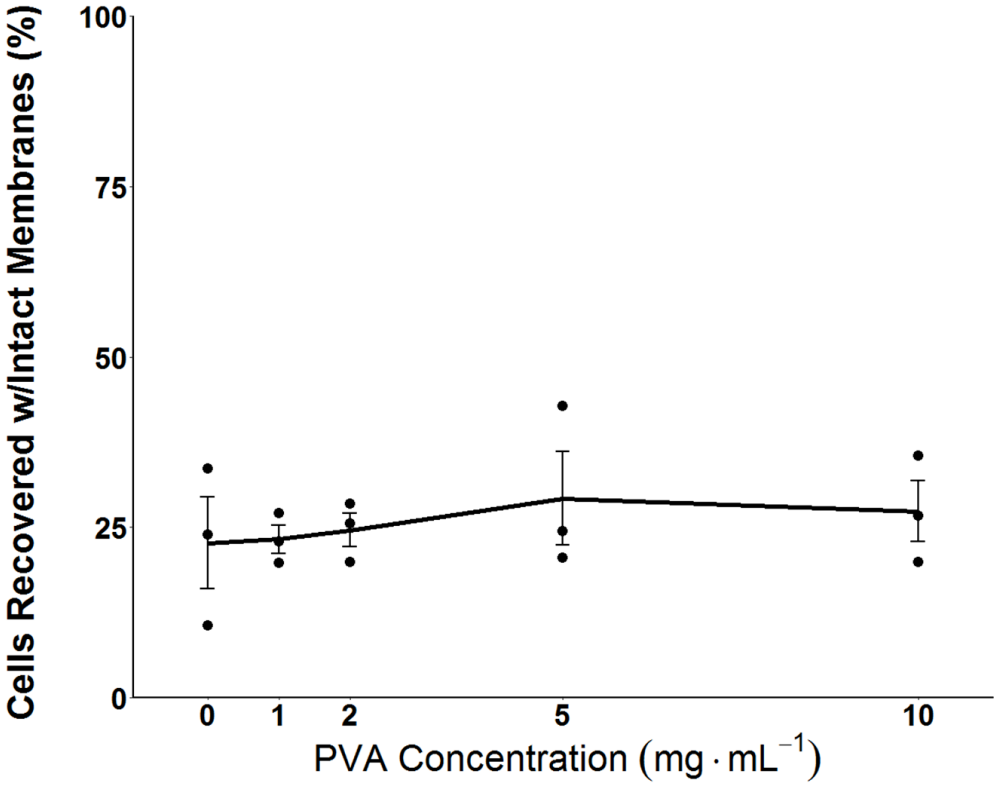

Figure 4.2. A549 PVA monolayer freezing. Cells recovered after freezing to -80 °C. Error bars represent ± SEM of 3 independent experiments with 2 nested replicates.

4.4.1.2 Combined Osmolyte PVA A549 Monolayer Freezing

In Chapter 1 we hypothesised that incubation with osmolytes may precondition the cells to improve cryopreservation outcomes, potentially by modifying metabolic or other processes, to 'prepare' them for cold stress. Therefore, we next combined an osmolyte incubation with PVA to assess if cryoprotection could be enhanced with this combination for monolayered cells as well as primary human cells in solution. We first tested our cells using a PVA concentration of 1 $mg \cdot mL^{-1}$ with variable proline (the osmolyte) incubation conditions to assess the optimal proline concentration (Fig 4.16). We next took our best performing proline

concentration and tested different PVA concentrations (Fig 4.17). The best performing PVA concentration from this assay (5 mg·mL^{-1} PVA) was then tested against variable concentrations of betaine (Fig 4.18) and alanine (Fig 4.19). Combining a uniform PVA concentration of 5 mg·mL^{-1} with the best performing concentration of each osmolyte for comparison, we saw a significant increase in recovery when cells were incubated in osmolyte solutions and cryopreserved in the presence of PVA (Fig 4.3, $n \geq 3$, $P = 0.0000005$). Cells frozen with no incubation and 10% DMSO resulted in only 16.9% (± 3.2) average recovery. The addition of 5 mg·mL^{-1} PVA to 10% DMSO resulted in 23.7% (± 2.8) recovery. Incubating cells in either 100 mM alanine or 100 mM betaine, and freezing with 10% DMSO, resulted in 24.1% (± 3.7) and 30% (± 3.7) recovery respectively and was not significantly higher than 10% DMSO or 5 mg·mL^{-1} PVA + 10% DMSO. Adding 5 mg·mL^{-1} PVA to both of these solutions resulted in a significant increase in recovery to 56.6% (± 1.8) for betaine incubated cells, yet had only a minimal effect on the alanine-treated cells. Incubating the cells in 200 mM proline and freezing with 10% DMSO resulted in a significant increase to 45.7% (± 5.2) recovery, and incubation of cells in 200 mM proline with a CPA of 5 mg·mL^{-1} PVA + 10% DMSO resulted in our highest recovery of 62.7% (± 4.2). Incubation in proline and betaine significantly increased the post-thaw recovery of our A549 monolayers. We believe this is due to directly affecting cell processes, as we have shown these osmolytes do not have an impact on ice within our system. These interactions could be in the form of membrane protection (explored in Chapter 5), osmoregulation, metabolic preconditioning (as shown for proline in Section 3.4.2), protein regulation, or perhaps the mitigation of apoptotic processes.

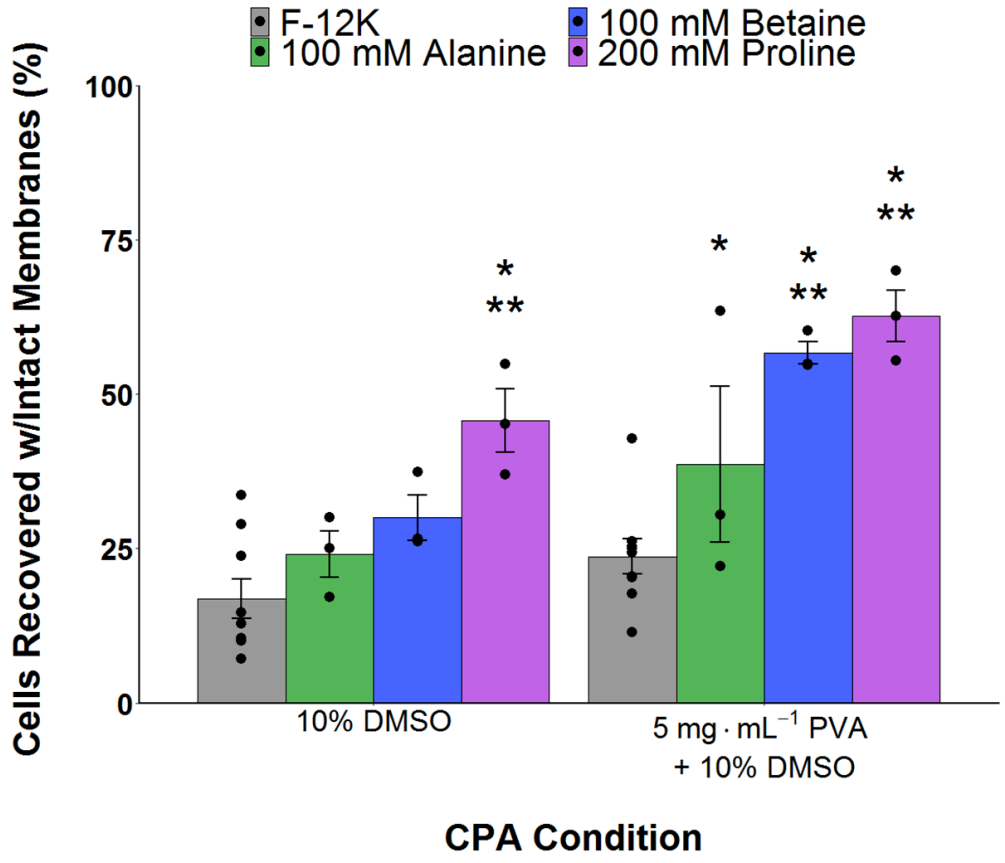

Figure 4.3. A549 osmolyte PVA monolayer freezing. Cells recovered after freezing to -80 °C. Error bars represent ± SEM of at least 3 independent experiments with two nested repeats. * P < 0.0001 from F-12K with 10% DMSO. ** P < 0.0001 from F-12K with 5 mg·mL^{-1} PVA + 10% DMSO.

This section has shown that pre-incubation of A549 cells with an osmolyte of proline or betaine and frozen in the presence of PVA + 10% DMSO significantly increased the post-thaw recovery of cells frozen as monolayers and shows that recrystallisation inhibitors can increase post-thaw cell recovery in pre-conditioned cells showing that combinations of cryoprotectants may be a viable strategy to enhance post-thaw outcomes.

4.4.1.3 Primary Endometrial Proline/PVA Suspension Freezing

Due to the high post-thaw recovery seen with the A549 monolayer cells, we next moved to test primary cells. Primary human cells are more sensitive and

challenging to cryopreserve and are less straightforward to culture, hence maximising their recovery is essential[19,20] as these cells are limited by the availability of donors and reduced cell counts post-thaw cannot be overcome by proliferation due to the short time span of primary cell growth. For this work we used human endometrial cells obtained from consenting donors via Dr Brosens' Implantation Clinic. The tissue was dissociated and two cells types were subsequently collected: endometrial stromal cells (ESC) and endometrial epithelial cells (EEC). Primary cells are usually cryopreserved in vials using standard methods, including slow cooling rates in combination with 5 – 10% DMSO supplemented with varying concentrations of foetal serum.[21–24] These cells were frozen in a suspension format, rather than a monolayer format, as the recovery of ESC/EEC frozen in suspension result in a low recovery, along with limited space available for sample storage. We first wanted to attempt to increase the recovery of these cells in suspension before moving on to a more challenging format. The cryopreservation protocol in the Brosens lab was 90% dextran-coated charcoal foetal calf serum (DCC) with 10% DMSO. DCC is very expensive and has been shown to stabilise bio-membranes and adjust osmotic pressure but it also contains a number of proteins and peptides which can cause an immune reaction after reinfusion.[25] Therefore, we wanted to start by selecting the proper base freezing media for primary endometrial cells, testing 90% DCC against completed cell media (DMEM) containing only 10% DCC for both cell types. We saw no significant difference between DCC and DMEM (supplemented with 10% DMSO) with or without 5 $mg \cdot mL^{-1}$ PVA for either ESC cells (Fig 4.4A) or EEC cells (Fig 4.4B). The recoveries of the ESC cells were very similar across all conditions, while the EEC cells recovered much better when frozen in DMEM rather than in DCC. From this, we selected DMEM as our base freezing media due to the higher recovery and the lower cost of the formula.

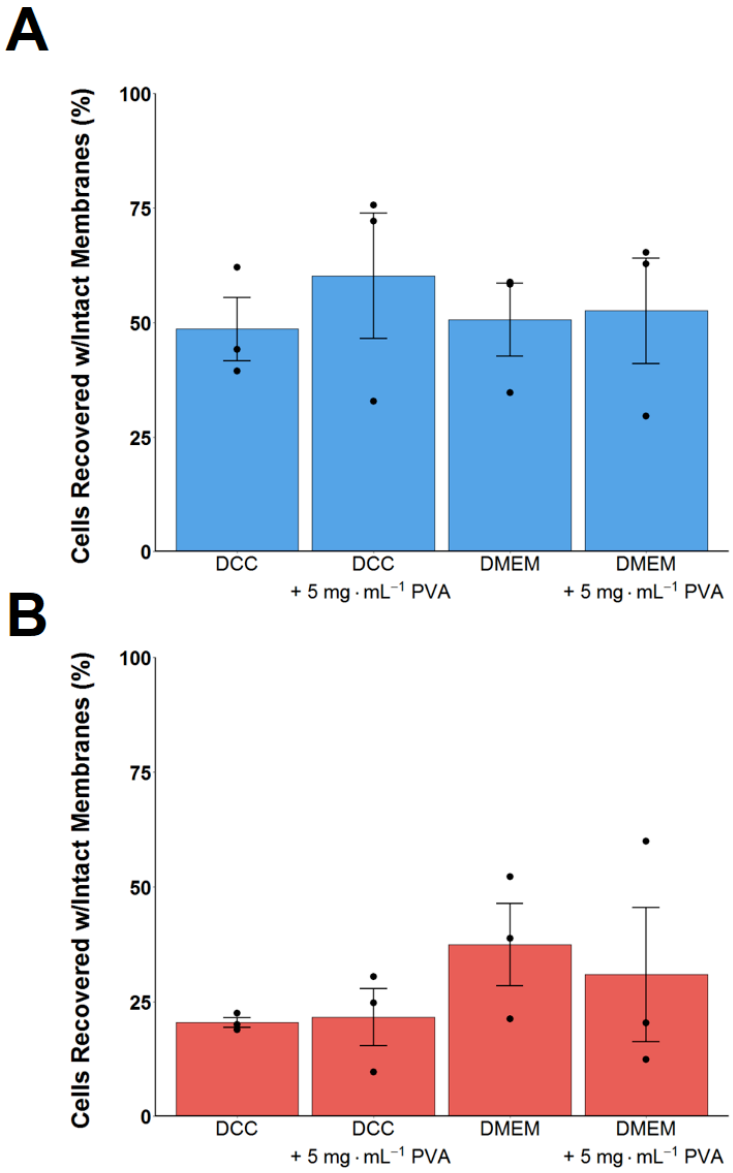

Figure 4.4. Media selection for primary human endometrial vial freezing. A) ESC cells recovered after freezing to -196 °C. **B)** EEC cells recovered after freezing to -196 °C. Error bars represent ± SEM of 3 independent experiments.

Now with the base freezing media set, we next wanted to see if proline could increase our post-thaw recovery with primary endothelial cells. In the previous experiments our monolayer cells were incubated in proline for 24 h. However, we wanted to work within the bounds of the Brosens' cryopreservation protocol, which involved freezing the cells immediately after dissociation and cell separation. This gave us two options for proline inclusion: adding the proline

directly into the freezing media or adding the proline to the 1 h digestion media. We saw no improvement in recovery for cells frozen with or without an incubation period for proline and with or without 5 $mg \cdot mL^{-1}$ PVA for ESC cells (Fig 4.5A) or for EEC cells (Fig 4.5B). There are several potential factors responsible for the lower recovery of our primary cells, most notably, the high variability of the results. This variation could be attributed to slight time-to-freeze disparities. This experiment was conducted within the large sample processing of the Brosens lab and the cells that were ready to freeze would often be held until the freezing container was full or all samples had been collected. This highlights the transition from lab setting to real-world application, as all factors, which may impact the outcome, cannot always be controlled. The high variability also speaks to the imperfect cryopreservation conditions for these cells as we see imprecise results in all conditions tested. There is much room for improvement in the storage of these cells, from adjusting the concentration and incubation time of the osmotic pre-conditioner, the concentration of the IRI compound, the concentration of DMSO, the number of cells frozen, and even the time to freeze.

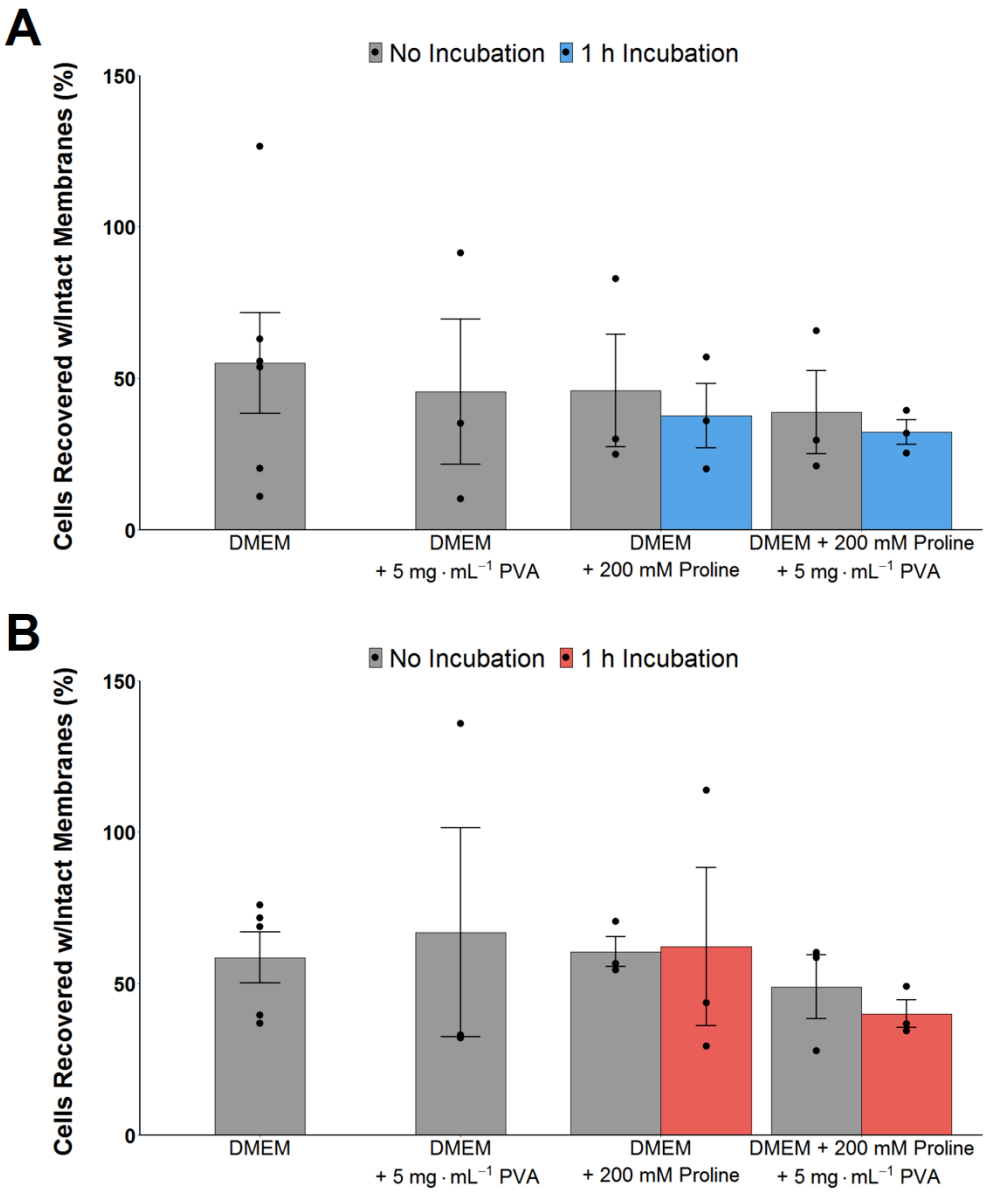

Figure 4.5. Primary endometrial epithelial proline/PVA vial freezing. Cells recovered after freezing to -196 °C. **A)** ESC cells frozen with 5 mg·mL^{-1} PVA, 200 mM proline, or a combination of proline and PVA. **B)** EEC cells frozen with 5 mg·mL^{-1} PVA, 200 mM proline, or a combination of proline and PVA. Error bars represent ± SEM of at least 3 independent experiments.

In this section we have shown that DMEM works better than DCC for primary human endometrial cell (ESC and EEC) vial cryopreservation. PVA or proline with PVA did not improve cryopreservation outcome for ESC or EEC cells frozen in suspension. We believe there is a large area for improvement in the

cryopreservation of primary human endometrial cells and optimisation of this protocol could vastly increase the recovery of these cells post-thaw.

4.4.1.4 Additional Immortalised Cell Monolayer Proline PVA Variable Concentration Freezing

Due to the poor recovery seen with human primary cells, we next wanted to test other immortalised cell lines in a monolayer format to see how our proline results would compare to those seen with A549 cells. We looked at two different cell lines: mouse calvarial osteoblastic (MC-3T3) and mouse brain neuroblastoma (Neuro-2a) cells.

4.4.1.4.1 MC-3T3 Proline PVA Variable Concentration Monolayer Freezing

Freezing monolayered MC-3T3 cells with 10% DMSO resulted in 11.8% (± 1.8) recovery (Fig 4.6A) and our largest improvement was with a 200 mM proline incubation in combination with 5 $mg \cdot mL^{-1}$ PVA + 10% DMSO, resulting in 27.7% (± 1.1) recovery. As MC-3T3 cells are known to have some attachment preferences, we also evaluated MC-3T3 cells frozen on collagen coated plates with 10% DMSO, which resulted in 9.5% (± 0.2) recovery (Fig 4.6B) and the inclusion of 200 mM proline and 5 $mg \cdot mL^{-1}$ PVA + 10% DMSO resulted in only 25.1% (± 7.3) recovery. While we did see some improvement in post-freeze recovery when proline and PVA were used, the recovery was not significantly different from cells frozen with only 10% DMSO. It has been shown that both the selection of an attachment substrate[26] and the pore size of substrate itself[27] effects adhesion, so it follows that collagen coating may not be a suitable substrate to retain cell attachment during the harsh event of monolayer freezing, which is reliant on attachment for cell retainability/recovery. MC-3T3 cells are also a contact inhibited cell line so we may have inadvertently programed them to arrest by simply creating a confluent monolayer. The lack of significant

improvement could also be due to the need for a different proline concentration, as MC-3T3 cells are considerably larger (20–50 μm)[28] than A549 cells (~15 μm)[29] and it would follow that ice would have more interaction with the larger membranes of these cells, especially if they haven't suitably shrunk prior to freezing. An additional mechanism may be through differentiation, as MC-3T3 confluent monolayers treated with 1% DMSO resulted in MC-3T3 differentiation and increased alkaline phosphatase (ALP) production,[30] as did simple mechanical strain,[31] and our cells are exposed to both of these throughout the cryopreservation process.

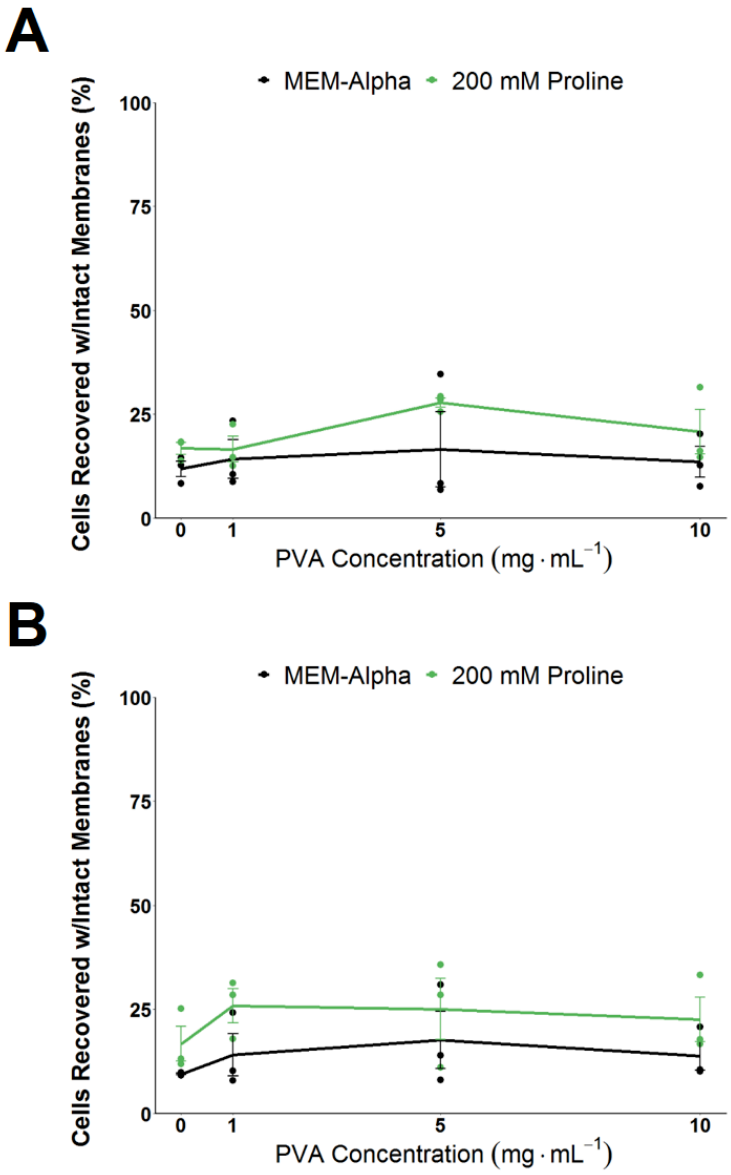

Figure 4.6. MC-3T3 proline PVA variable concentration monolayer freezing. Cells recovered after freezing to -80 °C. **A)** MC-3T3 cells frozen on bare plates. **B)** MC-3T3 cells frozen on collagen coated plates. Error bars represent ± SEM of 3 independent experiments with two nested repeats.

4.4.1.4.2 Neuro-2a Proline PVA Variable Concentration Monolayer Freezing

Freezing Neuro-2a monolayer cells on collagen-coated plates with 10% DMSO resulted in only an 18.9% (± 5.6) recovery (Fig 4.7) and our highest recovery was seen with a 200 mM proline incubation combined with 18 mg·mL^{-1} PVA, resulting in 37.5% (± 8.2) recovery. We saw no significant improvement for the monolayer freezing of Neuro-2a cells incubated in 200 mM proline and frozen with varying

concentrations of PVA on collagen coated plates. While our Neuro-2a cells were similar in size (10-14 μm)[32] to our A549 cells, neuronal cells are very sensitive to hypotonic conditions[33] so these cells may be much more sensitive to the harsh event of cryopreservation, thus a higher concentration of proline may be needed. We did see a somewhat PVA concentration-dependent increase in recovery, so it may also be that a higher concentration of IRI polymer is needed for these cells, however, PVA is not easily soluble past 20 mg·mL^{-1}.

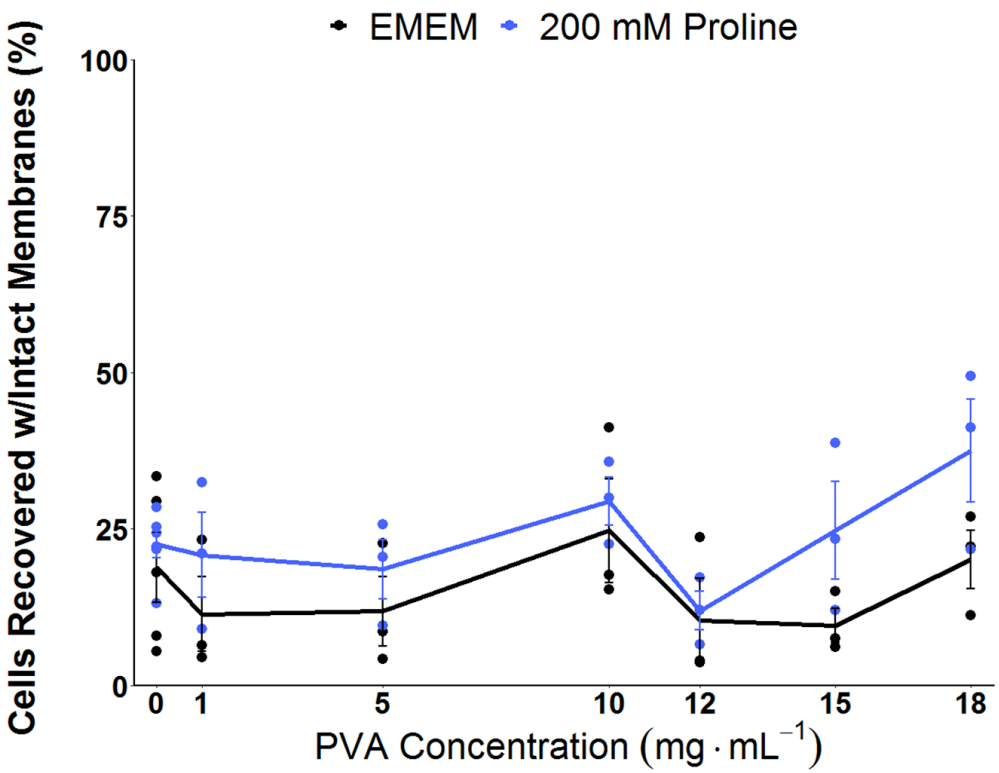

Figure 4.7. Neuro-2a proline PVA variable concentration monolayer freezing. Cells recovered after freezing to -80 °C. Error bars represent ± SEM of 3 independent experiments with two nested repeats.

In this section we attempted to improve the post-freeze recovery of MC-3T3 and Neuro-2a cells. While we did see some improvement with our solutions, we did not see any significant increases in recovery. We believe the formulation and process can be further optimised to provide increased recovery for these delicate

cell lines. These results further demonstrate how cryopreservation processes can be very cell-line dependent as different cell types will respond differently to particular treatments.

4.4.1.5 A549 Polyproline Monolayer Freezing

Having tested PVA as a cryoprotectant for several cell types, we next wanted to understand whether other macromolecular compounds had any cryoprotective benefit, either alone or in combination with osmolyte pre-conditioning. Addition of poly(L-proline) (which has moderate IRI activity) alone to 10% DMSO failed to give any significant increase in cell recovery, however, cells which were pre-conditioned with 200 mM proline for 24 h then treated with 10 $mg \cdot mL^{-1}$ polyproline + 10% DMSO doubled cell recovery to 53% compared to 10% DMSO alone (Fig 4.8, $n \geq 3$, $P = 0.000002$). Increasing the concentration of polyproline beyond 10 $mg \cdot mL^{-1}$ did not increase recovery further suggesting the additive benefits plateaued at 10 $mg \cdot mL^{-1}$. The highest recovery seen with proline + polyproline was 10% less than that seen with proline + PVA and this might be due to the differences in IRI activity, considering PVA is a highly active IRI polymer and polyproline showed only moderate IRI activity. These data suggest that in addition to IRI, other effects of polymers can lead to cryopreservation improvements, such as membrane interaction and/or protection.

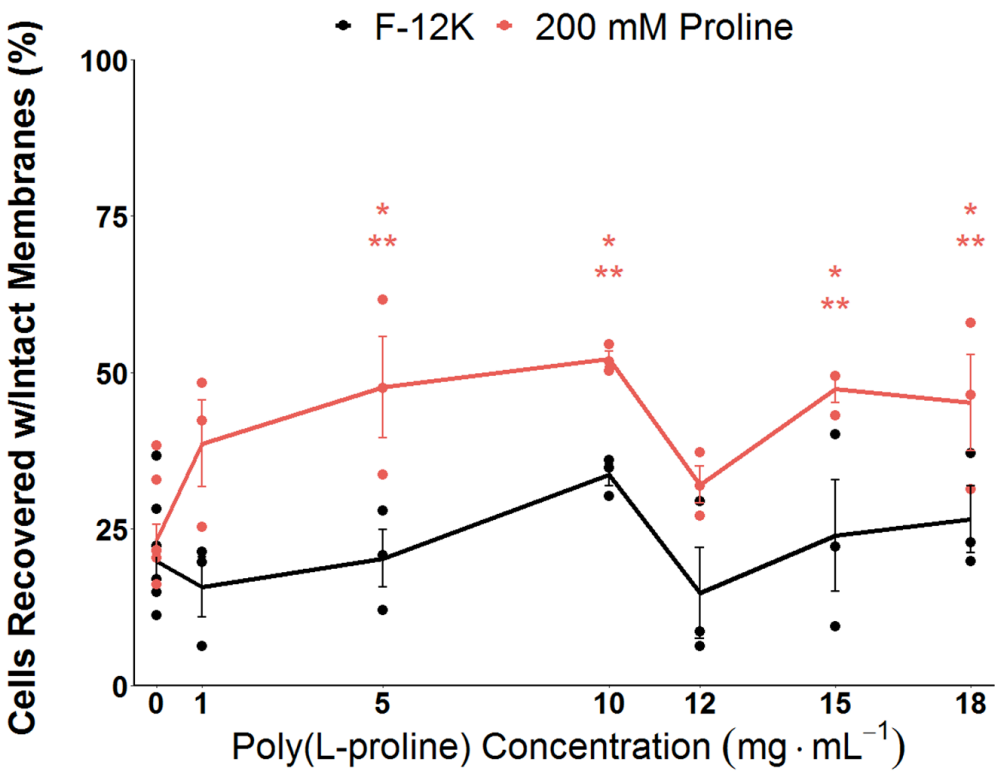

Figure 4.8. A549 proline polyproline variable concentration monolayer freezing. Cells recovered after freezing to -80 °C. Error bars represent ± SEM of at least 3 independent experiments with two nested repeats. * P < 0.0001 from 0 mg·mL^{-1} F-12K, ** P < 0.0001 from 0 mg·mL^{-1} 200 mM proline.

This section has shown that pre-incubation of A549 cells with proline and frozen in the presence of polyproline + 10% DMSO significantly increased the post-thaw recovery of cells frozen as monolayers.

4.4.1.6 Polyampholyte Monolayer Cryopreservation

4.4.1.6.1 A549 Polyampholyte Molecular Weight Variable Concentration Monolayer Freezing

We next sought to understand if polyampholyte had any cryoprotective benefits. As the start of our polyampholyte investigation, molecular weight effects of the polymer were screened (M_n = 20 kDa (P1), 80 kDa (P2), and 311 kDa (P3)). We found that all three molecular weights at 20 mg·mL^{-1} (in combination with 10%

DMSO) significantly improved the cryopreservation outcomes compared to cells frozen only with DMSO (Fig 4.9, $n \geq 3$, $P = 0.000006$). We further saw that P2 significantly protected cells at concentrations as low as 1 mg·mL^{-1}. While all three weights can be considered very potent cryoprotectants, we moved forward with our experiments utilising only P2 as the most promising candidate due to its protection at low concentrations.

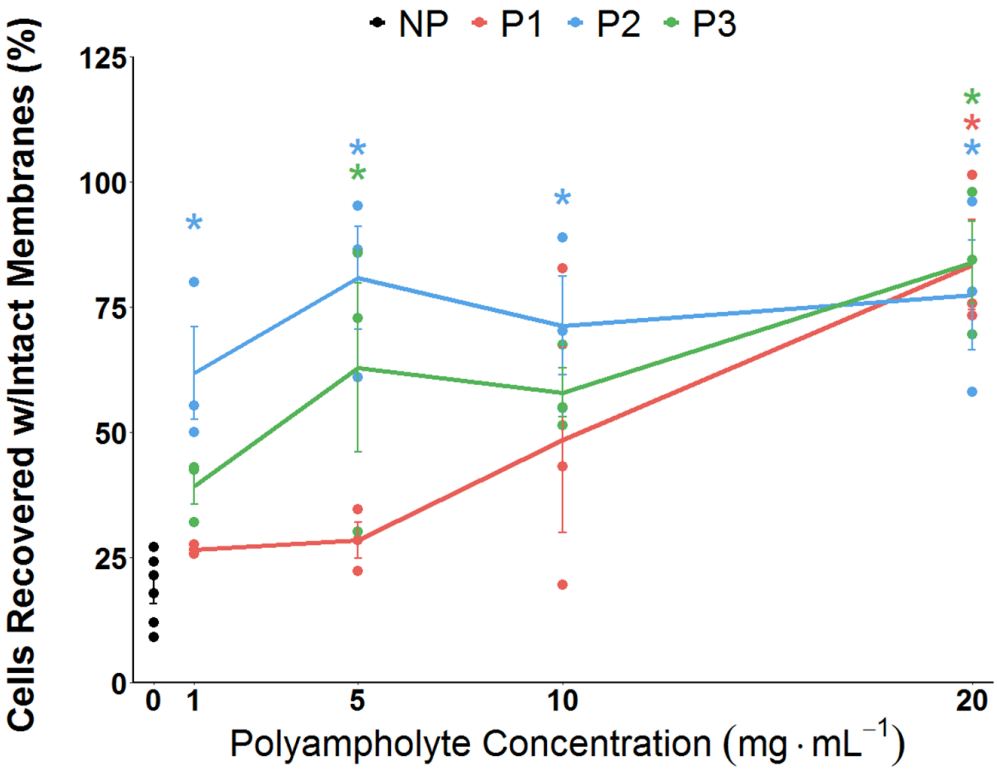

Figure 4.9. A549 polyampholyte molecular weight variable concentration monolayer freezing. Cells recovered after freezing to -80 °C. Error bars represent ± SEM of at least 3 independent experiments with two nested repeats. * P < 0.0001 from 0 mg·mL^{-1} NP (no polymer).

4.4.1.6.2 A549 Polyampholyte P2 Variable Concentration Proline Monolayer Freezing

We next tested a concentration range for P2 along with a proline incubation in combination with P2 to see how much protection we could afford our monolayers. We saw significant increases in cell recovery for all combinations tested (Fig

4.10, $n \geq 3$, $P = 0.000000004$). The highest recovery was seen with 30 mg·mL^{-1} for a recovery of 89.1% (±11.5%), however concentrations as low as 5 mg·mL^{-1} still provided a high recovery of 80.8% (±10.2%). Most surprisingly, we did not see any further increases in cell recovery for cells incubated with 200 mM proline and in most cases P2 actually performed better on its own. This could be due to proline and P2 sharing a protective mechanism to the point of a slight detrimental overload, however the mechanism of each compound requires further study.

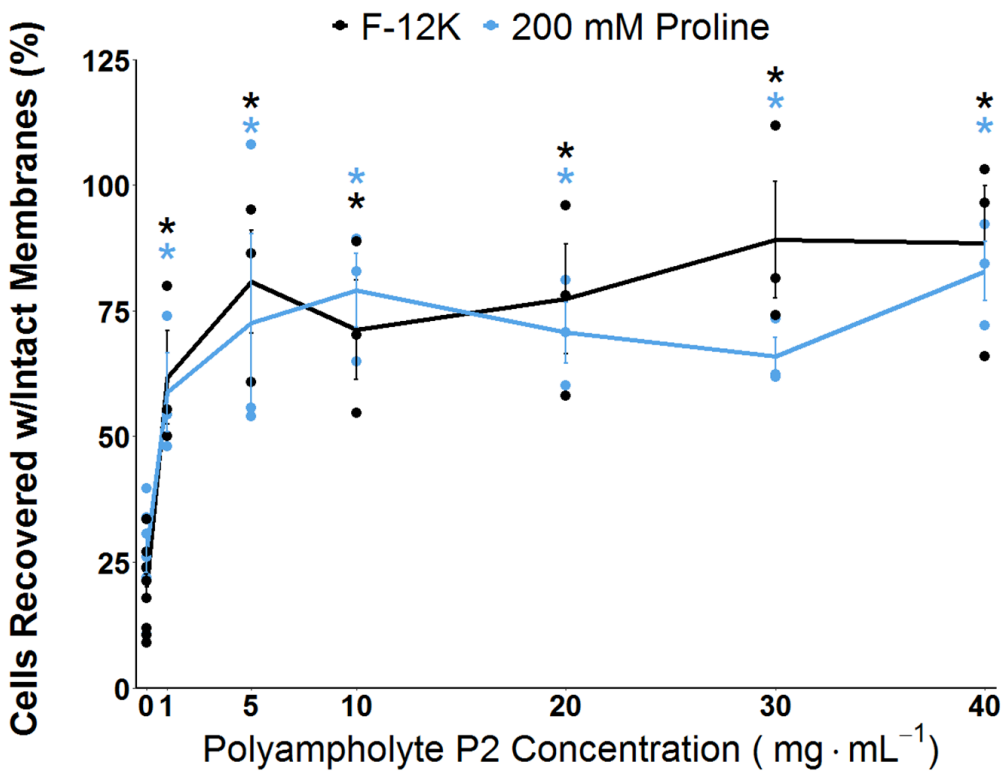

Figure 4.10. A549 polyampholyte P2 variable concentration monolayer freezing. Cells recovered after freezing to -80 °C. Error bars represent ± SEM of at least 3 independent experiments with two nested repeats. * P < 0.0001 from 0 mg·mL^{-1} F-12K.

4.4.1.6.3 A549 Polyampholyte P2 Reduced DMSO Monolayer Freezing

Due to the high recovery seen with P2 combined with 10% DMSO, we next tested to see if we could reduce the percentage of DMSO used during

cryopreservation. We tested three different polymer concentrations against five different DMSO percentages. We found that cells frozen with 40 mg·mL^{-1} and 5% DMSO had significantly higher recoveries than cells frozen with 10% DMSO alone (Fig 4.11, n = 3, P = 0.0000000001). We additionally observed that cells frozen with 10 mg·mL^{-1} and 5% DMSO along with 40 mg·mL^{-1} and 2% DMSO showed recoveries similar to cells frozen with 10% DMSO alone. The ability to lower the DMSO percentage while retaining recoveries similar to 10% DMSO alone could facilitate the storage of DMSO sensitive cells.

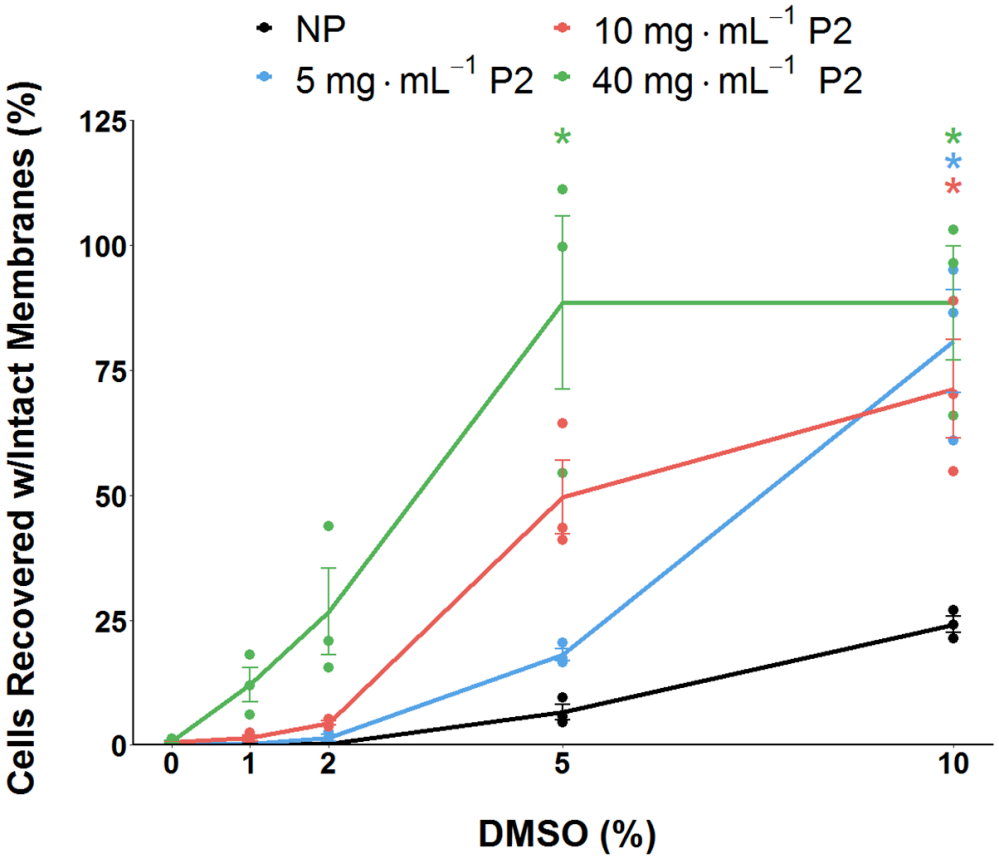

Figure 4.11. A549 polyampholyte P2 DMSO percentage monolayer freezing. Cells recovered after freezing to -80 °C. Error bars represent ± SEM of 3 independent experiments with two nested repeats. * P < 0.0001 from 10% DMSO NP (NP = no polymer).

4.4.1.6.4 MC-3T3 and Neuro-2a Polyampholyte P2 Variable Concentration Monolayer Freezing

As a final investigation into the cryoprotection of P2 polyampholyte, we tested the more sensitive immortalised cell lines of MC-3T3 and Neuro-2a. For MC-3T3 cells we saw that 5 and 30 mg·mL^{-1} resulted in significant increases from cells frozen with only 10% DMSO and for Neuro-2a cells we saw that 10, 20, and 30 mg·mL^{-1} resulted in significantly higher recovery than cells frozen with only 10% DMSO (Fig 4.12, $n \geq 3$, $P = 0.02$).

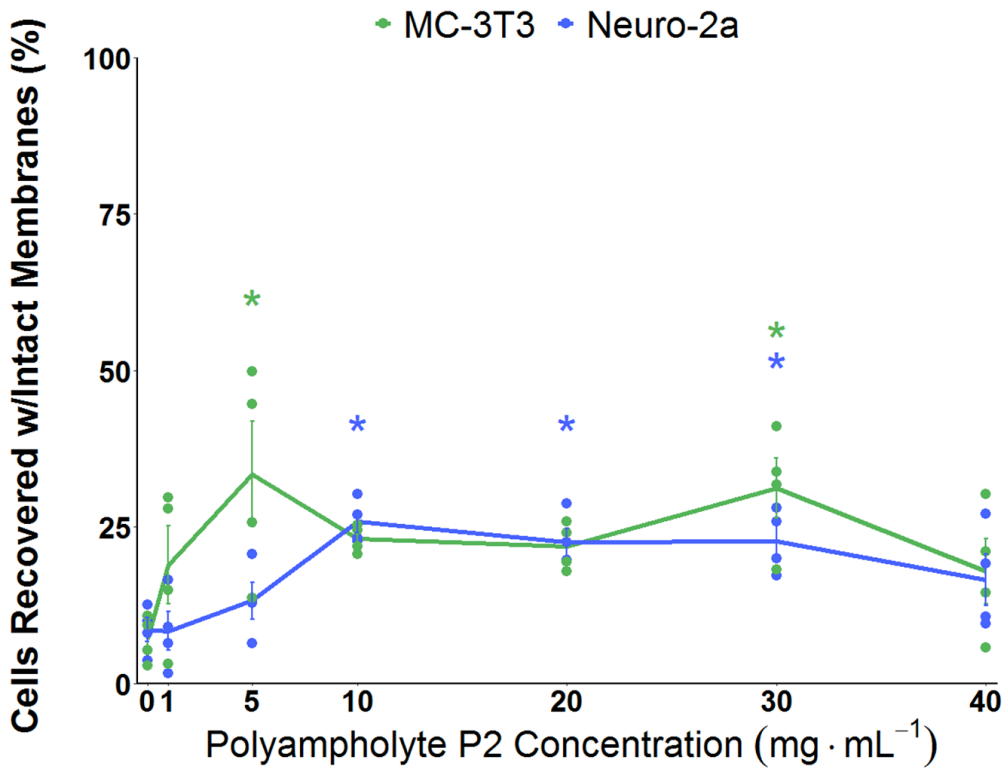

Figure 4.12. MC-3T3 and Neuro-2a polyampholyte P2 variable concentration monolayer freezing. Cells recovered after freezing to -80 °C. Error bars represent ± SEM of 3 independent experiments with two nested repeats. * P < 0.05 from 0 mg·mL^{-1} (of the same cell type).

This section has shown that the polyampholyte P2 is a powerful cryoprotectant not only for the robust A549 cell line but also the more delicate cells lines of MC-3T3 and Neuro-2a frozen as attached monolayers. These results indicate that P2

could be a universal cryoprotectant for many different cell types. We also demonstrated the ability to reduce the concentration of DMSO used while retaining recoveries similar to 10% DMSO. The ability to lower the DMSO concentration could dramatically increase the availability of cells that could otherwise not be used due to downstream DMSO toxicity issues.

4.4.2 Post-Freeze Viability

In order to assess the health of our cells post-freeze, utilising A549 cells, we conducted a growth viability assay of the cells after thawing. Typically with cryopreservation studies, either post-thaw recovery (how many cells are recovered after freezing) or post-thaw viability (how well the cells metabolise, grow, or behave after freezing) are reported, not always both. These are two independent measurements on the success of cryopreservation, and we feel both assays should be conducted to understand the full breadth of protection for the compound being tested. Our post-freeze viability assay was conducted in a similar manner as the growth assay in Section 3.4.2. Following a 24 h post-thaw incubation, the cells were detached and plated at identical densities, then assessed daily via the trypan blue exclusion assay to determine cell growth over 6 days. We were again looking for growth rates comparable to unfrozen controls.

4.4.2.1 Osmolyte PVA Post-Freeze Growth Rates

We conducted a 6-day post-freeze viability on cells frozen with 5 mg·mL^{-1} PVA, with or without a 24 h pre-incubation with our individual osmolyte compounds (Fig 4.20-4.23). Combining these results for rate of growth analysis, we found unfrozen control cells to have a day 6 rate of growth of 0.68 – 0.74 while cells frozen with 10% DMSO had a day 6 rate of 0.52 – 0.65 (Fig 4.13A, n = 3). Alanine (N = 2) had rates of 0.71 – 0.76, betaine showed rates of 0.59 – 0.71 and proline had rates of 0.53 – 0.65, respectively. These results were highly variable

and none of the conditions differed significantly from unfrozen control cells. Increasing the sample size may allow for more precise statistical analysis to determine significant differences in post-freeze growth rates for cells frozen with osmolyte pre-treatments. For cells frozen with 5 $mg \cdot mL^{-1}$ PVA included in the CPA we found a significantly lower rate of 0.55 – 0.60 compared to unfrozen control cells (Fig 4.13B, n = 3, P = 0.026), with this data set also showing 10% DMSO to have a significantly lower growth rate. For cells pre-incubated in osmolyte solutions and then frozen with PVA we found that alanine+PVA had a rate of 0.61 – 0.66, betaine+PVA showed a rate of 0.62 – 0.73 and proline+PVA had rates of 0.62 – 0.66. All cells with an osmolyte pre-incubation and frozen with PVA in the CPA had post-freeze rates of growth comparable to unfrozen control cells.

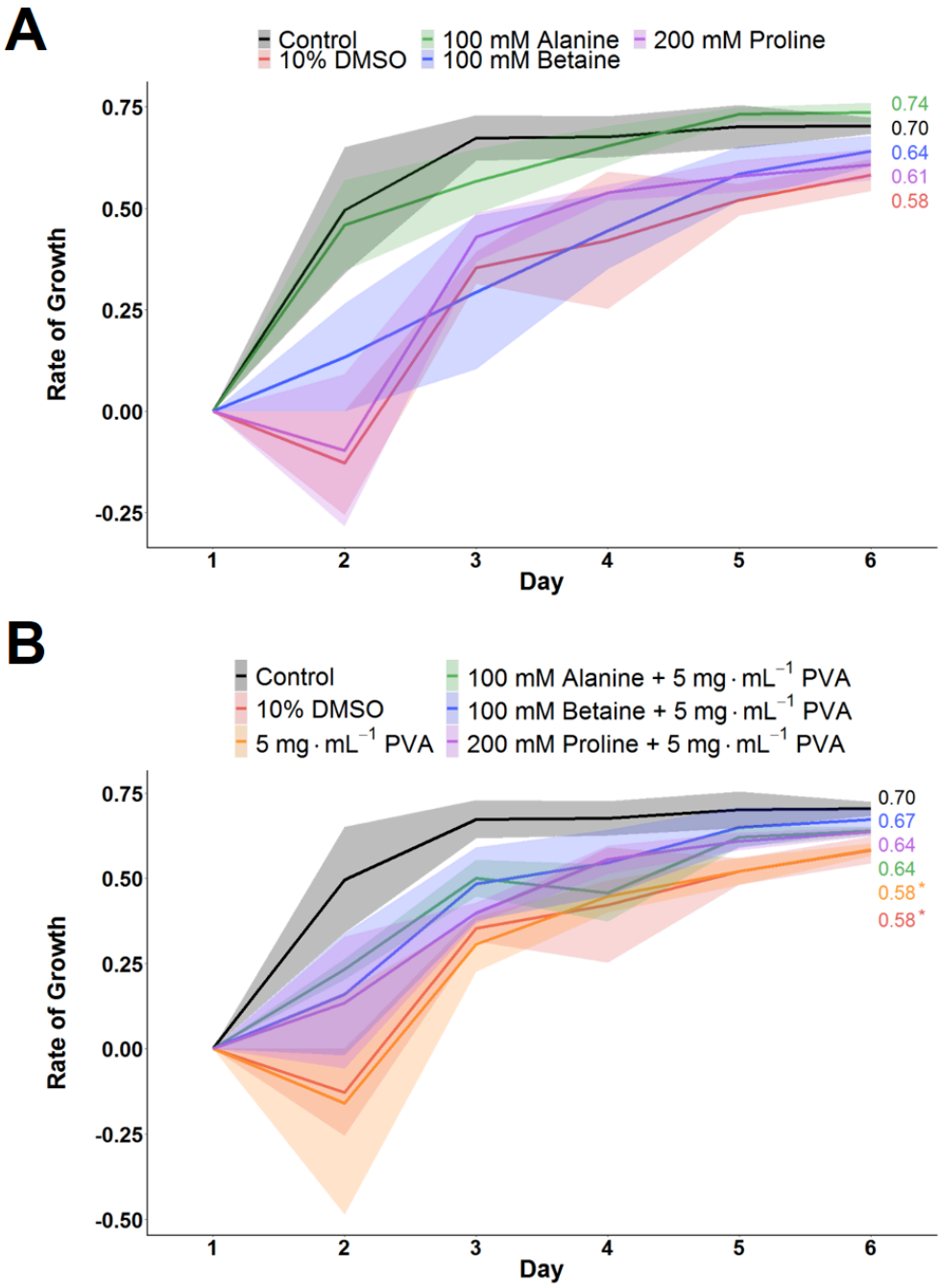

Figure 4.13. A549 osmolyte post-freeze growth rates. Rate of growth after freezing to -80 °C. **A)** Rate of growth following freezing with osmolyte solutions (100 mM alanine N=2; 10% DMSO and 100 mM betaine day 2 had no cells thus resulting in an 'undefined' rate for one data point each). **B)** Rate of growth following freezing with osmolyte solutions and PVA (10% DMSO-day 2 had no cells thus resulting in an 'undefined' rate for one data point, * $P < 0.03$ from control cells). Error represents ± SEM of 3 independent experiments

Overall, these results have shown that cells frozen in osmolyte solutions or an osmolyte solution with 5 mg·mL^{-1} PVA + 10% DMSO grew better than cells frozen

in just 10% DMSO or 5 mg·mL^{-1} PVA + 10% DMSO, highlighting the long term effect of the protective osmolytes of betaine and proline. This further shows that if post-thaw growth was our only post-freeze assessment, alanine would look like a suitable osmotic cryoprotectant, even though it resulted in much lower post-freeze cell recovery.

4.4.2.2 Polyproline Proline Post-Freeze Growth Rates

Monitoring the growth of the cells frozen with polyproline or 200 mM proline + polyproline revealed cells frozen with just 10 mg·mL^{-1} polyproline + 10% DMSO had a rate of growth of 0.60 – 0.66 (Fig 4.14, *n* = 3). Cells incubated in proline for 24 h then frozen with 10 mg·mL^{-1} polyproline + 10% DMSO had a rate of growth of 0.67 – 0.69, with all polyproline conditions comparable to unfrozen controls.

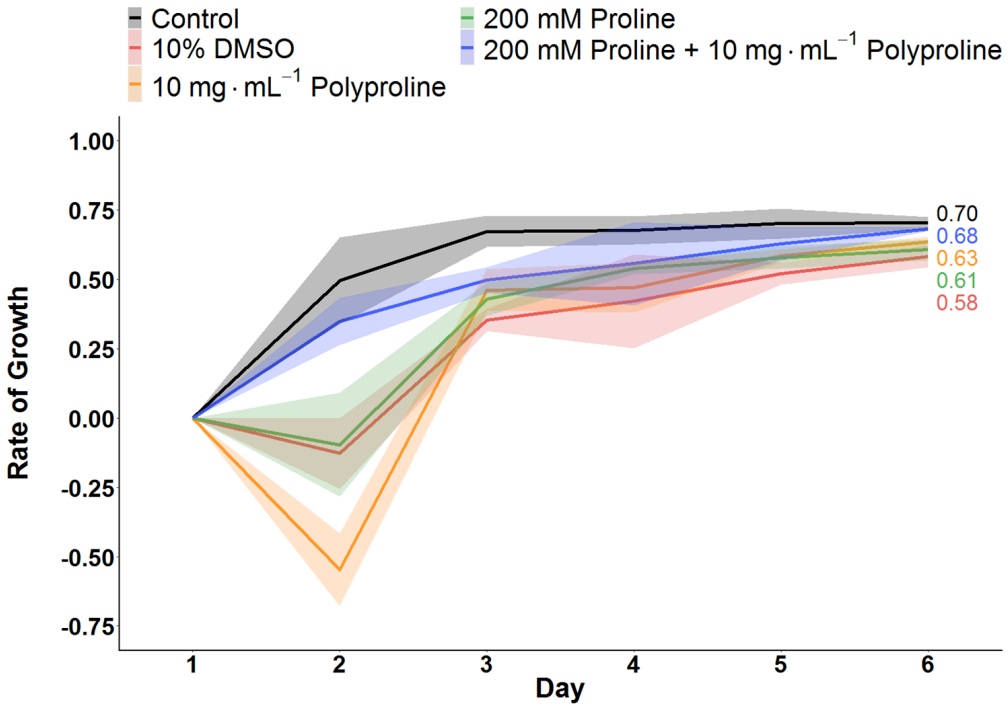

Figure 4.14. A549 polyproline post-freeze growth rates. Fold change after freezing to -80 °C. (10% DMSO-day 2 and 10 mg·mL^{-1} polyproline-day 3 had no cells thus resulting in an 'undefined' rate for one data point each). Error represents ± SEM of 3 independent experiments.

4.4.2.3 Polyampholyte Post-Freeze Growth Rates

Monitoring the growth of the cells frozen with polyampholyte revealed cells frozen with 10 mg·mL^{-1} P2 + 10% DMSO had a rate of growth of 0.57 – 0.64 (Fig 4.15, *n* = 3). All conditions frozen with 40 mg·mL^{-1} P2, regardless of DMSO concentration, showed lower growth rates than cells frozen with just 10% DMSO. We found that 40 mg·mL^{-1} P2 frozen with 2% DMSO had rates of 0.47 – 0.59, 40 mg·mL^{-1} P2 frozen with 5% DMSO had rates of 0.35 – 0.57, and 40 mg·mL^{-1} P2 frozen with 10% DMSO had rates of 0.49 – 0.59. All conditions were statistically similar to control cells, as there is large variability in this data set. Regardless, we believe that 10 mg·mL^{-1} P2 is the optimum concentration of for A549 cells and the trade-off between slower growth rates for higher concentrations/lower DMSO percentages should be considered based on the limiting factors of the cells (such as DMSO sensitivity).

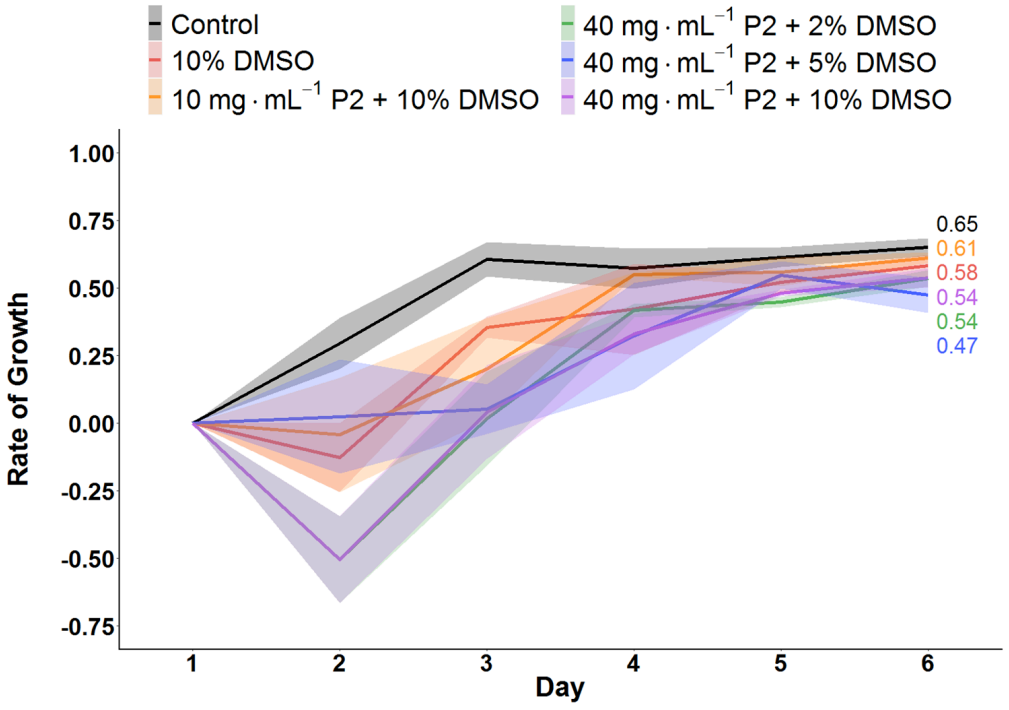

Figure 4.15. A549 polyampholyte P2 post-freeze growth rates. Fold change after freezing to -80 °C (10% DMSO-day 2 had no cells thus resulting in an 'undefined' rate for one data point). Error represents ± SEM of 3 independent experiments.

4.5 Conclusion

We have shown that combination of betaine or proline with PVA resulted in a significantly higher post-thaw recovery of A549 monolayers but the combination of proline with PVA was not successful for the cryopreservation of suspension human endometrial cells, MC-3T3 monolayers, or Neuro-2a monolayers. All A549 monolayers frozen with osmolytes and PVA grew better than cells frozen with only 10% DMSO. These results suggest that PVA's IRI (as demonstrated in Chapter 2) on its own is not sufficient for the cryopreservation of cell monolayers and that the extra necessary component for successful cryopreservation is seen in the preconditioning with betaine and proline, perhaps through osmo-protection or membrane protection. Polyproline, in combination with proline incubation, resulted in significantly higher recoveries for A549 cells frozen as monolayers compared to cells frozen with 10% DMSO. The combination of polyproline and proline also resulted in higher post-thaw growth rates. These results, correlated with our PVA results suggest that perhaps there is only a minimal amount of IRI necessary for the increased protection of cell monolayers. Polyproline was shown to have minimal IRI activity in Chapter 2 and yet, it performs similarly to the highly active IRI polymer PVA, both in its inability to provide protection on its own and in the presence of betaine or proline polyproline provides enhanced cryoprotection. This suggests that only a small amount of IRI may be necessary to provide improved cryoprotection. The polyampholyte P2 resulted in significantly higher post-thaw recoveries at all concentrations tested and the inclusion of proline did not further increase the recoveries seen for A549 monolayers. P2 also protected Neuro-2a and MC-3T3 cells, and also allowed for the lowering of DMSO down to 2% with recoveries comparable to 10% DMSO alone. Cells frozen with 10 $mg \cdot mL^{-1}$ P2 also grew better post-freeze compared to cells frozen with only 10% DMSO. Similar to polyproline, P2 showed minimal IRI activity in Chapter 2, however the added protection provided by proline was not necessary for improved

cryopreservation outcomes with P2. This suggest that P2 has a dual action of minimal IRI and membrane or osmo-protection, or that it acts in a singular fashion such that the membrane or osmo-protection is great enough that IRI does not damage the cells, or that proline and P2 have overlapping mechanisms to the point of being detrimental. Our results with PVA highlight how different cell types respond differently to CPA treatments, however, the apparent universal protection offered by P2 shows exciting potential as a powerful new cryoprotectant. Our results have been summarised in Table 4.1. There are several exciting avenues to follow up the questions remaining in this work. Since PVA's IRI activity has been linked to concentration and polymer length, it is possible to engineer a polymer with the same IRI activity as P2 to test if the same cryoprotection is observed with the less active IRI PVA (in the presence of a protective osmolyte), potentially demonstrating an IRI minimal threshold for cryoprotection. Another area for investigation would be to cryopreserve cells in the presence of PVA and P2 to evaluate if any further protection is gained, which would help to delineate the role of IRI as a mechanism of P2 if increased post-thaw viability is observed, it could be that P2 has a minimal role as an IRI active polymer and further protection can be obtained by the combination of the two polymers.

Table 4.1. Chapter 4 results summary. Significantly higher than control, significantly lower than control (*N=2).

Target	**A549 Monolayer Cryopreservation** ↑	Post-Freeze Growth Rate (Day 6)
Unfrozen Control	-	0.70
10% DMSO	16.9	**0.58**
5 mg·mL^{-1} PVA	23.7	**0.58**
100 mM Alanine	24.1	0.74
Alanine + PVA	**38.7**	0.64
100 mM Betaine	30.0	0.64
Betaine + PVA	**56.7**	0.67
200 mM Proline	**45.7**	0.61
Proline + PVA	**62.7**	0.64
10 mg·mL^{-1} Polyproline	20.3	0.63
Proline + Polyproline	**47.6**	0.68
10 mg·mL^{-1} P2 Polyampholyte	**71.2**	0.61

4.6 Materials and Methods

4.6.1 Reagents

All non-specified chemicals were obtained from Sigma Aldrich Co Ltd, (Irvine, UK).

Polyproline was synthesised as in Section 2.6.1.1.

Polyampholyte was synthesised as in Section 2.6.1.2.

4.6.2 A549 Cell Culture

A549 cells were cultured as per Section 3.6.2.

4.6.3 Neuro-2a Cell Culture

Mouse brain neuroblastoma cells (Neuro-2a) were obtained from American Tissue Culture Collection (ATCC) (Middlesex, UK) and grown in 75 cm^2 cell culture Nunc flasks. Standard cell culture medium was composed of Eagle's Minimum Essential Media (EMEM) (Gibco) supplemented with 10 % USA-origin foetal bovine serum (FBS), 100 units·mL^{-1} penicillin, 100 µg·mL^{-1} streptomycin, and 250 ng·mL^{-1} amphotericin B (PSA). Neuro-2a cells were maintained in a humidified atmosphere of 5% CO_2 and 95% air at 37 °C and the culture medium was renewed every 3 - 4 days. The cells were subcultured every 7 days or before reaching 90% confluency. To subculture, cells were dissociated using 0.25% trypsin plus 1 mM EDTA in balanced salt solution (Gibco) and reseeded at $7.5 \cdot 10^4$ cells per 75 cm^2 cell culture flasks.

4.6.4 MC-3T3 Cell Culture

Mouse calvarial osteoblastic cells (MC-3T3-E1) were obtained from ECACC and grown in 75 cm^2 cell culture Nunc flasks. Standard cell culture medium was composed of Minimum Essential Medium α (MEM-Alpha) (Gibco) supplemented with 10 % USA-origin foetal bovine serum (FBS), 100 units·mL^{-1} penicillin, 100 µg·mL^{-1} streptomycin, and 250 ng·mL^{-1} amphotericin B (PSA). MC-3T3 cells were maintained in a humidified atmosphere of 5% CO_2 and 95% air at 37 °C and the culture medium was renewed every 3–4 days. The cells were subcultured every 7 days or before reaching 90% confluency. To subculture, cells were dissociated using 0.25% trypsin plus 1 mM EDTA in balanced salt solution (Gibco) and reseeded at $1.87 \cdot 10^5$ cells per 75 cm^2 cell culture flasks.

4.6.5 Primary Endothelial Cell Culture

Methods adapted from Barros (2016)[34]. Endometrial biopsies were obtained by Dr Jan Brosens from women attending the Implantation Clinic, a dedicated

research clinic at University Hospitals Coventry and Warwickshire National Health Service Trust. All research was undertaken with full ethical approval and with written informed consent obtained from all participants in accordance with the guidelines in The Declaration of Helsinki 2000. Biopsies were taken during the secretory phase of the menstrual cycle using an Endocell cannula, starting from the uterine fundus and moving downward to the internal cervical ostium. The endometrial biopsy was placed in a labelled Bijoux tube containing 5 ml cell culture media and processed immediately.

Tissue was diced for 5 min with a scalpel to dissociate the tissue. Sample was then incubated in digestion media containing additive-free Dulbecco's minimum essential media (DMEM) (Gibco), 0.5 $mg \cdot mL^{-1}$ collagenase (Sigma-Aldrich), and 0.1 $mg \cdot mL^{-1}$ DNase I (Roche Diagnostics) for 1 h to promote further dissociation; sample was shaken every 15 minutes. Sample was then passed through a 0.2 µm membrane to allow endometrial stromal cells (ESC) and red blood cells to pass through. The membrane was then back washed to collect endometrial epithelial cells (EEC). Samples were spun at 2 g for 5 min, supernatant removed, and cells were resuspended in DMEM containing 10% dextran-coated charcoal FCS (DCC) (Gibco).

4.6.6 Solution Preparation

Solutions for cell experiments were prepared by dissolving the individual compounds in base cell media supplemented with 10% FBS and 1x PSA (solutions used as freezing buffers did not contain PSA) and sterile filtering prior to use.

4.6.7 Monolayer plate collagen coating

As indicated in experiments, to promote attachment of cells, collagen I from rat tail (Sigma-Aldrich) was diluted to 50 $\mu g \cdot mL^{-1}$ in 200 mM acetic acid (Sigma) and

added to each well of a 24-well cell culture plate at 5 µg collagen·cm^{-2}. Plates were incubated with the dissolved collagen for 1 h at room temperature. After this incubation period the collagen solution was removed and the plates were rinsed three times with 200 µL Dulbecco's phosphate buffered saline (Thermo Fisher) to remove any residual acetic acid solution. The collagen treated plates were allowed to dry for 1 h in a laminar flow hood and stored for less than 1 week at 4 °C prior to use.

4.6.8 Cryopreservation of Cell Monolayers

Methods adapted from Bailey.[9] Cells to be frozen in monolayer format were seeded at 0.4·10^6 (A549) or 0.5·10^6 (Neuro-2a, MC-3T3) cells per well in 500 µL of cell culture medium in 24-well plates (Corning Incorporated, Corning, NY). Plates had a total available volume of 3.4 mL with an approximate growth area of 1.9 cm^2, no coverslips were used and plates were used with the accompanying lid. Cells were allowed to attach to the entire free surface of the bottom of the well and formed a confluent layer not greater in height than one cell. Before experimental treatments, cells were allowed to attach for 2 h to the plates in a humidified atmosphere of 5% CO_2 and 95% air at 37 °C. The medium was exchanged against medium that was or was not supplemented with solutes as indicated in the figures. Control cells received no additional solutes and experimental cells were incubated in indicated solutions for 24 h in a humidified atmosphere of 5% CO_2 and 95% air at 37 °C. Following the incubation period, the culture medium was removed and cells were exposed for 10 min at room temperature to different concentrations of solutes dissolved in base media supplemented with 10% FBS and indicated concentrations of DMSO. After 10 min, the freezing solutions were removed and the plate placed inside a CoolCell® MP plate (BioCision, LLC, Larkspur, CA), transferred to a -80 °C freezer and frozen at a rate of 1 °C·min^{-1}. After 24 h at -80 °C, cells were rapidly thawed by

addition of 500 µL complete cell culture medium warmed to 37 °C. Cells were placed in a humidified atmosphere for 24 h and then dissociated using 0.25% trypsin plus 1 mM EDTA in balanced salt solution. The number of viable cells was then determined by counting with a hemocytometer (Sigma Aldrich) at room temperature after 1:1 dilution of the sample with 0.4% trypan blue solution (Sigma Aldrich). The initial cell medium was discarded such that any non-attached cells were not included in the assessment. The percentage of recovered cells was calculated by dividing the number of cells with intact membranes after freezing and thawing by the number of cells present prior to freezing (i.e. after application of pre-treatments), multiplied by 100.

4.6.9 Primary Endothelial Suspension Freezing

Cells were counted to determine starting number and diluted such that 500 µL of cell solution was placed into cryovials with 500 µL of different freezing mediums containing 10% DMSO. Cryovials were placed in a Mr. Frosty (Nalgene) and placed inside a -80 °C freezer for 24 h. Samples were then moved into liquid nitrogen (-196 °C) for 6 days. Samples were thawed by placing them in a 37 °C water bath. Post-thaw cells were plated in T-25 flasks (Thermo Fisher) in DMEM containing 10% DCC for 24 h. ESCs were dissociated using 0.25% trypsin plus 1mM EDTA in balanced salt solution. EECs were not attached and were simply washed off the flask and collected. The number of viable cells was determined by counting with a hemocytometer after 1:1 dilution of the sample with 0.4% trypan blue solution.

4.6.10 Post-freezing Cell Viability Assay

Cells were frozen as indicated in Section 4.6.8. Cells were then seeded at $12.5 \cdot 10^3$ per well in 6-well plates in 2 mL of complete cell media. Cells were placed in a humidified atmosphere of 5% CO_2 and 95% air at 37 °C and allowed

to grow, with counts starting on day two and commencing on day six. Cell media was renewed on day three. Cells were dissociated using 0.25% trypsin plus 1 mM EDTA in balanced salt solution. The number of viable cells was then determined by counting with a hemocytometer at room temperature after 1:1 dilution of the sample with 0.4% trypan blue solution. Fold increase of cells was calculated by dividing the number of cells with intact cell membranes by the number of cells initially plated.

4.6.11 Statistical Analysis

Data were analysed with a one-way analysis of variance (ANOVA) on ranks followed by comparison of experimental groups with the appropriate control group (Holm–Sidak method) followed by Tukey's post hoc test. Excel 2013 (Microsoft, Redmond, WA) and R were used for the analyses and graphs. Data sets are presented as mean ± (SEM).

4.7 Appendix

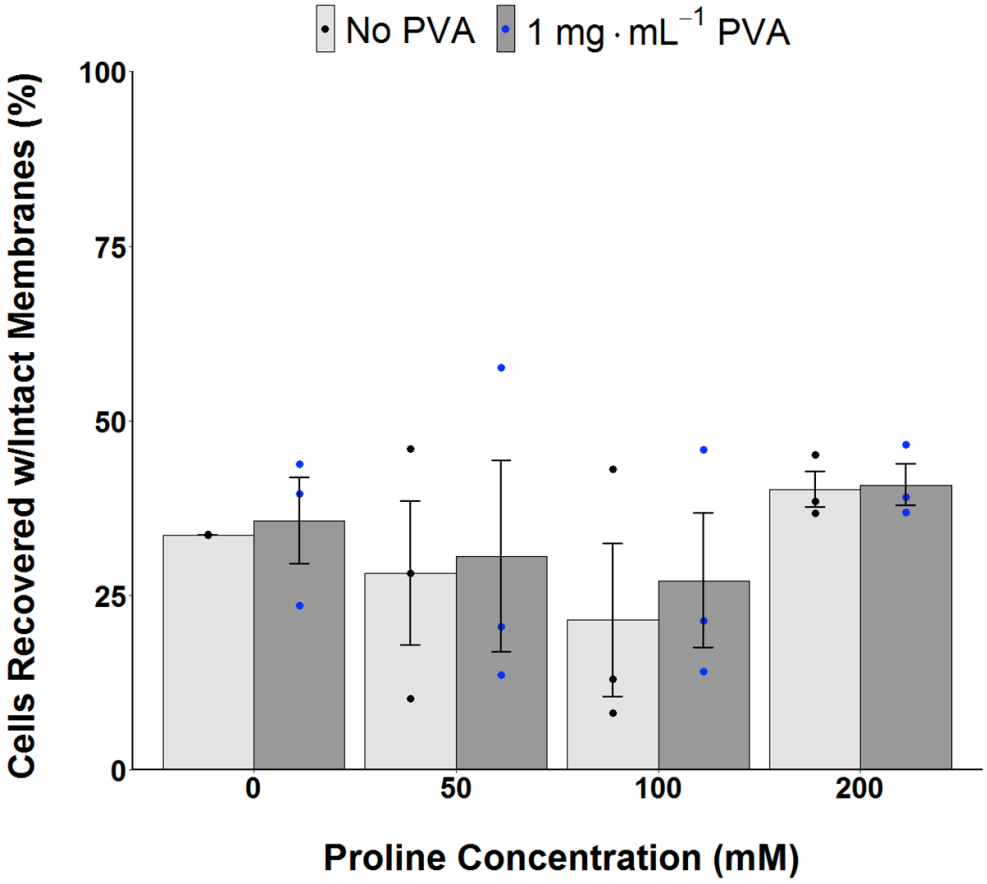

Figure 4.16. A549 proline concentration monolayer freezing. Cells recovered after freezing to -80 °C. Error bars represent ± SEM of 3 independent experiments with two nested replicates.

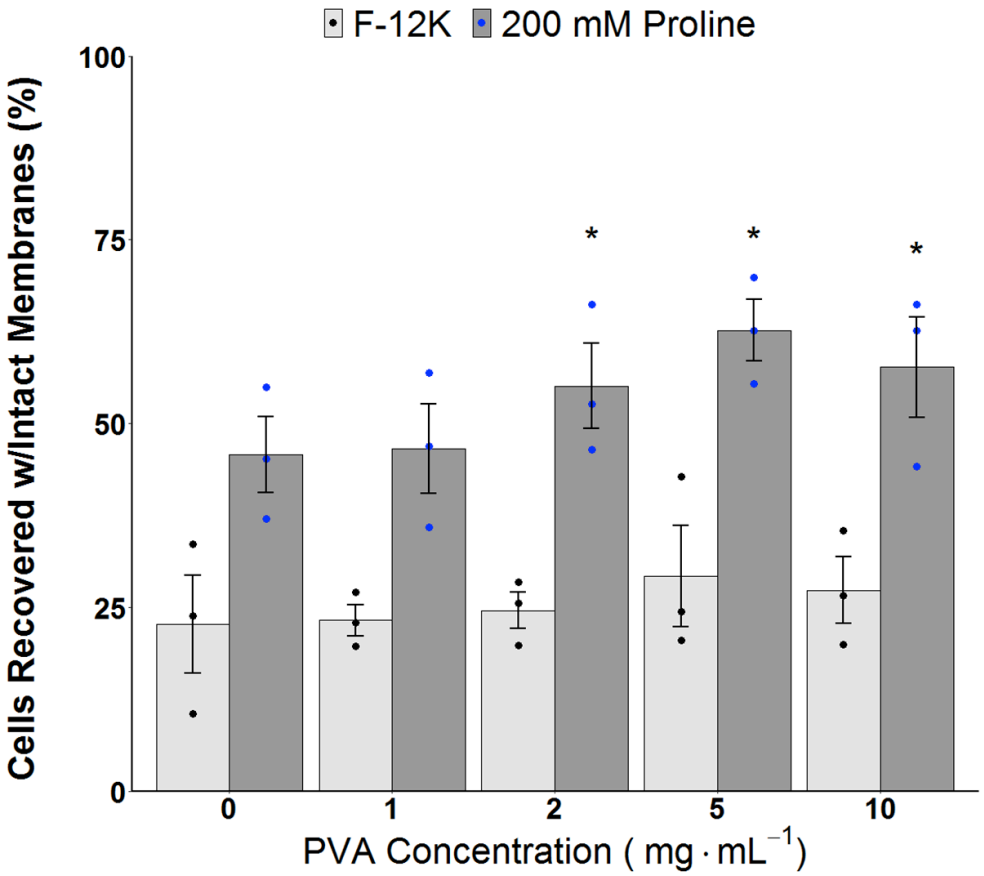

Figure 4.17. A549 proline PVA concentration monolayer freezing. Cells recovered after freezing to -80 °C. Error bars represent ± SEM of 3 independent experiments with two nested replicates. * P < 0.00001 from control (0 mg·mL^{-1} in F-12K).

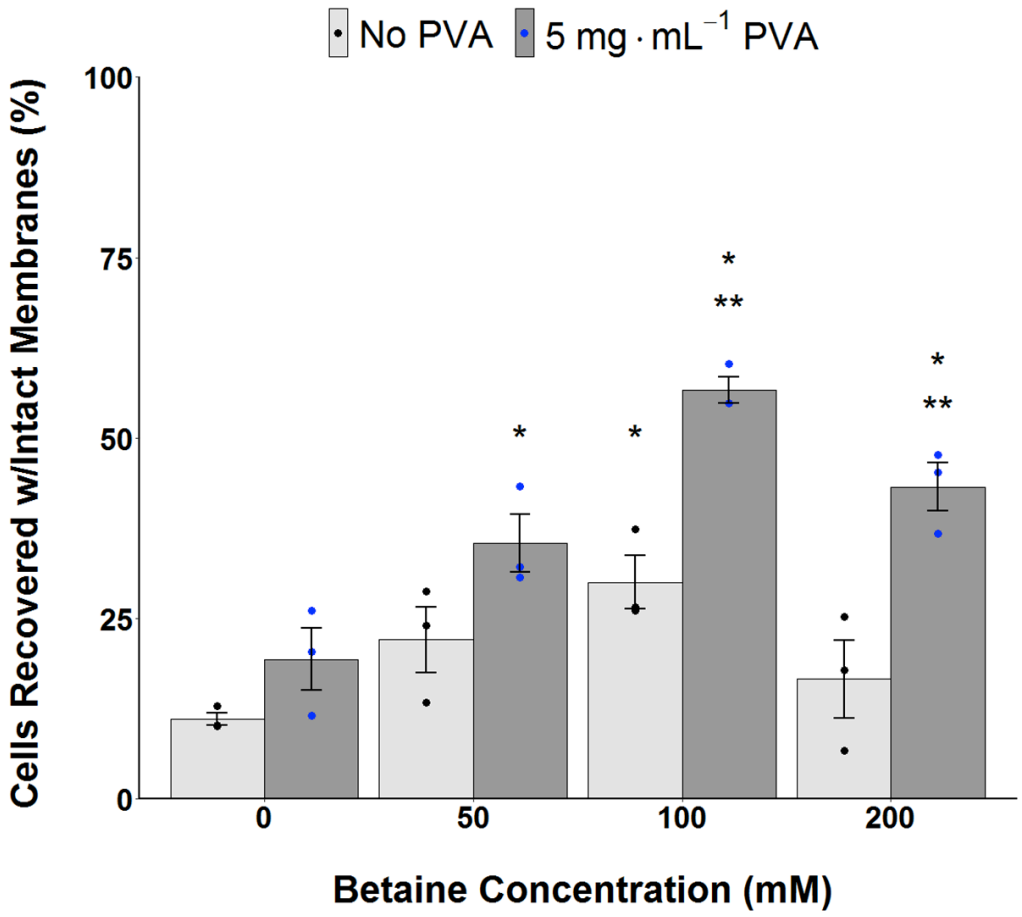

Figure 4.18. A549 betaine concentration monolayer freezing. Cells recovered after freezing to -80 °C. Error bars represent ± SEM of 3 independent experiments with two nested replicates. * P < 0.00001 from control (0 mM no PVA). ** P < 0.0001 from control with 5 mg·mL^{-1} PVA.

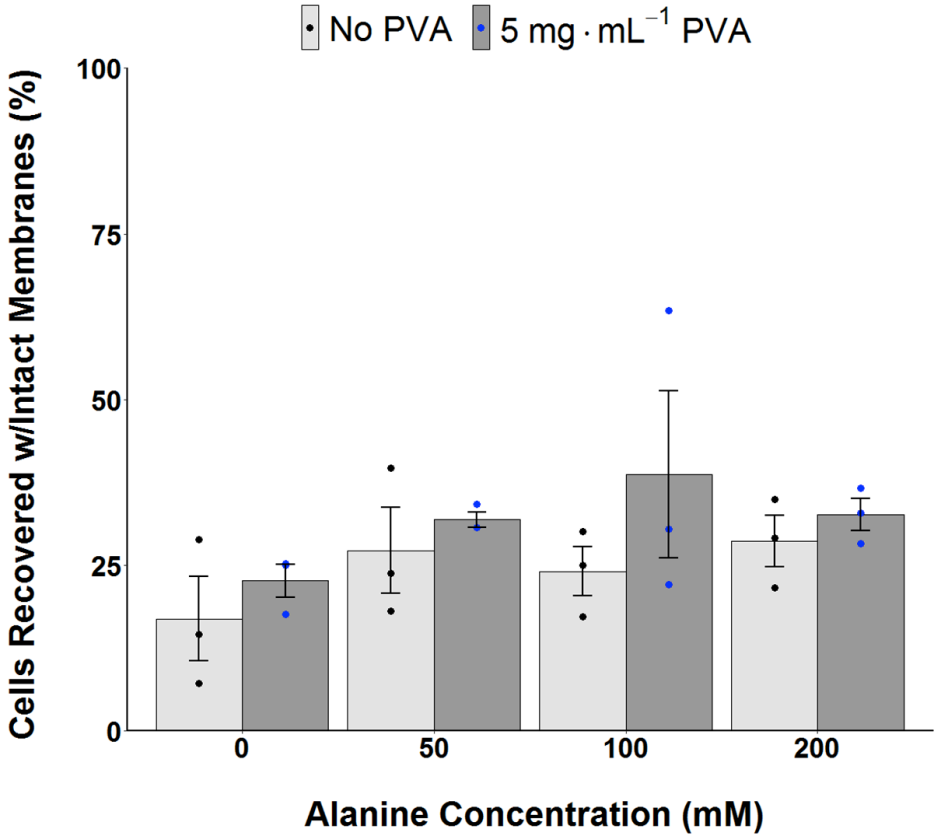

Figure 4.19. A549 alanine concentration monolayer freezing. Cells recovered after freezing to -80 °C. Error bars represent ± SEM of 3 independent experiments with two nested replicates.

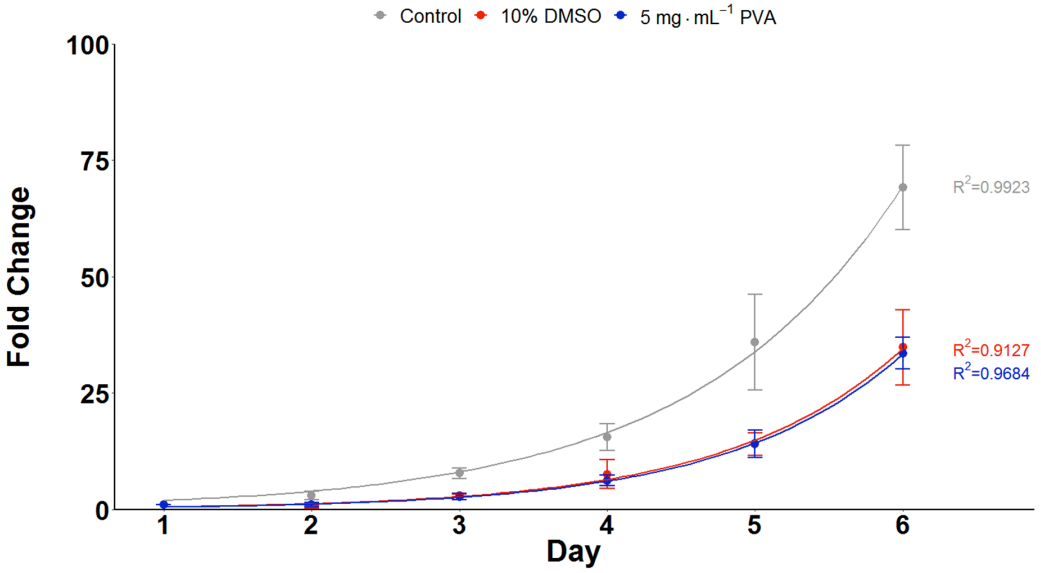

Figure 4.20. A549 PVA post-freeze growth rates. Growth rates after freezing to -80 °C. Error bars represent ± SEM of 3 independent experiments.

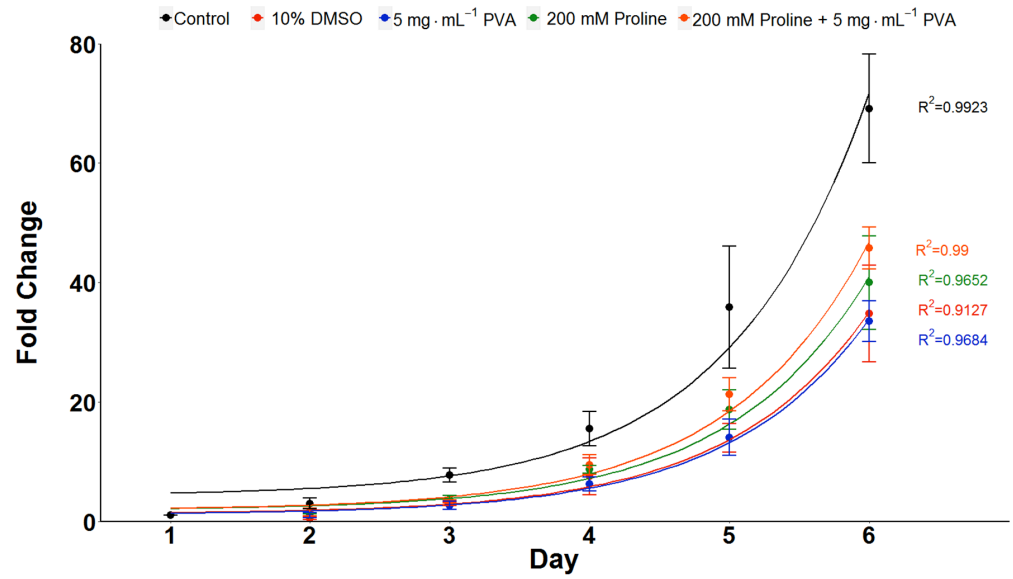

Figure 4.21. A549 proline post-freeze growth rates. Growth rates after freezing to -80 °C. Error bars represent ± SEM of 3 independent experiments.

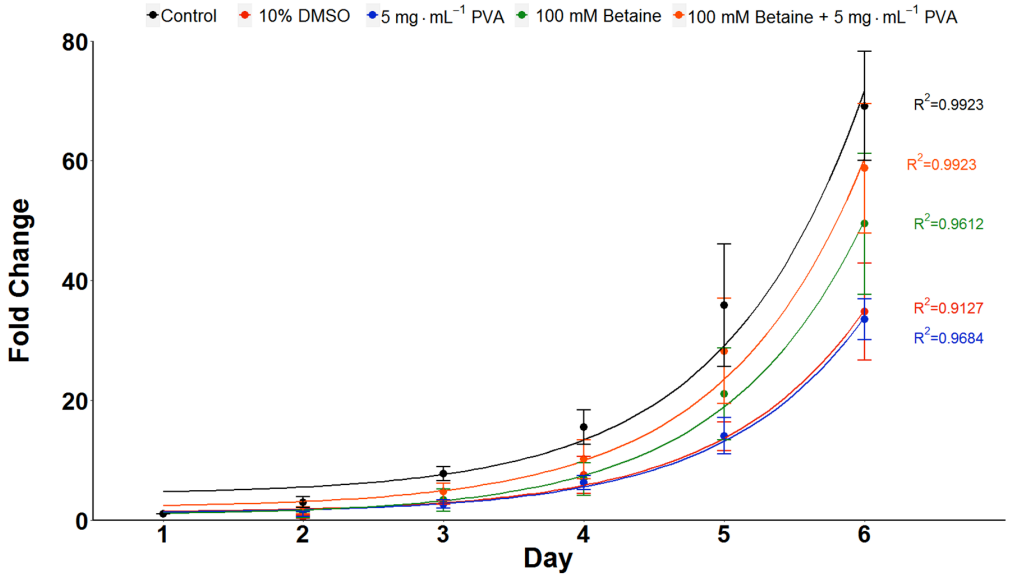

Figure 4.22. A549 betaine post-freeze growth rates. Growth rates after freezing to -80 °C. Error bars represent ± SEM of 3 independent experiments.

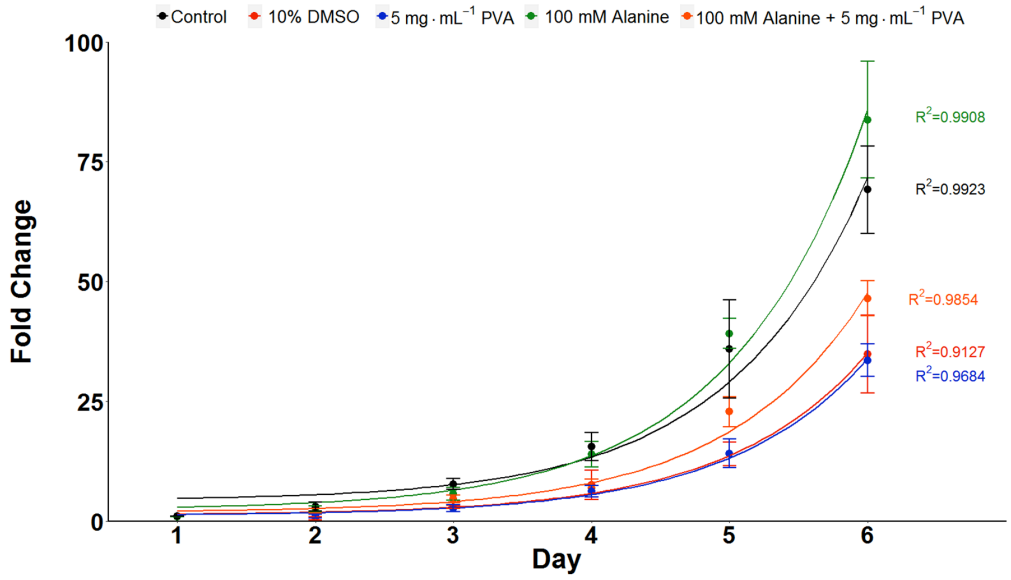

Figure 4.23. A549 alanine post-freeze growth rates. Growth rates after freezing to -80 °C. Error bars represent ± SEM of 3 independent experiments (100 mM alanine N=2).

4.8 References

(1) Matsumura, K.; Kawamoto, K.; Takeuchi, M.; Yoshimura, S.; Tanaka, D.; Hyon, S.-H. H. Cryopreservation of a Two-Dimensional Monolayer Using a Slow Vitrification Method with Polyampholyte to Inhibit Ice Crystal Formation. *ACS Biomater. Sci. Eng.* **2016**, *2* (6), 1023–1029. https://doi.org/10.1021/acsbiomaterials.6b00150.

(2) Bahari, L.; Bein, A.; Yashunsky, V.; Braslavsky, I. Directional Freezing for the Cryopreservation of Adherent Mammalian Cells on a Substrate. *PLoS One* **2018**, *13* (2), e0192265. https://doi.org/10.1371/journal.pone.0192265.

(3) Pless-Petig, G.; Knoop, S.; Rauen, U. Serum- and Albumin-Free Cryopreservation of Endothelial Monolayers with a New Solution. *Organogenesis* **2018**, *14* (2), 107–121. https://doi.org/10.1080/15476278.2018.1501136.

(4) Miyamoto, Y.; Enosawa, S.; Takeuchi, T.; Takezawa, T. Cryopreservation in Situ of Cell Monolayers on Collagen Vitrigel Membrane Culture Substrata: Ready-to-Use Preparation of Primary Hepatocytes and ES Cells. *Cell Transplant.* **2009**, *18* (5–6), 619–626. https://doi.org/10.1016/j.cryobiol.2009.10.036.

(5) Stevenson, D. J.; Morgan, C.; Goldie, E.; Connel, G.; Grant, M. H. Cryopreservation of Viable Hepatocyte Monolayers in Cryoprotectant Media with High Serum Content: Metabolism of Testosterone and Kaempherol Post-Cryopreservation. *Cryobiology* **2004**, *49* (2), 97–113. https://doi.org/10.1016/j.cryobiol.2004.05.006.

(6) Pasch, J.; Schiefer, A.; Heschel, I.; Rau, G. Cryopreservation of Keratinocytes in a Monolayer. *Cryobiology* **1999**, *39* (2), 158–168. https://doi.org/10.1006/cryo.1999.2197.

(7) Pasch, J.; Schiefer, A.; Heschel, I.; Dimoudis, N.; Rau, G. Variation of the HES Concentration for the Cryopreservation of Keratinocytes in Suspensions and in Monolayers. *Cryobiology* **2000**, *41* (2), 89–96. https://doi.org/10.1006/cryo.2000.2270.

(8) Stokich, B.; Osgood, Q.; Grimm, D.; Moorthy, S.; Chakraborty, N.; Menze, M. A. Cryopreservation of Hepatocyte (HepG2) Cell Monolayers: Impact of Trehalose. *Cryobiology* **2014**, *69* (2), 281–290. https://doi.org/10.1016/j.cryobiol.2014.08.001.

(9) Bailey, T. L.; Wang, M.; Solocinski, J.; Nathan, B. P.; Chakraborty, N.; Menze, M. A. Protective Effects of Osmolytes in Cryopreserving Adherent Neuroblastoma (Neuro-2a) Cells. *Cryobiology* **2015**, *71* (3), 472–480. https://doi.org/10.1016/j.cryobiol.2015.08.015.

(10) Tomás, R. M. F.; Bailey, T. L.; Hasan, M.; Gibson, M. I. Extracellular Antifreeze Protein Significantly Enhances the Cryopreservation of Cell Monolayers. *Biomacromolecules* **2019**, *20* (10), 3864–3872. https://doi.org/10.1021/acs.biomac.9b00951.

(11) Eskandari, N.; Marquez-Curtis, L. A.; McGann, L. E.; Elliott, J. A. W. Cryopreservation of Human Umbilical Vein and Porcine Corneal Endothelial Cell Monolayers. *Cryobiology* **2018**, *85* (September), 63–72. https://doi.org/10.1016/j.cryobiol.2018.10.001.

(12) Heng, B. C.; Ye, C. P.; Liu, H.; Toh, W. S.; Rufaihah, A. J.; Yang, Z.; Bay, B. H.; Ge, Z.; Ouyang, H. W.; Lee, E. H.; Cao, T. Loss of Viability during Freeze-Thaw of Intact and Adherent Human Embryonic Stem Cells with Conventional Slow-

Cooling Protocols Is Predominantly Due to Apoptosis Rather than Cellular Necrosis. *J. Biomed. Sci.* **2006**, *13* (3), 433–445. https://doi.org/10.1007/s11373-005-9051-9.

(13) De Loecker, P.; Fuller, B. J.; Koptelov, V. A.; De Loecker, W. Metabolic Activity of Freshly Prepared and Cryopreserved Hepatocytes in Monolayer Culture. *Cryobiology* **1993**, *30* (1), 12–18. https://doi.org/10.1006/cryo.1993.1002.

(14) Watts, P.; Grant, M. H. Cryopreservation of Rat Hepatocyte Monolayer Cultures. *Hum. Exp. Toxicol.* **1996**, *15* (1), 30–37. https://doi.org/10.1177/096032719601500106.

(15) McKay, G. C.; Henderson, C.; Goldie, E.; Connel, G.; Westmoreland, C.; Grant, M. H. Cryopreservation of Rat Hepatocyte Monolayers: Cell Viability and Cytochrome P450 Content in Post-Thaw Cultures. *Toxicol. Vitr.* **2002**, *16* (1), 71–79. https://doi.org/10.1016/S0887-2333(01)00096-0.

(16) Deller, R. C.; Vatish, M.; Mitchell, D. A.; Gibson, M. I. Synthetic Polymers Enable Non-Vitreous Cellular Cryopreservation by Reducing Ice Crystal Growth during Thawing. *Nat. Commun.* **2014**, *5*, 1–7. https://doi.org/10.1038/ncomms4244.

(17) Bailey, T. L.; Stubbs, C.; Murray, K.; Tomás, R. M. F.; Otten, L.; Gibson, M. I. Synthetically Scalable Poly(Ampholyte) Which Dramatically Enhances Cellular Cryopreservation. *Biomacromolecules* **2019**, *20* (8), 3104–3114. https://doi.org/10.1021/acs.biomac.9b00681.

(18) Spindler, R.; Rosenhahn, B.; Hofmann, N.; Glasmacher, B. Video Analysis of Osmotic Cell Response during Cryopreservation. *Cryobiology* **2012**, *64* (3), 250–260. https://doi.org/10.1016/j.cryobiol.2012.02.008.

(19) Meryman, H. T. Cryopreservation of Living Cells: Principles and Practice. *Transfusion* **2007**, *47* (5), 935–945. https://doi.org/10.1111/j.1537-2995.2007.01212.x.

(20) Sosef, M. N.; Baust, J. M.; Sugimachi, K.; Fowler, A.; Tompkins, R. G.; Toner, M. Cryopreservation of Isolated Primary Rat Hepatocytes: Enhanced Survival and Long-Term Hepatospecific Function. *Ann. Surg.* **2005**, *241* (1), 125–133. https://doi.org/10.1097/01.sla.0000149303.48692.0f.

(21) Tarasov, A. I.; Petrenko, A. Y.; Jones, D. R. E. The Osmotic Characteristics of Human Fetal Liver-Derived Hematopoietic Stem Cell Candidates. *Cryobiology* **2004**, *48* (3), 333–340. https://doi.org/10.1016/j.cryobiol.2004.02.010.

(22) Shichkin, V. P.; Gorbach, O. I.; Zuieva, O. A.; Grabchenko, N. I.; Aksyonova, I. A.; Todurov, B. M. Effect of Cryopreservation on Viability and Growth Efficiency of Stromal-Epithelial Cells Derived from Neonatal Human Thymus. *Cryobiology* **2017**, *78*, 70–79. https://doi.org/10.1016/j.cryobiol.2017.06.010.

(23) Zhao, J.; Hao, H. N.; Thomas, R. L.; Lyman, W. D. An Efficient Method for the Cryopreservation of Fetal Human Liver Hematopoeitic Progenitor Cells. *Stem Cells* **2001**, *19* (3), 212–218. https://doi.org/10.1634/stemcells.19-3-212.

(24) Petrenko, Y. A.; Jones, D. R. E.; Petrenko, A. Y. Cryopreservation of Human Fetal Liver Hematopoietic Stem/Progenitor Cells Using Sucrose as an Additive to the Cryoprotective Medium. *Cryobiology* **2008**, *57* (3), 195–200. https://doi.org/10.1016/j.cryobiol.2008.08.003.

(25) Mackensen, A.; Dräger, R.; Schlesier, M.; Mertelsmann, R.; Lindemann, A. Presence of IgE Antibodies to Bovine Serum Albumin in a Patient Developing Anaphylaxis after Vaccination with Human Peptide-Pulsed Dendritic Cells. *Cancer Immunol. Immunother.* **2000**, *49* (3), 152–156. https://doi.org/10.1007/s002620050614.

(26) Smith, I. O.; McCabe, L. R.; Baumann, M. J. MC3T3-E1 Osteoblast Attachment and Proliferation on Porous Hydroxyapatite Scaffolds Fabricated with Nanophase Powder. *Int. J. Nanomedicine* **2006**, *1* (2), 189–194. https://doi.org/10.2147/nano.2006.1.2.189.

(27) O'Brien, F. J.; Harley, B. A.; Yannas, I. V.; Gibson, L. J. The Effect of Pore Size on Cell Adhesion in Collagen-GAG Scaffolds. *Biomaterials* **2005**, *26* (4), 433–441. https://doi.org/10.1016/j.biomaterials.2004.02.052.

(28) Sudo, H.; Kodama, H. A.; Amagai, Y.; Yamamoto, S.; Kasai, S. In Vitro Differentiation and Calcification in a New Clonal Osteogenic Cell Line Derived from Newborn Mouse Calvaria. *J. Cell Biol.* **1983**, *96* (1), 191–198. https://doi.org/10.1083/jcb.96.1.191.

(29) Jiang, R.; Shen, H.; Piao, Y.-J. The Morphometrical Analysis on the Ultrastructure of A549 Cells. *Rom. J. Morphol. Embryol.* **2010**, *51* (4), 663–667.

(30) Cheung, W. M. W.; Ng, W. W.; Kung, A. W. C. Dimethyl Sulfoxide as an Inducer of Differentiation in Preosteoblast MC3T3-E1 Cells. *FEBS Lett.* **2006**, *580* (1), 121–126. https://doi.org/10.1016/j.febslet.2005.11.062.

(31) Yan, Y.; Sun, H.; Gong, Y.; Yan, Z.; Zhang, X.; Guo, Y.; Wang, Y. Mechanical Strain Promotes Osteoblastic Differentiation through Integrin-B1-Mediated β-Catenin Signaling. *Int. J. Mol. Med.* **2016**, *38* (2), 594–600. https://doi.org/10.3892/ijmm.2016.2636.

(32) Zalis, M. C.; Reyes, J. F.; Augustsson, P.; Holmqvist, S.; Roybon, L.; Laurell, T.; Deierborg, T. Label-Free Concentration of Viable Neurons, HESCs and Cancer Cells by Means of Acoustophoresis. *Integr. Biol. (Camb).* **2016**, *8* (3), 332–340. https://doi.org/10.1039/c5ib00288e.

(33) Carpaneto, A.; Accardi, A.; Pisciotta, M.; Gambale, F. Chloride Channels Activated by Hypotonicity in N2A Neuroblastoma Cell Line. *Exp. brain Res.* **1999**, *124* (2), 193–199. https://doi.org/10.1007/s002210050614.

(34) Barros, F.; Brosens, J.; Brighton, P. Isolation and Primary Culture of Various Cell Types from Whole Human Endometrial Biopsies. *Bio-Protocol* **2016**, *6* (22), 1–13. https://doi.org/10.21769/bioprotoc.2028.

CHAPTER 5

5. IMPACT OF MOLECULAR AND MACROMOLECULAR CRYOPROTECTANTS ON MEMBRANE INTEGRITY BEFORE AND AFTER CRYOPRESERVATION

5.1 DECLARATIONS

All polyampholyte polymers were synthesised by Dr Christopher Stubbs and polyproline polymers were synthesised by Dr Ben Graham under the supervision of Prof Matthew Gibson. Confocal imaging assistance was provided by Ruben Tomás and confocal images were processed solely by Ruben Tomás under the supervision of Prof Matthew Gibson.

5.2 CHAPTER SUMMARY

Cell membranes are an integral component of cell survival; irreversible damage to a membrane is considered a catastrophic event. Dehydration during the freezing process is essential to prevent intracellular ice, and thus ultimately, cell recovery, and the integrity of the membrane is a determinant for this process. In this chapter we examine the effect of our molecular and macromolecular cryoprotectants on the cell membrane. We found that the macromolecular cryoprotectants of PVA, polyproline, and polyampholyte did not have an impact on membrane permeability during short exposures at room temperature and the osmolytes of alanine, betaine, or proline did not affect permeability for long exposures at physiological temperatures. Following cryopreservation, we

discovered that cell permeability after storage with our cryoprotectants were comparable to those seen with 10% DMSO, with the exception of polyampholyte treatment, which showed significantly lower permeability. Additionally, the polyampholyte induced a unique phenotype not observed in our other macromolecular cryoprotectants and was investigated to rule out the cause as lipid bodies, polymer aggregation, phagocytes, or membrane poration.

5.3 INTRODUCTION

Cell membranes are large flexible bilayers that serve as the boundaries of cells and their intracellular organelles. Membranes literally define what a cell is (the outer membrane and the contents contained within) and what is not. Membranes are assembled by the non-covalent association of their components, the primary building blocks being phospholipids consisting of two long-chain, nonpolar fatty acid groups linked (usually by an ester bond) to small, highly polar groups, including a phosphor-glycerol unit. The plasma membrane serves as both a permeability barrier and a conduit, allowing the import of essential nutrients, ensuring that metabolic intermediates remain in the cells, and enabling waste products to leave the cell, while also permitting the selective transport of material and information between the cell's exterior and interior spaces.

Maximov suggested in 1929 that disruption of the plasma membrane was the primary cause of freezing injury[1] and in 1938 Siminovitch & Scarth concluded that both intracellular and extracellular ice formation resulted in damage to the plasma membrane, for separate reasons,[2] and this went on to help shape Mazur's two-factor hypothesis of freezing injury.[3] For cells in a partially frozen solution, the intracellular solution must come into equilibrium with the extracellular ice, either by intracellular ice formation or cell dehydration[4] and the plasma membrane plays a central role in determining the manner of this equilibrium. This is due to two

factors: the first is that the intact membrane acts as an effective barrier to extracellular ice[5,6] along with a lack of effective intracellular ice nucleators,[6] the intracellular solution will remain unfrozen. Secondly, due to the semipermeable nature of the plasma membrane, the cell will dehydrate in response to the lower potential of the extracellular solution.[7] Whether the cell achieves equilibrium by dehydration or intracellular ice formation is ultimately a consequence of the stability of the plasma membrane.[4] This emphasises how important the stability of the cell membrane is, even if all other mechanisms of damage are mitigated, irreparable damage to the cell membrane is not recoverable regardless of how well other factors are managed.

Cellular plasma membranes are selectively permeable such that only small hydrophobic or non-charged molecules, along with water, can pass through the membrane quickly without assistance (Fig 5.1). We can exploit this characteristic to probe membrane health; by using markers of either permeable or non-permeable molecules we can test the stability and permeability of the cell membrane.

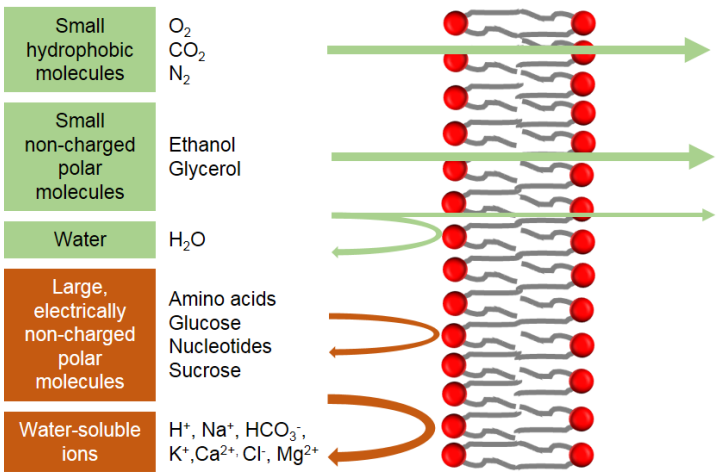

Figure 5.1. Selective membrane permeability. Bidirectional membrane permeability parameters.

DMSO is thought to introduce transient pores into the membrane during the freezing process, therefore we wanted to evaluate the membrane permeability of our compounds under physiological conditions to determine if there was any alteration in permeability that may be affording protection. This will be accomplished via a calcein-AM retention kinetic assay to measure any permeability as it happens in real time. Additionally, permeability after cryopreservation is a commonly used means of assessment in cell cryopreservation so we will evaluate post-freeze permeability via calcein-AM/EthD-1 retention and uptake prior to removing the cells from the plate through the damaging trypsinisation process. In this chapter, the membrane permeability at various steps throughout our freezing processes was assessed to determine if, (i) our macromolecules used as cryoprotective agents (CPAs) altered the membrane permeability under normal conditions, (ii) small molecule osmolyte incubation altered the membrane permeability under normal conditions, and (iii) the membrane permeability was altered after freezing in each of our conditions. The results of this chapter will allow us to evaluate if there is any impact on the permeability of the cell membrane due to our cells being in the presence of our compounds. Additionally, we will be able to evaluate potential cell damage of our cryopreserved monolayers before any outside manipulation occurs to remove them from the plate. This will help us to identify potential areas of cell damage during the cryopreservation process.

5.4 RESULTS AND DISCUSSION

5.4.1 Permeability Kinetics

We first wanted to look at the membrane impacts of our macromolecules being used as CPAs. As demonstrated in Chapter 4, our macromolecular CPAs are in contact with our cells for a relatively short period of time in the monolayer format.

They experience a 10 min CPA incubation prior to freezing, the CPA solution is then removed (some will remain behind at the cell surface) and the cells are then frozen at a rate of 1 °C·min^{-1} down to -80 °C (~103 min). Therefore, we needed an assay that would quickly capture any impacts our CPAs were having on cell membranes in less than 2 h. One method to quickly evaluate the stability of a cell membrane is through the uptake of a retained fluorescent molecule such as calcein-AM. Calcein-AM is freely permeable to the cell and can also be transported out via the P-glycoprotein (P-gp) transporter. Once inside the cells, calcein-AM is hydrolysed by endogenous esterases into the negatively charged green fluorescent calcein, which is retained in the cytoplasm. Calcein is not cell permeable and is not effluxed by P-gp. One limitation to this assay is in the event of a loss of membrane stability, such that the fluorescent calcein is released into the solution, which can result in inaccurate fluorescent readings. Fortunately, this problem has a solution. Utilising a membrane flux assay modified from Su *et al.,*[8] the calcein quencher trypan blue was exogenously added, allowing membrane flux to be continuously monitored by a reduction in retained calcein-associated fluorescence (Fig 5.2). The exogenously added trypan blue will quench any lost fluorescence from calcein which has leached from the cell (as well as permeate damaged membranes) and allow accurate readings of cell-retained calcein. For this assay, cells were loaded with calcein-AM then plated and exposed to the CPAs for 4 h at 37 ˚C, with readings taken every 10 min. Lower fluorescent values indicate cell leakage, and therefore membrane permeability. A slight increase in cell permeability could be beneficial to our cells during the freezing process, allowing them to dehydrate faster, but a large increase in permeability would be fatal if the integrity of the bilayer was lost.

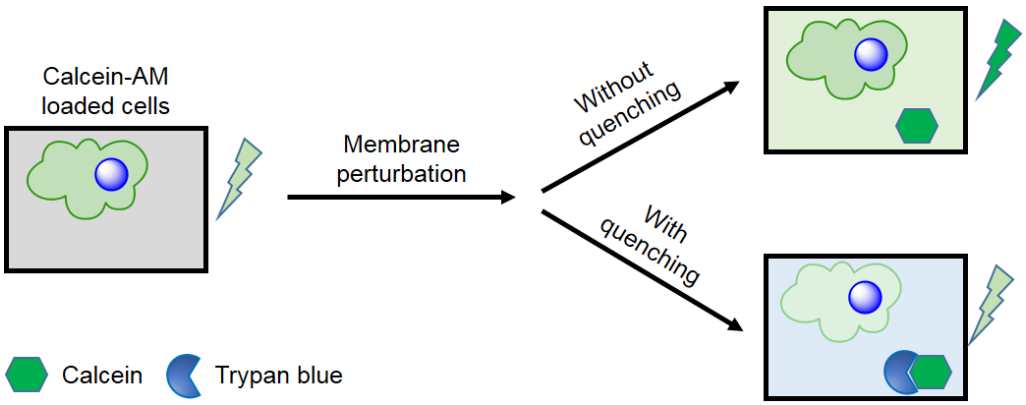

Figure 5.2. Schematic representation of membrane permeability kinetics assay.

5.4.1.1 Standard Membrane Permeability Kinetics

We first tested the permeability kinetics for our standards of cell media (Ham's F-12K (Kaighn's) Medium (F-12K)) and the standard cryoprotectant of dimethyl sulfoxide (DMSO). Control cells were incubated in complete cell media (F-12K) and experimental cells (10 and 20% DMSO) were incubated in the indicated solutions for the duration of the experiment (4 h). Control cells showed the expected exponential decay of the fluorophore, with 10% DMSO exhibiting the same decay trend, although with a slightly higher initial fluorescence retention (Fig 5.3, n = 3). The higher retention for 10% DMSO may be due to DMSO increasing cell permeability or inducing water pores,[9] thereby allowing more calcein-AM to enter. We saw that cells treated with 20% DMSO showed a large decrease in fluorescence over a short period of time (45 minutes), suggesting that 20% DMSO caused the cell membranes to become very permeable resulting in a loss of structural integrity. However, DMSO is known to be toxic at room temperature[10] so these results were not overall unexpected for the high concentration of DMSO used.

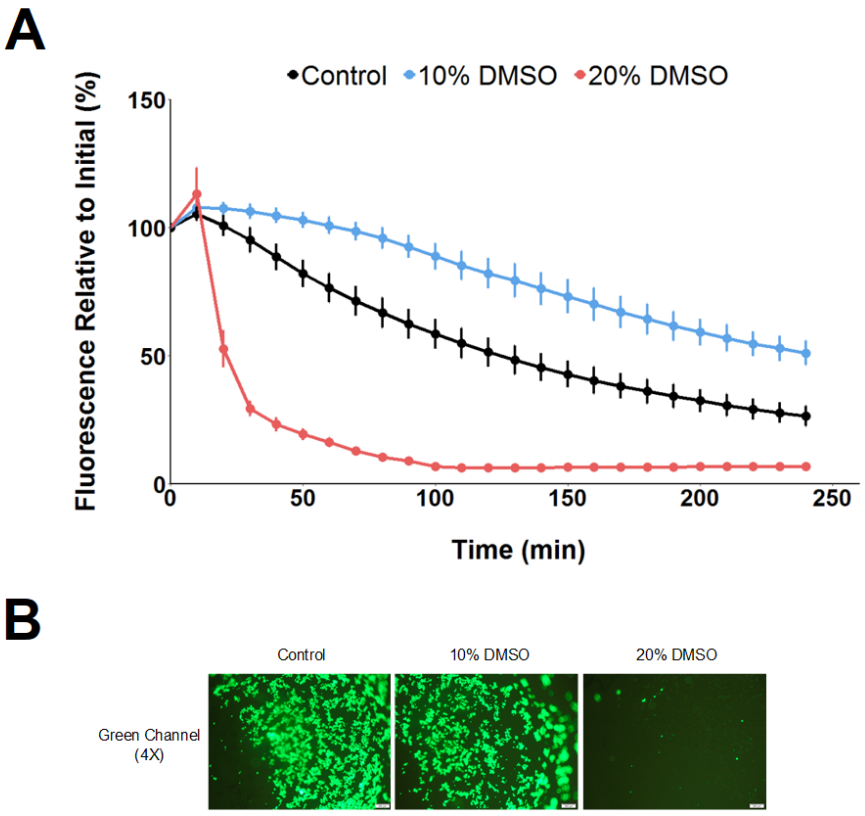

Figure 5.3. Permeability kinetics of control cells and DMSO. A) Plate readings of calcein fluorescence. **B)** Bright-field images of cells at 4 h (460 nmλ illumination). Scale bar = 200 µm.

These results show that this assay is a useful indicator of membrane permeability and provides a fast and reliable reporting method. We have additionally demonstrated that 20% DMSO results in catastrophic membrane permeability leading to a fatal loss of membrane integrity at room temperature in less than 45 minutes.

5.4.1.2 PVA and Polyproline Membrane Permeability Kinetics

We next looked at the membrane permeability of two of our macromolecular CPA compounds, PVA and polyproline. Neither of these compounds are highly soluble, with a max solubility of approximately 20 $mg \cdot mL^{-1}$ (for the molecular weight used here). Due to the nature of this assay, such as the timing and the

volumes used, a 4X experimental solution is required, therefore the highest concentration tested for PVA and polyproline was 5 mg·mL^{-1}. We saw no significant change in permeability for either PVA or polyproline, with values below that of 10% DMSO but just slightly above control values (Fig 5.4, n = 3).

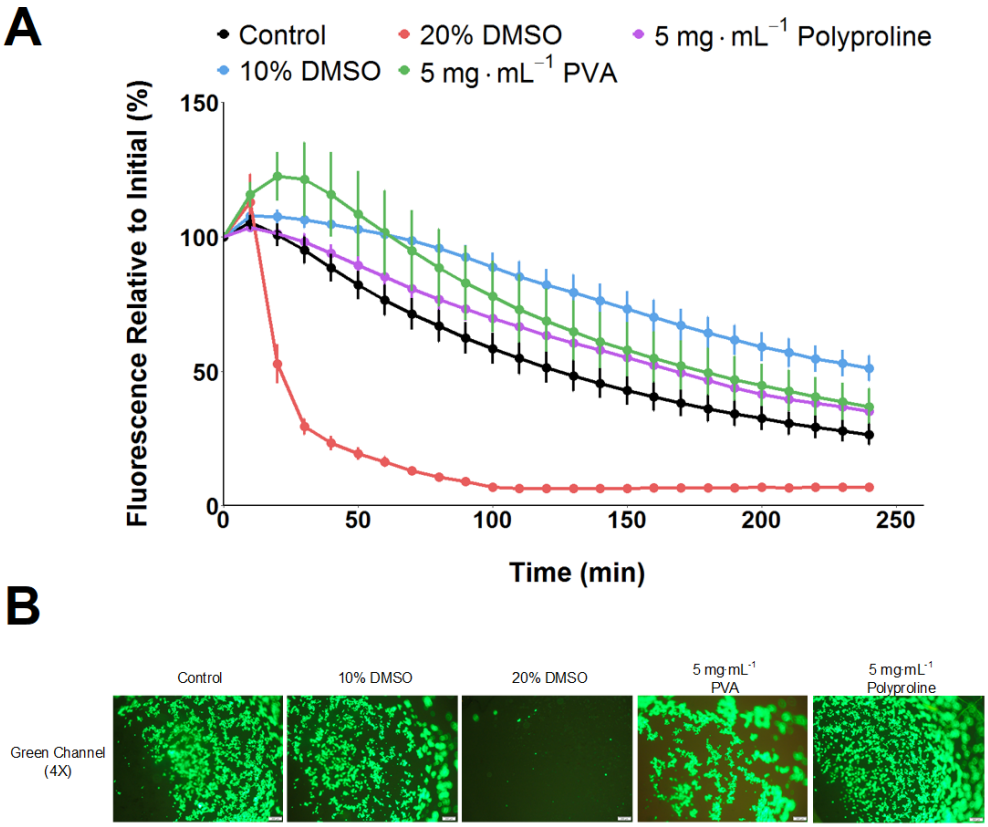

Figure 5.4. Permeability kinetics of PVA and polyproline. A) Plate readings of calcein fluorescence. **B)** Bright-field images of cells at 4 h (460 nmλ illumination). Scale bar = 200 µm.

PVA is not considered to be highly membrane active, for example, when used as a hydrogel it has poor cell attachment due to its highly hydrophilic nature.[11] Additionally, polyproline showed no inherent membrane permeability when tested against red blood cells for hemolysis,[12] also aligning with our results. From this we can conclude that the macromolecular CPA agents of PVA and polyproline do

not inherently induce cell permeation at room temperature for the concentrations tested.

5.4.1.3 Polyampholyte Membrane Permeability Kinetics

We next tested the membrane permeability of polyampholyte, which is highly soluble, allowing us to test concentrations from 1 to 40 $mg \cdot mL^{-1}$. We saw fluorescence retention values higher than control cells but comparable to values obtained with 10% DMSO (Fig 5.5, $n = 3$).

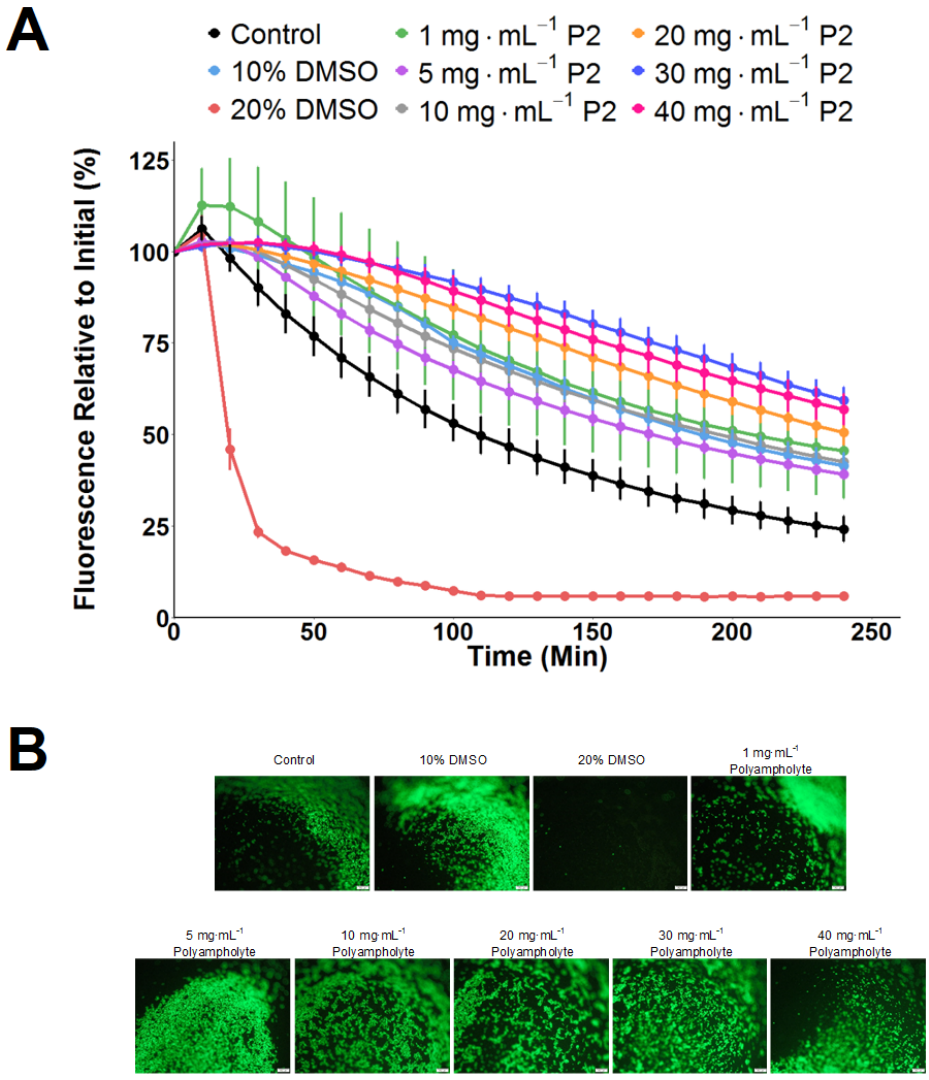

Figure 5.5. Permeability kinetics of polyampholyte. A) Plate readings of calcein fluorescence. **B)** Bright-field images of cells at 4 h (460 nmλ illumination). Scale bar = 200 µm.

Cells incubated with varying concentrations of polyampholyte had retention values comparable to 10% DMSO and we saw no reduction in fluorescence retention, demonstrating that polyampholyte does not increase permeability at room temperature over 4 h. Polyampholytes have been shown to interact with the membrane and protect it from freezing-induced damage;[13] our results suggest no loss of membrane stability when cells are incubated with polyampholytes.

These results show that our additives used as macromolecular CPAs do not affect the membrane permeability at room temperature. It would be interesting to test the stability of our additives in combination with 20% DMSO, to assess if our macromolecular CPAs could mitigate the membrane damage from high concentration DMSO exposure.

5.4.2 Osmolyte Incubation Pre-Freezing Membrane Permeability

After evaluating the membrane permeability of short exposure macromolecular CPAs, we next wanted to assay the permeability impact of the osmolytes of alanine, betaine, and proline. These compounds are incubated with cells for 24 h prior to cryopreservation, since as we established in Chapter 4, this pre-incubation period dramatically improves post-thaw recoveries for betaine and proline. Therefore, due to the 24 h exposure time, permeability kinetics would only be useful to pinpoint the time at which permeability may happen, assuming it does it all. With that in mind, we conducted a static permeability assay following osmolyte incubations at 24 h. For this assay, we utilised the well-established calcein-AM/ethidium homodimer-1 (EthD-1) assay, commonly known as the LIVE/DEAD assay. This assay works similar to the calcein-AM assay in Section 5.4.1, where healthy cells convert calcein-AM to calcein. In addition, EthD-1 is not freely permeable and cannot enter cells unless the membrane is damaged, once EthD-1 enters the cells, it binds to nucleic acids and its fluorescence is increased 40 fold. In this assay, the cells are incubated in the osmolyte compounds for 24 h, then treated with calcein-AM/EthD-1 for 45 min at room temperature, rinsed, analysed on a plate reader, and then imaged. Healthy cells will have a higher reading on the calcein channel (green) and damaged cells will have a higher reading on the EthD-1 channel (red) (Fig 5.6).

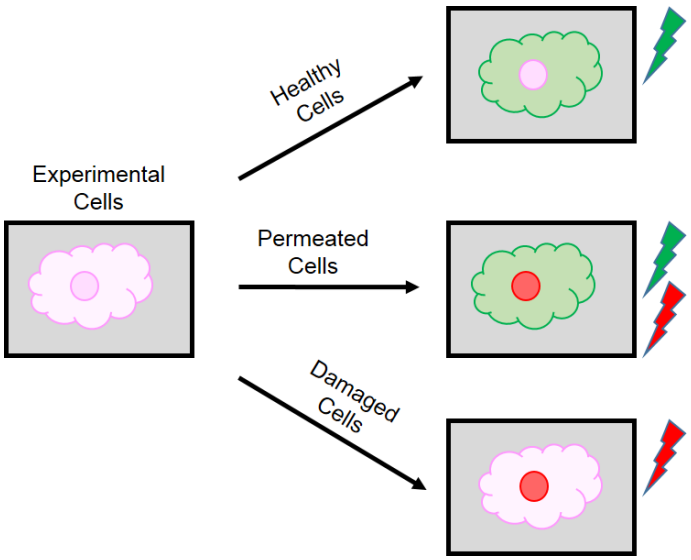

Figure 5.6. Schematic representation of calcein/ethidium homodimer-1 membrane permeability assay.

Incubating cells in osmolyte solutions for 24 h did not significantly change their permeability relative to control cells (F-12K) (Fig 5.7). There was no significant difference in calcein fluorescence (green) for cells incubated in osmolyte solutions (Fig 5.8A) and cells incubated in 200 mM proline had significantly lower EthD-1 fluorescence (red) compared to 100 mM alanine and 100 mM betaine (Fig 5.8B, n = 3, P = 0.02) but all conditions were comparable to control cells. Incubating cells in osmolyte solutions for 24 h did not significantly alter the permeability of the cells relative to control cells.

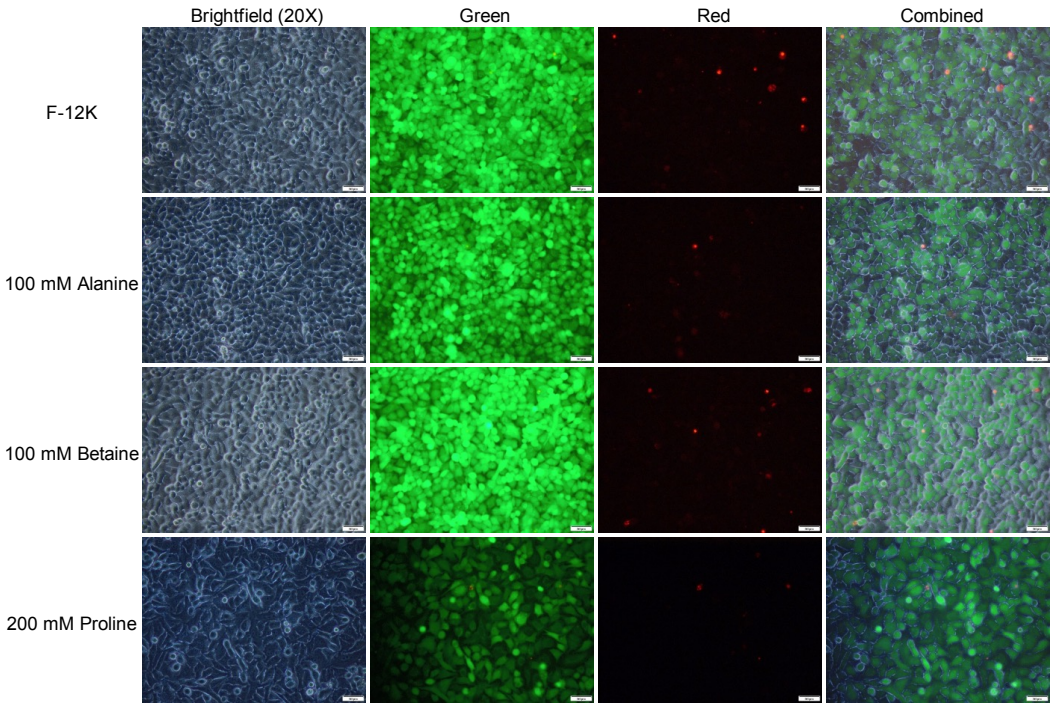

Figure 5.7. Calcein/EthD-1 bright-field images of A549 cells incubated in osmolyte solutions for 24 h. (Green = 460 nmλ illumination, red = 525-660 nmλ illumination) Scale bar = 50 µm.

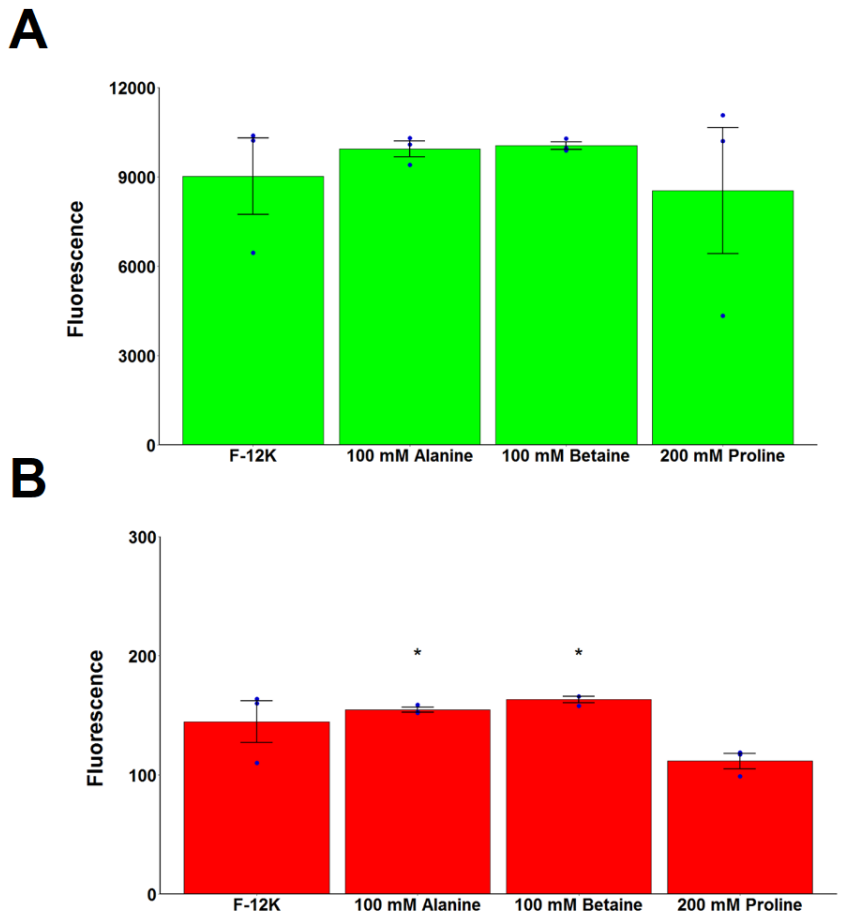

Figure 5.8. Calcein/EthD-1 fluorescent readings of A549 cells incubated in osmolyte solutions for 24 h. A) Calcein readings. **B)** Ethidium homodimer-1 readings. * P < 0.03 from 200 mM proline.

These results are not unsurprising, as these compounds are compatible osmolytes, which means they typically do not act in detrimental ways, and the stabilising ability of these compounds appear to be used only when there are stressors that destabilise membranes.[14]

5.4.3 Post-Freeze Membrane Permeability

Since we didn't see any significant membrane permeability with either macromolecular CPAs or osmolyte compounds under normal conditions, we next wanted to evaluate the permeability of the membrane after freezing and thawing

our cells with our various treatments. This section utilises the same assay as in Section 5.4.2, except in this experiment the cells have been frozen and thawed as in Section 4.6.8 prior to calcein-AM/EthD-1 treatment.

5.4.3.1 Osmolyte PVA Post-Freeze Membrane Permeability

Cells were incubated in osmolyte pre-treatments for 24 h (as indicated) then treated with the specified CPA for 10 min, frozen for 24 h to -80 °C, thawed with 37 °C cell media (F-12K) and incubated for 24 h, then treated with calcein-AM and EthD-1 (Fig 5.9). Cells frozen with osmolyte pre-incubation and with or without PVA did not significantly differ in their calcein-AM or EthD-1 uptake from 10% DMSO, with the exception of 100 mM alanine which had significantly higher EthD-1 fluorescence (Fig 5.10, $n = 3$, $P = 0.00006$).

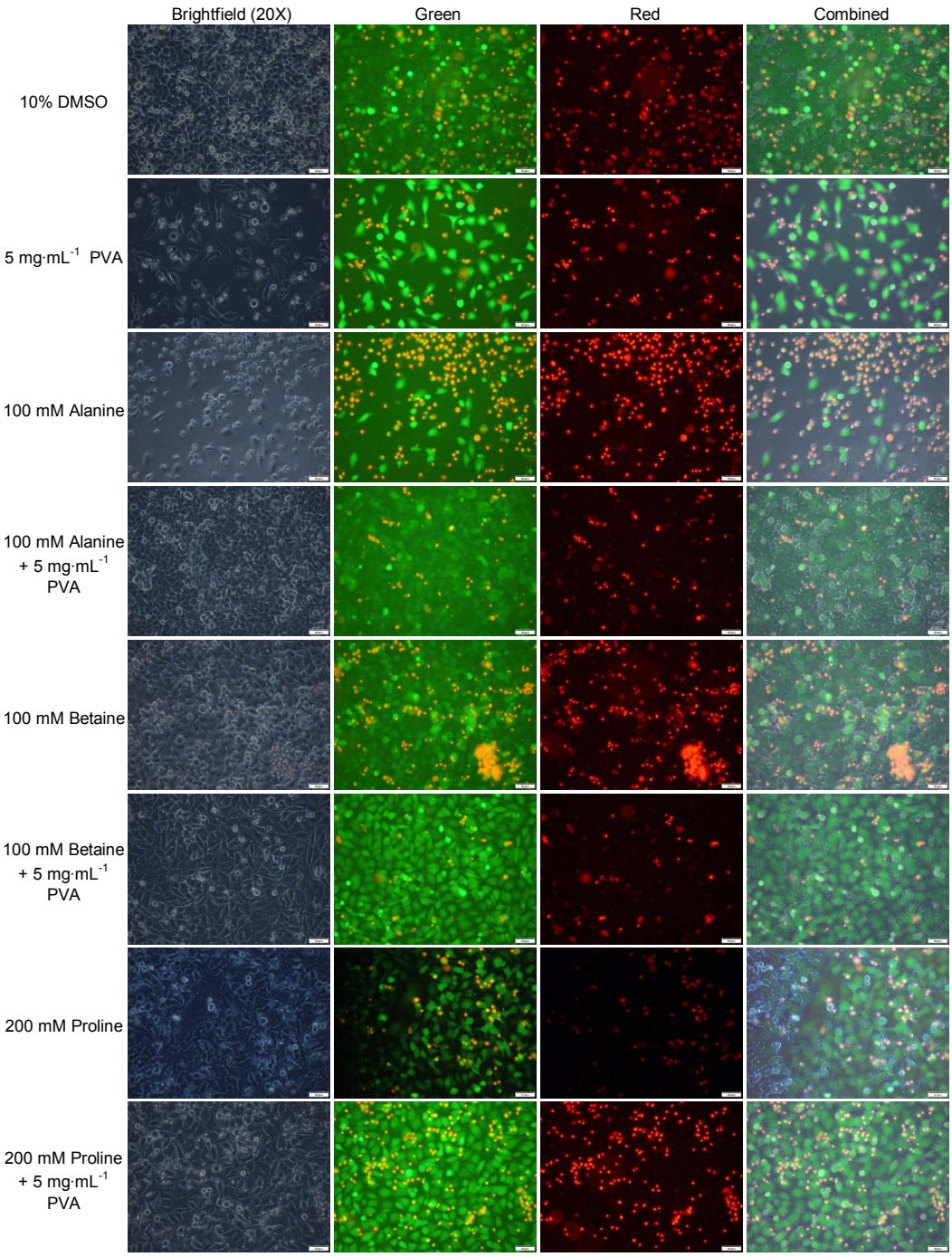

Figure 5.9. Membrane permeability of frozen/thawed A549 cells with osmolyte incubation and CPA treatments. Bright-field images of calcein-AM / EthD-1 treated cells 24 h post-thaw (green = 460 nmλ illumination, red = 525-660 nmλ illumination). Scale bar = 50 µm.

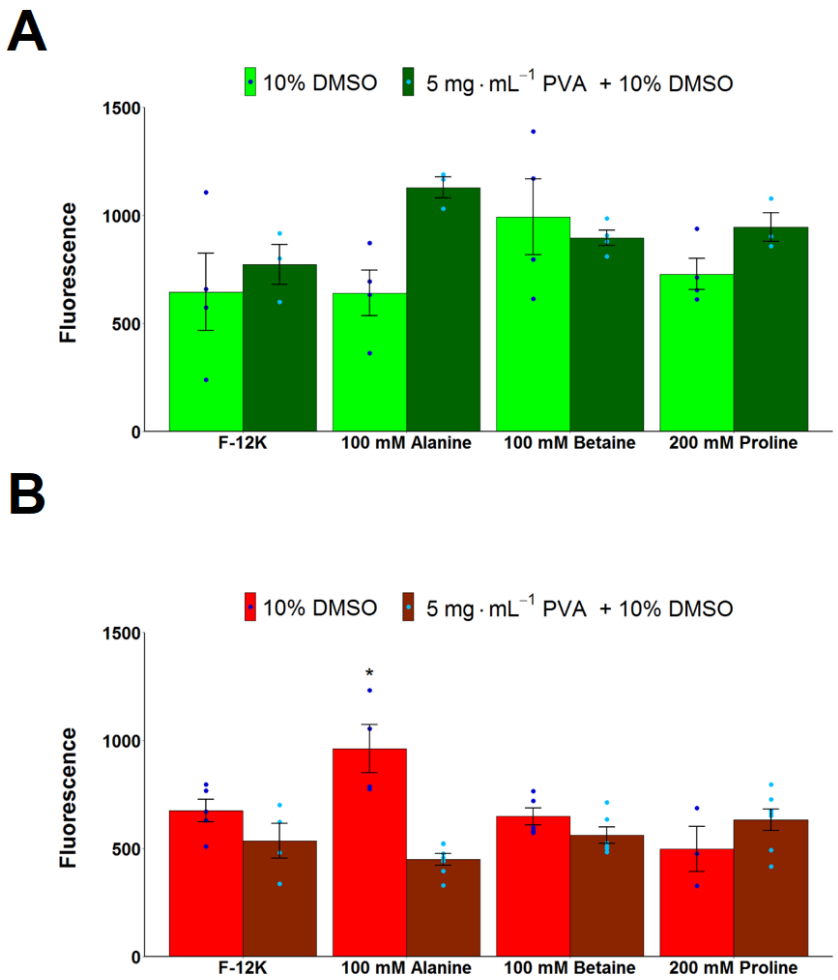

Figure 5.10. Calcein/EthD-1 fluorescent readings of frozen/thawed A549 cells with osmolyte and PVA treatments. A) Calcein readings. **B)** Ethidium homodimer-1 readings. * P < 0.001 from 10% DMSO in F-12K.

The fact that we only saw a significant difference in EthD-1 fluorescence with 100 mM Alanine was surprising, since this does not match the trend seen with cells recovered in Section 4.4.1.2 (combined for comparison in Fig 5.11), as we would expect to see increasing calcein fluorescence/decreasing EthD-1 fluorescence with increasing cell recovery. There could be several reasons for this discrepancy, the simplest being that this assay alone is not a good determinant of cell recovery for cryopreserved cells. Perhaps the cells remain partially functional while attached to the plate but the membranes of our low recovery conditions are too fragile to survive being removed from their culture

plate during trypsinisation for cell recovery assessment. This is an interesting finding as the calcein-AM/EthD-1 assay is often used as the only measurement of cell recovery in cryopreservation studies and by comparing our combined results, we can see that it may not be an accurate measurement of recovery on its own.

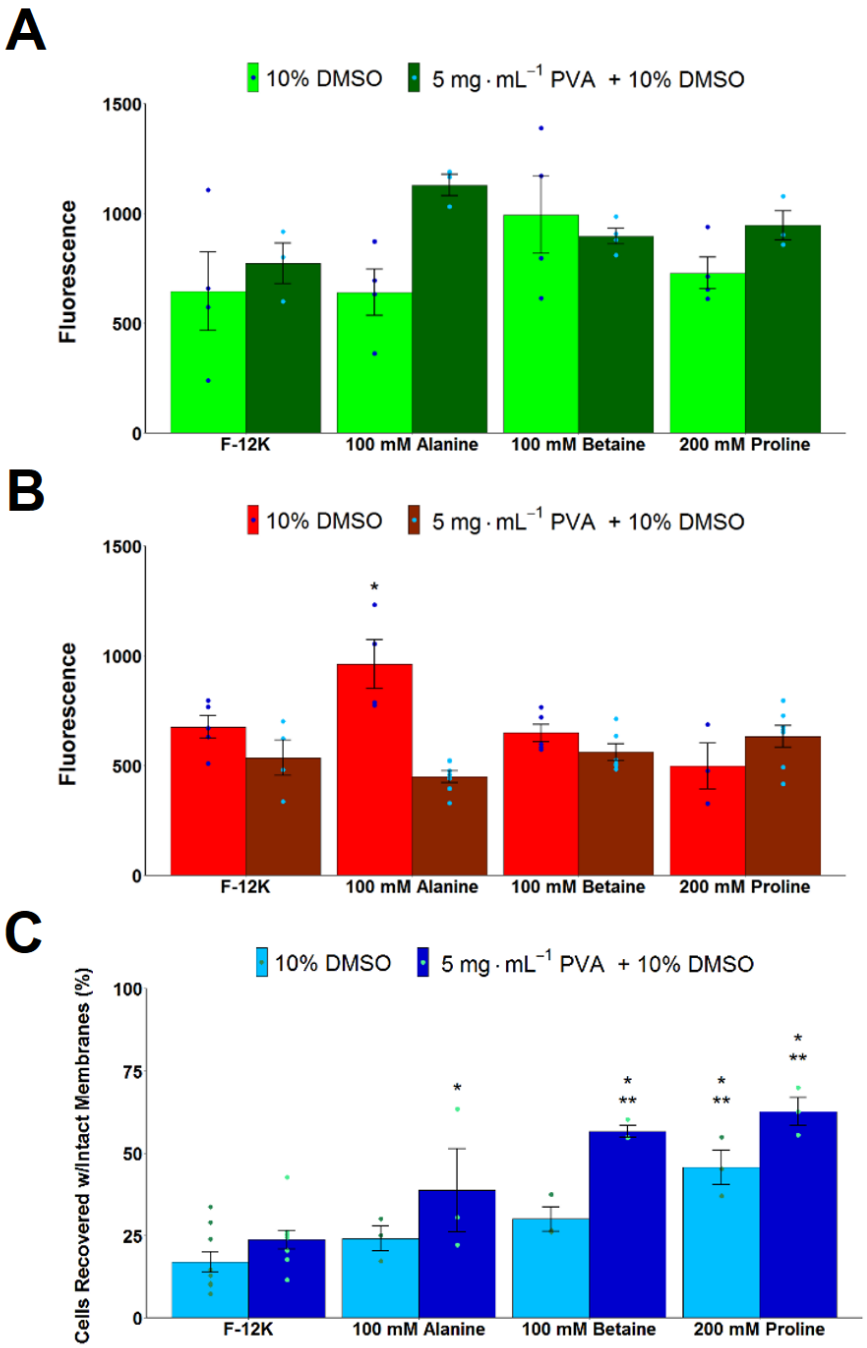

Figure 5.11. Calcein/EthD-1 fluorescent readings and cell recovery of frozen/thawed A549 cells with osmolyte and PVA treatments. A) Calcein readings. **B)** Ethidium homodimer-1 readings. * $P < 0.001$ from 10% DMSO in F-12K. **C)** Cells recovered with intact membranes. * $P < 0.001$ from 10% DMSO in F-12K, ** $P < 0.001$ from 10% DMSO+5 mg·ml^{-1} PVA in F-12K.

5.4.3.2 Polyproline Post-Freeze Membrane Permeability

To determine the effect of polyproline on cell membrane permeability post-thaw, A549 cells were plated and incubated for 24 h, then treated with the polyproline (+ 10 % DMSO) for 10 min, frozen for 24 h to -80 °C, thawed with 37 °C cell media (F-12K) and incubated for 24 h. Cells were then treated with calcein-AM and EthD-1 24 h post-thaw after freezing with polyproline in the CPA (Fig 5.12). Cells frozen with polyproline did not significantly differ in their calcein or EthD-1 uptake from 10% DMSO (Fig 5.13, *n* = 3).

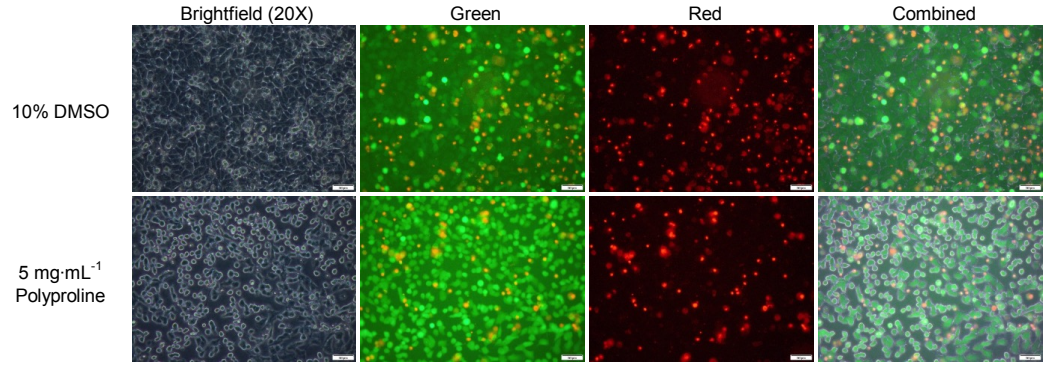

Figure 5.12. Membrane permeability of frozen/thawed A549 cells polyproline treatments. Bright-field images of calcein-AM / EthD-1 treated cells 24 h post-thaw (green = 460 nmλ illumination, red = 525-660 nmλ illumination). Scale bar = 50 µm.

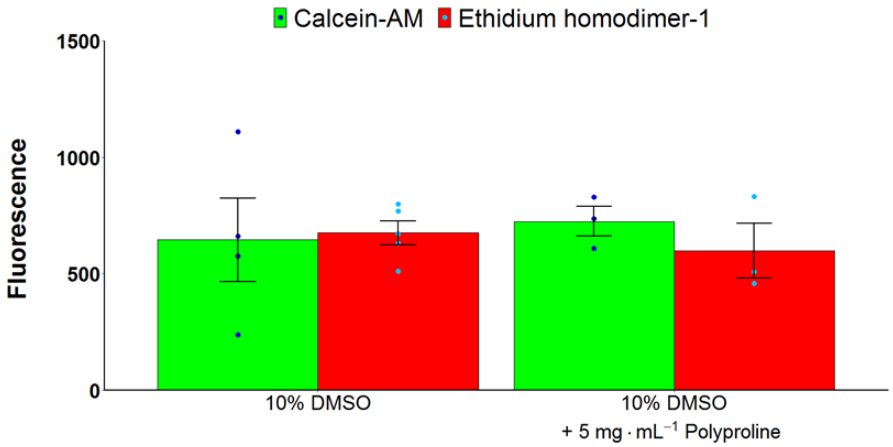

Figure 5.13. Calcein/EthD-1 fluorescent readings of frozen/thawed A549 cells with polyproline.

Polyproline did not appear to alter the post-freeze/thaw membrane permeability compared to 10% DMSO and this correlates with our previous cell recovery data from Section 4.4.1.5 where 10% DMSO had a recovery of 19.8% and 5 mg·ml^{-1} polyproline had a recovery of 20.3%.

5.4.3.3 Polyampholyte Post-Freeze Membrane Permeability

Similar to PVA and polyproline, we wanted to determine the effect that polyampholyte (P2) had on cell membrane permeability after freezing. Cells were plated and incubated for 24 h then treated with polyampholyte (+ 10% DMSO) for 10 min, frozen for 24 h to -80 °C, thawed with 37 °C cell media (F-12K) and incubated for 24 h, then treated with calcein-AM and EthD-1 (Fig 5.14). Cells frozen with 5 mg·mL^{-1} polyampholyte had significantly higher calcein uptake and significantly lower EthD-1 uptake from 10% DMSO (Fig 5.15, n = 3, P = 0.004).

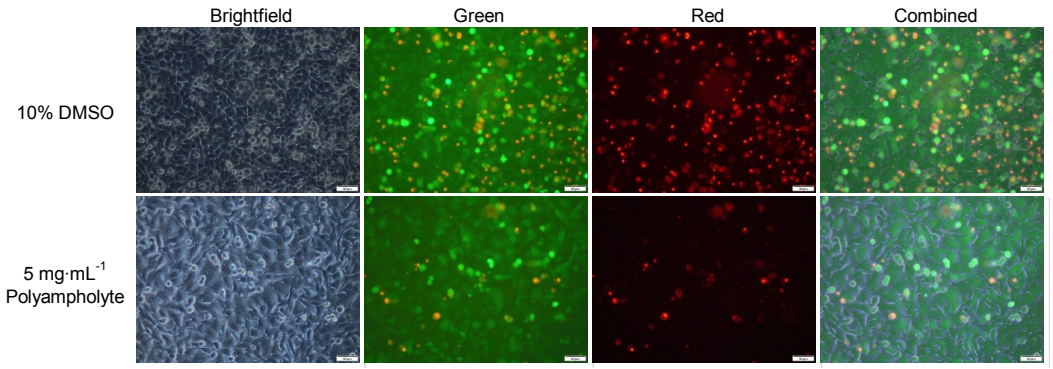

Figure 5.14. Membrane permeability of frozen/thawed A549 cells with polyampholyte treatment. Bright-field images of calcein-AM/EthD-1 treated cells 24 h post-thaw (green = 460 nmλ illumination, red = 525-660 nmλ illumination). Scale bar = 50 µm.

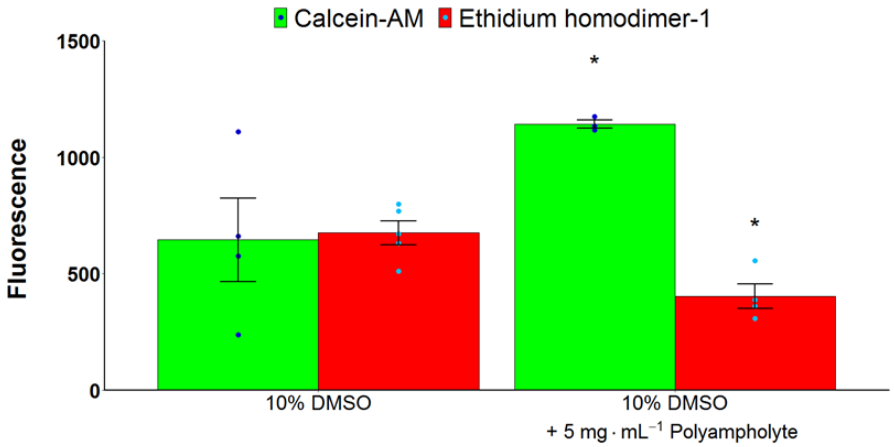

Figure 5.15. Calcein/EthD-1 fluorescent readings of frozen/thawed A549 cells with polyampholyte. * P < 0.01 from 10% DMSO.

Cells frozen with 5 mg·mL^{-1} polyampholyte had a significantly higher calcein-AM uptake with a significantly lower EthD-1 uptake than cells frozen with just 10% DMSO. These results do trend with our recovery results from Section 4.4.1.6.2; 10% DMSO had 19% recovery with an 81% recovery for 5 mg·mL^{-1} polyampholyte. This could imply that the calcein-AM/EthD-1 assay only trends correctly when there are large disparities between the recoveries. It could alternatively imply that the osmolyte/PVA treatment and the polyampholyte treatment protect cells through different mechanisms.

These results have shown that none of our macromolecular cryoprotectants or small molecule osmolytes increased membrane permeability at room temperature. PVA, a highly IRI active polymer, and polyproline, a weakly IRI active polymer, did not show increased calcein uptake/retention (showing membrane health) following cryopreservation. Polyampholyte, a weakly IRI active polymer, did show significant increases in calcein uptake and retention following cryopreservation. These results could imply that PVA and polyproline offer incomplete protection that is manifested primarily when the cells are manipulated off the plate, while polyampholyte provides membrane protection which is evident directly after thawing. Alternatively, it could imply that the calcein/EthD-1 assay is not well suited for analysing medium variability differences (i.e. 19%:55% vs. 19%:80%).

5.4.4 Polyampholyte Phenotype Investigation

An unknown circular phenotype was noticed during toxicity screening of polyampholyte (Section 3.4.1.3) as shown in (Fig 5.16). This phenotype was not observed when cells were treated with either PVA or polyproline, suggesting it is a unique attribute of polyampholyte and begs further investigation. The phenotype presented for high concentrations (≥ 20 $mg \cdot mL^{-1}$) for 10 min exposures and at lower concentrations (≤ 10 $mg \cdot mL^{-1}$) for 24 h exposures. While the simplest explanation for this phenotype would simply be degradation of the cell and membrane, our toxicity results show that cell metabolism (assessed by alamarBlue reduction) was only significantly lower for concentrations > 10 $mg \cdot mL^{-1}$ after 24 h incubation. In addition, the phenotype was present at lower concentrations where the cells appear to be metabolising normally.

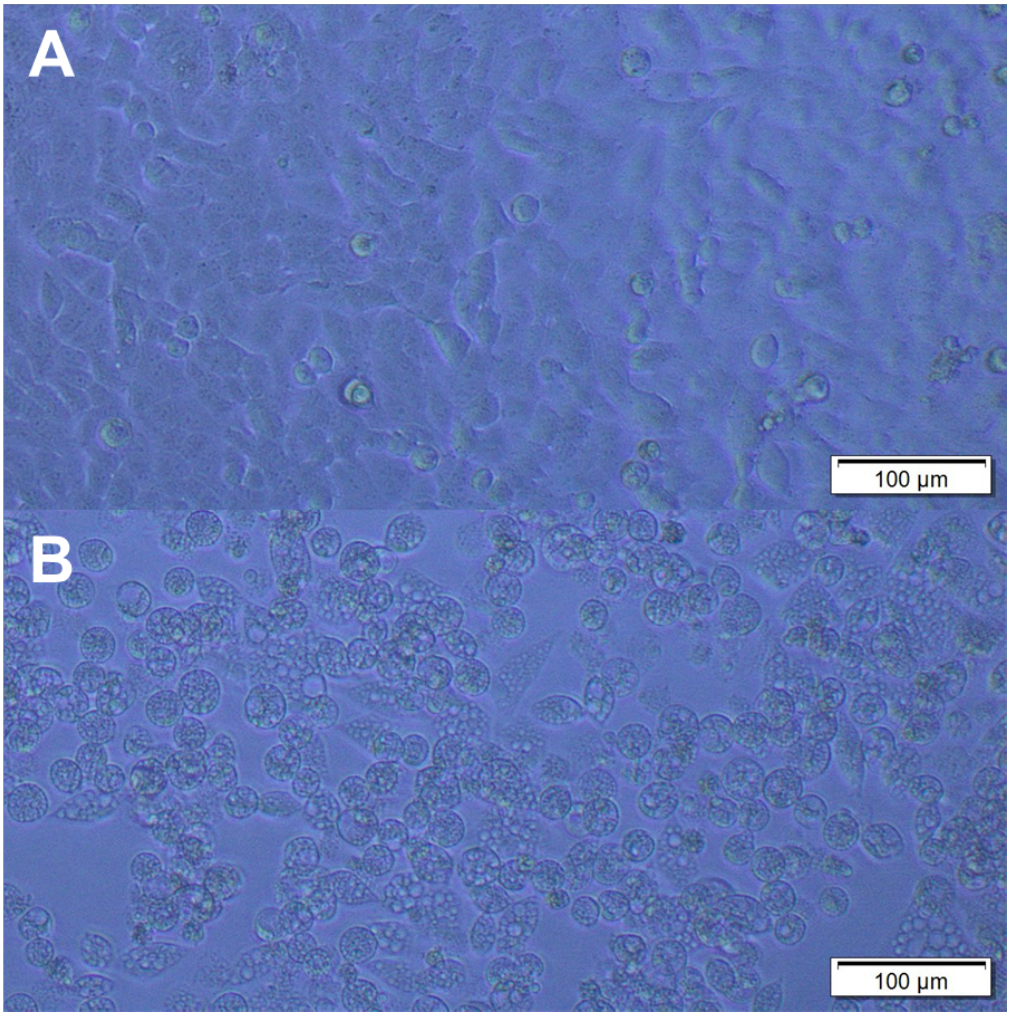

Figure 5.16. Polyampholyte observed phenotype. A) Control cells. **B)** 10 mg·mL^{-1} polyampholyte P2 (24 h). Scale bar = 100 µm.

The observed phenotype was first investigated to determine if it was due to lipid droplet formation. Lipid droplets are lipid-rich cellular organelles and their biogenesis is a highly regulated cellular process that culminates in the compartmentalisation of lipids and enzymes, protein kinases and other proteins. It is thought that lipid droplets are inducible organelles with roles in cell signaling, regulation of lipid metabolism, membrane trafficking and control of the synthesis and secretion of inflammatory mediators.[15] Nile red is a dye that can be applied to cells in an aqueous solvent and it dissolves preferentially in lipids; its fluorescence is quenched in an aqueous environment so it is seen only in the

substances it is intended to stain, and its fluorescence color changes in the presence of very hydrophobic lipids (Fig 5.17).[16]

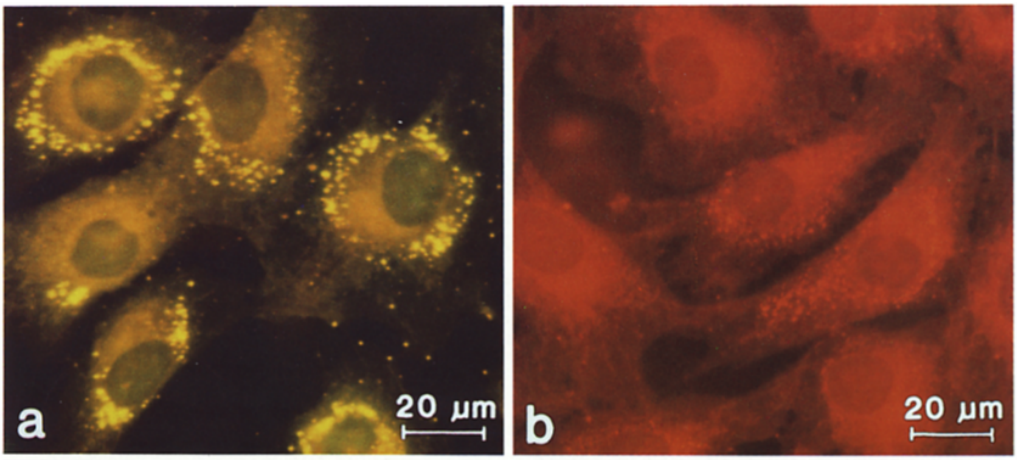

Figure 5.17. Nile red staining. Nile red fluorescence of cultured monkey aortic smooth muscle cells and mouse peritoneal macrophages. (a and b). Adapted with permission from Greenspan *et al.* (1985).[16]

Cells were incubated in varying concentrations of polyampholyte for 10 min and 24 h then treated with nile red and imaged on a fluorescent microscope to assess the presence of lipid droplets. Cells did not fluoresce for the presence of lipid droplets as phenotype circles remained unfluoresced (Fig 5.24) with the unflouresced circle shown (Fig 5.25). As a further assessment, cells were incubated with polyampholyte P2 then analysed by confocal microscopy, to obtain more detailed cell images. Z-stack images were collected to allow the whole cell to be captured. Confocal images were taken following nile red treatment (Fig 5.26) and to definitively show that there were no lipid droplets externally or internally, z-stack images were addtionally taken (Fig 5.18).

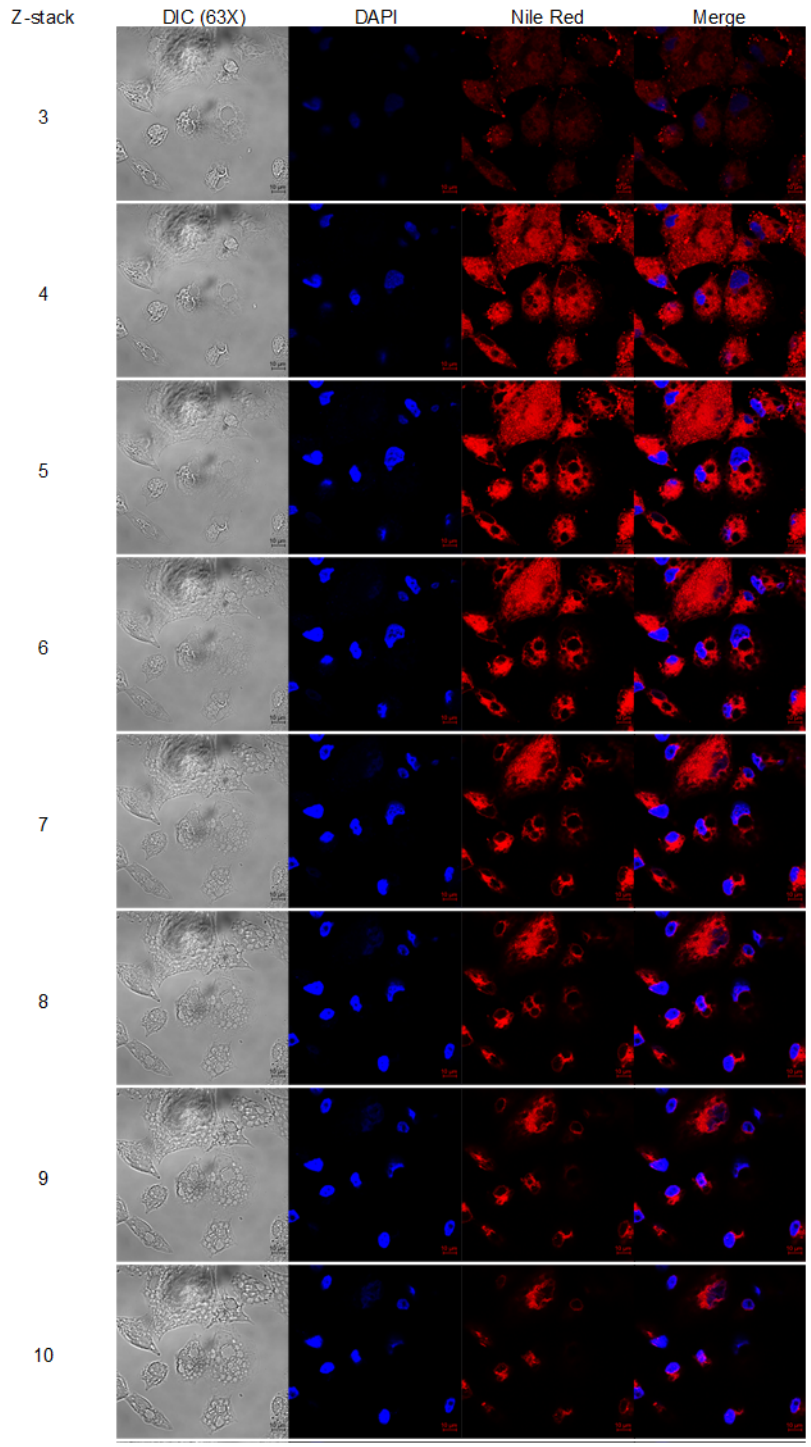

Figure 5.18. Confocal z-stack imaging of nile red treatment of cells incubated with 5 mg·mL^{-1} polyampholyte for 24 h. Scale bar = 10 µm.

From the z-stack images, we again see a lack of nile red staining within the circular phenotype, which instead appear as holes moving through the body of

the cell. If they are indeed holes, we would expect the membrane to be permeable, which is what we next investigated.

To explore membrane permeability, the cells were again incubated in varying concentrations of polyampholyte for 10 min and 24 h. Calcein-AM and ethidium homodimer-1 (EthD-1) were then added and cells imaged after a 45 min incubation. Surprisingly, we saw no increase in permeability for the cells that contained the circular phenotype (Fig 5.27) and we observed a lack of fluorescence within the circles (Fig 5.19).

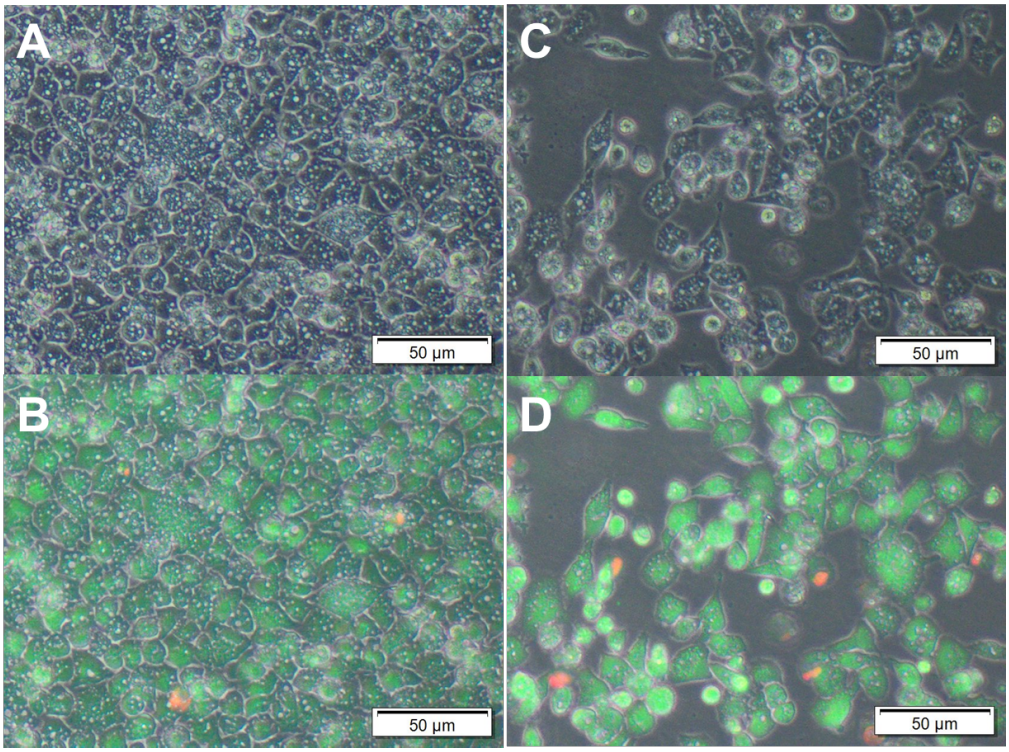

Figure 5.19. Bright-field images of polyampholyte incubated membrane permeability of 5 and 10 mg·ml^{-1} polyampholyte incubated cells. A) 5 mg·mL^{-1} (24 h) bright-field. **B)** 5 mg·mL^{-1} (24 h) combined channels (green = 460 nmλ illumination, red = 525-660 nmλ illumination). **C)** 10 mg·mL^{-1} (24 h) bright-field. **D)** 10 mg·mL^{-1} (24 h) combined channels. Scale bar = 50 µm.

If the circular phenotype is indeed holes, they appear to be non-permeable, such as a toroid, membranes with a "doughnut-like" toroidal shape[17] (Fig 5.20[18]).

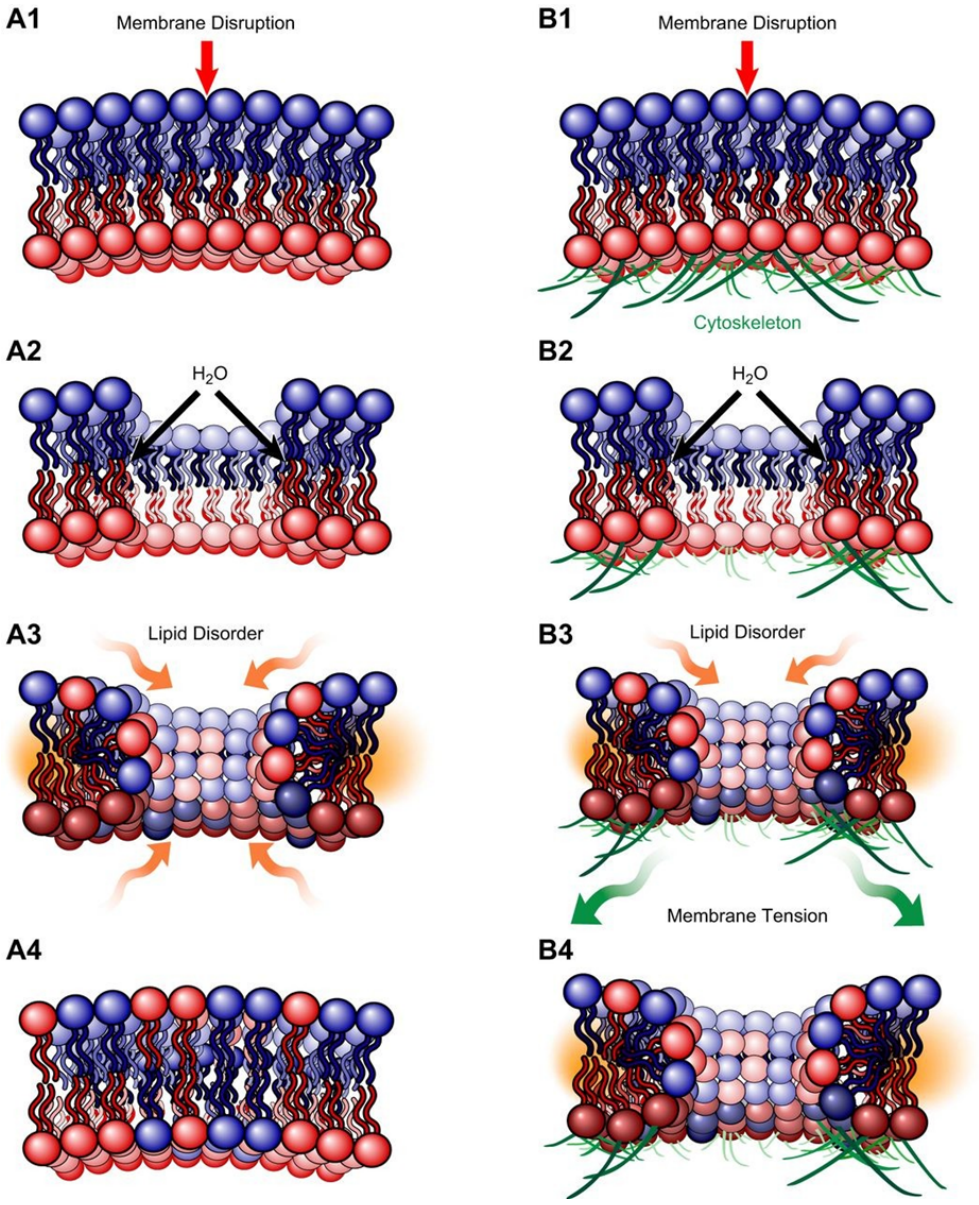

Figure 5.20. Spontaneous membrane resealing. Spontaneous resealing of plasma membrane injuries in the nanometer range is opposed by the forces of the underlying membrane cytoskeleton. For an injury to a phospholipid bilayer alone (*A1-4*), the lipid disorder present on the curved edges of the disruption provides the driving force to spontaneously reseal the injury and is a function of disruption diameter squared. However, if the injured phospholipid bilayer is tethered to underlying cytoskeleton (*B1-4*), the membrane tension from adhesion to the cytoskeleton confers an opposing force for resealing, a function of disruption diameter cubed, and prevents spontaneous repair of membrane disruptions that exceed diameters in the nanometer range. Reprinted with permission from Cooper and McNeil (2015).[18]

We next investigated if the circles might be a result of the polyampholyte triggering the formation of phagocytes, a process where cells ingest a harmful foreign substance. Neutral red is a pH indicating histological stain and will stain

phagocytes purple.[19] We observed no significant purple staining of the cells with neutral red (Fig 5.28) and when looking at the cells we observed no staining at all within the circular phenotype (Fig 5.21).

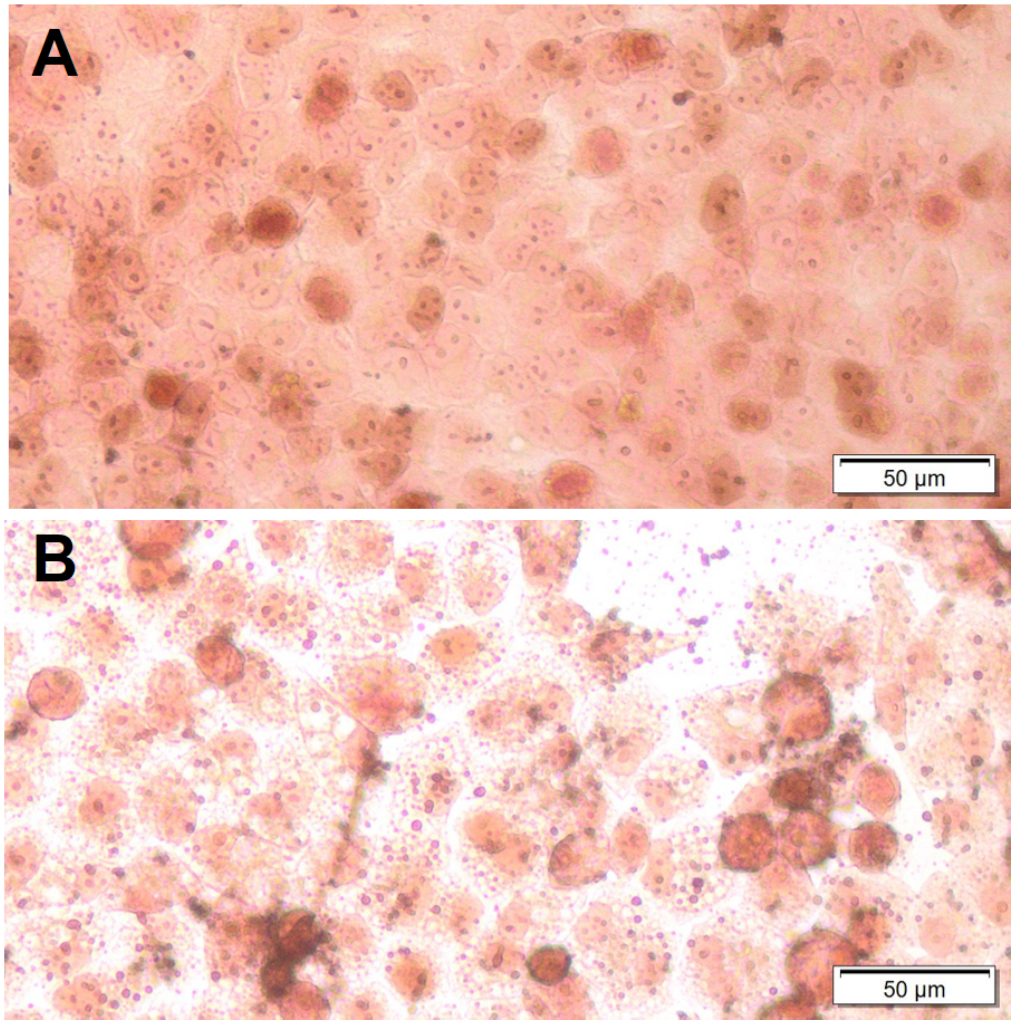

Figure 5.21. Enhanced images of neutral red staining. A) Control cells. **B)** 10 mg·mL^{-1} polyampholyte (24 h). Scale bar = 50 µm.

Since the phenotype did not appear to be either lipid droplets or phagocytes, we next investigated if the phenotype might be due to aggregated polymer vesicles. Utilising a rhodamine-6G fluorescently tagged polyampholyte, we again incubated our cells and imaged them for the presence of internalised polyampholyte. We saw no internalised vesicles of polymer with the tagged-

polymer incubated cells (Fig 5.22). To completely rule out the presence of internal polyampholyte, confocal imaging was conducted with the tagged-polyampholyte. Again, we observed no fluorescence for the cells incubated with tagged-polymer (Fig 5.29) and moving through the z-stack image there was no visible fluorescence in any of the planes (Fig 5.23).

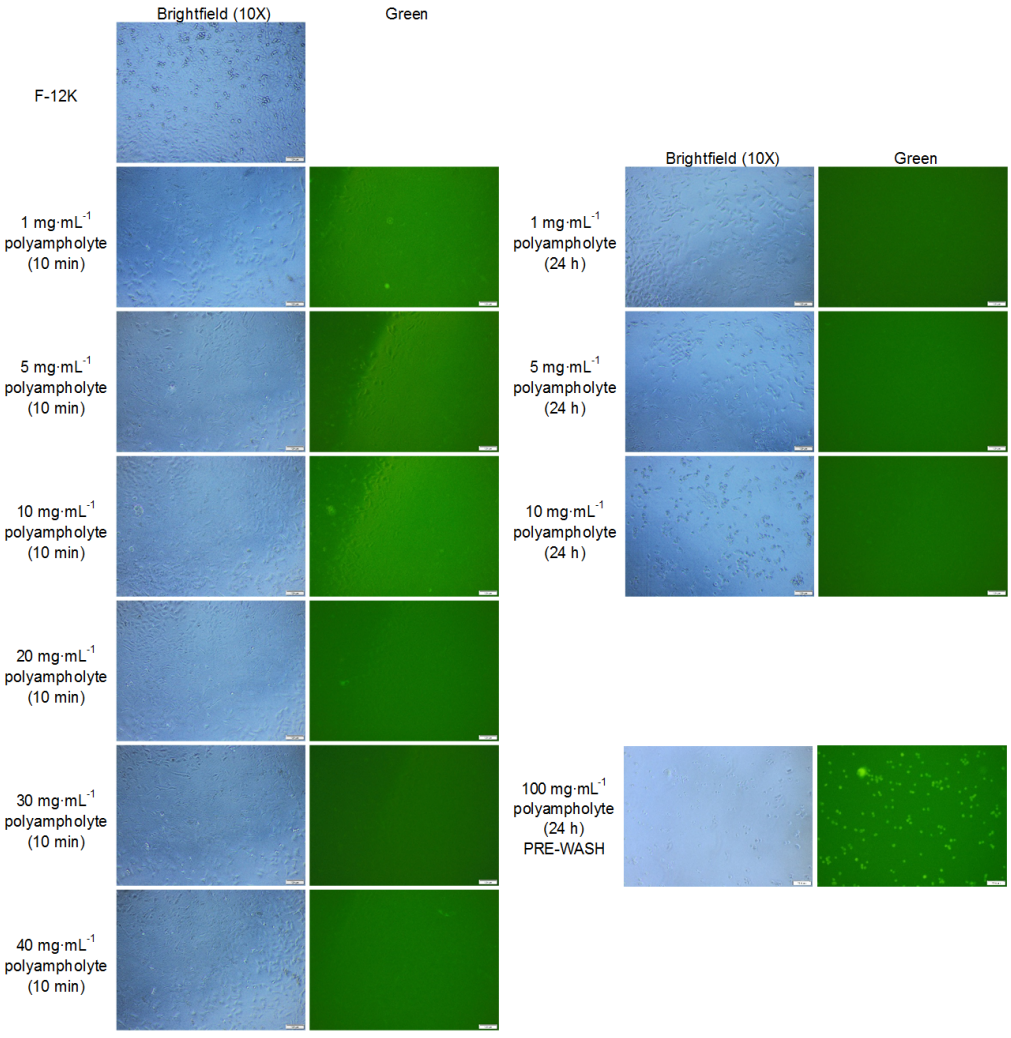

Figure 5.22. Imaging of rhodamine-6G tagged-polyampholyte incubated cells. Images of treated cells (green = 460 nmλ illumination). Scale bar = 100 μm.

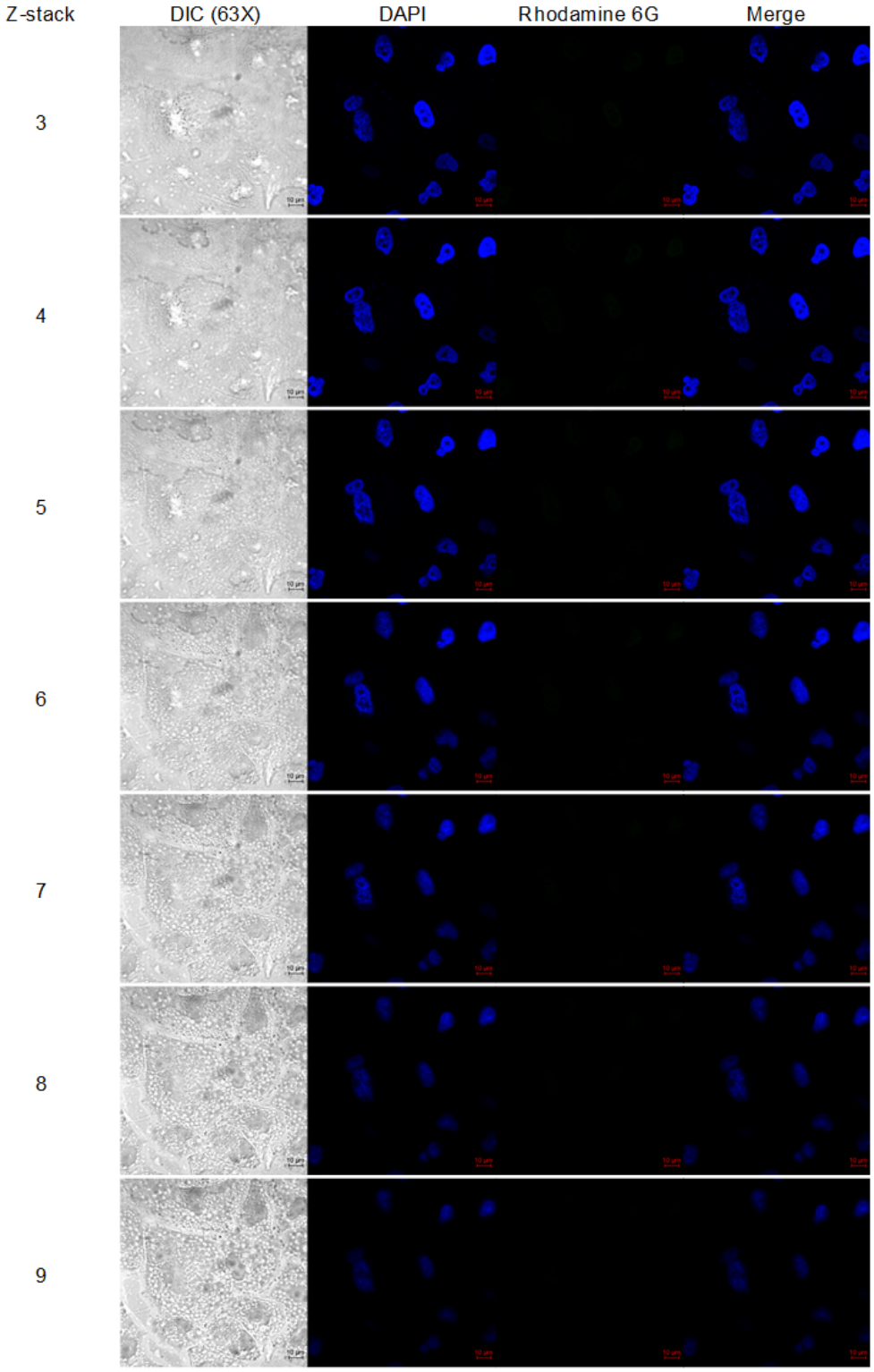

Figure 5.23. Confocal z-stack imaging of cells incubated with 5 mg·mL^{-1} rhodamine-6G tagged-polyampholyte for 24 h. Scale bar = 10 µm.

While we were unable to find a definitive cause for the observed phenotype, we were able to rule out lipid bodies, phagocytes, polymer vesicles, and most surprisingly, membrane permeability. Future studies are needed to determine the cause of this phenotype and if it has any impact on the cryoprotection seen with polyampholyte.

5.5 Conclusions

We have shown that our CPA compounds do not impact the membrane permeability of cells at 37 ˚C. Similarly, we found that the osmolyte incubation also did not impact permeability under physiological conditions. From post-freeze analysis, we found that cells frozen with osmolyte pre-treatment along with PVA did not show significantly different permeability from cells frozen with just DMSO, even though the post-freeze cell recoveries for these conditions were significantly different in Chapter 4. These disparities between post-freeze permeability when compared to post-freeze viability may indicate that the trypsinisation process is a major area of potential damage exposure following the stressful event of cryopreservation, such that less protected cells will not endure the process of being removed from the plate as well as better protected cells. The post-freeze permeability for cells frozen with polyampholyte did show significant differences, correlating with their post-freeze cell recoveries observed in Chapter 4. It has been shown that DMSO dehydrates the phospholipid head-groups, whereas other CPAs (glycerol, ethylene glycol, dimethyl formamide, and propylene glycol) caused an increase in the hydration level of the lipid head-groups; resulting in the freezing-and-thawing of liposomes in the presence of CPAs showing carboxyfluorescein (CF)-retention at the same levels as before freezing (with the exception of glycerol), which implied it is the exposure to CPAs and not the freezing step itself that causes CF-leakage during cryopreservation processing.[20]

However, exposure to high CPA concentrations already caused leakage before freezing, increasing in the order DMSO, ethylene glycol, dimethyl formamide/propylene glycol, and glycerol.[20] Our results suggest that all of our CPAs act similarly to those previously studied, with the exception of polyampholyte, which appears to cause no leakage, either before, during, or after cryopreservation. We additionally examined an observed phenotype for the presence of lipid bodies, membrane permeability, phagocytes, and polymer vesicles and found none of those to be the cause of the morphology. While we were unable to determine a definitive cause, we were able to rule out several of the most obvious reasons for the observed phenotype. Freeze-fracturing and atomic force microscopy may be able to help to identify the cause of the observed phenotype.

5.6 Materials and Methods

5.6.1 Reagents

All non-specified cell related chemicals were obtained from Sigma Aldrich Co Ltd, (Irvine, UK).

Polyproline was synthesised as in Section 2.6.1.1.

Polyampholyte was synthesised as in Section 2.6.1.2.

5.6.1.1 Synthesis of fluorescently labelled polyampholytes

Performed and written by Dr Christopher Stubbs. As a representative example, poly(methyl vinyl ether-*alt*-maleic anhydride), average M_n ~80,000 Da, (300 mg) was dissolved in tetrahydrofuran (50 mL) and heated to 50 °C with stirring. After dissolution, *N*-[4-(aminomethyl)benzyl]rhodamine 6G-amide bis(trifluoroacetate) (3 mg) and triethylamine (10 mg) were added and left for 20 minutes before dimethylamino ethanol (2 g) was added in excess, forming a pink

waxy solid, which was allowed to stir for 30 minutes. 50 mL water was added, and the reaction left to stir overnight followed by purification in dialysis tubing (Spectrapor, 12 – 14 kDa MWCO) for 48 hours with 7 water changes. The resulting solution was freeze-dried to evolve a white solid.

5.6.2 Cell Culture

A549 cells were cultured as per Section 3.6.2

5.6.3 Membrane Kinetics

Methods adapted from Su.[8] A549 cells were dissociated and incubated with 1 μM of calcein-AM (BD Biosciences, Workingham, UK) in completed cell media for 30 min at 37 °C with frequent mixing. Cells were then centrifuged and rinsed twice with media. Cells were plated at a density of $4 \cdot 10^5$ in 100 μL in 96-U-well suspension plates (Sarstedt Ltd., Leicester, UK) and centrifuged at 500 rpm for 2 min. Experimental solutions of 50 μL were added at 4x and 50 μL of 0.32% trypan blue was added for a final concentration of 0.08%. Plate was placed in the BioTek plate reader at 37 °C and read every 10 min at 494/517 nm for 4 h. Plate was then imaged with the CKX41 microscope with LED illumination, the XC30 camera, and processed using the CellSens software.

5.6.4 Osmolyte Incubation Calcein/Ethidium Homodimer-1 Uptake

A549 cells were seeded at $4 \cdot 10^6$ cells per well in 500 μL of cell culture medium in 24-well plates. Cells were incubated with osmolyte solutions for 24 h in a humidified atmosphere of 5% CO_2 and 95% air at 37 °C. Following the 24 h incubation, cells were incubated with 0.3 μM calcein-AM (ThermoFisher) and 10 μM ethidium homodimer-1 (ThermoFisher) in PBS. Cells were incubated at room temperature for 45 min. Solution was removed and wells were washed twice with PBS. Plate was read using the BioTex plate reader at 494/517 nm and 528/617

nm. Plate was then imaged with the CKX41 microscope with pE-300-W LED illumination, the XC30 camera, and processed using the CellSens software.

5.6.5 Post-Freeze Membrane Calcein/Ethidium Homodimer-1 Uptake

A549 cells were cryopreserved as monolayers as previously indicated in Section 4.6.8. Following the 24 h post-thaw incubation, cells were incubated with 0.3 µM calcein and 10 µM ethidium homodimer-1 in PBS. Cells were incubated at room temperature for 45 min. Solution was removed and wells were washed twice with PBS. Plate was read using the BioTex plate reader at 494/517 nm and 528/617 nm. Plate was then imaged with the CKX41 microscope with pE-300-W LED illumination, the XC30 camera, and processed using the CellSens software.

5.6.6 Nile Red Staining

5.6.6.1 Bright-field Nile Red Staining

A549 cells were seeded at $4 \cdot 10^4$ cells per well in 200 µL of cell culture medium with indicated concentrations of polyampholyte in 96-well plates. Cells were incubated with polymer for 10 min and exchanged against completed cell media or incubated with polymer for 24 h in a humidified atmosphere of 5% CO_2 and 95% air at 37 °C. Following the incubation period, 200 nM nile red (Sigma-Aldrich) in PBS was added to the wells. Plate was incubated for 10 min at room temperature. Nile red solution was removed and wells were washed with PBS. Cells were then imaged using a CKX41 microscope with pE-300-W LED illumination (CoolLED, Andover, UK), the XC30 camera, and processed using the CellSens software.

5.6.6.2 Confocal Nile Red Staining

A549 cells were seeded at $5 \cdot 10^5$ cells per well in 1 mL of cell culture medium with indicated concentrations of polyampholyte in 12-well plates (ThermoFisher) with 12 mm coverslips (Appleton Woods). Cells were incubated with polymer for 10

min and exchanged against completed cell media or incubated with polymer for 24 h in a humidified atmosphere of 5% CO_2 and 95% air at 37 °C. Following the incubation period, 200 nM nile red in phosphate buffered saline PBS was added. Plate was incubated for 10 min at room temperature. Nile red solution was removed and wells were washed with PBS. Cells were subsequently stained with NucBlue™ Live ReadyProbes™ nuclear stain reagent (ThermoFisher), fixed with 4% paraformaldehyde and imaged. ***Confocal imaging capture performed with assistance from Ruben Tomás and imaging processing was performed solely by Ruben Tomás.*** Confocal imaging was completed using a Zeiss LSM 710 inverted microscope with 63x oil immersion objective lenses, equipped with three photomultiplier detectors (GaAsP, multialkali and BiG.2) and multichannel spectral imaging with an ultra-sensitive GASP detector. The UV and VIS Laser Modules allowed selection of six lasers with wavelengths of 633, 594, 561, 543, 514, 488, 458, 405 and 355 nm. Zeiss ZEN (blue edition) 2.3 lite was utilised for image collection and processing.

5.6.7 Polyampholyte Incubation Calcein/Ethidium Homodimer-1 Uptake

A549 cells seeded at $4 \cdot 10^6$ cells per well in 500 µL of cell culture medium in 24-well plates. Cells were incubated with polymer for 10 min and exchanged against completed cell media or incubated with polymer for 24 h in a humidified atmosphere of 5% CO_2 and 95% air at 37 °C. Following the 24 h incubation, cells were incubated with 0.3 µM calcein (ThermoFisher) and 10 µM ethidium homodimer-1 (ThermoFisher) in PBS. Cells were incubated at room temperature for 45 min. Solution was removed and wells were washed twice with PBS. Plate was read using the BioTex plate reader at 494/517 nm and 528/617 nm. Plate was then imaged with the CKX41 microscope with pE-300-W LED illumination, the XC30 camera, and processed using the CellSens software.

5.6.8 Neutral Red Staining

A549 cells were seeded at $4 \cdot 10^4$ cells per well in 200 µL of cell culture medium with indicated concentrations of polyampholyte in 96-well plates. Cells were incubated with polymer for 10 min and exchanged against completed cell media or incubated with polymer for 24 h in a humidified atmosphere of 5% CO_2 and 95% air at 37 °C. Following the incubation period, 100 µL neutral red was added and plate was incubated for 2 h at 37 °C. Plate was washed with PBS and then 150 µL of destain solution, consisting of 50% ethanol (VWR International, Leicestershire, UK), 49% deionised water, 1% glacial acetic acid (Sigma-Aldrich), was added for 10 min with shaking. Cells were then imaged using a CKX41 microscope, the XC30 camera, and processed using the CellSens software.

5.6.9 Fluorescently Labelled Polyampholytes

5.6.9.1 Bright-field Fluorescent Labelled Polyampholyte Uptake

A549 cells were seeded at $4 \cdot 10^4$ cells per well in 200 µL of cell culture medium with indicated concentrations of rhodamine-6G tagged polyampholyte in 96-well plates. Cells were incubated with polymer for 10 min and exchanged against completed cell media or incubated with polymer for 24 h in a humidified atmosphere of 5% CO_2 and 95% air at 37 °C. Following the incubation period, polyampholyte solution was removed and wells were washed with PBS. Cells were then imaged using a CKX41 microscope with pE-300-W LED illumination (CoolLED, Andover, UK), the XC30 camera, and processed using the CellSens software.

5.6.9.2 Confocal Fluorescent Labelled Polyampholyte Uptake

A549 cells were seeded at $5 \cdot 10^5$ cells per well in 1 mL of cell culture medium with indicated concentrations of rhodamine-6G tagged polyampholyte in 12-well plates with 12 mm coverslips. Cells were incubated with tagged polymer for 10 min and

exchanged against completed cell media or incubated with polymer for 24 h in a humidified atmosphere of 5% CO_2 and 95% air at 37 °C. Following the incubation period, cells were stained with NucBlue™ Live ReadyProbes™ nuclear stain reagent, fixed with 4% paraformaldehyde and imaged as detailed previously in Section 5.6.6.1.

5.6.10 Statistical Analysis

Data were analysed with a one-way analysis of variance (ANOVA) on ranks followed by comparison of experimental groups with the appropriate control group (Holm–Sidak method) followed by Tukey's post hoc test. Excel 2013 (Microsoft, Redmond, WA) and R were used for the analyses and graphs. Data sets are presented as mean ± (SEM).

5.7 APPENDIX

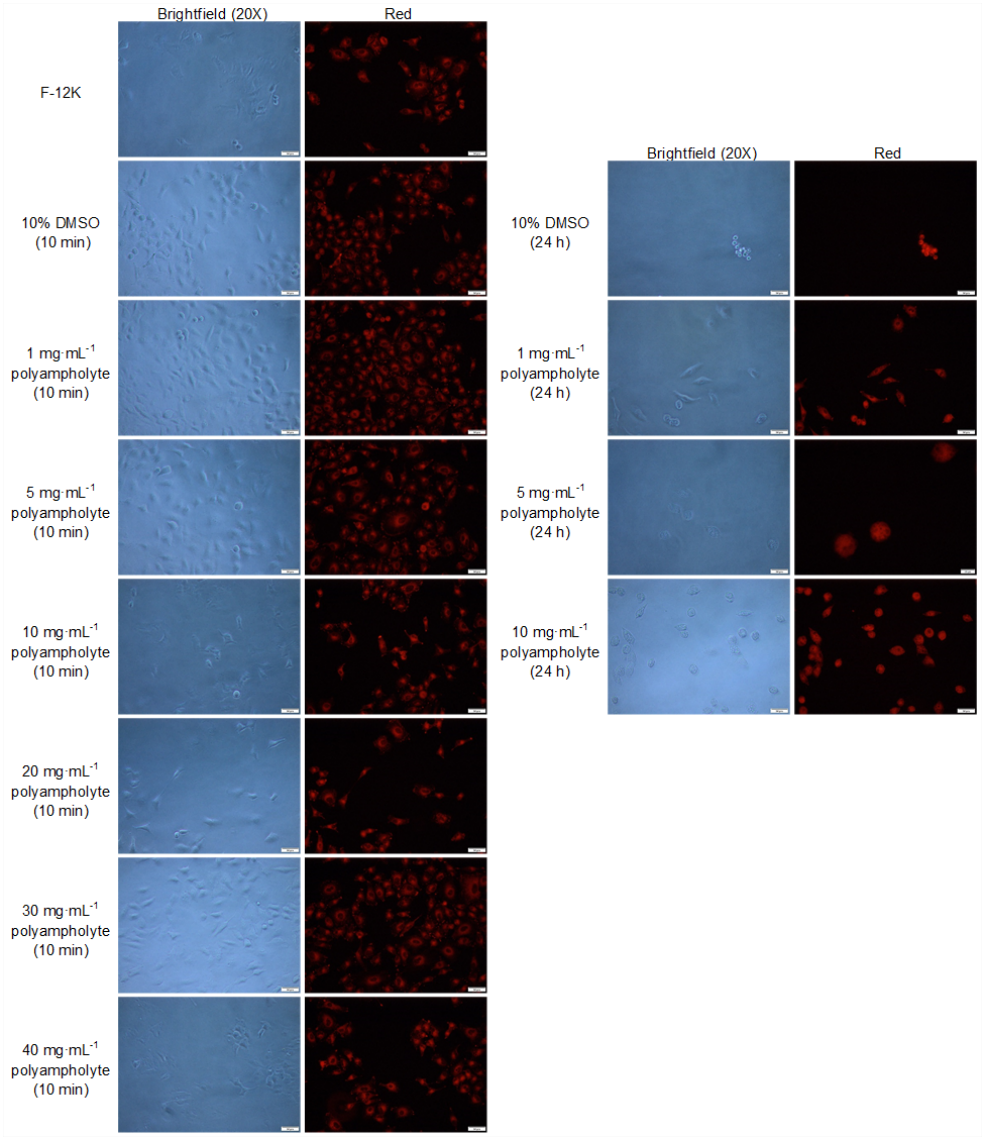

Figure 5.24. Nile red treatment of cells incubated with polyampholyte. Scale bar = 50 µm.

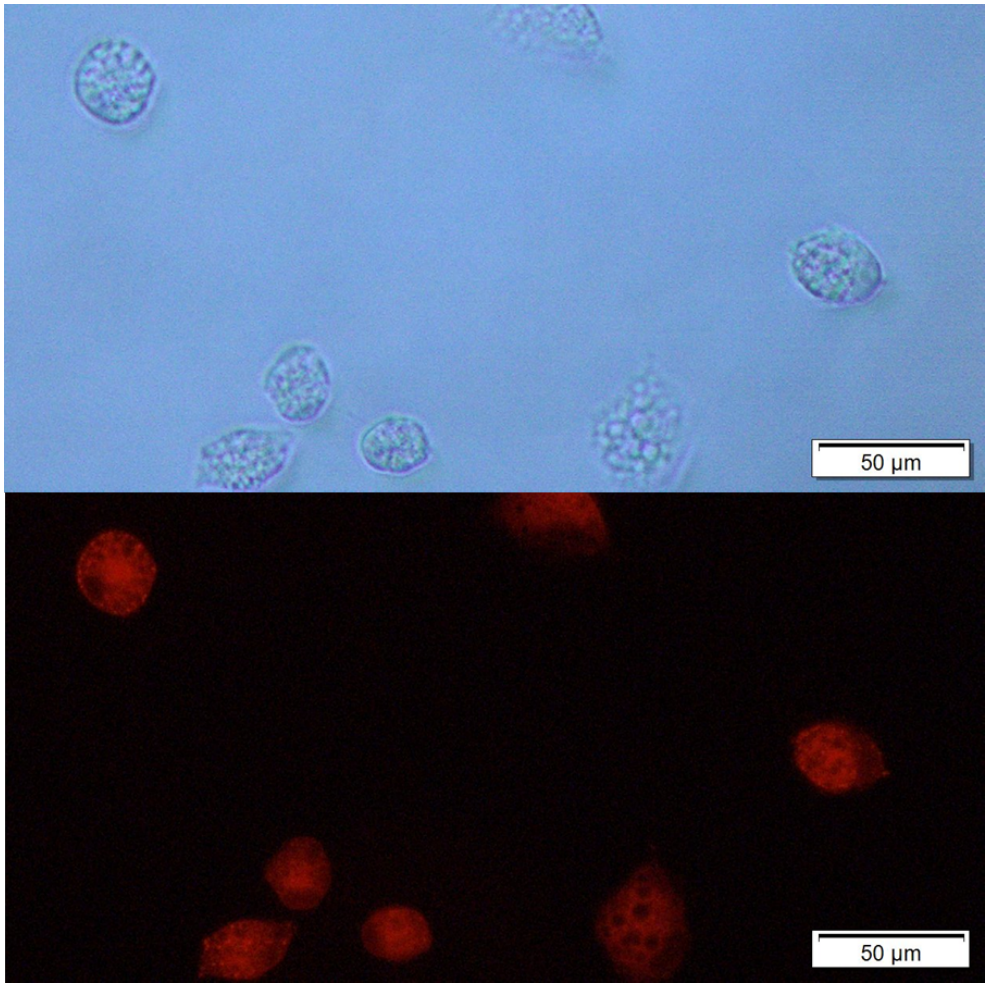

Figure 5.25. Nile red treatment of cells incubated with 10 mg·mL^{-1} polyampholyte for 24 h. Scale bar = 50 µm.

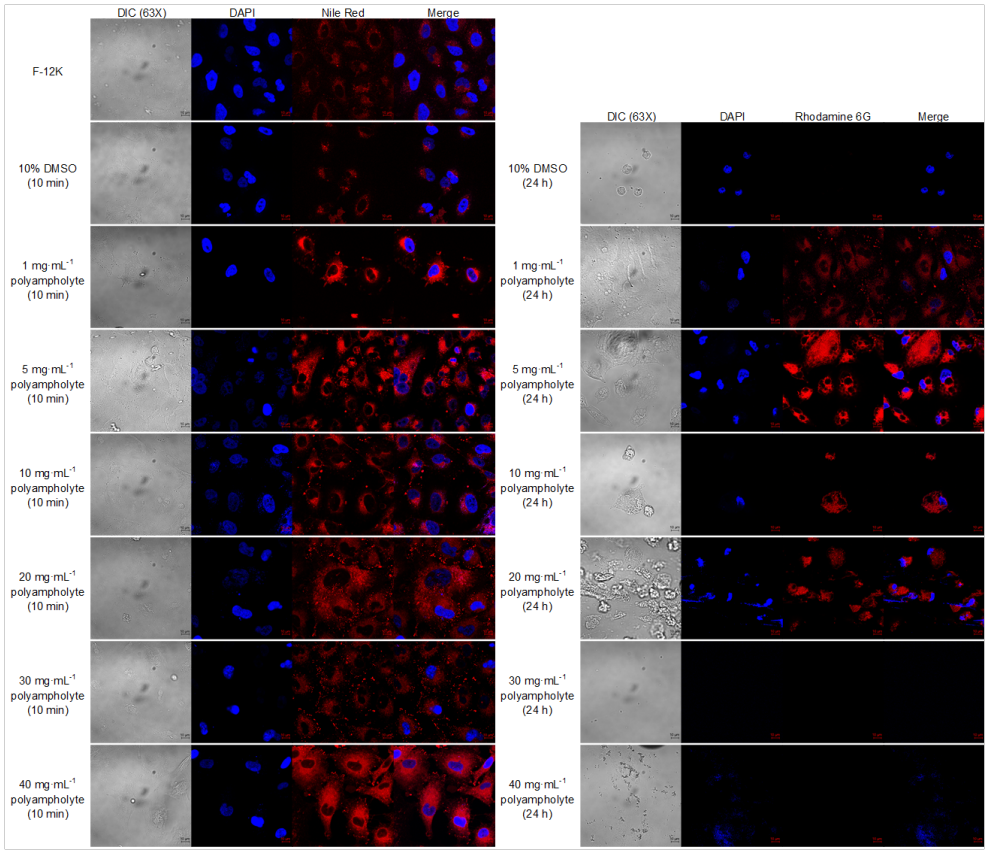

Figure 5.26. Confocal imaging of nile red treatment of cells incubated with polyampholyte. Scale bar = 10 µm.

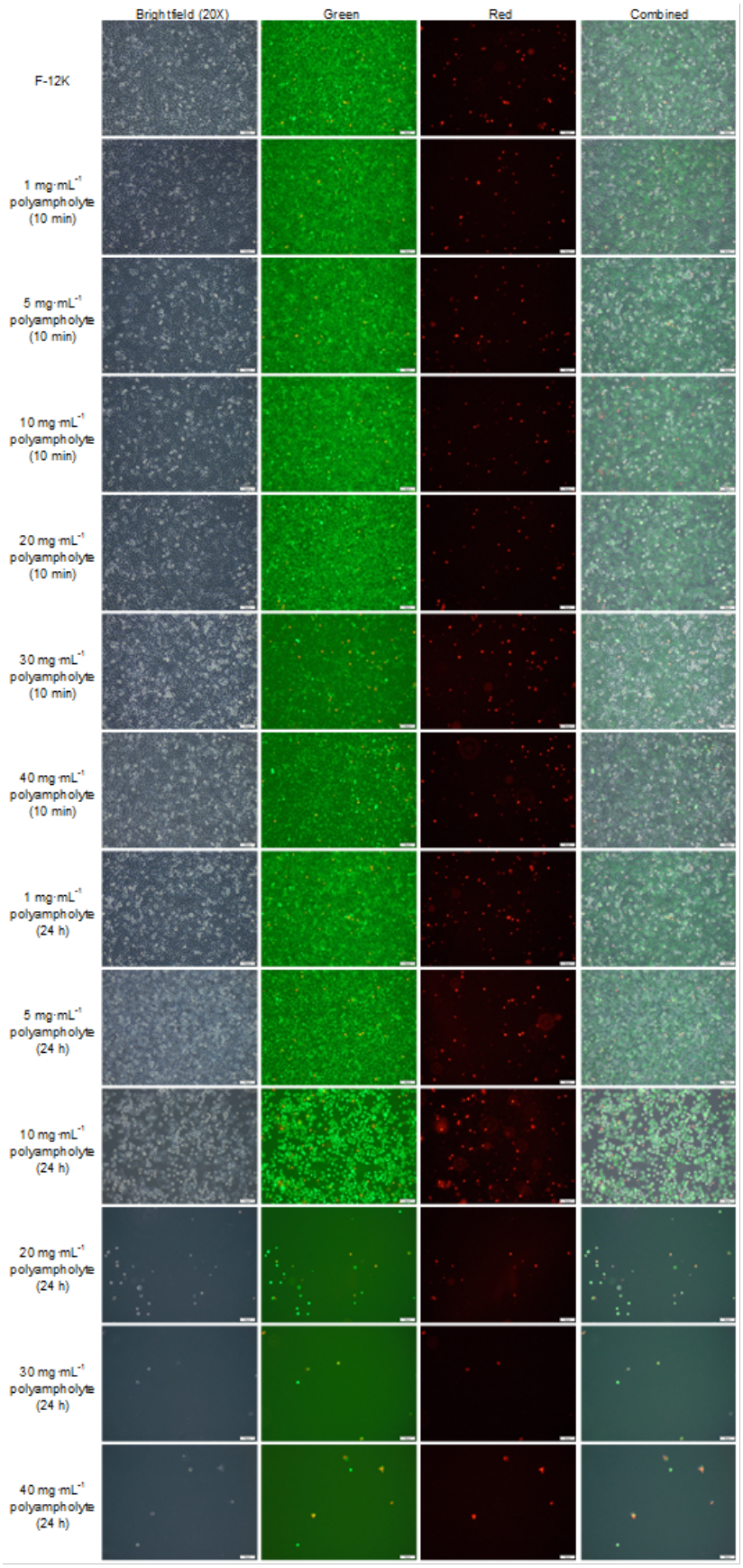

Figure 5.27. Membrane permeability of polyampholyte incubated cells. Images of calcein-AM/EthD-1 treated cells. Scale bar = 50 µm.

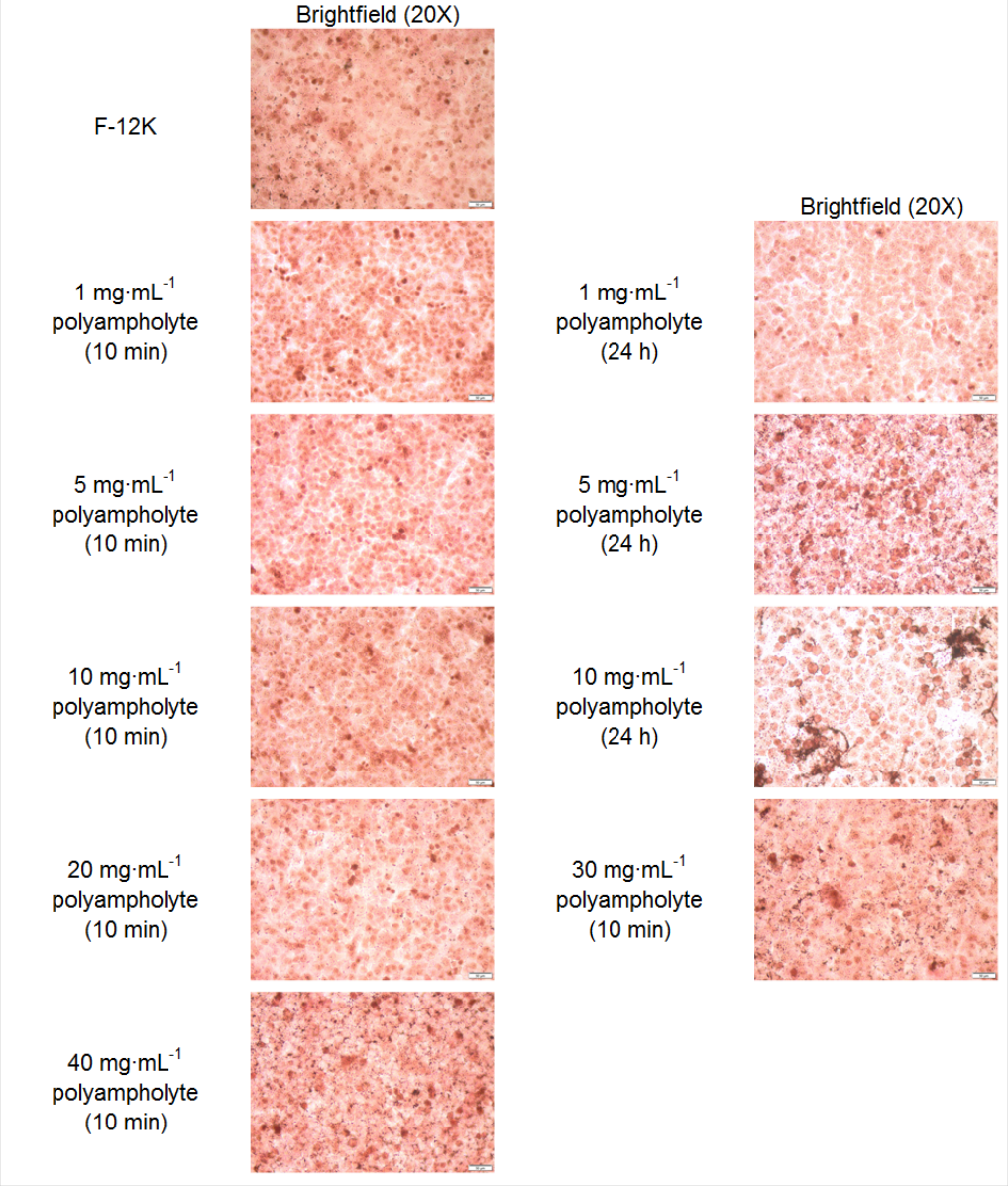

Figure 5.28. Neutral red staining of polyampholyte incubated cells. Images of treated cells. Scale bar = 50 µm.

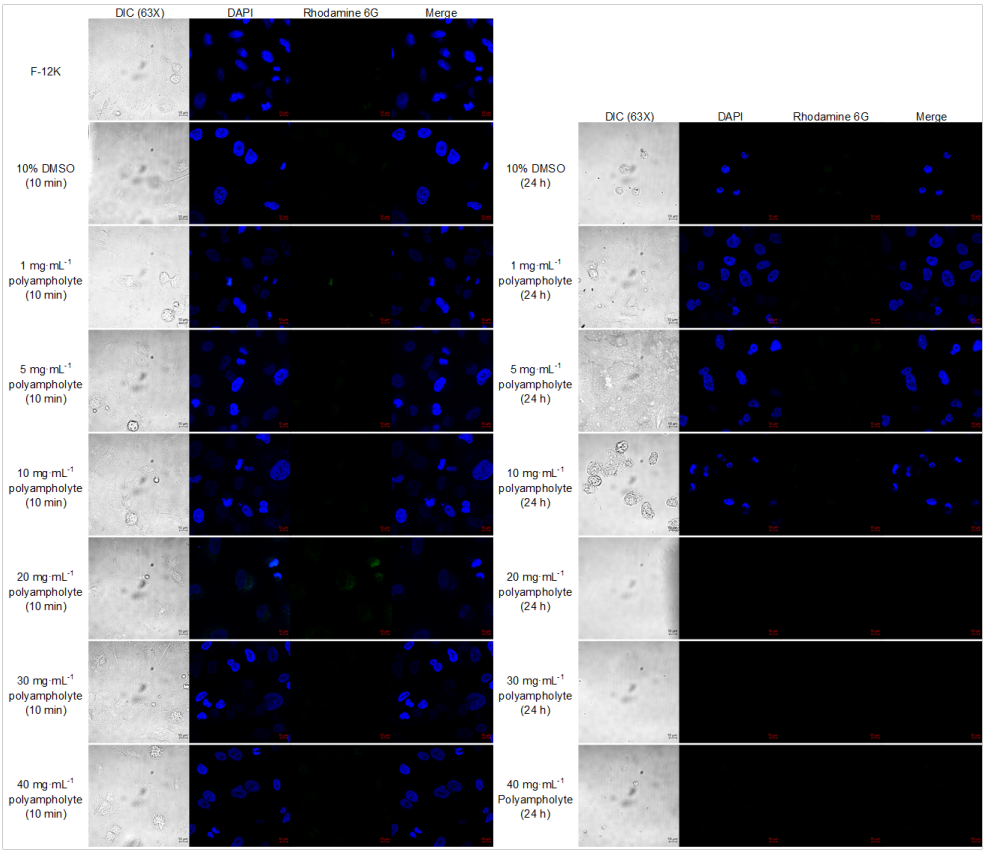

Figure 5.29. Confocal imaging of rhodamine-6G tagged-polyampholyte incubated cells. Images of treated cells. Scale bar = 10 μm.

5.8 References

(1) Maximov, N. A. Internal Factors of Frost and Drought Resistance in Plants. *Protoplasma* **1929**, *7* (1), 259–291. https://doi.org/10.1007/BF01612809.

(2) Siminovitch, D.; Scarth, G. W. A Study of the Mechanism of Frost Injury to Plants. *Can. J. Res.* **1938**, *16c* (11), 467–481. https://doi.org/10.1139/cjr38c-043.

(3) Mazur, P.; Leibo, S. P.; Chu, E. H. Y. A Two-Factor Hypothesis of Freezing Injury. Evidence from Chinese Hamster Tissue-Culture Cells. *Exp. Cell Res.* **1972**, *71* (2), 345–355. https://doi.org/10.1016/0014-4827(72)90303-5.

(4) Steponkus, P. L. Role of the Plasma Membrane in Freezing Injury and Cold Acclimation. *Annu. Rev. Plant Physiol.* **1984**, *35* (1), 543–584.

https://doi.org/10.1146/annurev.pp.35.060184.002551.

(5) Mazur, P. The Role of Cell Membranes in the Freezing of Yeast and Other Single Cells. *Ann. N. Y. Acad. Sci.* **1965**, *125* (2), 658–676. https://doi.org/10.1111/j.1749-6632.1965.tb45420.x.

(6) Mazur, P. The Role of Intracellular Freezing in the Death of Cells Cooled at Supraoptimal Rates. *Cryobiology* **1977**, *14* (3), 251–272. https://doi.org/10.1016/0011-2240(77)90175-4.

(7) de Gier, J. Osmotic Behaviour and Permeability Properties of Liposomes. *Chem. Phys. Lipids* **1993**, *64* (1–3), 187–196. https://doi.org/10.1016/0009-3084(93)90065-b.

(8) Su, M.; He, C.; West, C. A.; Mentzer, S. J. Cytolytic Peptides Induce Biphasic Permeability Changes in Mammalian Cell Membranes. *J. Immunol. Methods* **2001**, *252* (1–2), 63–71. https://doi.org/10.1016/S0022-1759(01)00334-9.

(9) He, F.; Liu, W.; Zheng, S.; Zhou, L.; Ye, B.; Qi, Z. Ion Transport through Dimethyl Sulfoxide (DMSO) Induced Transient Water Pores in Cell Membranes. *Mol. Membr. Biol.* **2012**, *29* (3–4), 107–113. https://doi.org/10.3109/09687688.2012.687460.

(10) Fahy, G. M. The Relevance of Cryoprotectant “Toxicity” to Cryobiology. *Cryobiology* **1986**, *23* (1), 1–13. https://doi.org/10.1016/0011-2240(86)90013-1.

(11) Liu, Y.; Vrana, N. E.; Cahill, P. A.; McGuinness, G. B. Physically Crosslinked Composite Hydrogels of PVA with Natural Macromolecules: Structure, Mechanical Properties, and Endothelial Cell Compatibility. *J. Biomed. Mater. Res. B. Appl. Biomater.* **2009**, *90* (2), 492–502. https://doi.org/10.1002/jbm.b.31310.

(12) Graham, B.; Bailey, T. L.; Healey, J. R. J.; Marcellini, M.; Deville, S.; Gibson, M. I. Polyproline as a Minimal Antifreeze Protein Mimic That

Enhances the Cryopreservation of Cell Monolayers. *Angew. Chem. Int. Ed. Engl.* **2017**, *56* (50), 15941–15944. https://doi.org/10.1002/anie.201706703.

(13) Rajan, R.; Hayashi, F.; Nagashima, T.; Matsumura, K. Toward a Molecular Understanding of the Mechanism of Cryopreservation by Polyampholytes: Cell Membrane Interactions and Hydrophobicity. *Biomacromolecules* **2016**, *17* (5), 1882–1893. https://doi.org/10.1021/acs.biomac.6b00343.

(14) Yancey, P. H. Organic Osmolytes as Compatible, Metabolic and Counteracting Cytoprotectants in High Osmolarity and Other Stresses. *J. Exp. Biol.* **2005**, *208* (Pt 15), 2819–2830. https://doi.org/10.1242/jeb.01730.

(15) Bozza, P. T.; Viola, J. P. B. Lipid Droplets in Inflammation and Cancer. *Prostaglandins. Leukot. Essent. Fatty Acids* **2010**, *82* (4–6), 243–250. https://doi.org/10.1016/j.plefa.2010.02.005.

(16) Greenspan, P.; Mayer, E. P.; Fowler, S. D. Nile Red: A Selective Fluorescent Stain for Intracellular Lipid Droplets. *J. Cell Biol.* **1985**, *100* (3), 965–973. https://doi.org/10.1083/jcb.100.3.965.

(17) Vadivelu, R. K.; Kamble, H.; Munaz, A.; Nguyen, N. T. Liquid Marble as Bioreactor for Engineering Three-Dimensional Toroid Tissues. *Sci. Rep.* **2017**, *7* (1), 1–14. https://doi.org/10.1038/s41598-017-12636-5.

(18) Cooper, S. T.; McNeil, P. L. Membrane Repair: Mechanisms and Pathophysiology. *Physiol. Rev.* **2015**, *95* (4), 1205–1240. https://doi.org/10.1152/physrev.00037.2014.

(19) Repetto, G.; Peso, A.; Zurita, J. L. Neutral Red Uptake Assay for the Estimation of Cell Viability/Cytotoxicity. *Nat. Protoc.* **2008**, *3* (7), 1125–1131. https://doi.org/10.1038/nprot.2008.75.

(20) Sydykov, B.; Oldenhof, H.; de Oliveira Barros, L.; Sieme, H.; Wolkers, W. F. Membrane Permeabilization of Phosphatidylcholine Liposomes Induced

by Cryopreservation and Vitrification Solutions. *Biochim. Biophys. Acta - Biomembr.* **2018**, *1860* (2), 467–474. https://doi.org/10.1016/j.bbamem.2017.10.031.

CONCLUSIONS

The overall aim of this thesis was to develop a simple and effective method to cryopreserve adherent mammalian cells. The ability to cryopreserve monolayered cells would facilitate drug development by providing phenotypically identical cells for assays as well as provide insights into the cryopreservation of more complex biological material such as spheroids or tissues but established methods have failed to achieve this. In this thesis we investigated three different macromolecular cryoprotectants and three different small molecule osmolytes. Poly(vinyl alcohol), (PVA) was chosen due to its high ice recrystallisation inhibition (IRI) activity and its success in cryopreserving cells in suspension. Polyproline was chosen as a possible AF(G)P mimic due to its amphiphilicity and tertiary structure. Polyampholytes bearing mixed positive and negative charges have been studied for cryopreservation and our polyampholyte of interest was chosen due to its scalable synthesis of a cheap precursor and precise 1:1 ratio of cationic/anionic groups. Alanine was selected due to the heavy alanine rich regions of AF(G)Ps, betaine was selected for its osmoprotecting properties, and proline was chosen due to its previous use as a cryoprotectant and its implications as an osmoprotectant.

The first aim of this thesis was to examine the cryoprotective agents' physical interactions with ice. This allowed an investigation into how the compounds may be affording their protection. Initially, we investigated the IRI activity of our macromolecular compounds and small molecule osmolytes. In this work we confirmed that PVA is a potent IRI polymer, regardless of solvent (PBS or cell media) while polyproline and polyampholyte showed significantly less IRI activity in comparison. The osmolytes themselves showed little IRI activity yet did not inhibit PVA's high IRI activity. We additionally demonstrated that all our solutions

containing macromolecular cryoprotectants, osmolytes, DMSO, or combinations of, freeze (i.e. ice forms, rather than vitrification) and the polymers and/or osmolytes did not affect DMSO's phase transitions (Chapter 2).

The next aim of this thesis was to evaluate if any of our macromolecular cryoprotectants or small molecule osmolytes were inherently toxic to our cells and if the osmolytes affected the proliferation rate of the cells. We found that none of our macromolecular cryoprotectants were toxic to our cells for a 10 min exposure (relevant for cryopreservation) and none of our osmolytes were toxic to the cells after 24 hours. Proline was the only osmolyte to affect the growth of our cells, significantly down-regulating growth during incubation; however, we saw no differences in our preliminary cell cycle analysis (Chapter 3).

The next aim of this thesis was to evaluate if our small molecule osmolytes and/or macromolecular cryoprotectants were able to successfully cryopreserve mammalian cells and how viable the cells were post-freeze. We found that the combination of betaine or proline with PVA resulted in a significantly higher post-thaw recovery of A549 monolayers compared to 10% DMSO, however, the combination of proline with PVA was not successful for the cryopreservation of suspension human endometrial cells, MC-3T3 monolayers, or Neuro-2a monolayers. All A549 monolayers frozen with osmolytes and PVA grew better than cells frozen with only 10% DMSO. Polyproline, in combination with proline incubation, resulted in significantly higher recoveries for A549 cells frozen as monolayers compared to cells frozen with 10% DMSO. The combination of polyproline and proline also resulted in higher post-thaw growth rates. This is an interesting finding as polyproline showed weak IRI, yet provided cell recovery equivalent to PVA, which is highly IRI active. It would be interesting to explore if there is a minimal amount of IRI that is sufficient to provide protection to cell monolayers. The polyampholyte resulted in significantly higher post-thaw recoveries at all concentrations tested and the inclusion of proline did not further

increase the recoveries seen for A549 monolayers. This is also an interesting finding that may be worth exploring, as proline and the polyampholyte may have overlapping protection mechanisms or may be protecting cells through two wholly different pathways. The polyampholyte also protected Neuro-2a and MC-3T3 cells, as well allowed for the lowering of DMSO down to 2% with recoveries comparable to 10% DMSO alone. Cells frozen with 10 $mg \cdot mL^{-1}$ polyampholyte P2 also grew better post-freeze compared to cells frozen with only 10% DMSO (Chapter 4).

The last aim of this thesis was to evaluate the membrane permeability at various steps throughout our freezing processes to determine if our macromolecular and small molecule compounds had any effect on the permeability of the cells. We found that our CPA compounds did not impact the membrane permeability of cells at room temperature. Similarly, we found that our osmolyte incubation also did not impact permeability under physiological conditions. For our post-freeze analysis, we found that cells frozen with osmolyte pre-treatment along with PVA did not show significantly different permeability from cells frozen with just DMSO, even though the post-freeze cell recoveries for these conditions were significantly different. The post-freeze permeability for cells frozen with polyampholyte did show significant differences, correlating with their post-freeze cell recoveries. This is a significant finding for future study, as it could imply that the calcein/EthD-1 assay, a commonly used assay, is not sensitive enough to capture differences for small significant differences. However, it could be that the cells are viable post-thaw but are damaged through the trypsinisation process (a necessary step to assess cell recovery), introducing a new mode of analysis/damage for cryopreserved monolayers (Chapter 5).

Our overall significant results have been compiled in Table C.1. Throughout this work we have developed three different strategies for the cryopreservation of adherent mammalian cells. We were unable to pinpoint a unifying mechanism for

these compounds, paving the way for future work to investigate how these compounds may be affording their protection. Ultimately, the high recovery, along with the relative ease of synthesis and use, seen with polyampholyte could position it as a next generation cryopreservation solution for many different cell types.

Table C.1. Compiled significant results. Significantly higher than control, significantly lower than control, significantly lower than control but higher than 5 mg·mL^{-1} PVA.

Target	Average Ice Crystal Size (μm^2) ↓	AlamarBlue Reduction (24 h) (%) ↑	Rate of Growth (Day 6) –	Recovery Rate of Growth (Day 6) –	A549 Monolayer Cryopreservation (%) ↑	Post-Freeze Growth Rate (Day 6) -
Unfrozen Control	4519.59	100.0	0.69	0.39	–	0.70
10% DMSO	–	**31.9**	–	–	16.9	**0.58**
5 mg·mL^{-1} PVA	**365.87**	88.3	–	–	23.7	**0.58**
100 mM Alanine	2326.05	93.5	0.66	0.43	24.1	0.74
Alanine + PVA	**117.9**	–	–	–	**38.7**	0.64
100 mM Betaine	3641.71	95.4	0.74	0.43	30.0	0.64
Betaine + PVA	**354.71**	–	–	–	**56.7**	0.67
200 mM Proline	2657.67	82.1	**0.51**	**0.49**	**45.7**	0.61
Proline + PVA	**344.34**	–	–	–	**62.7**	0.64
5 mg·mL^{-1} Polyproline	1323.41	**67.5**	–	–	20.3	0.63
Proline + Polyproline	–	–	–	–	**47.6**	0.68
10 mg·mL^{-1} P2 Polyampholyte	2622.38	79.1	–	–	**71.2**	0.61

CONTRIBUTIONS TO PUBLISHED WORK

The following details personal contributions to published work subjected to peer review.

R. M. F. Tomás, **T. L. Bailey**, M. Hasan, and M. I. Gibson, “Extracellular Antifreeze Protein Significantly Enhances the Cryopreservation of Cell Monolayers,” *Biomacromolecules*, vol. 20, no. 10, pp. 3864–3872, 2019.

Contributed to experimental design and assisted in review of article during the publication process.

T. L. Bailey, C. Stubbs, K. Murray, R. M. F. Tomás, L. Otten, and M. I. Gibson, “Synthetically Scalable Poly(ampholyte) Which Dramatically Enhances Cellular Cryopreservation.,” Biomacromolecules, vol. 20, no. 8, pp. 3104–3114, Aug. 2019.

Contributed to experimental design and assisted in obtaining all experimental data involved in mammalian cell cryopreservation, performed a significant amount of the data analysis prior to assisting in the writing and reviewing of the article during the publication process.

R. M. F. Tomás, B. Martyn, **T. L. Bailey**, and M. I. Gibson, “Engineering Cell Surfaces by Covalent Grafting of Synthetic Polymers to Metabolically-Labeled Glycans,” *ACS Macro Lett.*, pp. 1289–1294, 2018.

Contributed to experimental design, performed cell viability assay and initial screening of labelled glycans.

C. I. Biggs, **T. L. Bailey**, Ben Graham, C. Stubbs, A. Fayter, and M. I. Gibson, "Polymer mimics of biomacromolecular antifreezes," *Nat. Commun.*, vol. 8, no. 1, p. 1546, 2017.

Complied cell cryopreservation information and contributed to the writing of the article during the publication process.

B. Graham, **T. L. Bailey**, J. R. J. Healey, M. Marcellini, S. Deville, and M. I. Gibson, "Polyproline as a Minimal Antifreeze Protein Mimic That Enhances the Cryopreservation of Cell Monolayers," *Angew. Chemie - Int. Ed.*, vol. 56, no. 50, pp. 15941–15944, 2017.

Contributed to experimental design and assisted in obtaining all experimental data involved in mammalian cell cryopreservation, performed data analysis prior to assisting in the writing and reviewing of the article during the publication process.

C. S. Guy, E. Tichauer, G. L. Kay, D. J. Phillips, **T. L. Bailey**, J. Harrison, C. M. Furze, A. D. Millard, M. I. Gibson, M. J. Pallen, and E. Fullam, "Identification of the anti-mycobacterial functional properties of piperidinol derivatives," *Br. J. Pharmacol.*, vol. 174, no. 14, pp. 2183–2193, 2017.

Performed cell viability assays and contributed to the writing during the publication process.